NOVEL BENT-CORE METALLOMESOGENS

Kelly Ames, MSci.

Thesis submitted to the University of Nottingham

for the degree of Doctor of Philosophy

September 2005

For Grandad

Declaration

Except where specific reference has been made to other sources, the work presented in this thesis is the original work of the author. It has not been submitted, in whole or in part, for any other degree.

Kelly Ames

Abstract

Novel polycatenar bent-core Schiff-base metallomesogens from derivatives of 1,10-phenanthroline ($[MCl_2(L^{Phen\text{-}n})]$), 2,2-bipyridine ($[MCl_2(L^{Bipy\text{-}n})]$) and 5,5'-dimethyldipyrromethane ((tc)-$[M(L^{Dipy\text{-}n})]$ and ex-$[M(L^{Dipy\text{-}n})]$) have been investigated in this body of work. The mesomorphic properties of these first- and second-row transition metal complexes have been studied. Further to the examination of the compounds in the liquid crystalline state, single crystal X-ray studies of short chain analogues were performed to determine the coordination geometry and the degree of self-assembly of the molecules in the solid state.

Chapter 1 introduces the field of liquid crystals and metallomesogens, with a focus on thermotropic liquid crystals and their nomenclature, physical properties and applications. The historical background of the field is briefly explored and previous research on bent-core metallomesogens from the Schröder group in Nottingham has been reviewed. The characterisation of liquid crystalline mesophases, namely by polarised optical microscopy, differential scanning calorimetry and X-ray diffraction, are described. Further discussion is dedicated to the X-ray diffraction patterns generated by columnar mesophases. The chapter finishes with a description of the aims of the project.

Chapter 2 commences with an introduction to liquid crystals derived from 1,10-phenanthroline. Following this is a description of the synthesis and characterisation of mesomorphic metal-free ligands, $L^{Phen\text{-}n}$ (n = 10, 12, 14, 16), four novel series of metallomesogens and two non-mesomorphic series of complexes derived from 1,10-phenanthroline, $[MCl_2(L^{Phen\text{-}n})]$ (M = Mn^{2+}, Fe^{2+}, Co^{2+}, Ni^{2+}, Cu^{2+}, Zn^{2+}; L^{Phen} = 2,9-bis-[3',4',5'-tri(alkoxy)phenyliminomethyl]-

1,10-phenanthroline; n = 8, 10, 12, 14, 16). Structural determination by single crystal X-ray diffraction of the analogous methoxy complexes $[MCl_2(L^{Phen\text{-}1})]$ (M = Mn^{2+}, Co^{2+}, Ni^{2+}, Zn^{2+}), and the complex without any lateral aliphatic groups $[CuCl_2(L^{Phen\text{-}0})]$, revealed the metal(II) complexes to have either distorted trigonal bipyramidal, square pyramidal or octahedral coordination geometry. The mesomorphic behaviour of the complexes $[MCl_2(L^{Phen\text{-}n})]$ (M = Mn^{2+}, Co^{2+}, Ni^{2+}, Zn^{2+}; n = 8, 10, 12, 14, 16) and the metal-free ligands $L^{Phen\text{-}n}$ (n = 10, 12, 14, 16) is columnar (with the exception of the non-mesomorphic $[CoCl_2(L^{Phen\text{-}8})]$), and the 2D symmetries of these mesophases vary between hexagonal, rectangular and oblique.

Chapter 3 is introduced with a discussion of liquid crystalline compounds derived from 2,2'-bipyridine. Subsequently, the synthesis and characterisation of four new series of metallomesogens and two non-mesomorphic compounds derived from 2,2'-bipyridine, $[MCl_2(L^{Bipy\text{-}n})]$ (M = Mn^{2+}, Fe^{2+}, Co^{2+} Cu^{2+} and n = 16; M = Ni^{2+}, Zn^{2+} and n = 10, 12, 14, 16; L^{Bipy} = 6,6'-bis-[3',4',5'-tri(alkoxy)phenyliminomethyl]-2,2'-bipyridine) are detailed. Single crystal X-ray diffractometry revealed the coordination geometry of $[MnCl_2(L^{Bipy\text{-}1})]$, $[CoCl_2(L^{Bipy\text{-}1})]$ and $[NiCl_2(L^{Bipy\text{-}1})]$ to be octahedral, whereas $[ZnCl_2(L^{Bipy\text{-}1})]$ is distorted trigonal bipyramidal. The complexes $[MCl_2(L^{Bipy\text{-}n})]$ (M = Mn^{2+}, Co^{2+} and n = 16; M = Ni^{2+}, Zn^{2+} and n = 10, 12, 14, 16) exhibit mesomorphic character and again generate columnar mesophases.

Finally, Chapter 4 begins with a discussion on pyrrole-derived liquid crystals. Consequently, the synthesis and characterisation of hexacatenar compounds $[M(L^{Dipy\text{-}n})]_x$ (M = 2H, Zn^{2+}, Pd^{2+}; n = 10, 12, 14, 16; x = 1, 2),

tetracatenar compounds tc-$[M(L^{Dipy\text{-}16})]_x$ (M = 2H, Zn^{2+}, Pd^{2+}; x = 1, 2) and extended dicatenar compounds ex-$[M(L^{Dipy\text{-}n})]_x$ (M = 2H, Zn^{2+}, Pd^{2+}; x = 1, 2) are described. Characterisation by X-ray diffraction of single crystals of $[Zn(L^{Dipy\text{-}1})]_2$, ex-$[Zn(L^{Dipy\text{-}1})]_2$ show they exhibit a distorted tetrahedral geometry, forming double stranded helical structures, while ex-$[Pd(L^{Dipy1})]$ has a distorted square planar geometry. The metal-free ligands $H_2L^{Dipy\text{-}n}$ (n = 10, 12, 14, 16) and complexes $[Zn(L^{Dipy\text{-}16})]_2$ and $[Pd(L^{Dipy\text{-}n})]$ (n = 12, 14, 16) all exhibit narrow mesomorphic temperature ranges and unidentified mesophases. The tetracatenar compound tc-$[Zn(L^{Dipy\text{-}16})]_2$ generates a columnar hexagonal mesophase and the complex tc-$[Pd(L^{Dipy\text{-}16})]$ generates an unidentified liquid crystalline phase, whereas the metal-free ligand tc-$H_2L^{Dipy\text{-}16}$ has no mesomorphic character. Finally, two of the extended dicatenar compounds ex-$H_2L^{Dipy\text{-}16}$ and ex-$[Zn(L^{Dipy\text{-}16})]_2$ are non-mesomorphic, while ex-$[Pd(L^{Dipy\text{-}16})]$ was found to have a smectic A phase.

Acknowledgements

I would like to gratefully acknowledge my supervisor Prof. Martin Schröder for the opportunity to carry out three years of research, in addition to his support and encouragement throughout. I would also like to give special thanks to my second supervisor Dr. Simon Collinson, whose assistance, advice and support have been unparalleled over the past four years and most gratefully received. My thanks also extend to the Schröder group and the rest of the Inorganic floor for much valued friendship and good times, in particular Ash, Stu, Angela, Jen, George, Phil, Ian, Dave, Paul and Katie.

Much of the work in this thesis would not have been possible without the help and collaboration of a number of people. From the University of Nottingham I would like to acknowledge Dr. Claire Wilson and Dr. Sandy Blake for an abundance of help with crystallography and problematic disordered molecules, and Prof. Steve Howdle and Andy Naylor for access to and support in using their DSC machine. I am indebted to Prof. Duncan Bruce from the University of Exeter for allowing me to experience first-hand liquid crystal characterisation by POM and DSC. I am also thankful to Dr. Richard Date and Maja Sepelj for additional analysis of some liquid crystalline compounds in Exeter. I am extremely grateful to Dr. Bertrand Donnio for the opportunity he gave me to characterise my compounds by X-ray diffraction at the Institut de Physique et Chimie des Matériaux de Strasbourg.

Finally, my greatest thanks extends to my family for the unconditional support, understanding and encouragement they have provided me with over the last four years.

Abbreviations

a, *b*, γ	lattice parameters for mesophase unit cell
AcOH	acetic acid
Ar	argon
B	banana mesophase
Bipy	derivative of 2,2-bipyridine
Br_2	bromine
$CDCl_3$	deuterated chlorofrom
$CHCl_3$	chloroform
CH_2Cl_2	dichloromethane
CH_3CN	acetonitrile
CI MS	chemical ionisation mass spectrometry
$CoCl_2.6H_2O$	cobalt(II) chloride hexahydrate
Col	columnar mesophase
Col_h	columnar hexagonal mesophase
Col_o	columnar oblique mesophase
Col_r	columnar rectangular mesophase
Cr	crystalline or solid phase
Cs_2CO_3	cesium carbonate
Cub	cubic mesophase
$CuCl_2$	copper(II) chloride
d	repeat distance between lattice planes
δ	NMR shift in ppm
DCC	N,N'-dicyclohexylcarbodiimide
Dipy	derivative of 5,5'-dimethyldipyrromethane

DMAP	4-dimethylaminopyridine
DMF	dimethylformamide
DPPD	diketopyrrolopyrrole
DSC	differential scanning calorimetry
EI MS	electron ionisation mass spectrometry
ES MS	electrospray mass spectrometry
EtOAc	ethyl acetate
EtOH	ethanol
Et_2O	ether
ex	extended
FAB MS	fast atom bombardment mass spectrometry
$FeCl_2.4H_2O$	iron(II) chloride tetrahydrate
g	glass transition temperature
h	repeat unit along columnar axis of a mesophase
hk	indexation of two-dimensional lattice
HBr	hydrobromic acid
HCl	hydrochloric acid
HNO_3	nitric acid
I	isotropic liquid
K	crystalline or solid phase
KOH	potassium hydroxide
L	ligand
λ	wavelength
lc	uncharacterised liquid crystalline mesophase
LCD	liquid crystal display

MALDI-TOF MS	matrix-assisted laser desorption/ionisation mass spectrometry
MeOH	methanol
$MgSO_4$	magnesium sulphate
$MnCl_2.4H_2O$	manganese(II) chloride tetrahydrate
n	number of carbon atoms in an aliphatic chain
$\underline{n}$	director
N	nematic mesophase
N_2	nitrogen
Na_2CO_3	sodium carbonate
$NaNO_2$	sodium nitrite
NaOH	sodium hydroxide
Na_2SO_4	sodium sulphate
N_{Col}	columnar nematic mesophase
N_D	discotic nematic mesophase
NEt_3	triethylamine
$NiCl_2.6H_2O$	nickel(II) chloride hexahydrate
N_h, N_r, N_o	number of molecules per column cross-section for columnar hexagonal, rectangular and oblique phases, respectively
ν	wavenumber
$Pd(OAc)_2$	palladium(II) acetate
Phen	derivative of 1,10-phenanthroline
$POCl_3$	phosphorus oxychloride
POM	polarised optical microscopy

S	cross-sectional lattice parameter of columnar mesophase
SAXS	small angle X-ray scattering
SmA	smectic A mesophase
SmB	smectic B mesophase
SmC	smectic C mesophase
SmC*	ferroelectric smectic C mesophase
SmF	smectic F mesophase
SmI	smectic I mesophase
$SnCl_2.2H_2O$	tin(II) chloride dihydrate
τ	geometric parameter
T	temperature
tc	tetracatenar
THF	tetrahydrofuran
θ	angle of diffraction of X-rays
WAXS	wide angle X-ray scattering
XRD	X-ray diffraction
$ZnCl_2$	zinc(II) chloride
$Zn(OAc)_2.2H_2O$	zinc(II) acetate dihydrate

Table of Figures

Table of Schemes

Table of Tables

Table of Contents

CHAPTER 1:

INTRODUCTION TO METALLOMESOGENS

1. INTRODUCTION

1.1 GENERAL CONCEPTS: LIQUID CRYSTALS

1.1.1 States of Matter

The liquid crystalline state has often been referred to as "the fourth state of matter"[1] after the solid, liquid and gas phases. This unique state of matter actually lies between the solid and liquid states. Consequently, molecules that are liquid crystalline share properties from both. The fascinating properties displayed by liquid crystalline molecules have captured the imagination of numerous research groups over the last century, generating an intriguing array of results.

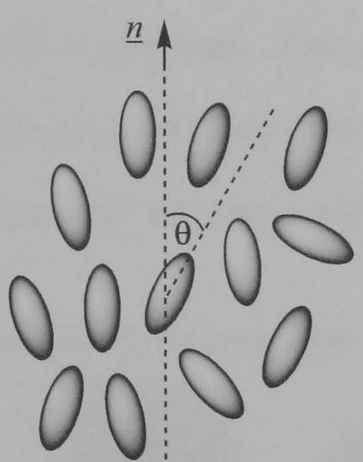

Figure 1.1. Molecules in the liquid crystal phase. The dashed arrow (director) shows the direction of preferred orientation. θ is the angle each molecule makes with the director (shown here for one molecule).

In the liquid crystal phase, molecules do not occupy fixed positions but are oriented in approximately the same direction. The average alignment is represented by the *director*, $\underline{n}$ (Figure 1.1). Such materials are fluid due to the lack of positional order, but also are anisotropic due to the presence of some orientational order. Consequently liquid crystals are described as

mesomorphic, coming from the Greek meaning between two states. The dominant forces promoting this orientational order are anisotropic dispersion forces,[2] and the extent of alignment along the director is given by the order parameter, $S = \frac{1}{2}(3\cos^2\theta - 1)$, where θ is the angle a molecule makes with the director. The order parameter decreases as temperature is increased, *i.e.* the more energy in the system, the more randomly oriented the molecules. Organic compounds displaying this phenomenon are described as *liquid crystalline*, whereas metal-containing species are often defined as *metallomesogens*.[3]

1.1.2 Classification of Liquid Crystals

Mesophases (liquid crystal phases) are only formed by certain molecules under a specific set of conditions. They can be categorised into two main groups depending on the mode of phase generation. *Thermotropic* liquid crystals[4] generate mesophases that are stable within a specific temperature range.

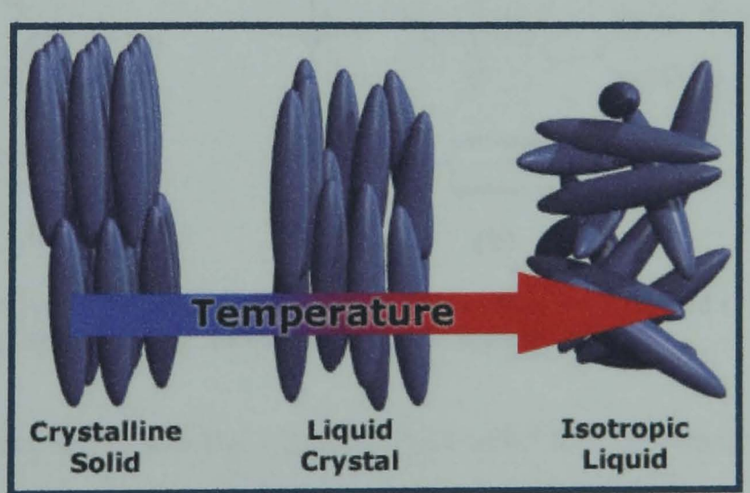

Figure 1.2. Schematic illustration of the solid, liquid crystal and liquid phases of thermotropic molecules.

At the *melting point* there is sufficient energy to disrupt the rigid positional and orientational order present in the solid state (*Cr*) resulting in a

liquid crystal phase. If the material is *polymorphic* further heating will result in the generation of more mesophases. At the temperature known as the *clearing point* all order is completely lost and the *isotropic liquid* (*I*) is formed (Figure 1.2). Generally, thermotropics form mesophases both on heating and cooling and are termed *enantiotropic*. However, thermotropics that only exhibit mesophases on cooling from the isotropic liquid are metastable and are termed *monotropic*.

The second class of liquid crystals are the *lyotropic* liquid crystals.[5] Lyotropic liquid crystals form mesophase*s* as a function of surfactant concentration with a solvent that is usually water. The molecules are *amphiphilic*, composed of hydrophilic and hydrophobic groups. Therefore, the difference in solubility properties of the component parts determines the arrangement of the amphiphilic molecules in both polar and non-polar solvents. Two examples of lyotropic liquid crystals, sodium stearate[6] and a phospholipid,[7] are shown below in Figure 1.3.

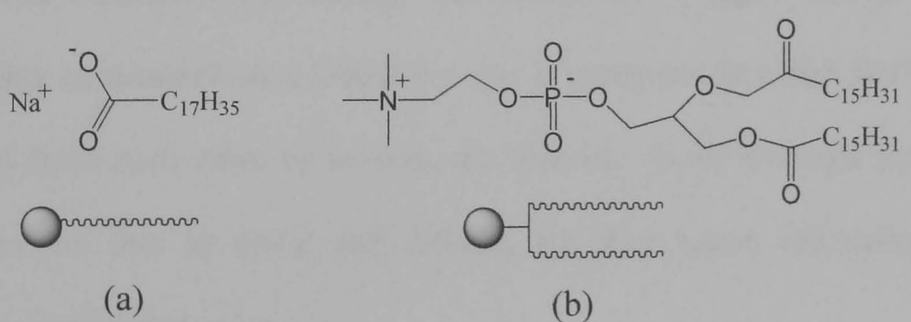

Figure 1.3. Two lyotropic liquid crystals (a) a soap, sodium stearate[6] and (b) a phospholipid, dipalmitoylphosphatidylcholine,[7] plus their schematic representations.

Both the soap and the phospholipid have a polar 'head' attached to a hydrocarbon 'tail' group. In a polar solvent such as water, the molecules will arrange themselves so that the hydrophilic heads are in contact with the water and the hydrophobic tails are shielded from it (Figure 1.4). Soap molecules assemble to form *micelles* and phospholipids assemble to form *vesicles*.

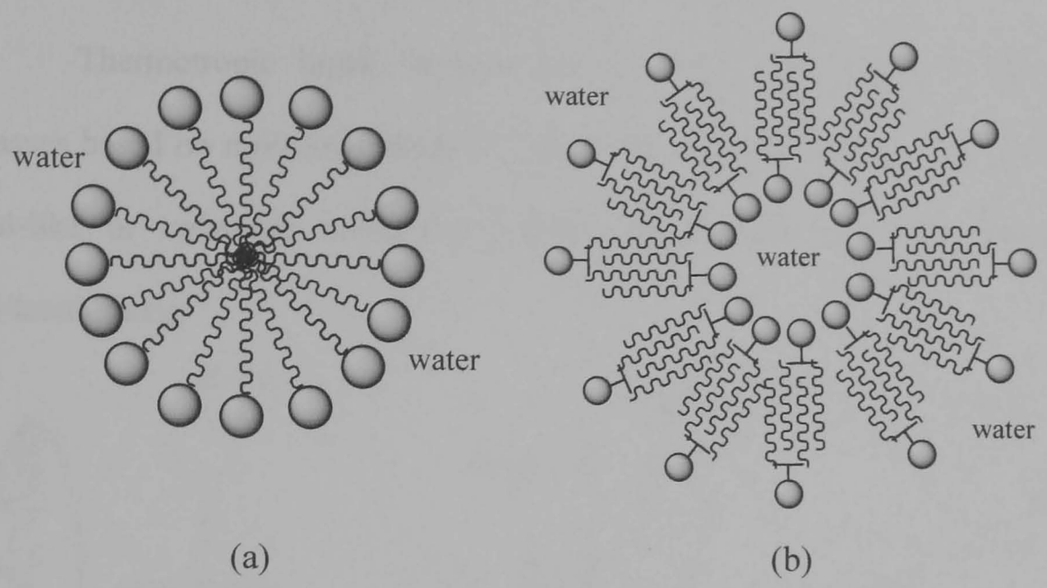

Figure 1.4. Cross-sectional diagrams of (a) a micelle and (b) a vesicle.

At concentrations above the *critical micelle concentration* the micelles and vesicles form larger arrays, which are the lyotropic mesophases. In the *hexagonal phase* long cylindrical rods of amphiphilic molecules are arranged with the long axes of the rods in a hexagonal array. At higher concentrations the (less common) *cubic phase* may form. This is composed of spheres of amphiphilic molecules that arrange themselves into a cubic lattice, while at even higher concentrations a *lamellar phase* is generated in which flat bilayers, separated from each other by solvent, are formed. In all lyotropic phases the molecules are free to move and diffuse, but they retain orientational and sometimes positional order.

There are some molecules which exhibit both thermotropic and lyotropic behaviour and these are termed *amphotropic* liquid crystals.[8] Since our research concerns liquid crystals that are generated as a function of temperature only, the following discussion is focussed solely on thermotropic liquid crystals.

1.1.3 Categorisation of Thermotropic Liquid Crystals

Thermotropic liquid crystals can be categorised into two principle classes based on molecular shape (Figure 1.5). The first class is described as rod-like or *calamitic* molecules (Figure 1.5a),[9] and have one elongated molecular axis.

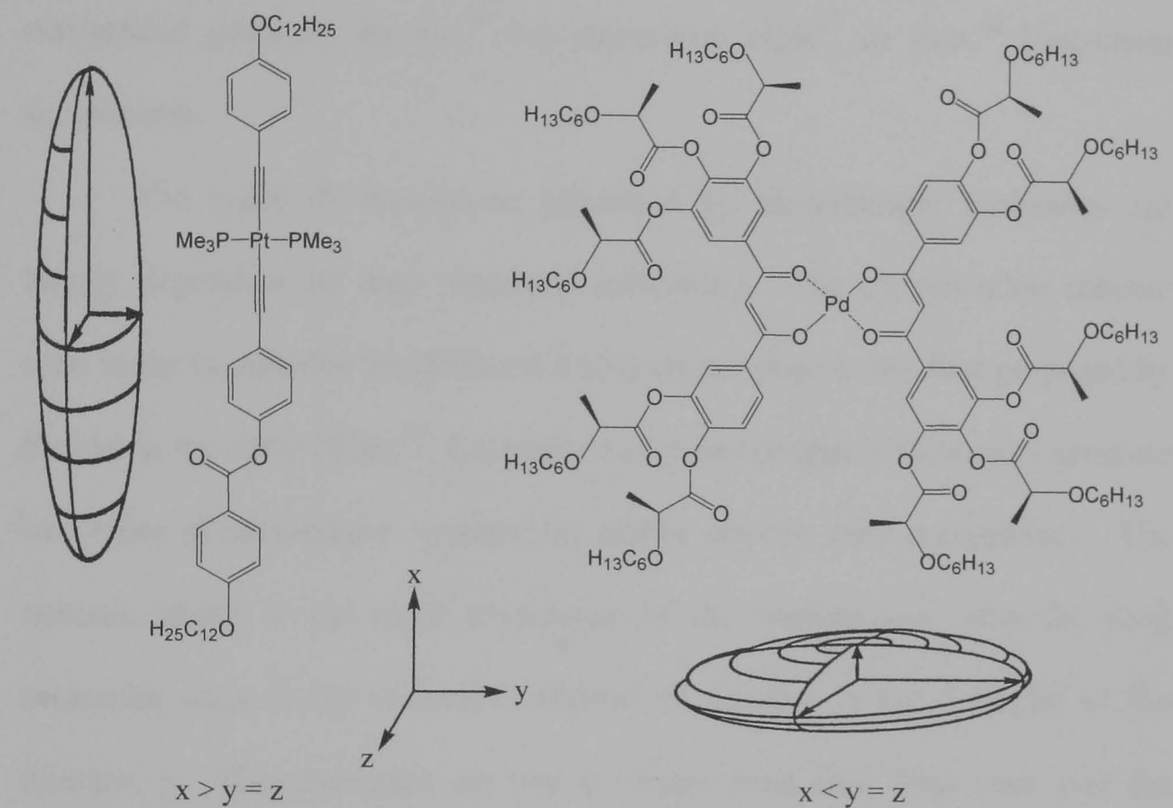

Figure 1.5. Examples of structural anisotropies in thermotropic liquid crystals: (a) is a calamitic molecule, a tertiary phosphine complex of Pt^{II}, which has an extended x axis relative to z and y;[10] (b) is a discotic molecule, a β-diketonate complex of Pd^{II}, which has a shortened x axis relative to z and y.[11] Transition temperatures are given in °C.

The general structural requirements for a calamitic molecule are that the rigid core comprises two or more aromatic (or heteroaromatic) rings connected by groups that may preserve the conjugation of the system in a linear arrangement. Terminal groups may either be identical,[12] such as alkyl or alkoxy groups to promote structural anisotropy and to lower the melting

temperature, or different,[13] for example one alkyl/alkoxy group plus a polar group.

The second class is disk-like or *discotic* (Figure 1.5b).[14] These have one short molecular axis and were not identified until 1977.[15] They are comprised of a rigid core, which is planar or almost planar, with the core surrounded generally by six,[16] but sometimes eight[17] or four,[18] long-chain substituents.

The types of mesophase generated by thermotropic molecules are largely dependent on their structural anisotropy. The classification scheme used today to describe the different liquid crystal phases was first proposed by Freidel in the early 1920s.[19] Calamitic molecules (Figure 1.6) broadly generate two types of mesophase: *nematic (N)* and/or *smectic (Sm)* mesophases. The nematic phase is the most disordered of the mesophases, with the long molecular axes of the molecules aligned on average in the direction of the director, $\underline{n}$. The molecules are free to rotate about their long axes, and the phase is very fluid because there is one-dimensional orientation order along the unique long axis but no positional order. Smectic phases are more ordered,[20] and involve both orientational order together with partial positional ordering of the molecules into layers. Despite this the molecules are free to diffuse between layers, promoting fluidity. There are several types of smectic phase with the simplest being the *smectic A* phase (*SmA*),[21] in which the long axes in each layer of the molecules are aligned approximately in the same direction perpendicular to the layer normal. If these molecules are tilted at some angle, θ, to the layer normal a *smectic C* phase (*SmC*)[22] is produced.

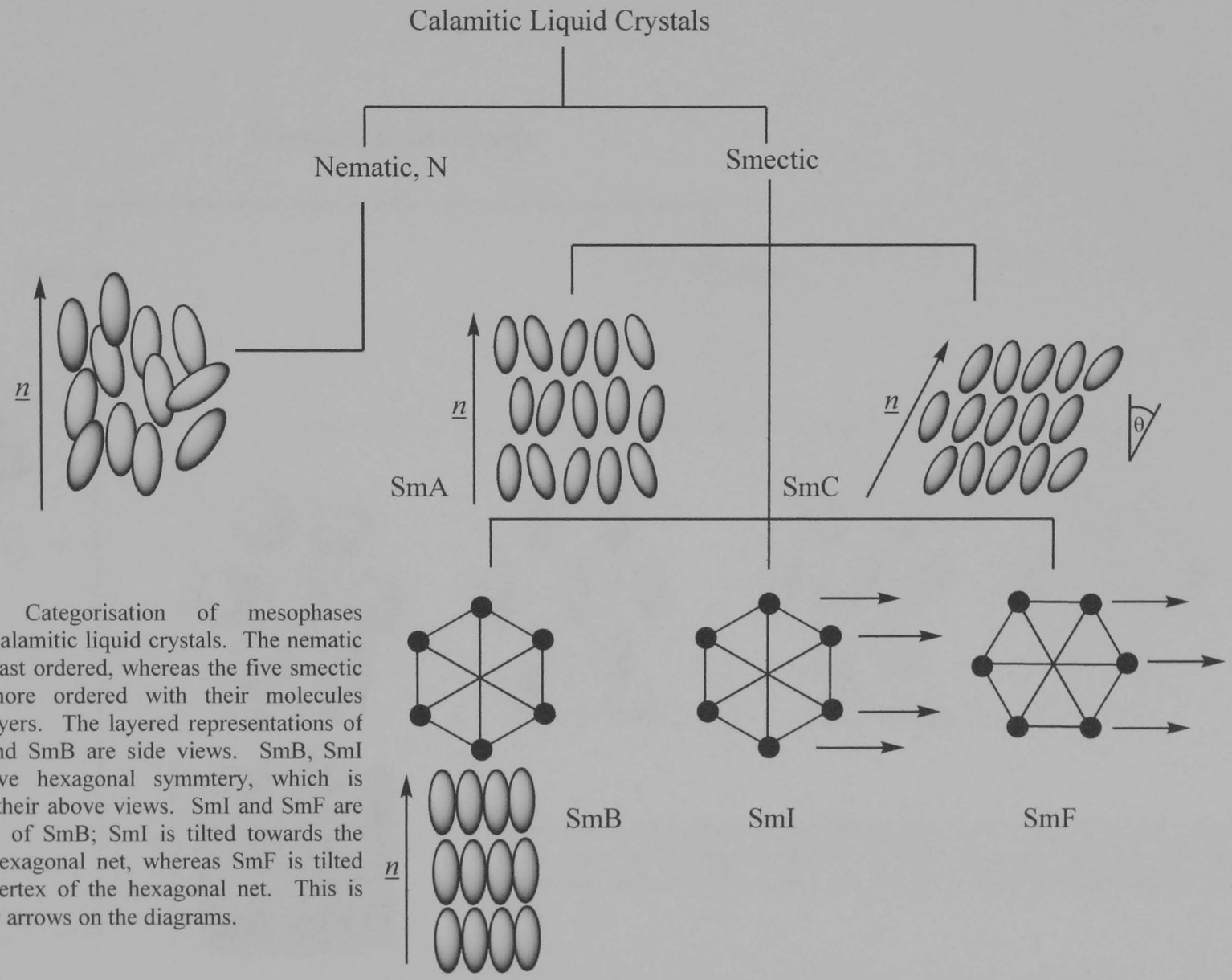

Figure 1.6. Categorisation of mesophases generated by calamitic liquid crystals. The nematic phase is the least ordered, whereas the five smectic phases are more ordered with their molecules arranged in layers. The layered representations of SmA, SmC and SmB are side views. SmB, SmI and SmF have hexagonal symmtery, which is illustrated by their above views. SmI and SmF are tilted versions of SmB; SmI is tilted towards the edge of the hexagonal net, whereas SmF is tilted towards the vertex of the hexagonal net. This is represented by arrows on the diagrams.

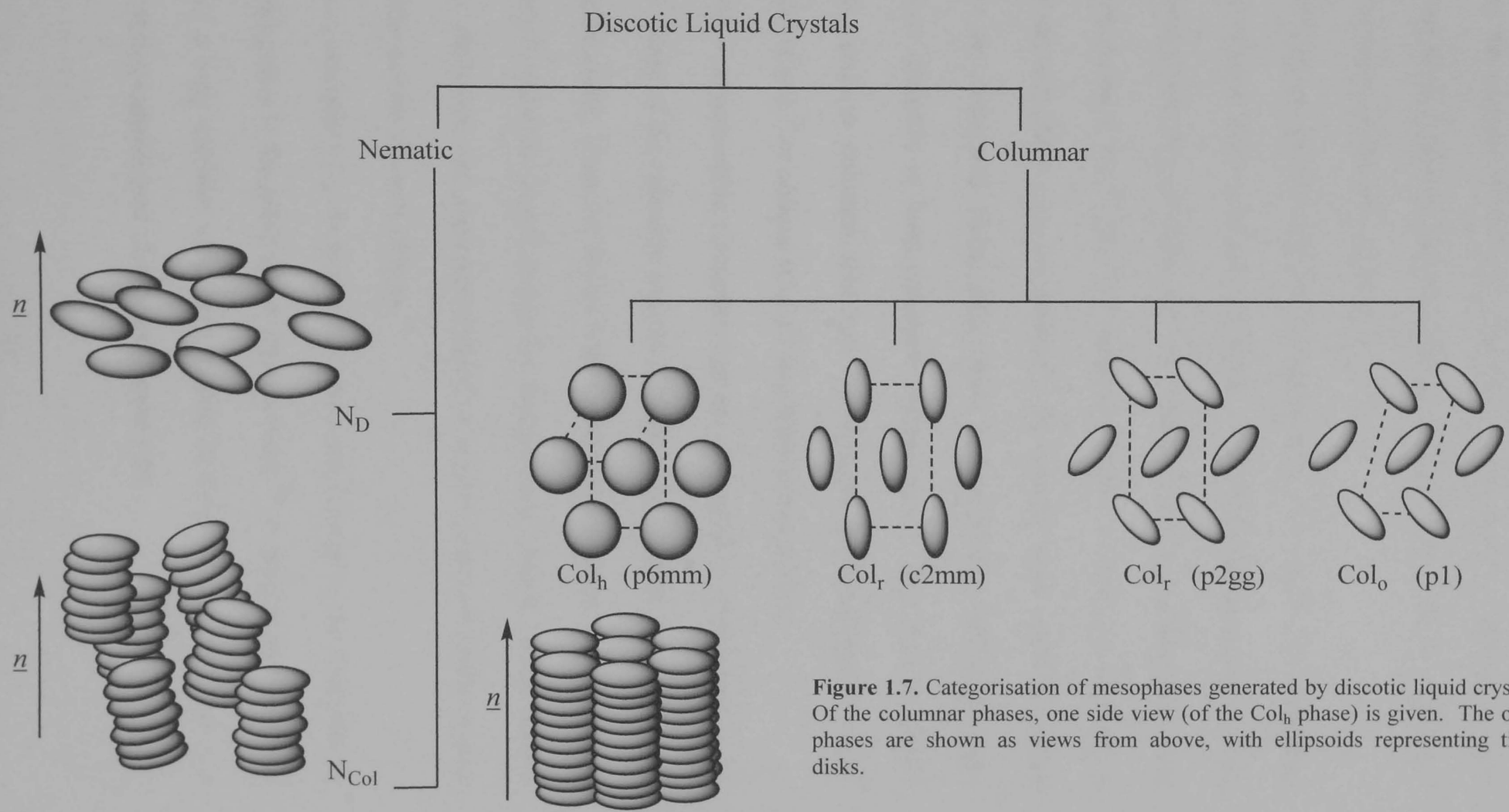

Figure 1.7. Categorisation of mesophases generated by discotic liquid crystals. Of the columnar phases, one side view (of the Col_h phase) is given. The other phases are shown as views from above, with ellipsoids representing tilted disks.

The *smectic B* (*SmB*)[23] phase is generated by further modification of the smectic A phase, whereby the overall positional order of the phase is increased relative to the smectic A phase by the hexagonal symmetry featured in each layer. Two further smectic phases, *smectic I* (*SmI*)[24] and *smectic F* (*SmF*),[25] are tilted versions of the smectic B phase.

Discotic molecules may also generate two main types of mesophase, which are nematic and/or columnar (Figure 1.7). Within the nematic category discotic molecules may produce *discotic nematic* (N_D) mesophases that have only orientational order,[26] like the calamitic nematic. Very occasionally a columnar nematic phase (N_{Col}) is formed.[27] In contrast to the calamitics these molecules are correlated along their *short* molecular axes and it is more common for discotics to form *columnar* mesophases.[28] In columnar phases molecules stack in columns that can be arranged in *hexagonal* (Col_h),[29] *rectangular* (Col_r),[30] or *oblique* (Col_o)[31] two-dimensional lattices.

These mesomorphic categories that are derived from and related to the molecular shape of the calamitic and the discotic molecules are generalised and may be misleading. There are in fact rod-shaped molecules that form columnar mesophases[32] and disk-shaped molecules that generate smectic mesophases.[33] Moreover, there are also mesogens whose molecular structure fulfils neither the calamitic nor the discotic criteria.[34]

One example of a molecule that does not belong in the calamitic or discotic categories is the *polycatenar* liquid crystal.[35] A polycatenar molecule consists of a long rod-like rigid core ending in two half-disk moieties – a hybrid of the aforementioned categories (Figure 1.8).

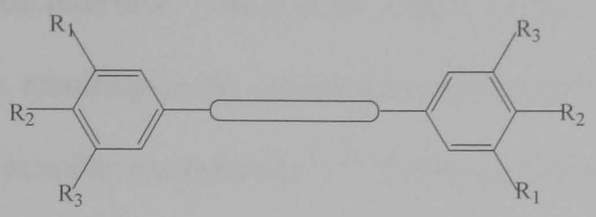

Figure 1.8. Schematic representation of a polycatenar molecule. In hexacatenar molecules, $R_1 = R_2 = R_3$, where typically R = alkoxy chain. In tetracatenar molecules, generally $R_1 = H$; $R_2 = R_3$.

Generally, the polycatenar core consists of four or five rings and the half-disks are composed of the terminal phenyl rings with two or three terminal paraffinic chains grafted on in *meta* and/or *para* positions. These molecules are of particular interest because they may sometimes exhibit behaviour crossing over from calamitic-like to discotic-like mesogens, *i.e.* they may produce both smectic and columnar mesophases, either within a single homologue series[36] or as a function of temperature from a single compound.[37,35(b)]

Tetracatenar compounds exhibit the richest variety of mesomorphic behaviour. Generally, at short chain lengths nematic or smectic mesophases are formed[35(e)] whereas at long chain lengths the compounds exhibit columnar phases.[38,35(e)] The competition between lamellar and columnar mesophases can result in the formation of a frustrated phase at intermediate chain lengths. Then the *cubic* phase arises due to the segregation of aromatic and aliphatic parts of the molecule, effectively resulting in an amphiphilic molecule.[39] One type of molecule capable of such seemingly contradictory behaviour is shown below, in Figure 1.9.[40] This tetracatenar compound exhibits smectic C, cubic and columnar hexagonal mesophases.

As implied above, mesophases generated by polycatenar liquid crystals are generally dependent on the length of the aliphatic chain.[35(a)] This is as a consequence of the segregation of molecular parts, which results in curvature at

the aromatic-aliphatic interface. Thus, as the length of the chain is increased so too is the curvature, resulting in the stabilisation of the columnar mesophase at the expense of the lamellar mesophases.[41,35(a)] It is the delicate balance of rigid and fluid moieties that determines the mesomorphic character of polycatenar molecules.

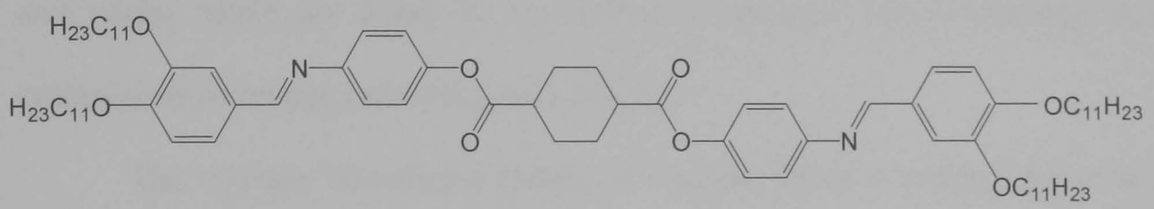

Cr 135 SmC 140 Cub 147 Col_h 158 I

Figure 1.9. Tetracatenar mesogen exhibiting polymorphism. Also included are the phase transition temperatures in °C.[40]

A model proposed by Guillon and co-workers[35(a)] accounts for the formation of the columnar phases by polycatenar molecules (Figure 1.10).

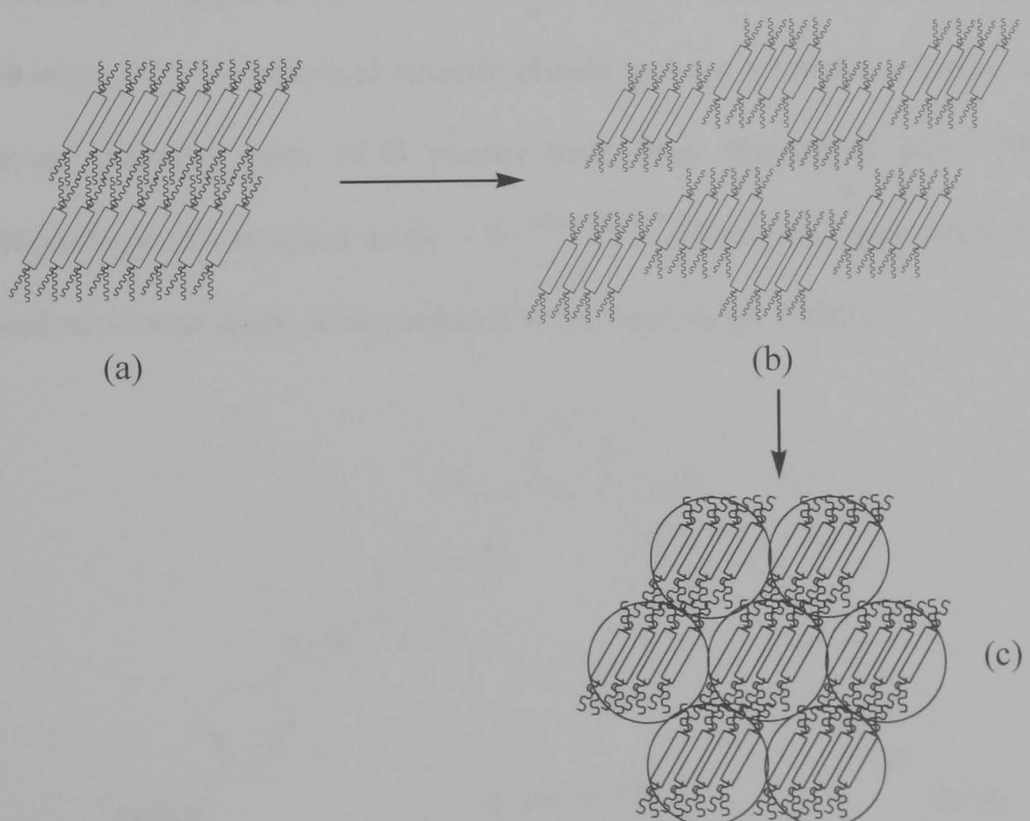

Figure 1.10. Schematic to show the transition from the SmC phase (a) through an intermediate (b) to the Col_h phase (c).[35(a)]

In the smectic C phase (Figure 1.10(a)) the interactions between adjacent planes are very weak due to the presence of the bulky aliphatic chains. When heated (and when the number of carbon atoms in the chain is increased) the interactions between the planes are weakened even more allowing the planes to undulate (Figure 1.10(b)). This creates discrete clusters of molecules and voids, which are filled by the sliding of adjacent layers resulting in a columnar-type arrangement (Figure 1.10(c)).

The recently discovered family of *banana liquid crystals* represents a new sub-field of the area.[42] These molecules are so called because of their bent molecular shape, and significantly, these achiral molecules can pack in such a way to induce chirality in the smectic layers and generate ferro-, ferri- or antiferroelectric properties. Additionally, some of these phases can be switched by application of an electrical field. These smectic phases are not miscible with the classical smectic phases and are termed *B phases*. At least seven different types of B phases have been discovered since 1996 and chronologically assigned as B_1 – B_7.[42(a),42(c),43] However, liquid crystals with a bent molecular shape were prepared as far back as the 1920's.

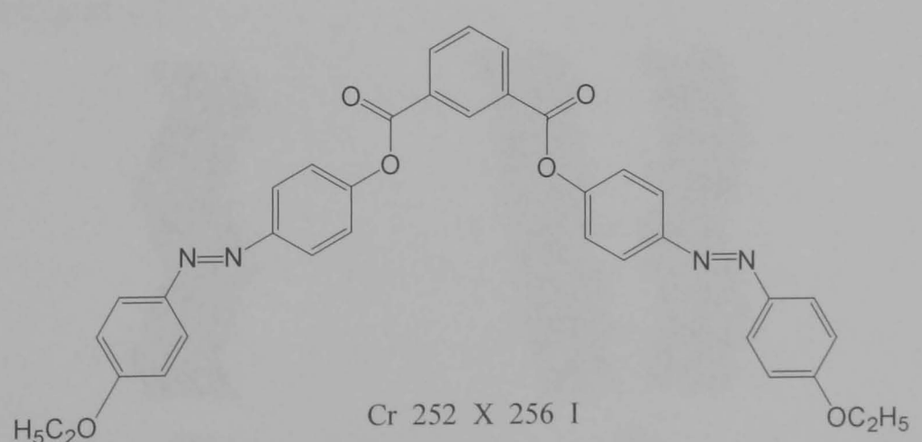

Figure 1.11. Schröter's bent molecules.[44] The phase transition temperatures in °C are included, where X = an unidentified mesophase.

In 1925 Schröter (from the research group of Vorländer, whose significance is discussed later on) synthesised five-ring molecules that exhibited an unidentified mesophase above 250°C (Figure 1.11).[44] However, it was not until 1996 that the unusual ferroelectric switching properties of banana molecules were observed by Watanabe and co-workers.[45] The molecule shown in Figure 1.12 was the first observed ferroelectric banana liquid crystal, and it generated what came to be known as B_3 and B_2 mesophases.

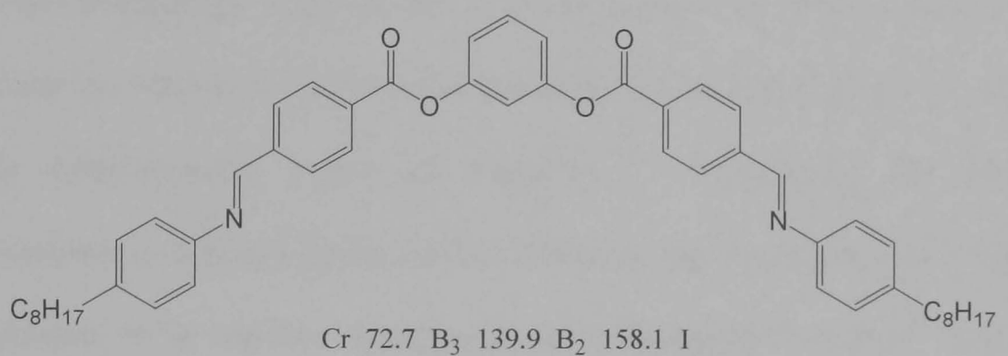

Figure 1.12. Wanatabe's banana molecules.[45] The phase transition temperatures in °C are also included, where B_3 and B_2 are banana mesophases.

The most widely studied of all the banana phases is the B_2 phase. This is a tilted antiferroelectric polar smectic ($SmCP_A$) phase with either synclinic or anticlinic structures. The sterically induced packing of the B_2 phase is shown below in Figure 1.13.

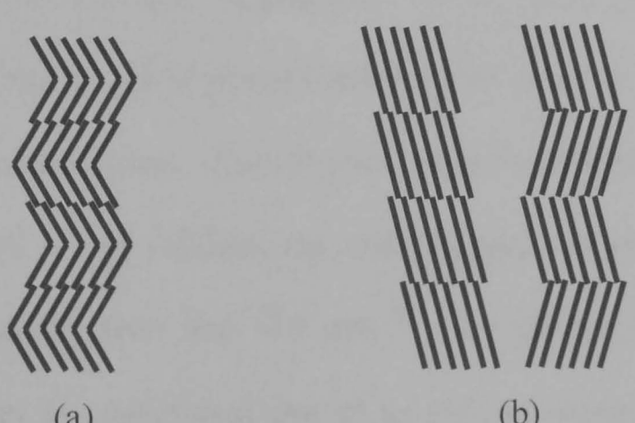

Figure 1.13. Representation of the B_2 phase. The front view is given in schematic (a), whereas the two possibilities for the side view are given in schematic (b).

Banana molecules generally consist of five, six or seven aromatic rings.[42(a)] The bend in the molecule, the types of linker groups and the presence or absence of substituents all have profound influence on phase behaviours.[42(a)] The influence of the terminal chains on mesomorphic behaviour is more difficult to judge, because phase behaviour relative to the length of the terminal chains is not comparable to that of calamitic liquid crystals. Calamitic molecules tend to have decreasing transition temperatures with increasing chain length up to a limiting number of carbon atoms. After this point the transition temperatures rise again as a result of excessive van der Waals intermolecular forces of attraction.[46] Conversely, the clearing temperatures in a homologous series of banana liquid crystals can be nearly independent of the number of carbon atoms in the aliphatic chains,[47] or it may increase,[48] or even decrease[49] with increasing number. To the best of our knowledge banana-shaped *metallomesogens* have yet to generate B phases.

1.1.4 Physical Properties and Applications of Liquid Crystals

Liquid crystals are structurally anisotropic, and therefore the resulting physical properties are also anisotropic. It is these properties and their interaction with the surrounding environment that generate phenomena unique to the liquid crystalline state. The physical properties responsible for the novel characteristics of liquid crystals are birefringence, polarisability, dielectric permittivity, diamagnetism and viscosity.[50] In addition to these properties banana molecules (as mentioned above) as well as some chiral and discotic compounds can be ferroelectric.[51] All of these properties are extremely

sensitive to external stimuli and hence can be exploited in applications such as display devices.

Liquid crystal display (LCD) devices are probably the most renowned applications for liquid crystals.[52] LCD's in watches and calculators are usually twisted nematic, whereas LCD's in televisions and computers are usually active matrix displays that incorporate dichroic dyes.[53] Other applications of liquid crystals include optical devices such as cameras and electronic books,[54] and temperature sensors such as thermometers and "battery tester" strips.[55] *Polymer dispersed liquid crystals* (*PDLCs*), in which liquid crystal droplets are embedded in a solid polymer matrix, have found application in switchable windows as a consequence of their light scattering properties.[56] Pictorial examples of some of these devices are shown below in Figure 1.14.

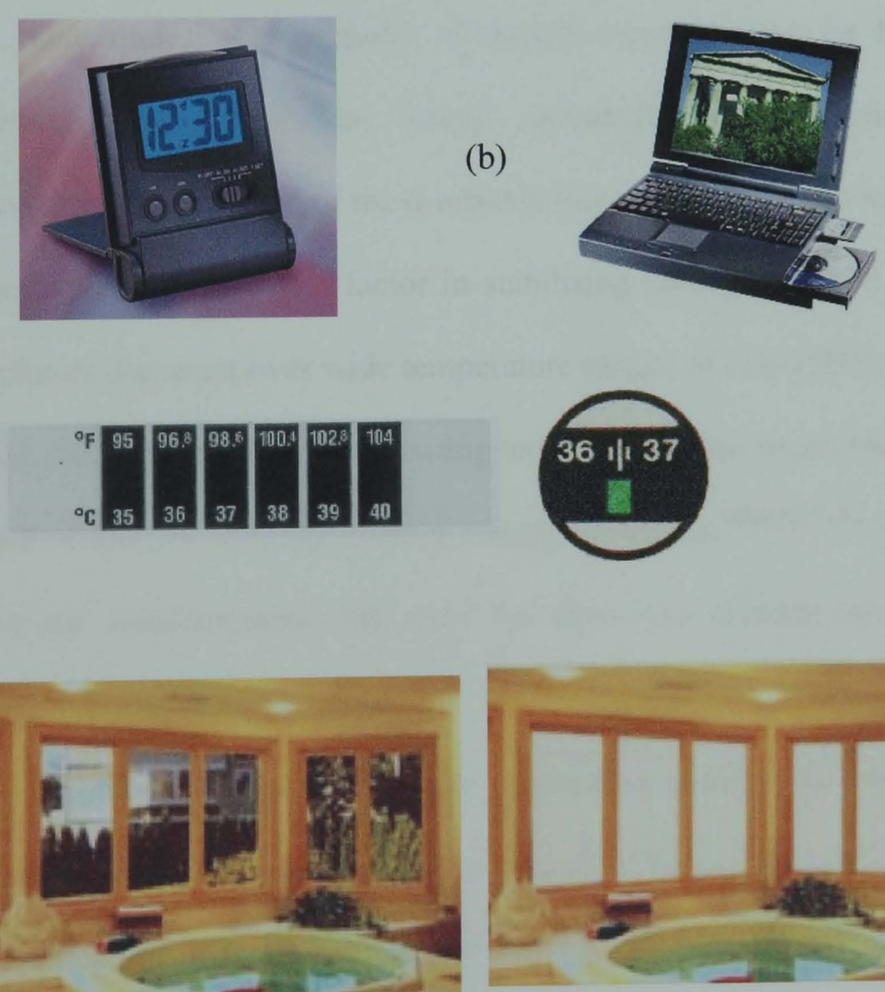

Figure 1.14. Some practical applications of liquid crystals (a) LCD clock, (b) laptop with a LCD, (c) non-invasive thermometer, (d) switchable windows.

1.1.5 Physical Properties and Applications of Metallomesogens

Metallomesogens also display anisotropic physical properties in common with organic liquid crystals. However, the key difference between metallomesogens and organic liquid crystals is the ability of metallomesogens to enhance common physical properties and introduce novel, interesting and useful ones. For example, the incorporation of a metal into the system may introduce paramagnetism,[57] colour,[58] redox activity[59] and a greater geometry range.[60] The high density of polarisable electrons at the metal centre increases the overall polarisability[61] of the molecule and consequently enhances birefringence[62,3(a)] and dielectric permittivity.[11] Furthermore, the metal may impose liquid crystalline behaviour on otherwise non-liquid crystalline ligands.[63]

One undesirable property of metallomesogens can be high melting temperatures resulting from strong intermolecular interactions.[9(a),57(d),64] However, the contribution of the d-orbitals from a metal atom to intermolecular interactions is an important factor in stabilising mesophases and can produce mesophases that exist over wide temperature ranges of 100-150°C (or larger).[65] Despite this, high melting and clearing temperatures can be problematic due to the lack of thermal stability in many metallomesogens.[64(a),65(d),66] Hence, this is one of the considerations that must be taken into account when designing metal-containing systems.

Another potential problem for metallomesogens is the high viscosity[11] of the materials in comparison to their organic counterparts, which would limit their application in fast-switching display devices. However, high viscosities are probably responsible for the *glass transitions* detected in many metal-

containing liquid crystals. The glassy states are mesophases that freeze below their melting temperatures preserving macroscopic mesophase structure. This increases the range of control over molecular order opening up the opportunity for application in nonlinear optics.[67]

Currently, for reasons mentioned above, the applications of metallomesogens are more limited than those of liquid crystals. Nevertheless, as a consequence of their colour, metallomesogens have been employed as dichroic dyes in host-guest devices.[3(a),68] Non-chiral metallomesogens have also found application in thermometers[68(b)], whereas thermochromism in non-chiral organic liquid crystals is rare. Columnar metallomesogens have potential to act as one-dimensional conductors[69] due to the ability of the metal centres and the delocalised π-systems to interact and create pathways for charge transport. With continued research and logical molecular design the applications of metallomesogens are certain to increase.

1.2 HISTORICAL PERSPECTIVE

1.2.1 Early Work on Liquid Crystals

The discovery of the liquid crystalline state is usually attributed to Reinitzer. In 1888, the Austrian botanist stated that cholesteryl benzoate (Figure 1.15) appeared to have two melting points, first melting at 145.5°C to an opaque liquid and then to a clear liquid at 178.5°C.[70] Reinitzer's observations were investigated by the German physicist Lehmann. Lehmann believed that the opaque phase was a uniform phase of matter and noted that this exceptional phase affected polarised light in ways associated with solid

crystals but had the flow properties of a liquid. He termed this phase the liquid crystalline state.[71]

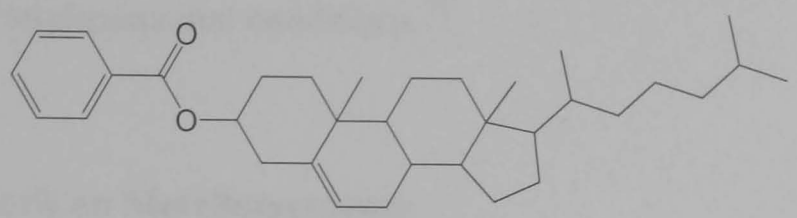

Cr 145.5 N* 178.5 I

Figure 1.15. The term 'liquid crystalline state' originated from the observed phase behaviour of cholesteryl benzoate.[70] Included above are the transition temperatures in °C.

Despite this field of research extending back 116 years, it has only been the last four decades that have witnessed the explosion in growth of liquid crystal research. This can be attributed to the successful commercial exploitation of the physical properties, giving rise to applications in devices such as electrooptical displays. In 1968 scientists at the RCA corporation in Princeton demonstrated the original liquid crystal display (*LCD*).[72] Thus, Heilmeier *et al.*[72] showed that a thin layer of liquid crystal was capable of switching from cloudy to clear on application of an electrical voltage. Research to overcome the flaws of the first LCD (high voltage required, too much power consumed, poor quality displays produced) reached a break-through in 1972, when Gray and co-workers discovered the family of cyano biphenyl liquid crystals (Figure 1.16).[73] These compounds have stable mesophases at around room temperature, requiring low voltages, consuming little power and producing high quality displays.

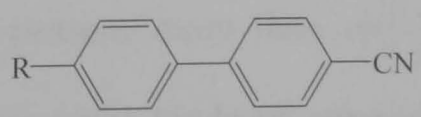

$R = C_nH_{2n+1}$

$R = C_5H_{11}$: Cr 22.5 N 35 I

Figure 1.16. Cyano biphenyl liquid crystals produced by Gray *et al.* Also included are the room-temperature transition temperatures in °C of the compound with $R = C_5H_{11}$.[73]

Over the last few decades the development of liquid crystals for display devices has progressed to include devices displaying more information over a wider range of environmental conditions.[74]

1.2.2 Early Work on Metallomesogens

The first metallomesogens were in fact observed some 30 years before Reinitzer and Lehmann's publications. In 1855 a report published by Heintz[75] detailed the unusual melting behaviour of an alkaline earth metal soap, which experienced a second melting point. However, Heintz did not elaborate further on the significance of his observations and so it took another three decades for this unique state of matter to be recognised. It is broadly accepted that the first report dealing with metallomesogens appeared in 1910,[76] when Vorländer[77] discovered that the alkali-metal carboxylates, $R(CH_2)_nCOONa$, formed classical lamellar phases on heating. In 1923 Vorländer also found that the diarylmercurials (Figure 1.17) formed nematic and/or smectic phases.[78]

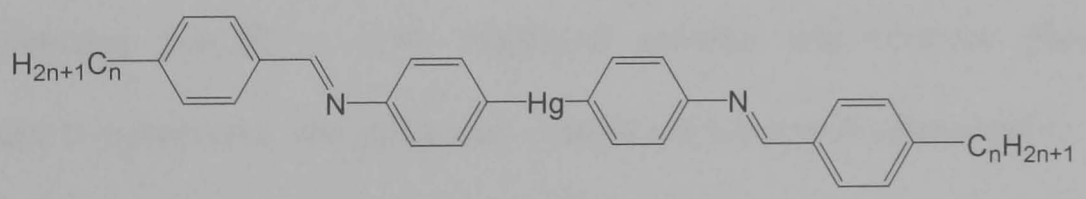

$R = C_2H_5$: Cr 204 N 272 I

Figure 1.17. Vorländer's diarylmercury complexes.[76] The phase transition temperatures in °C of the complex with $R = C_2H_5$ are also included.

Furthermore, Vorländer was the first to observe that a single substance could possess more than one liquid crystal phase.[79] His work led him to perceive what kinds of substances were likely to be liquid crystalline. His recognition that a linear molecular shape was of importance[80] influenced theoretical and experimental work for years to come, and the first well-

characterised organotransition metallomesogens appeared in the literature some 50 years later, when in 1976, Malthête and Billard[81] reported ferrocenyl Schiff base derivatives (Figure 1.18) exhibiting nematic phases.

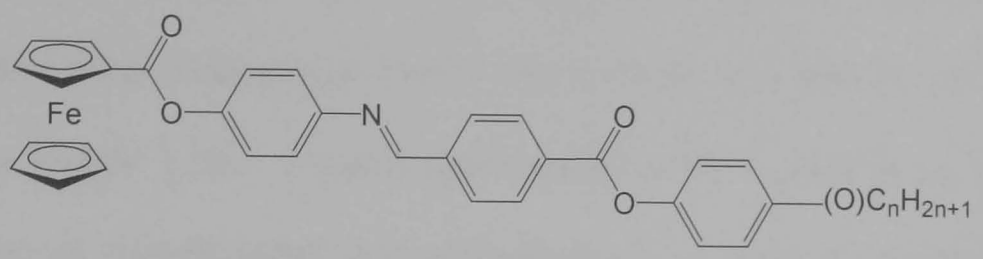

C_5H_{11}: Cr 182 (N 155) I
C_6H_{13}: Cr 164 (N 143) I
C_8H_{17}: Cr 152 (N 135) I

OC_8H_{17}: Cr 153 N 167 I
$OC_{10}H_{21}$: Cr 143 N 159 I

Figure 1.18. Ferrocene Schiff base derivatives synthesised by Malthête and Billard.[81] Transition temperatures are given in °C.

However, the work credited with truly starting systematic research into metallomesogens is that of Giroud and Müller-Westerhoff in 1977. Their study of dithiolene complexes of nickel(II) (Figure 1.19),[82] and subsequently complexes of platinum(II) and palladium(II),[83] showed that whilst the nickel and platinum complexes both displayed smectic and nematic phases at moderate temperatures, the palladium complexes were not mesomorphic. Such work stimulated research into the study of mesogens containing d-block elements.

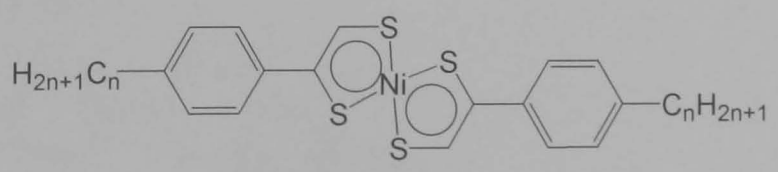

n = 8: Cr 109 SmC 184 I
n = 9: Cr 106.5 SmC 188 I

Figure 1.19. Nickel(II) dithiolene complexes studied by Giroud and Müller-Westerhoff.[82] Transition temperatures are given in °C.

Consequently, metallomesogens containing an extremely diverse range of metals and ligands have subsequently been prepared and studied. Selected examples are shown in Figures 1.20 – 1.26 and discussed briefly below.

Calamitic metallomesogens derived from monodentate alkoxystilbazole ligands have been studied extensively. One example of a silver(I) complex[84] is shown in Figure 1.20. 4-Alkoxystilbazole-derived ligands have also been complexed to palladium(II) and platinum(II),[85] as well as rhodium(I) and iridium(I),[86] generating either nematic or smectic mesophases.

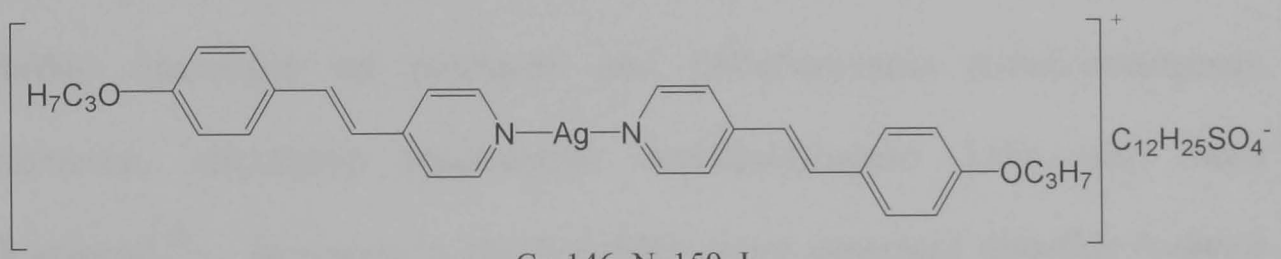

Figure 1.20. Example of a 4-alkoxystilbazole silver(I) complex, prepared by Bruce and co-workers.[84(d)] Transition temperatures are given in °C.

Another highly significant class of metallomesogens is the salicylaldimine-derived group. These ligands act as bidentate chelating groups, forming six-membered rings with the metal centre. The liquid crystalline properties of metal-salicylaldimine complexes up to 1998 have been reviewed by Hoshino,[64(b)] and an example of a branch of this class of metallomesogen is given in Figure 1.21.[87]

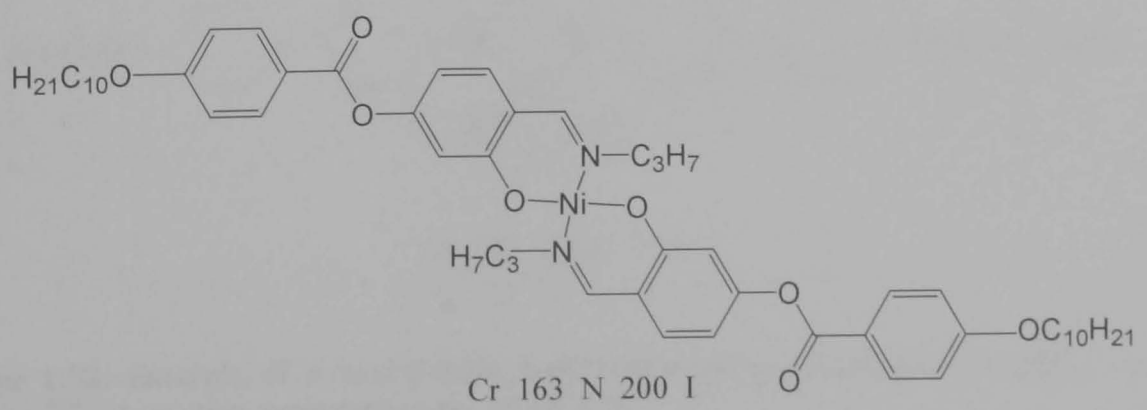

Figure 1.21. Example of a salicylaldimine-derived nickel(II) complex, synthesised by Hoshino *et al.* [87] Transition temperatures are given in °C.

For example, salicylaldimine ligands are highly suitable in metallomesogen systems due to their ability to form stable complexes with a wide range of transition metal and lanthanide cations. A range of vanadyl(IV),[60(g),87,88] chloroiron(III),[89] nickel(II),[88] copper(II)[57(e),60(d),88,90] and palladium(II)[91] metallomesogens have been successfully prepared, as well as a variety of lanthanide(III) complexes.[92]

Research into macrocyclic metallomesogens has most commonly focussed on porphyrin and phthalocyanine-derived ligands, where columnar mesophases are prevalent (the reader is referred to Chapter 4, Section 4.1.1 for further discussion on porphyrin and phthalocyanine metallomesogens). However, alternative macrocyclic metallomesogens have also been developed.[93] Research in the Schröder group generated thioether S-donor crowns complexed to palladium(II) cations.[94] These compounds were oligobenzoate derivatives of $(RO)_2$[14]aneS_4 and $(RO)_2$[16]aneS_4. Figure 1.22 provides one example.[94(a)] The metal-free ligands were non-mesogenic, whereas complexation to palladium(II) conformationally locks the macrocyclic ring providing sufficient rigidity to enhance anisotropy and induce mesomorphism. The mesomorphic complexes generated either smectic or nematic mesophases.

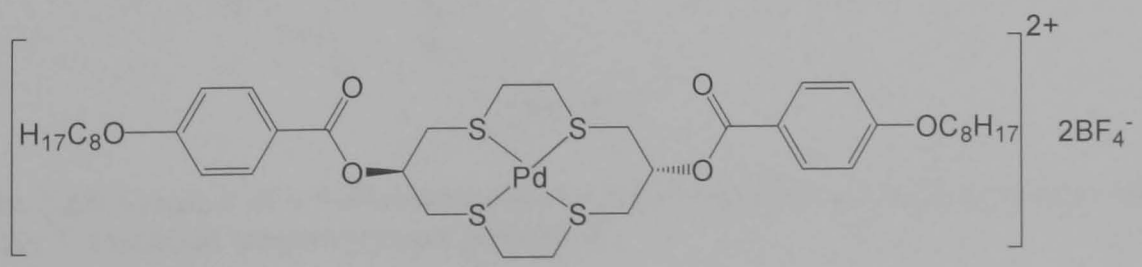

Cr 222 (SmC 164) I

Figure 1.22. Example of a macrocyclic metallomesogen synthesised by Schröder and co-workers.[94(a)] Transition temperatures are given in °C.

β-Diketonate and related molecules form another class of ligands that are utilised in metallomesomorphic compounds. The molecules generally form bis-ligand complexes with a variety of metals that can take up square planar geometries, such as palladium(II),[11,95] copper(II)[11,34(a),95] and square pyramidal vanadyl(IV).[11] Swager *et al.* synthesised unusual tetrakis-β–diketonate zirconium(IV) metallomesogens that are eight coordinate,[31] and one example is given in Figure 1.23.[31] These complexes exhibit columnar hexagonal mesophases at room temperature, and related tris(diketonate) octahedral metallomesogens with iron(III), manganese(III) and chromium(III) centres have also been synthesised by Swager.[96] The more typical bis-β-diketonate complexes of palladium(II), copper(II) and vanadyl(IV) generate either columnar, smectic or nematic phases, although this mesophase formation is highly dependent on the substitution about the β-diketonate molecule. For example, complexes with two pairs of *p*-substituted phenyls situated 1,3- on each diketone, plus a total of at least eight peripheral aliphatic chains are likely to generate columnar mesophases.[95]

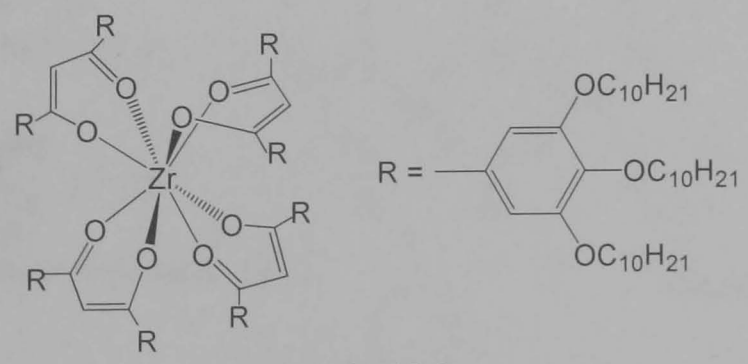

Col_h 45 I

Figure 1.23. Example of a β-diketonate-derived metallomesogen prepared by Swager and co-workers.[31] Transition temperatures are given in °C.

Orthometallated metallomesogens can be broadly categorised into two groups, which are bridged dimeric complexes and monomeric species. The bridged dimeric complexes tend to incorporate palladium[3(a),(b),9(a)] or

occasionally platinum[67(b),97] binuclear centres. Planar compounds result when the ligands are derived from azobenzenes (Figure 1.24(a))[97] or arylimines (Figure 1.24(b))[65(a)] and metal centres linked by dihalogen bridges.

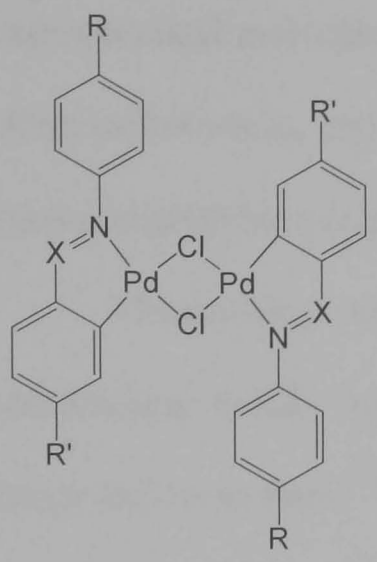

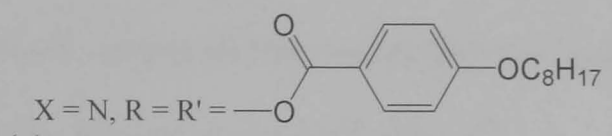

(a) Cr 149 Cr' 250 SmC 331 I

X = C–Me, R = $C_{10}H_{21}$, R' = $OC_{10}H_{21}$

(b) Cr 112 SmC 135 SmA 238 I

Figure 1.24. Examples of (a) an azobenzene-derived metallomesogen[97] and (b) an arylimine-derived metallomesogen.[65(a)] Transition temperatures are given in °C.

Despite the disk-like shape of the core the complexes generate nematic and/or smectic mesophases, since the distribution of the cores is insufficient to stabilise columnar mesophases.

(a) R = Me, n = 10
Cr 132 SmC 151 I

(b) R = 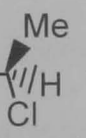

, n = 10
Cr 102 SmC* 119 SmA 149 I

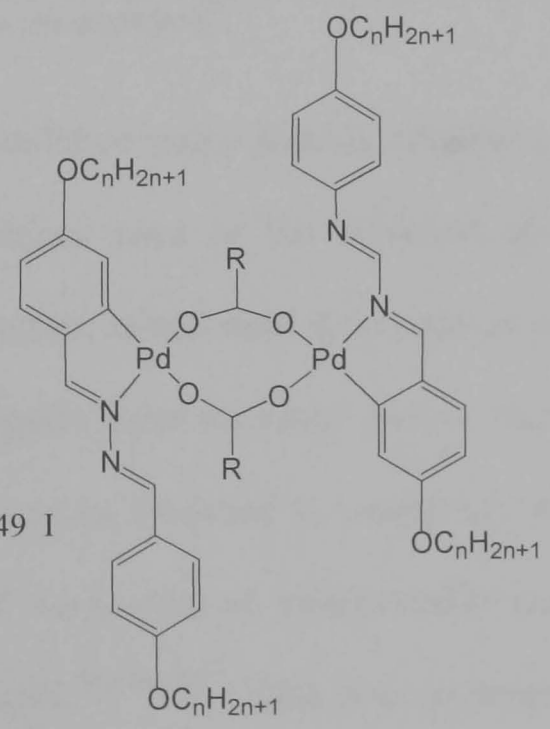

Figure 1.25. Examples of diarylazine-derived metallomesogens synthesised by Espinet and co-workers (a)[98] and (b).[99] Transition temperatures are given °C.

Diarylazine-derived ligands can generate a more unusual molecular shape (Figure 1.25(a) and (b)),[34(e),98,99] and μ-carboxylato ligands can constrain

the molecules to be non-planar, generating butterfly-shaped molecules. These bridged dimeric complexes also give rise to mesophases associated with rod-like shaped compounds, namely nematic and smectic phases, despite their unprecedented molecular shape. Chirality may be introduced by the means of chiral carboxylates, and the *trans* isomer of the compound in Figure 1.25(b) is known to generate a related ferroelectric smectic C* phase.[99]

Mononuclear orthometallated liquid crystals may incorporate higher-coordinating metals, specifically manganese(I) and rhenium(I) as studied by Bruce and co-workers[60(a),(b),100] (Figure 1.26).

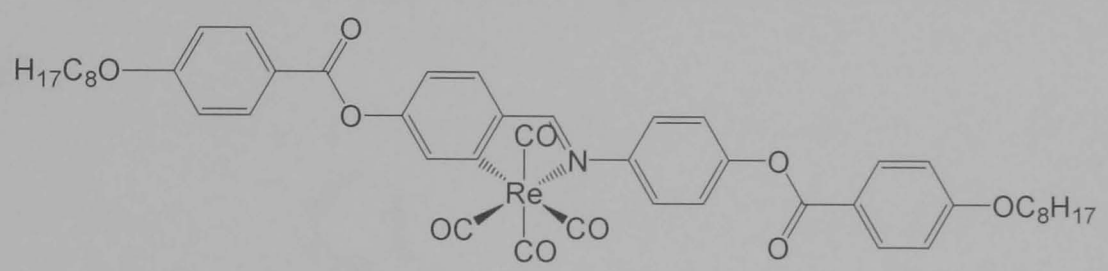

Cr 154 N 176 I

Figure 1.26. Example of a mononuclear orthometallated metallomesogen synthesised by Bruce *et al.*[60(a)] Transition temperatures are given in °C.

However, these orthometallated imine ligands (Figure 1.26) must be extended relative to the arylimines used in the binuclear species (Figure 1.24(b)). This is due to the reduction in structural anisotropy as a consequence of the introduction of further ligands about the metal centre. Accordingly, the anisotropy of the imine ligand must be increased to compensate for this effect. The octahedral orthometallated complexes of manganese(I) and rhenium(I) only generate nematic mesophases.[60(a),(b),100] This is in contrast to both the metal-free ligands and the binuclear species in Figure 1.24(b), which also form smectic phases, the suppression of the smectic phases being due to the perturbation of anisotropy. An additional consequence of the octahedral coordination geometry is reduction in mesophase stability.

The possibilities facing the development of metallomesogens are vast, and the aforementioned complexes illustrate a range of different metallomesogens incorporating various metals and ligands, but this discussion is by no means exhaustive.

1.2.3 Bent-Core Metallomesogens Prepared Previously in the Schröder Group

The study of bent-core metallomesogens in the Schröder group was initiated by Finn[101] and explored further by Morale.[102] The three ligands they investigated incorporated pyridine- and phenol-based cores as shown in Figure 1.27.

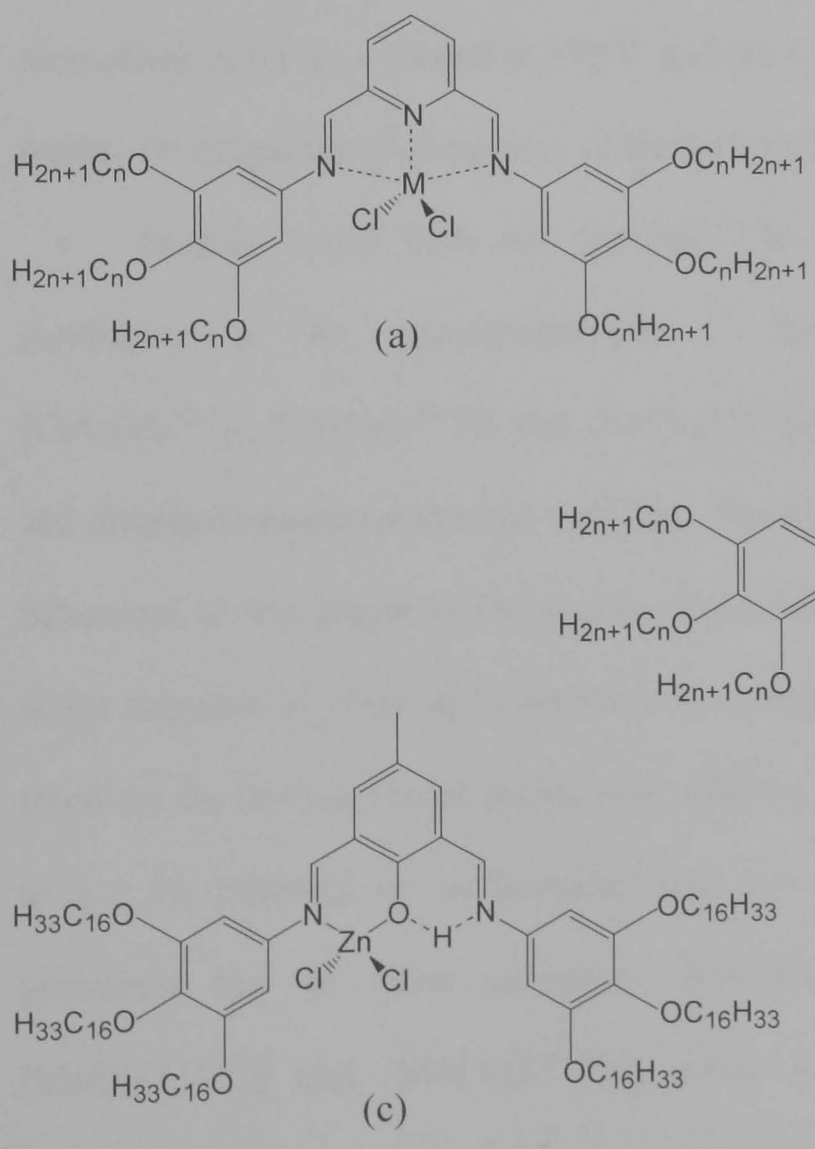

Figure 1.27. Bent-core metallomesogens previously studied in the Schröder group: (a) $[MCl_2(L^{py\text{-}n})]$, where M = Mn^{2+}, Co^{2+}, Ni^{2+} and Cu^{2+}, and n = 8, 10, 12, 14, 16; (b) $[MCl_2(L^{ol\text{-}n})]$, where M = Mn^{2+} and Zn^{2+}, and n = 16; and (c) $[ZnCl_2(L^{ol'\text{-}16})]$.[101,102]

Finn instigated the group's study of bent-core metallomesogens with the synthesis and investigation of two complexes $[ZnCl_2(L^{py\text{-}16})]$ and $[ZnCl_2(L^{ol'\text{-}16})]$, while Morale extended this study to complexes $[MCl_2(L^{py\text{-}n})]$, with M = Mn^{2+}, Fe^{2+}, Co^{2+}, Ni^{2+}, Cu^{2+} and Zn^{2+}, and n = 8, 10, 12, 14 and 16, as well as complexes $[MCl_2(L^{ol\text{-}n})]$, with M = Mn^{2+} and Zn^{2+}, and n = 16.

The results of these studies are summarised in Tables 1.1 and 1.2 and an outline of the findings is given in the discussion below.

Finn's preliminary results indicated that the bi-compartmental complex $[ZnCl_2(L^{ol'\text{-}16})]$ generated one unidentified columnar mesophase at 35°C and cleared into the isotropic liquid at 133°C. The increased thermal stability of the pyridine-based complex $[ZnCl_2(L^{py\text{-}16})]$, which melted into one columnar mesophase at 62°C, a second at 179°C and the isotropic liquid at 230°C, led to further investigation of complexes of the type $[MCl_2(L^{py\text{-}n})]$.

Morale found both the $[FeCl_2(L^{py\text{-}n})]$ and $[CuCl_2(L^{py\text{-}n})]$ series of complexes to be non-mesomorphic. However, the $[MnCl_2(L^{py\text{-}n})]$, $[CoCl_2(L^{py\text{-}n})]$, $[NiCl_2(L^{py\text{-}n})]$ and $[ZnCl_2(L^{py\text{-}n})]$ series were all mesomorphic and displayed excellent thermal stability. The dependence of the mesomorphic behaviour on the length of the alkoxy chains was illustrated in general by the slight decrease in clearing temperature on going from n = 8 to n = 16. The trend for the melting temperatures was different, at first decreasing from n = 8 to n = 10 followed by an increase from n = 12 onwards. All complexes generated two or more columnar mesophases with the exception of $[MnCl_2(L^{py\text{-}14})]$ and $[MnCl_2(L^{py\text{-}16})]$, which both displayed one columnar mesophase only.

Table 1.1. Results obtained for the previous bent-core metallomesogens prepared in the Schröder group derived from pyridine, $[MCl_2(L^{py\text{-}n})]$.

M	*n*	$[MCl_2(L^{py\text{-}n})]$ (Transition Temperatures, °C)
Zn	**8**	Cr 111 Col_{r1} 138 Col_{r2} 237 Col_{r3} 270 Col_h 285 I
	10	Cr 52 Col_r 235 Col_h 285 I
	12	Cr 48 Col_r 170 Col_h 262 I
	14	Cr 63 Col_r 145 Col_h 248 I
	16	Cr 65 Col_r 105 Col_h 235 I
Co	**8**	Cr 78 Col_o 151 Col_r 275 Col_h 303 I
	10	Cr 60 Col_r 210 Col_h 281 I
	12	Cr 46 Col_r 175 Col_h 256 I
	14	Cr 48 Col_r 170 Col_h 258 I
	16	Cr 65 Col_r 125 Col_h 255 I
Mn	**8**	Cr 83 Col_r 185 Col_h 315 I
	10	Cr 46 Col_r 143 Col_h 290 I
	12	Cr 55 Col_r 120 Col_h 280 I
	14	Cr 52 Col_h 278 I
	16	Cr 61 Col_h 248 I
Ni	**8**	Cr 148 Col_{r1} 210 Col_{r2} 293 I
	10	Cr 90 Col_{r1} 125 Col_{r2} 249 Col_h 265 I
	12	Cr 57 Col_{r1} 105 Col_{r2} 190 Col_h 256 I
	14	Cr 48 Col_r 175 Col_h 243 I
	16	Cr 62 Col_r 155 Col_h 240 I

Hexagonal columnar symmetry was prevalent throughout the study of $[MCl_2(L^{py\text{-}n})]$ with the only exception being $[NiCl_2(L^{py\text{-}8})]$. Accompanying the columnar hexagonal mesophase in all examples, apart from the monomorphic $[MnCl_2(L^{py\text{-}14})]$ and $[MnCl_2(L^{py\text{-}16})]$ complexes, was rectangular columnar symmetry (Col_r). In addition $[CoCl_2(L^{py\text{-}8})]$ also generated an oblique columnar phase (Col_o) at temperatures below the columnar rectangular phase.

The general conclusion drawn from these results was that as *n* increases the stability of the hexagonal columnar phase increases at the expense of the mesomorphic range of the rectangular mesophase.

The influence of the metal on the melting points of the complexes appeared to be negligible for all but the compounds $[NiCl_2(L^{py\text{-}n})]$, because complexes with identical *n* had similar melting points, and the complexes $[NiCl_2(L^{py\text{-}n})]$ showed the highest melting temperatures on average. However, the clearing temperatures were more metal-dependent. Thus, the complexes $[MnCl_2(L^{py\text{-}n})]$ and $[CoCl_2(L^{py\text{-}n})]$ generally cleared at higher temperatures than the analogous transitions of the complexes $[NiCl_2(L^{py\text{-}n})]$ and $[ZnCl_2(L^{py\text{-}n})]$. Overall, mesophases of the same symmetry and with the same chain-length had different temperature ranges and thermodynamic stabilities and hence were metal-dependent.

Preliminary investigations into the mesomorphic behaviour of bi-compartmental complexes $[MnCl_2(L^{ol\text{-}16})]$ and $[ZnCl_2(L^{ol\text{-}16})]$ revealed the metal-dependent nature of the mesomorphism. $[MnCl_2(L^{ol\text{-}16})]$ melted into one columnar mesophase at 41°C and cleared into the isotropic liquid at 285°C, thus demonstrating its greater thermal stability over the $[ZnCl_2(L^{ol\text{-}16})]$ analogue, which melted at 65°C and cleared at 152°C.

Table 1.2. Results obtained for the previous bent-core metallomesogens prepared in the Schröder group derived from phenol, $[MCl_2(L^{ol\text{-}n})]$ and $[MCl_2(L^{ol'\text{-}n})]$.

M	*n*	**$[MCl_2(L^{ol\text{-}n})]$** (Transition Temperatures, °C)
Mn	**16**	Cr 41 Col 285 I
Zn	**16**	Cr 65 Col 152 I
		$[MCl_2(L^{ol'\text{-}n})]$ (Transition Temperatures, °C)
Zn	**16**	Cr 35 Col 133 I

The influence of the ligand core is apparent from comparing the three complexes $[ZnCl_2(L^{ol\text{-}16})]$, $[ZnCl_2(L^{ol'\text{-}16})]$ and $[ZnCl_2(L^{py\text{-}16})]$ (Figure 1.27). The phenol-based complexes generated only one columnar mesophase, compared to the two generated by the pyridine-based complex. In addition, thermal stability was far greater for the pyridine complex.

1.3 CHARACTERISATION OF MESOPHASES

There are three main techniques employed in the characterisation of liquid crystal mesophases: p*olarised optical microscopy* (*POM*),[103] d*ifferential scanning calorimetry* (*DSC*)[104] and *X-ray diffractometry* (*XRD*).[105] POM and DSC are mutually complimentary techniques, while XRD provides unambiguous mesophase assignment. A discussion of each technique follows.

1.3.1 Polarised Optical Microscopy

Characterisation using polarising optical microscopy is dependent on the birefringent nature of liquid crystals, because identification requires the interpretation of characteristic interference patterns. A simplified schematic of the microscope is shown below in Figure 1.28.

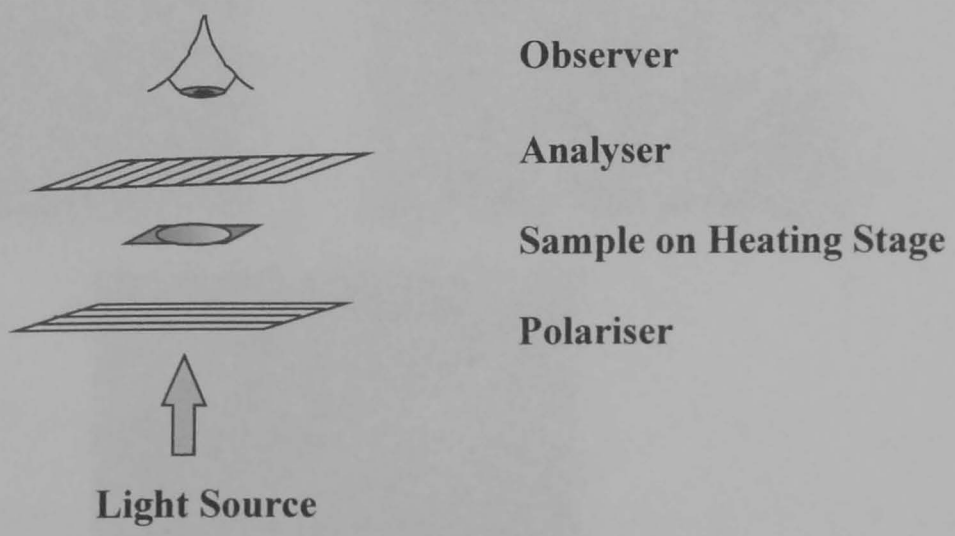

Figure 1.28. Schematic representation of a polarised optical microscope.

Plane polarised light is shone through a sample placed between cover slips on a microscope with a controllable heating stage. Above the sample is a second polariser (the analyser), which is at 90° to the first polariser, and therefore any light that passes through the analyser is observed.

Isotropic liquids appear black because plane polarised light passes though unaffected and is consequently absorbed by the analyser. Liquid crystals, however, are birefringent and therefore plane polarisation of light is lost and becomes elliptically polarised. Thus, there are two refracted rays that become out of phase to give an interference pattern. The appearance of this texture is dependent on the symmetry of the mesophase, and is therefore a method of phase identification.

The beautiful brightly-coloured regions of texture are also accompanied by dark areas. These *disclinations* are regions where the director is undefined because it points in many directions in an extremely small area. In other words, the orientation of the director changes abruptly at that particular point. These disclinations are defects and it is these that determine the appearance of the liquid crystal phase between crossed polarisers.

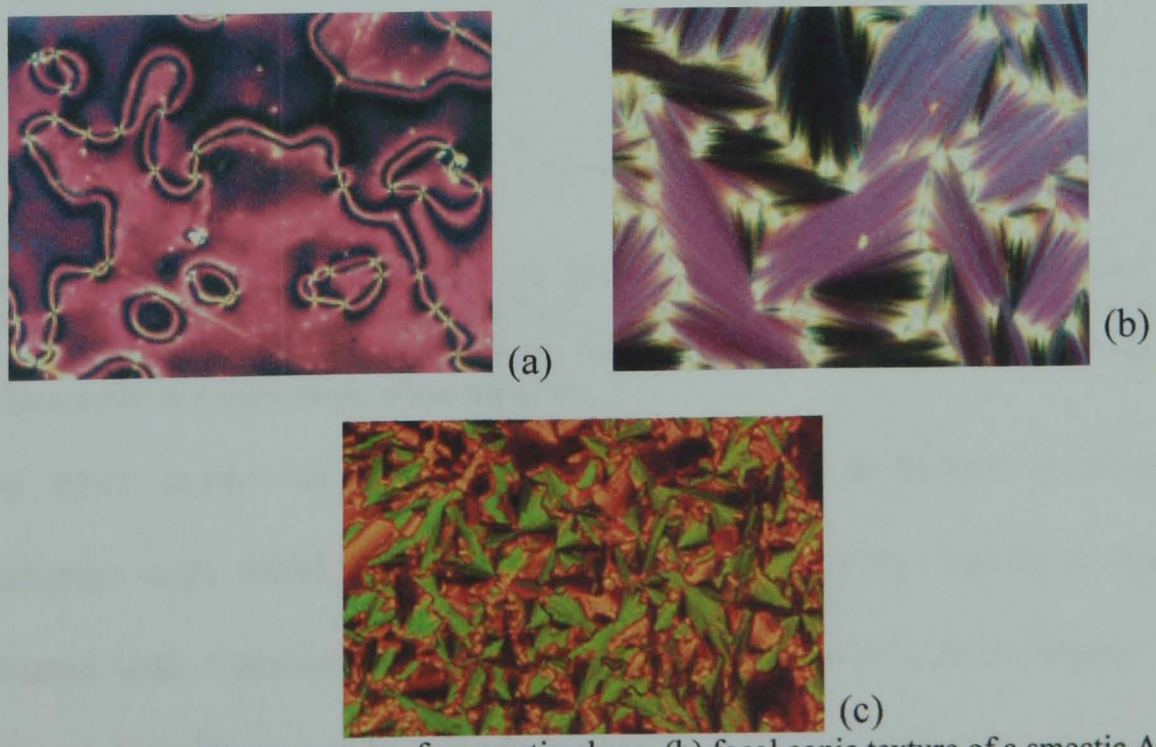

Figure 1.29. (a) Schlieren texture of a nematic phase, (b) focal conic texture of a smectic A phase and (c) dendritic texture of a columnar phase.

Examples of liquid crystalline textures include the thread-like *Schlieren* texture of the nematic phase, the *focal conic fan* textures of smectic A and C phases and the *dendritic* textures produced by columnar phases (Figure 1.29).

1.3.2 Differential Scanning Calorimetry

Differential scanning calorimetry (DSC) is a technique that detects phase transitions by measuring changes in heat capacity as a function of temperature. Hence, when a sample undergoes a phase transition the enthalpy and entropy changes accompanying that phase change are observed in the DSC trace (an example is given in Figure 1.30).

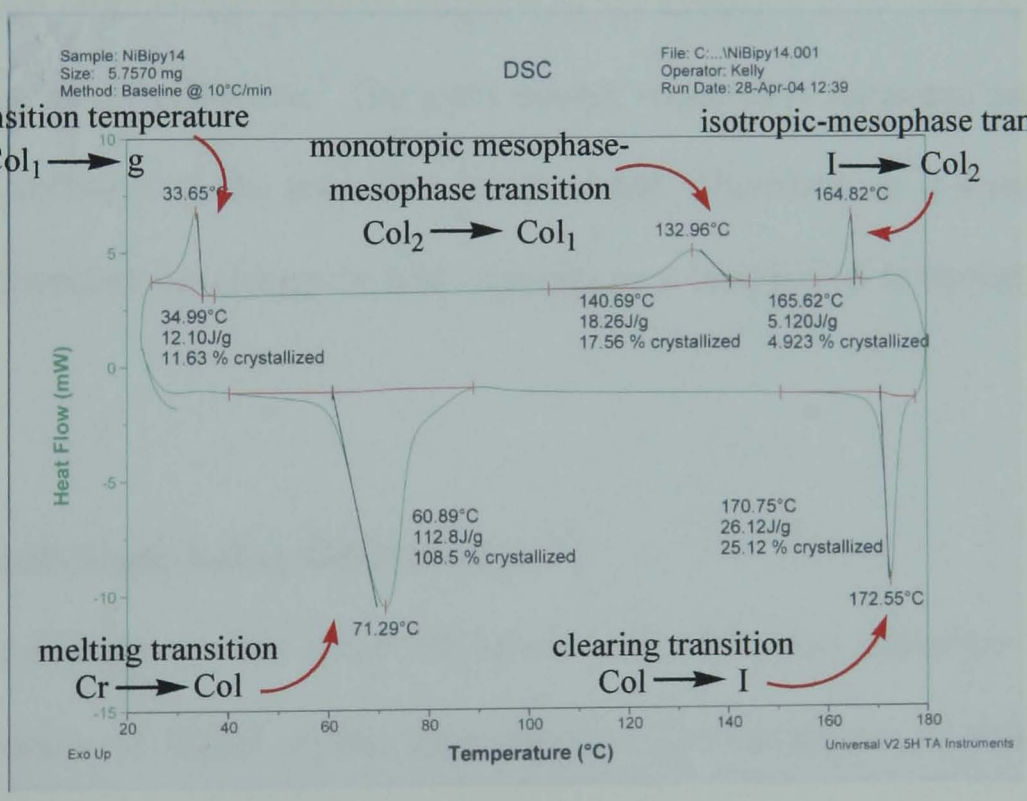

Figure 1.30. Example of a DSC trace for $[NiCl_2(L^{Bipy\text{-}14})]$, as prepared by ourselves and discussed further in Chapter 3, Section 3.2.6.2. The heating trace is shown on the bottom, where the melting and isotropic transitions are visible. The cooling trace is shown on top and includes a peak for a monotropic phase transition.

Phase *types* cannot be identified by DSC, so the technique is used in conjunction with POM. However, the magnitude of the enthalpy change associated with a transition is related to the degree of structural change that occurs, so inferences can be drawn from the size of an enthalpy change and

confirmed by POM. For example, melting enthalpies (solid to liquid crystal) are much larger than mesophase-to–mesophase or mesophase-to-isotropic liquid transitions and are typically around 16-48kJmol^{-1}, compared to 0-5kJmol^{-1} for the latter two transitions.[106] DSC compliments POM since not all changes in optical texture may correspond to a phase transition.

In the differential scanning calorimetry experiment between 5-10mg of the sample is sealed in an aluminium pan and placed in a microfurnace. A reference pan is placed in a separate microfurnace, which is connected to the other by two control loops. The loops control the heating rate and ensure that the temperature of the two pans always remains the same. Therefore, if the sample melts more energy must be supplied to the sample to keep it at the same temperature as the reference. The extra energy required is measured and the change in enthalpy of the transition is calculated. Therefore, as a sample is heated and cooled the change in heat capacity as a function of temperature is recorded.

1.3.3 Small-Angle X-Ray Diffraction

Small-angle powder X-ray diffraction is the definitive technique in the characterisation of liquid crystal mesophases. This technique is based on Bragg's Law, $n\lambda=2d_{hkl}sin\theta$, which states that when X-rays of wavelength, λ, are reflected from adjacent planes separated by a distance, d_{hkl}, at the same angle, θ, they will interfere constructively if the path difference ($2d_{hkl}\sin\theta$) between them is an integer multiple of the wavelength used.

The illustration in Figure 1.31 provides a diagrammatic representation of the Bragg equation, with the three crystallographic planes separated by a

distance, *d*, described with Miller indices *hkl*. If three incident X-ray beams are reflected by each plane with an angle of reflection, θ, the wave reflected from the second plane will travel further than the wave reflected from the top plane by a distance of ABC. Similarly, the wave reflected from the third plane will travel an additional distance of DEF. Therefore, waves 2 and 3 are phase retarded with respect to wave 1 causing interference. If the distance ABC is equal to one wavelength, λ, it follows that the distance DEF is equal to 2λ. If we assume that the waves were initially in phase with one another, then when ABC = λ all waves will emerge in phase resulting in constructive interference and hence diffraction.

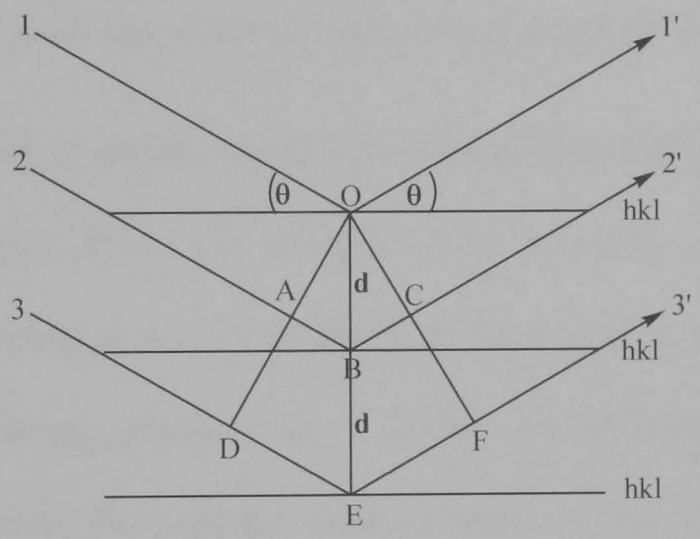

Figure 1.31. Diagrammatic representation of the Bragg equation.

Liquid crystals diffract due to their periodicities, and when Bragg's Law is satisfied, constructive interference occurs and a peak is observed. These Bragg peaks provide information on inter-planar distances and molecular organisation, giving conclusive characterisation of the mesophase.

The four basic parts of the instrumentation required for powder X-ray diffraction are shown in Figure 1.32, and the X-ray source is often a generator using a sealed tube. The polychromatic beam of X-rays then enters the monochromator (often a quartz crystal), which selects a single wavelength of

radiation. The monochromatic beam then passes through the sample in the sample chamber, which is temperature controlled. Finally, the diffracted rays reach the detector set at a predetermined angle of 2θ and known distance to the sample chamber.

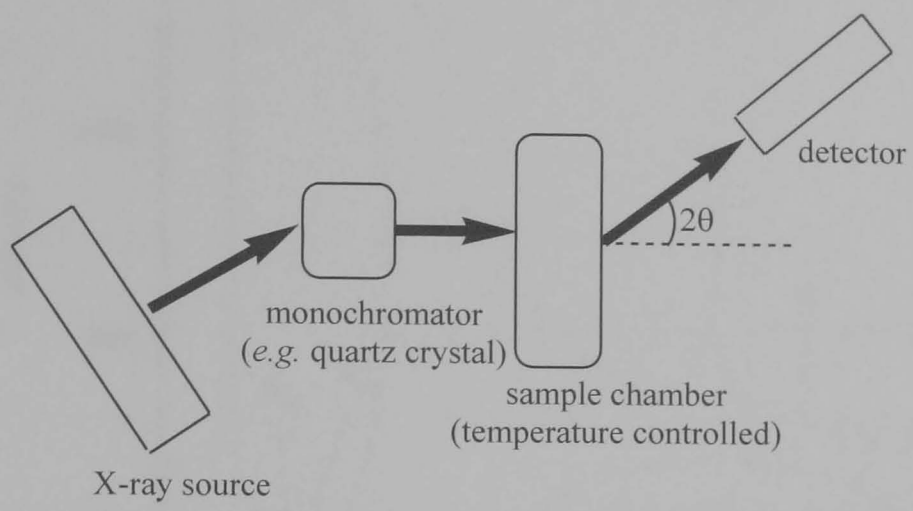

Figure 1.32. Basic instrumentation required for powder X-ray diffractometry.

The detector is usually either a two-dimensional detector or an image-plate. The output from the detector will normally provide sufficient information to determine the 2D symmetry of the liquid crystal phase, because the terms of the Bragg equation, $n\lambda = 2dsin\theta$, are all known except for the spacings, *d*, between the periodic lattice planes. Once the *d* spacings are derived, the 2D symmetry is known and the lattice parameters *a* and *b* can also be calculated, which describe the unit cell dimensions of the mesophase.

An example of a powder X-ray diffraction pattern is shown in Figure 1.33, with the wide angle (*WAXS*) and small angle (*SAXS*) regions of the data revealed. It is necessary to observe both these regions because sharp reflections from liquid crystals corresponding to the characteristic long periodic spacings, *d*, occur in the small angle region. This is due to the inverse relationship between *d* and θ in the Bragg equation, which means that widely-spaced periodic planes will diffract X-rays at small angles. In the wide-angle

region, a broad peak is present typically at 4.5Å corresponding to short-range correlations between the molten hydrocarbon chains. It is the presence of this halo that confirms the liquid crystallinity of the sample at a given temperature.

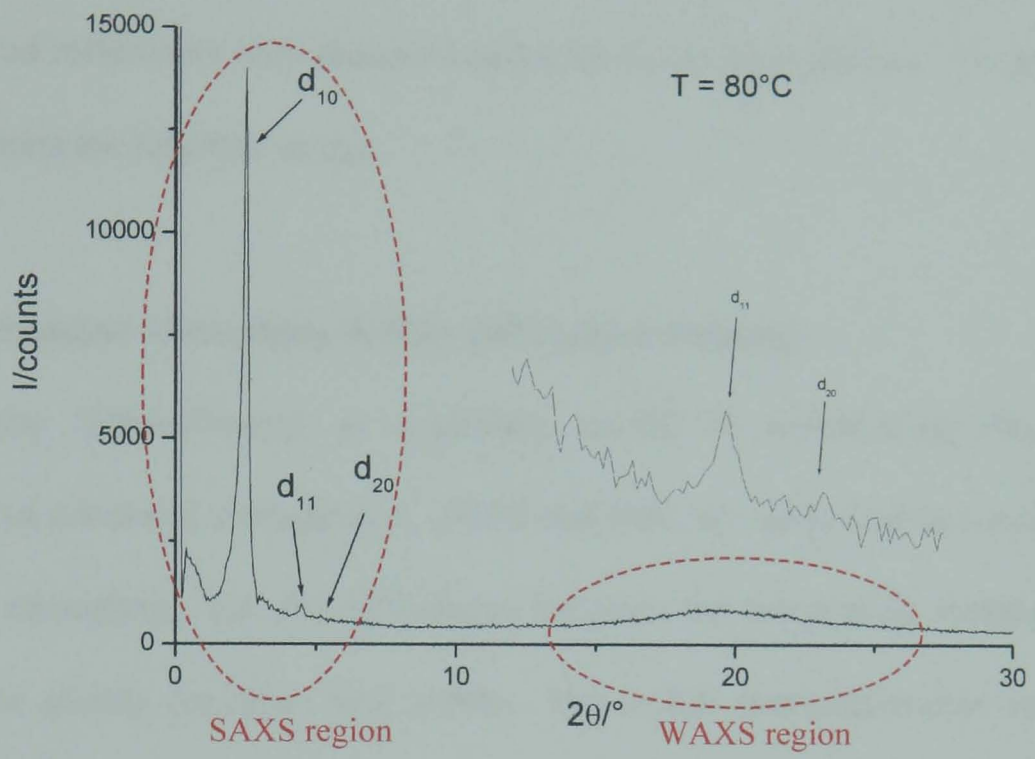

Figure 1.33. Powder X-ray diffraction pattern for a columnar hexagonal mesophase. The sharp reflections in the SAXS region correspond to the Bragg peaks, or *d* spacings, whereas the broad reflection in the WAXS region corresponds to the hydrocarbon chains and provides evidence of liquid crystallinity.

Image plates generate the same information, albeit in a different format. The film shows (Figure 1.34) the reflections in the SAXS region as a series of sharp rings. A diffuse halo in the WAXS region represents the liquid-like hydrocarbon chains and provides confirmation of the mesomorphic properties.

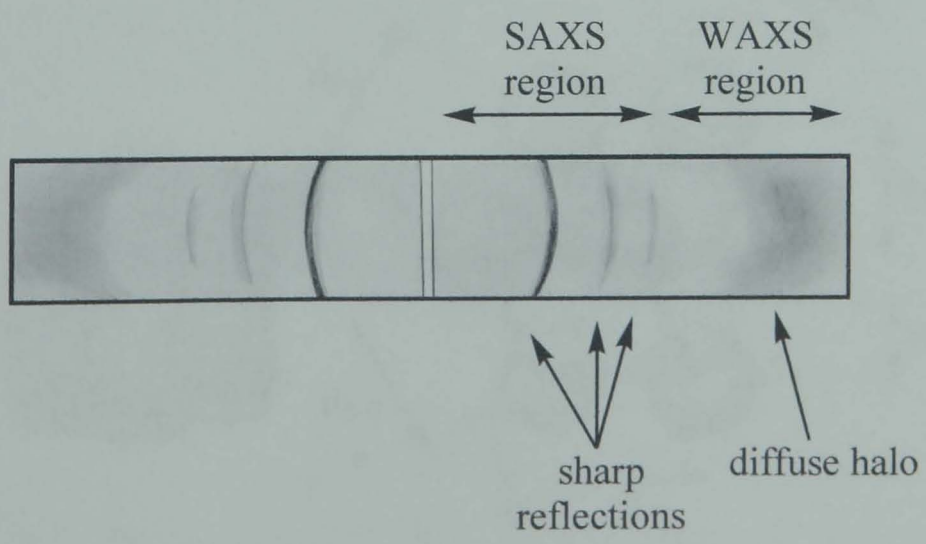

Figure 1.34. Image plating film showing the sharp (*d* spacing) reflections and the broad halo corresponding to the hydrocarbon chains.

When powder X-ray diffraction is performed on non-liquid crystalline crystallites, the observed reflections, *d*, have the accompanying Miller indices *h*, *k* and *l* as subscripts. Due to the two-dimensional nature of liquid crystals the observed reflections only require *h* and *k* for indexing purposes. Therefore, the reflections are reported as d_{hk}.

1.3.3.1 Columnar Mesophase X-Ray Diffraction Patterns

X-ray diffractometry is especially useful in determining the 2D symmetry of columnar mesophases. POM and DSC are sufficient to confirm a *columnar* mesophase, but the differences between the hexagonal, rectangular and oblique phases are often very subtle. Hence full characterisation usually requires further study by XRD. As mentioned earlier in this chapter, the molecules in columnar mesophases are arranged as disks and are stacked in columns with respect to one another. X-ray diffractometry provides the data necessary to be able to calculate the intercolumnar spacings, d_{hk}. It is the characteristic ratios of the d_{hk} values that describe the 2D symmetry type of the phase and, in turn, allow calculation of the lattice parameters, *a*, *b* and *S*.

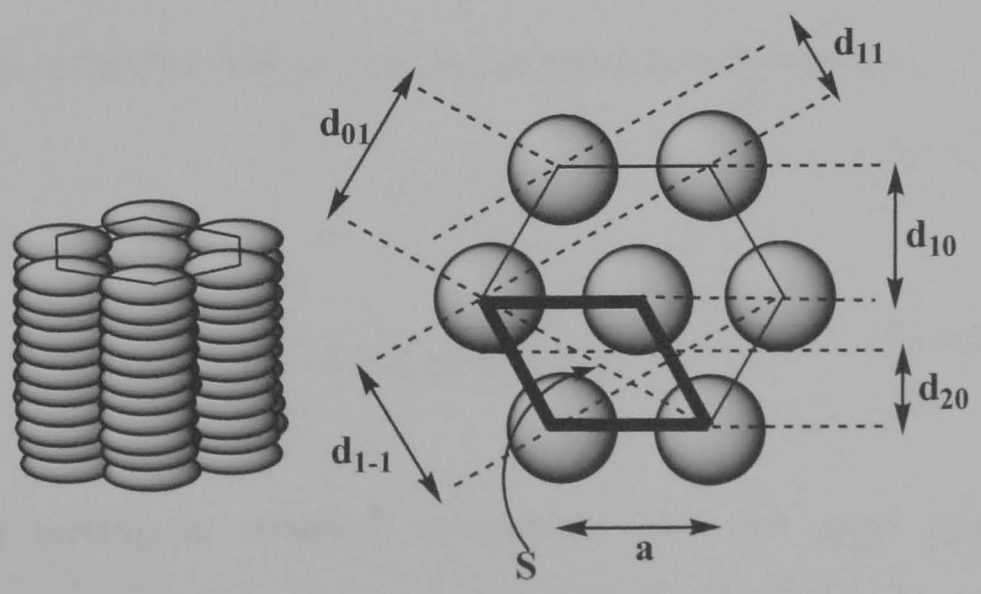

Figure 1.35. Side and cross-sectional views of the molecular symmetry of a Col_h, *p6mm*, arrangement of molecules.

The X-ray diffraction pattern for a Col_h phase was shown previously in Figure 1.33 and will now be explained in further detail with regards to the molecular symmetry. The hexagonal nature of the columnar stacking is demonstrated in Figure 1.35 and includes a cross-sectional view from above. The disks are perpendicular to the column axis and hence have a circular cross section.

Calculation of all the possible d_{hk} ratios is given by Equation 1.1.

$$d_{hk} = \sqrt{(h^2 + k^2 + hk)} \qquad \text{(Equation 1.1)}$$

Thus, for Col_h: $d_{10} = d_{01} = d_{1\text{-}1} = 1$;

$$d_{11} = \sqrt{3};$$

and $d_{20} = \sqrt{4}$.

Hence the intercolumnar periodic spacings for Col_h are in the ratio $1:\sqrt{3}:\sqrt{4}$, with a much greater intensity for the d_{10} reflection due to coincidence with the $d_{1\text{-}1}$ and d_{20} reflections. The d_{10} reflection has the largest value and so occurs at the smallest angle in the pattern ($n\lambda = 2d_{hk}sin\theta$). The space group for Col_h is designated *p6mm*.

The lattice parameter, a, for the mesophase Col_h can be calculated from Equation 1.2. The surface area, S, corresponding to the cross-sectional area of one column in the Col_h unit cell can be calculated from Equation 1.3.

$$a = \frac{2d_{10}}{\sqrt{3}} \text{Å} \qquad \text{(Equation 1.2)}$$

$$S = d_{10}a = \frac{2d_{10}^2}{\sqrt{3}} \text{Å}^2 \qquad \text{(Equation 1.3)}$$

For rectangular columnar mesophases Col_r two space groups are possible, namely the *c2mm* and *p2gg* planar groups (Figures 1.36 and 1.37).

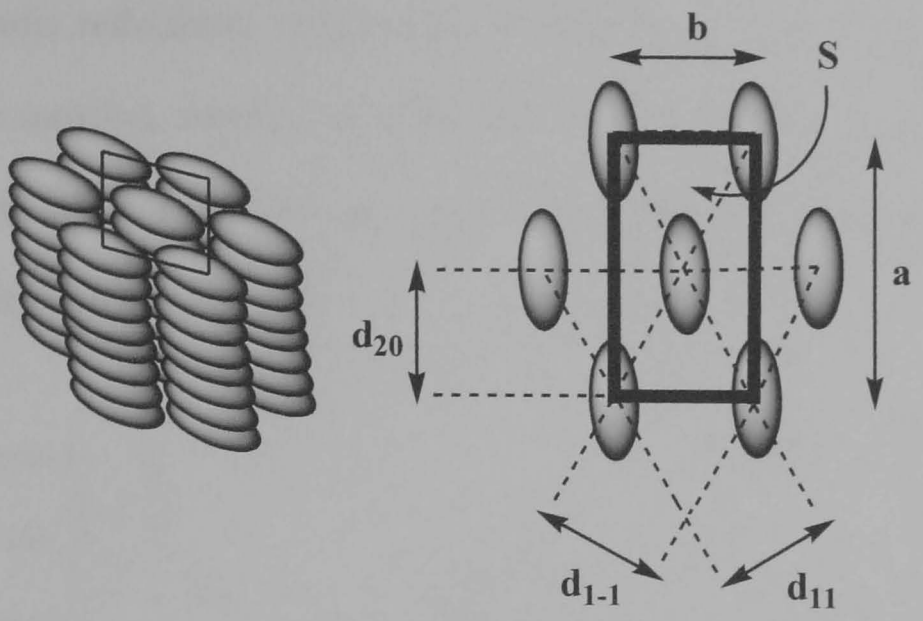

Figure 1.36. Side and cross-sectional views of the molecular symmetry of a Col_r, *c2mm*, arrangement of molecules. The 'disks' are tilted relative to the columnar axes, hence they are represented by ellipses and not circles.

Figures 1.36 and 1.37 show that the disks in the columns are tilted, giving elliptical cross sections. For space group *c2mm* (Figure 1.36), the long axes of the ellipses are oriented in a single direction, whereas for *p2gg* (Figure 1.37) the axes are oriented alternatively along two different directions, resulting in herringbone packing.

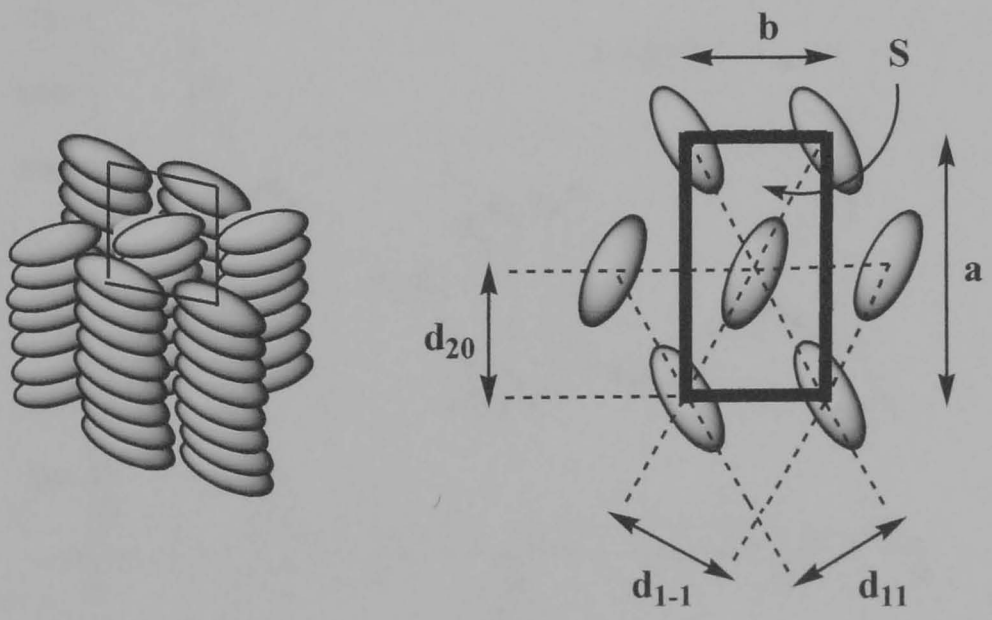

Figure 1.37. Side and cross-sectional views of the molecular symmetry of a Col_r, *p2gg*, arrangement of molecules. The 'disks' are tilted relative to the columnar axes, hence they are represented by ellipses and not circles. The symmetry of the *p2gg* mesophase differs from that of the *c2mm* phase, as a result of the alternating direction of tilt between each layer.

Examination of the X-ray diffraction pattern can often be used to distinguish between the *c2mm* and *p2gg* lattices by studying the fundamental

and higher order reflections. Since, in *c2mm* symmetry, the condition $h + k = 2n$ must be satisfied, whereas no such condition exists for *p2gg* symmetry, discrimination is often possible as long as the higher order reflections are present and of sufficient intensity.

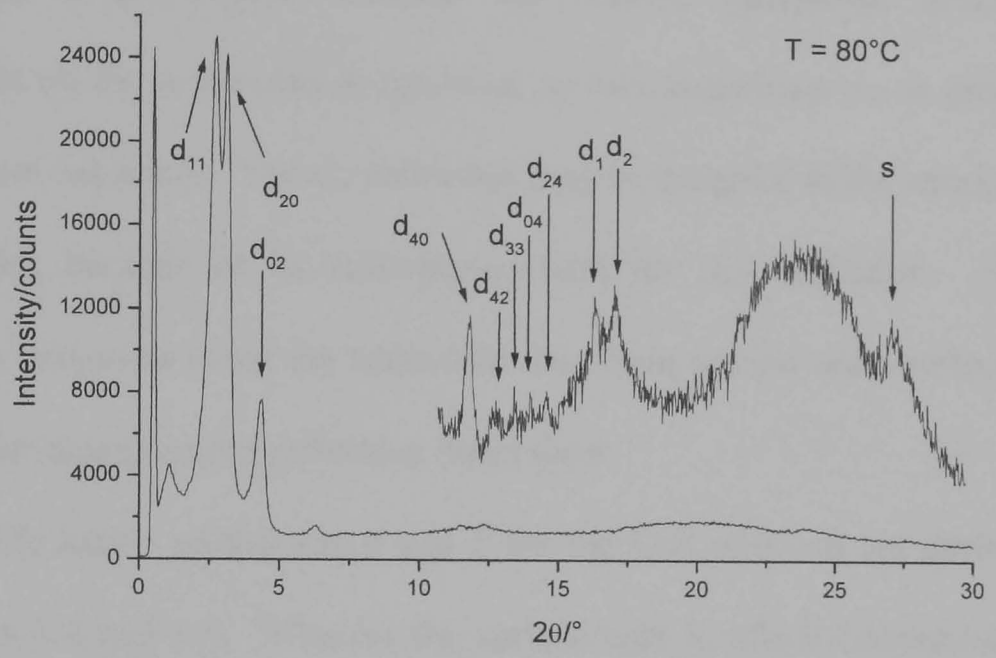

Figure 1.38. Powder X-Ray diffraction pattern of a Col_r mesophase, *c2mm*.

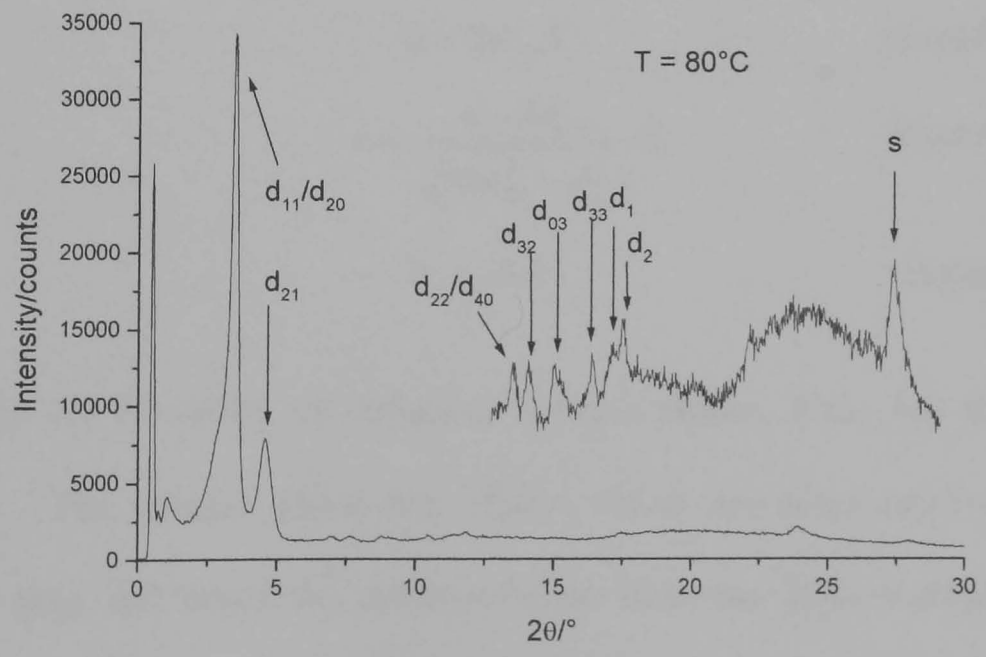

Figure 1.39. Powder X-Ray diffraction pattern of a Col_r mesophase, *p2gg*.

The Figures 1.36 and 1.37 and the XRD patterns in Figures 1.38 and 1.39 indicate that two first-order reflections are to be expected in the small-

angle regions of both *c2mm* and *p2gg*. These reflections are d_{11} (which is coincident with $d_{1\text{-}1}$) and d_{20}. However, the interplanar spacings for these two peaks are so similar that the reflections in the XRD pattern occur very close to each other and often occur as 'twin peaks'. The assignment of the d_{11} and d_{20} reflections is problematic because the relative interplanar spacings are dependent on the molecules in question, so that sometimes d_{11} is greater than d_{20}, but not explicitly. The d_{11} reflection may be assigned as the stronger of the two peaks, because of its coincidence with the $d_{1\text{-}1}$ reflection. However, computer programs using the additional data from second order reflections are utilised for unambiguous reflection indexation.

The lattice parameters a and b for the Col_r unit cell are derived from Equations 1.4 and 1.5. Whereas the surface area S, which corresponds to the cross-sectional area of two columns in the unit cell Col_r, is derived from Equation 1.6.

$$a = 2d_{20}\text{Å} \qquad \text{(Equation 1.4)}$$

$$b = \frac{d_{11}.2d_{20}}{\sqrt{(4d_{20}^2 - d_{11}^2)}}\text{Å} \qquad \text{(Equation 1.5)}$$

$$S = ab\text{Å}^2 \qquad \text{(Equation 1.6)}$$

The 2D symmetry of columnar oblique phases, Col_o, has the space group *p1*. The oblique phase has 'disks' which are tilted relative to the columnar axes and hence the cross-sectional view has disks represented by ellipses (Figure 1.40). These 'disks' alternate in tilt angle from layer-to-layer. The Col_o phase differs from the rectangular *p2gg* lattice by the offset angle of the layers, which occur at γ, an angle other than 90°.

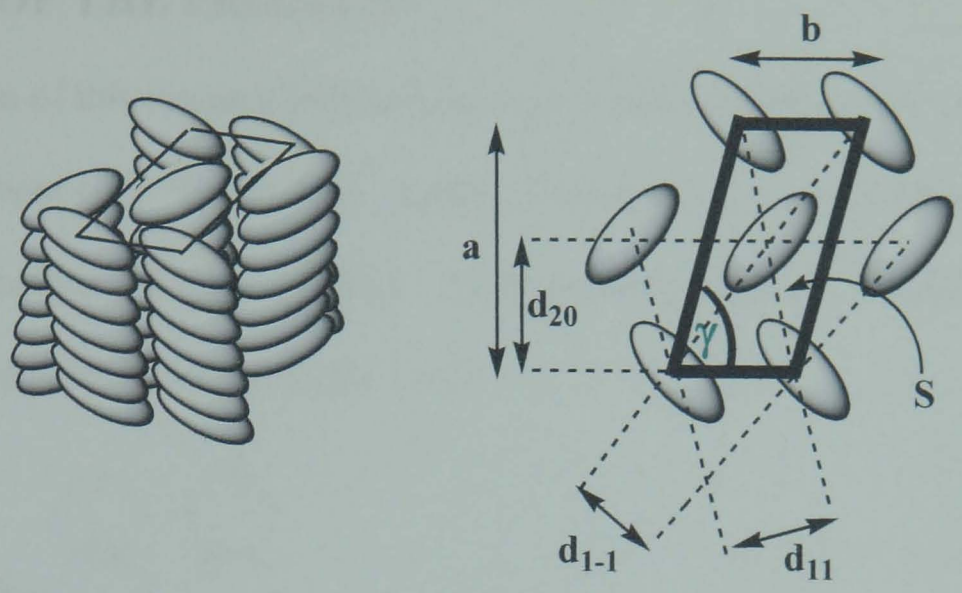

Figure 1.40. Side and cross-sectional views of the molecular symmetry of a Col_o, *p1*, arrangement of molecules. The 'disks' are tilted relative to the columnar axes, hence they are represented by ellipses and not circles. The layers of 'disks' are offset by an angle of γ.

The XRD pattern of the Col_o phase is recognisable by the appearance of three fundamental reflections in the small-angle region corresponding to d_{11}, d_{1-1} and d_{20} (Figure 1.41). The indexing of the reflections, along with the determination of the lattice parameters (a, b, γ and S), requires resolution by the relevant computer programs. The surface area S (where $S = ab$) corresponds to the cross-sectional area of two columns in the unit cell Col_o.

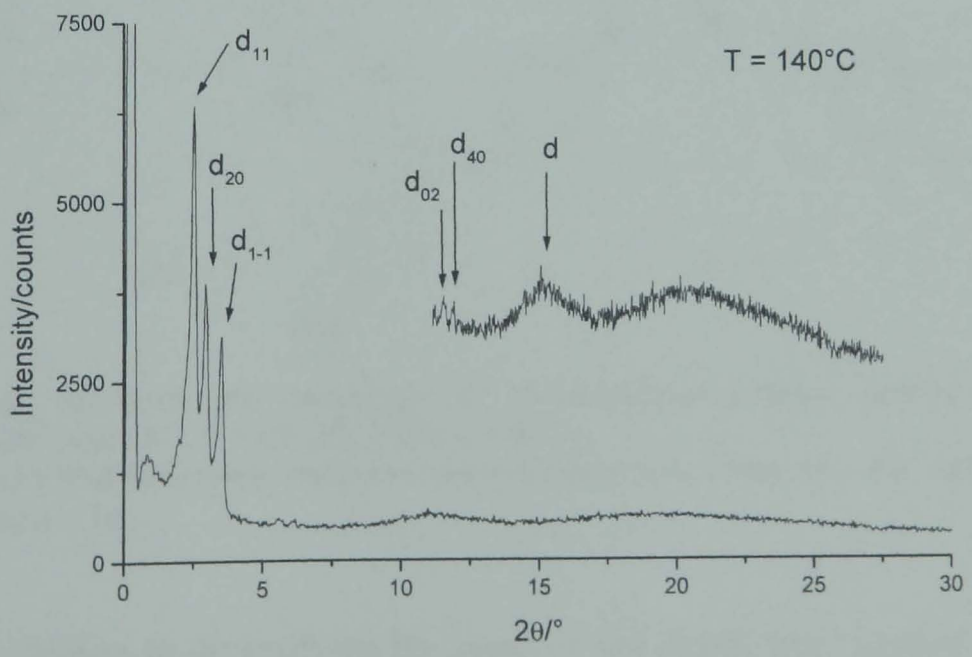

Figure 1.41. Powder XRD pattern of a Col_o mesophase, *p1*.

1.4 AIM OF THE PROJECT

The aim of this research project was to synthesise and characterise novel polycatenar bent-core Schiff-base metallomesogens from derivatives of 1,10-phenanthroline (Figure 1.42a), 2,2-bipyridine (Figure 1.42b) and 5,5'-dimethyldipyrromethane (Figure 1.43).

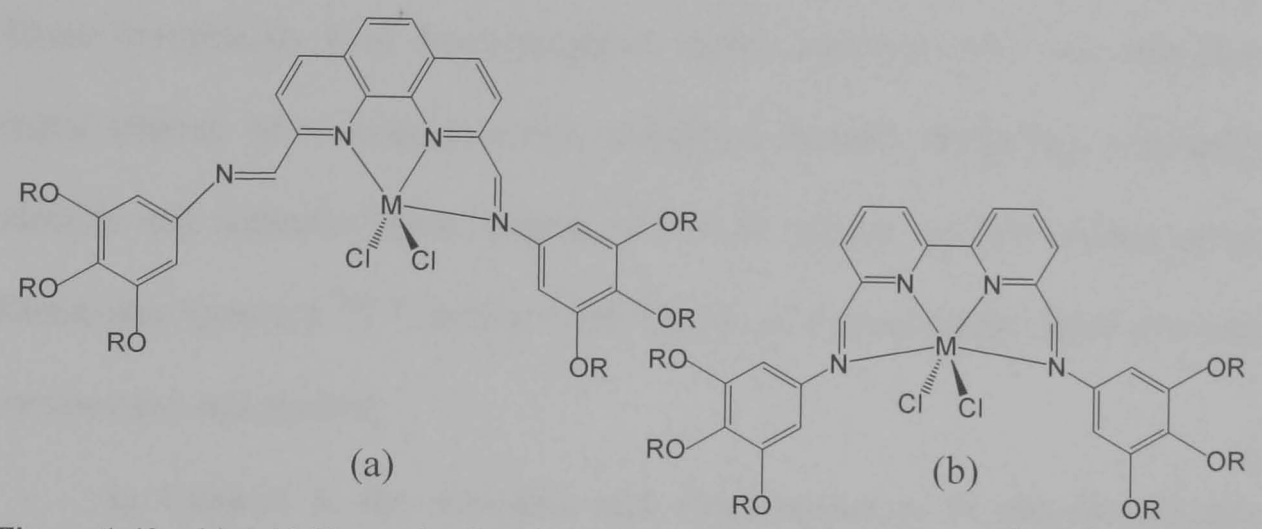

Figure 1.42. (a) 1,10-Phenanthroline derived complexes, where M = Mn^{2+}, Fe^{2+}, Co^{2+}, Ni^{2+}, Cu^{2+}, Zn^{2+}, R = C_nH_{2n+1} and n = 8, 10, 12, 14, 16;
(b) 2,2'-bipyridine derived complexes, where R = C_nH_{2n+1}, n = 16 and M = Mn^{2+}, Fe^{2+}, Co^{2+}, Ni^{2+}, Cu^{2+}, Zn^{2+}. Additionally, M = Ni^{2+} and Zn^{2+} complexes were prepared with n = 10, 12 and 14 carbon atoms.

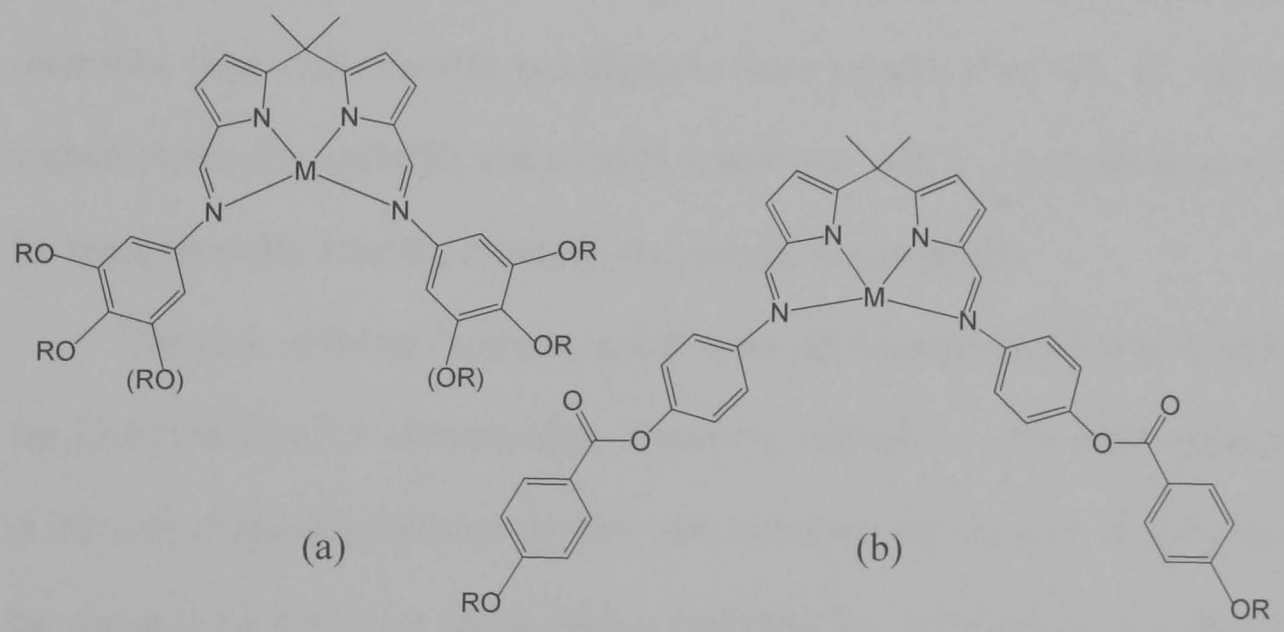

Figure 1.43. (a) Hexa- and tetracatenar 5,5'-dimethyldipyrromethane derived complexes, where M = Zn^{2+} and Pd^{2+}, R = OC_nH_{2n+1} and n = 16;
(b) Extended 5,5'-dimethyldipyrromethane derived complexes, where M = Zn^{2+} and Pd^{2+}, R = OC_nH_{2n+1} and n = 16.

In addition to diversifying the cores of the Schiff-base ligands with bis-[3',4',5'-tri(alkoxy)phenyliminomethyl] pendant arms, both the metal centres and length of the aliphatic chains have also been varied. Further to the study of

the compounds in the liquid crystalline state, single crystal X-ray studies of short chain analogues were performed to determine the degree of self-assembly of the molecules on the solid state.

The synthesis and characterisation of metallomesogens derived from 1,10-phenanthroline $[MCl_2(L^{Phen\text{-}n})]$ (Figure 1.42a) are described in Chapter 2. These compounds have been prepared with mid-to-late first row transition metal cations M = manganese(II), iron(II), cobalt(II), nickel(II), copper(II), zinc(II) and aliphatic chain lengths of n = 8, 10, 12, 14, 16 carbon atoms. Metal-free ligands $L^{Phen\text{-}n}$, with n = 10, 12, 14, 16 carbon atoms, have also been synthesised and studied.

In Chapter 3, the synthesis and characterisation of metallomesogens derived from 2,2'-bipyridine, $[MCl_2(L^{Bipy\text{-}n})]$ (Figure 1.42b), are discussed. These complexes were prepared with M = manganese(II), iron(II), cobalt(II), nickel(II), copper(II), zinc(II), and aliphatic chain lengths of n = 10, 12, 14, 16 carbon atoms for nickel(II) and zinc(II) complexes, and n = 16 carbon atoms for manganese(II), iron(II), cobalt(II) and copper(II) complexes.

The core of the molecule is varied more significantly in Chapter 4, with the inclusion of a 5,5'-dimethyldipyrromethane derivative. The metal centres at the core of these species are the first row transition metal cation zinc(II) and the second row transition metal cation palladium(II). Hexacatenar complexes of $[Zn(L^{Dipy\text{-}n})]_2$ and $[Pd(L^{Dipy\text{-}n})]$ along with the metal-free ligands $H_2L^{Dipy\text{-}n}$ have been prepared with an aliphatic chain length of n = 16 carbon atoms (Figure 1.43a). In order to determine the influence of the aliphatic chain density on the liquid crystalline properties, analogous tetracatenar complexes (*tc*) and metal-free ligands tc-$[Zn(L^{Dipy\text{-}16})]_2$, tc-$[Pd(L^{Dipy\text{-}16})]$ and tc-$H_2L^{Dipy\text{-}16}$

were also synthesised (Figure 1.43a). Further modifications were made to the 5,5'-dimethyldipyrromethane derived ligand with the extension (*ex*) of the molecule, incorporating additional phenyl rings with ester linkers, and the reduction of the number of terminal chains to two (Figure 1.43b). The complexes ex-$[Zn(L^{Dipy\text{-}16})]_2$, ex-$[Pd(L^{Dipy\text{-}16})]$ and metal-free ligand ex-$H_2L^{Dipy\text{-}16}$ were prepared with the intention of generating alternative mesophases to those formed by the aforementioned hexa- and tetracatenar compounds. The length and shape of the extended compounds indicate that banana mesophases may be generated.

1.5 REFERENCES

[1] *Liquid Crystals, The Fourth State of Matter*, ed. F. D. Saeva, Marcel Dekker, Inc., New York, 1979.

[2] N. Hoshino, *Coord. Chem. Rev.*, 1998, **174**, 77.

[3] Reviews: (a) A.-M. Giroud-Godquin and P. M. Maitlis, *Angew. Chem. Int. Ed. Engl.*, 1991, **30**, 375; (b) R. W. Date, E. F. Igesias, K. E. Rowe, J. M. Elliott and D. W. Bruce, *Dalton Trans.*, 2003, **10**, 1914; (c) R. Giménez, D. P. Lydon and J. L. Serrano, *Curr, Opin. Solid St. M.*, 2002, **6**, 527; (d) D. W. Bruce, *J. Chem. Soc. Dalton*, 1993, **20**, 2983; (e) P. M. Maitlis, D. W. Bruce, R. Dhillon, D. A. Dunmur, F. P. Fanizzi, S. E. Hunt, R. Le Lagadec, E. Lalinde, R. Orr, J. P. Rourke, N. J. S. Salt, J. P. Stacey and P. Styring, *New J. Chem.*, 1990, **14**, 549; (f) A. P. Polishchuk and T. V. Timofeeva, *Russ. Chem. Rev.*, 1993, **62**, 291; (g) P. Espinet, M. A. Esteruelas, L. A. Oro, J. L. Serrano and E. Sola, *Coord. Chem. Rev.*, 1992, **117**, 215; (h) A.-M. Giroud-Godquin,

Handbook of Liquid Crystals, Vol. 2B, ed. D. Demus, J. Goodby, G. W. Gray, H.-W. Speiss and V. Vill, Wiley-VCH, Weinheim, 1998, Chapter XIV: (i) A.-M. Giroud-Godquin, *Coord. Chem. Rev.*, 1998, **178**, 1485; (j) S. R. Collinson and D. W. Bruce, *Transition Metals in Supramolecular Chemistry*, ed. J. P. Sauvage, Wiley, New York, 1999, Chapter 7; (k) *Metallomesogens: Synthesis, Properites and Applications*, ed. J. L. Serrano, VCH:Weinheim, 1996; (l) B. Donnio, D. Guillon, R. Deschenaux and D. W. Bruce, *Comprehensive Coord. Chem. II*, ed. J. A. McCleverty and T. J. Meyer, Oxford: Elsevier, 2004, **7**, 357.

[4] (a) *Thermotropic Liquid Crystals*, ed. G. W. Gray, John Wiley & Sons, Chichester, 1987; (b) P. J. Collings and M. Hird, *Introduction to Liquid Crystals – Chemistry and Physics*, Taylor & Francis Ltd., London, 1997; (c) *Handbook of Liquid Crystals, Vol. 2B*, ed. D. Demus, J. Goodby, G. W. Gray, H.-W. Speiss and V. Vill, Wiley-VCH, Weinheim, 1998.

[5] For a more comprehensive review of lyotropic liquid crystals the reader is referred to the following articles (a) B. Donnio, *Curr. Opin. Colloid In.* 2002, **7**, 371; (b) M. R. Alcantara and E. G. Fernandes Jr., *Braz. J. Phys.*, 2002, **32**, 509; (c) A. S. Sonin, *J. Mater. Chem.*, 1998, **8**, 2557; G. J. T. Tiddy, *Phys. Rep.*, 1980, **57**, 2.

[6] T. A. Mirnaya, V. D. Prisyazhnyi and V. A. Shcherbakov, *Russ. Chem. Rev.*, 1989, **58**, 821.

[7] F. Reiss-Husson, *J. Mol. Biol.*, 1967, **25**, 363.

[8] C. Tschierske, *Curr. Opin. Colloid In.*, 2002, **7**, 355 and references therein.

[9] (a) S. A. Hudson and P. M. Maitlis, *Chem. Rev.*, 1993, **93**, 861; (b) K.Toyne, *Thermotropic Liquid Crystals*, ed. G. W. Gray, John Wiley & Sons, Chichester, 1987, 28.

[10] T. Kaharu, H. Matsubara and S. Takahashi, *J. Mater. Chem.*, 1991, **1**, 145.

[11] J. Barberá, R. Iglesias, J. L. Serrano, T. Sierra, M. R. de la Fuente, B. Palacios, M. A. Pérez-Jubindo and J. T. Vázquez, *J. Am. Chem. Soc.*, 1998, **120**, 2908.

[12] (a) H. Adams, A. C. Albeniz, N. A. Bailey, D. W. Bruce, A. S. Cherodian, R. Dhillon, D. A. Dunmar, P. Espinet, J. L. Feijoo, E. Lalinde, P. M. Maitlis, R. M. Richardson and G. Ungar, *J. Mater. Chem.*, 1991, **1**, 843; (b) D. W. Bruce, E. Lalinde, P. Styring, D. A. Dunmur and P. M. Maitlis, *J. Chem. Soc., Chem. Commun.*, 1986, 581; (c) D. W. Bruce, D. A. Dunmur, E. Lalinde, P. M. Maitlis, P. Styring, *Liq. Cryst.*, 1988, **3**, 385.

[13] (a) H. Adams, N. A. Bailey, D. W. Bruce, R. Dhillon, D. A. Dunmur, S. E. Hunt, E. Lalinde, A. A. Maggs, R. Orr, P. Styring, M. S. Wragg, and P. M. Maitlis, *Polyhedron*, 1988, **7**, 1861; (b) M. A. Esteruelas, L. A. Oro, E. Sola, M. B. Ros, and J. L. Serrano, *J. Chem. Soc., Chem. Commun.*, 1989, 55; (c) R. Eidenschink, D. Erdmann, J. Krause and L. Pohl, *Angew. Chem. Int. Ed.*, 1978, **17**, 133.

[14] (a) S. Chandrasekhar, *Phil. Trans. R. Soc. Lond. A*, 1983, **309**, 93; (b) S. Chandrasekhar, *Handbook of Liquid Crystals, Vol. 2B*, ed. D. Demus, J. Goodby, G. W. Gray, H.-W. Speiss and V. Vill, Wiley-VCH, Weinheim, 1998, Chapter VIII; (c) R. J. Bushby and O. R. Lozman, *Curr. Opin. Colloid In.*, 2002, **7**, 343.

[15] S. Chandrasekhar, B. K. Sadashiva and K. A. Suresh, *Pramana*, 1977, **9**, 471.

[16] (a) J. C. Dubois, *Ann. Phys.*, 1978, 131; (b) N. H. Tinh, C. Destrade and H. Gasparoux, *Phys. Lett.*, 1979, **72A**, 251; (c) B. Y. Tang, J. J. Ge, A. Zhang, B.

Calhoun, P. Chu, H. Wang, Z. Shen, F. W. Harris and S. Z. D. Cheng, *Chem. Mater.*, 2001, **13**, 78;

[17] (a) J. W. Goodby, P. S. Robinson, B. K. Teo and P. E. Cladis, *Mol. Cryst. Liq. Cryst. Lett.*, 1980, **56**, 303; (b) H. Bock and W. Helfrich, *Liq. Cryst.*, 1992, **12**, 697; (c) K. Ohta, M. Ikejima, M. Moriya, H. Hasebe and I. Yamamoto, *J. Mater. Chem.*, 1998, **8**, 1971.

[18] (a) A. M. Giroud-Godquin and J. Billard, *Mol. Cryst. Liq. Cryst.*, 1981, **66**, 147; (b) R. Fugnitto, H. Strzelecka, A. Zann, J.-C. Dubois and J. Billard, *J. Chem. Soc., Chem. Commun.*, 1980, 271.

[19] G. Friedel, *Ann. Phys.*, 1922, **18**, 273.

[20] H. Sackmann, *Liq.Cryst.*, 1989, **5**, 43.

[21] J. P. Rourke, F. P. Fanizzi, N. J. S. Salt, D. W. Bruce, D. A. Dunmur and P. M. Maitlis, *J. Chem. Soc. Chem. Commun.*, 1990, 229.

[22] H. A. Ellis, *Mol. Cryst. Liq. Cryst.*, 1986, **139**, 281.

[23] Z. Liu, L. Zhu, W. S. Zhou, S. Z. D. Cheng, V. Percec and G. Ungar, *Chem. Mater.*, 2002, **14**, 2384.

[24] M.-A. Guillevic, M. E. Light, S. J. Coles, T. Gelbrich, M. B. Hursthouse and D. W. Bruce, *J. Chem. Soc., Dalton Trans.*, 2000, 1437.

[25] Y. Zhang, W. Zhu, W. Wang, H. Tian, J. Su and W. Wang, *J, Mater. Chem.*, 2002, **12**, 1294.

[26] (a) N. H. Tinh, H. Gasparoux and C. Destrade, *Mol. Cryst. Liq. Cryst.*, 1981, **68**, 101; (b) B. Kohne and K. Praefcke, *Chimia*, 1987, **41**, 196; (c) C. Destrade, H. Gasparoux, A. Babeau, N. H. Tinh and J. Malthête, *Mol. Cryst. Liq. Cryst.*, 1981, **67**, 37; (d) S. Kumar, S. K. Varshney, *Angew. Chem. Int. Ed.*, 2000, **39**, 3140.

[27] (a) K. Praefcke, D. Singer, B. Kohne, M. Ebert, A. Liebmann and J. H. Wendorff, *Liq. Cryst.*, 1991, **10**, 147; (b) K. Praefcke, D. Singer, M. Langer, B. Kohne, M. Ebert, A. Liebmann and J. H. Wendorff, *Mol. Cryst. Liq. Cryst.*, 1992, **215**, 121.

[28] (a) S. Chandrasekhar and G. S. Ranganath, *Rep. Prog. Phys.*, 1990, **53**, 57; (b) D. Guillon, B. Donnio and D. W. Bruce, *Mol. Cryst. Liq. Cryst.*, 2003, **396**, 141.

[29] U. Pietrasik, J. Szyłowska and A. Krówczyński, *Chem. Mater.*, 2004, **16**, 1485.

[30] J. Barberá, L. Puig, J. L. Serrano and T. Sierra, *Chem. Mater.*, 2004, **16**, 3308.

[31] S. T. Trzaska, H. Zheng and T. M. Swager, *Chem. Mater.*, 1999, **11**, 130.

[32] (a) K. Borisch, S. Diele. P. Göring and C. Tschierske, *Chem. Commun.*, 1996, **2**, 237; (b) K. Borisch, S. Diele, P. Göring, H. Kresse and C. Tschierske, *Angew. Chem., Int. Ed. Engl.*, 1997, **36**, 2087; (c) M. Lee, N. –K. Oh and W. –C. Zin, *Chem. Commun.*, 1996, 1787.

[33] (a) N. J. Thompson, G. W. Gray, J. W. Goodby, and K. J. Toyne, *Mol. Cryst. Liq. Cryst.*, 1991, **200**, 109; (b) U. Stebani, G. Lattermann, R. Festtag, M. Wittenberg and J. H. Wendorff, *J. Mater. Chem.*, 1995, **5**, 2247; (c) D. W. Bruce, D. A. Dunmur, L. S. Santa and M. A. Wali, *J. Mater. Chem.*, 1992, **2**, 363; (d) B. Neumann, C. Sauer, S. Diele and C. Tshierske, *J. Mater. Chem.*, 1996, **6**, 1087.

[34] (a) H. Zheng, B. Xu and T. M. Swager, *Chem. Mater.*, 1996, **8**, 907; (b) H. Nozar, C. Piguet, J.-P. Rivera, P. Tissot, G. Bernardinelli, N. Vulliermet, J. Weber and J.-C. G. Bünzli, *Inorg. Chem.*, 2000, **39**, 5286; (c) C. K. Lai, A. G.

Serrette and T. M. Swager, *J. Am. Chem. Soc.*, 1992, **114**, 7948; (d) K. Kishikawa, S. Furusawa, T. Yamaki, S. Kohmoto, M. Yamamoto and K. Yamaguchi, *J. Am. Chem. Soc.*, 2002, **124**, 1597; (e) P. Espinet. J. Perez, M. Marcos, M. B. Ros, J. L. Serrano, J. Barberá and A. M. Levelut, *Organometallics*, 1990, **9**, 2028; (f) C. Tschierske, *J. Mater. Chem.*, 1998, **8**, 1485 and references therein; (g) C. Tschierske, *J. Mater. Chem.*, 2001, **11**, 2647 and references therein.

[35] (a) H.-T. Nguyen, C. Destrade and J. Malthête, *Handbook of Liquid Crystals, Vol. 2B*, ed. D. Demus, J. Goodby, G. W. Gray, H.-W. Speiss and V. Vill, Wiley-VCH, Weinheim, 1998, Chapter XII; (b) M. Gharbia, A. Gharbi, H. T. Nguyen and J. Malthête, *Curr. Opin. Colloid In.*, 2002, **7**, 312; (c) J. Malthête, H.-T. Nguyen and C. Destrade, *Liq. Cryst.*, 1993, **13**, 171; (d) H.-T. Nguyen, C. Destrade and J. Malthête, *Adv. Mater.*, 1997, **9**, 375; (e) D. Fazio, C. Mongin, B. Donnio, Y. Galerne, D. Guillon and D. W. Bruce, *J. Mater. Chem.*, 2001, **11**, 2852.

[36] (a) B. Donnio and D. W. Bruce, *J. Chem. Soc., Dalton Trans.*, 1997, 2745; (b) C. Tschierske, *Angew. Chem. Int. Ed.*, 2000, **39**, 2454; (c) J. M. Elloitt, J. R. Chipperfield, S. Clark and E. Sinn, *Inorg. Chem. Commun.*, 2002, **5**, 99.

[37] J. M. Elliott, J. R. Chipperfield and S. Clark, *Inorg. Chem.*, 2001, **40**, 6390.

[38] B. K. Sadashiva and V. A. Raghunathan, *Pramana – J. Phys.*, 2003, **61**, 219.

[39] B. Donnio and D. W. Bruce, *New J. Chem.*, 1999, 275.

[40] H. T. Nguyen, C. Destrade and J. Malthête, 1990, *Liq. Cryst.*, **8**, 797.

[41] B. Donnio and D. W. Bruce, *J. Chem. Soc., Dalton Trans.*, 1997, 2745.

[42] (a) G. Pelzl, S. Diele and W. Weissflog, *Adv. Mater.*, 1999, **11**, 707; (b) K. Fodor-Csorba, A. Vajda, G. Galli, A. Jákli, D. Demus, S. Holly, E. Gács-Baitz,

Macromol. Chem. Phys., 2002, **203**, 1556; (c) C. Tschierske and G. Dantlgraber, *Pramana – J. Phys.*, 2003, **61**, 455; (d) T. C. Lubensky, *Science*, 2000, **288**, 2146.

[43] T. C. Lubensky and L. Radzihovsky, *Phys. Rev. E*, 2002, **66**, 031704.

[44] E. Schröter, Ph.D. Thesis, The University of Halle, Halle, 1925.

[45] T. Niori, T. Sekine, J. Watanabe, T. Furukawa and H. Takezoe, *J. Mater. Chem.*, 1996, **6**, 1231.

[46] P. J. Collings and M. Hird, *Introduction to Liquid Crystals – Chemistry and Physics*, Taylor & Francis Ltd., London, 1997, Chapter 3.

[47] G. Pelzl, S. Diele, A. Jákli, C. Lischka, I. Wirth and W. Weissflog, *Liq. Cryst.*, 1999, **26**, 135.

[48] G. Pelzl, S. Diele, S. Grande, A. Jákli, C. Lischka, H. Kresse, H. Schmalfuss, I. Wirth, W. Weissflog, *Liq. Cryst.*, 1999, **26**, 401.

[49] W. Weissflog, C. Lichka, I. Benné, T. Scharf, G. Pelzl, S. Diele, H. Kruth, *Proc. SPIE: Int. Soc. Opt. Eng.*, 1998, **14**, 3319.

[50] (a) D. Dunmur, K. Toriyama, F. Schneider, H. Kneppe, L. M. Blinov and P. Palffy-Muhoray, *Physical Properties of Liquid Crystals*, ed. D. Demus, J. Goodby, G. W. Gray, H.-W. Spiess and V. Vill, Wiley, Chichester, 1999, Chapter IV; (b) L. Pohl and U. Finkenzeller, *Liquid Crystals - Applications and Uses (Vol 1)*, ed. B. Bahadur, World Scientific, London, 1995, Chapter 4.

[51] (a) S. Chanrasekhar and S. K. Prasad, *Contemp. Phys.*, 1999, **40**, 237; (b) R. B. Meyer, L. Liébert, L. Strzelecki and P. Keller, *J. Phys. Lett. – Paris*, 1975, **36**, 69; (c) D. M. Walba, M. B. Ros, N. A. Clark, R. Shao, M. G. Robinson, J.-Y. Liu, K. M. Johnson and D. Doroski, *J. Am. Chem. Soc.*, 1991, **113**, 5471; (d) P. Espinet, J. Etxebarría, M. Marcos, J. Pérez, A. Remón and J. L. Serrano,

Angew. Chem. Int. Ed. Engl., 1989, **28**, 1065: (e) G. Heppke, D. Krüerke, C. Löhning, D. Lötzsch, D. Moro, M. Müller and H. Sawade, *J. Mater. Chem.*, 2000, **10**, 2657; (f) L. M. Blinov, *Liquid Cryst.*, 1998, **24**, 143.

[52] (a) D. Pauluth and K. Tarumi, *J. Mater. Chem.*, 2004, **14**, 1219: (b) D. Coates, *Ed. Chem.*, 2000, 153; (c) G. W. Gray and S. M. Kelly, *J. Mater. Chem.*, 1999, **9**, 2037; (d) M. Bremshey-Wilhelm, *Liquid Crystals – Merck Makes Bits and Bytes Visible.* http://www.media-highlights.merck.de/servlet/PB/show/1075410/Merck_TopTopics_LC_EN.pdf; (e) W. R. Boulton, *Note on the Liquid Crystal Display Industry*, 1995. http://www.business.auburn.edu/~boultwr/lcdnote.pdf.

[53] (a) T. Geelhaar, *Liq. Cryst.*, 1998, **24**, 91; (b) T. Scheffer and J. Nehring, *Liquid Crystals - Applications and Uses (Vol 1)*, ed. B. Bahadur, World Scientific, London, 1995, Chapter 10; (c) F. C. Luo, *Liquid Crystals - Applications and Uses (Vol 1)*, ed. B. Bahadur, World Scientific, London, 1995, Chapter 15.

[54] Y. Matsuda, *Jpn. Kokai Tokkyo Koho*, JP 2005-128416A, 2005.

[55] D. G. McDonnell, *Thermotropic Liquid Crystals*, ed. G. W. Gray, John Wiley & Sons, Chichester, 1987, Chapter 5.

[56] (a) J. W. Doane, *Liquid Crystals - Applications and Uses (Vol 1)*, ed. B. Bahadur, World Scientific, London, 1995, Chapter 14; (b) J. W. Doane, A. Golemme, J. L. West, J. B. Whitehead and B.-G. Wu, *Mol. Cryst. Liq. Cryst.*, 1988, **165**, 511.

[57] (a) Marcos, J. L. Serrano, T. Sierra and M. J. Giménez, *Angew. Chem. Int. Ed. Engl.*, 1992, **31**, 1471; (b) Y. G. Galyametdinov, G. I. Ivanova and I. V. Ovchinnikov, *Izv. Akad. Nauk SSSR Ser. Khim.*, 1989, 1931; (c) A.-M. Giroud-

Godquin, J.-M. Latour and J.-C. Marchon, *Inorg. Chem.*, 1985, **24**, 4452; (d) H. Hoshino, A. Kodama, T. Shiuya, Y. Matsunga and S. Miyajima, *Inorg. Chem.*, 1991, **30**, 3091; (e) C. P. Roll, A. G. Martin, H. Görls, G. Leibeling, D. Guillon, B. Donnio and W. Weigand, *J. Mater. Chem.*, 2004, **14**, 1722.

[58] (a) K. Ohta, H. Hasebe, M. Moriya, T. Fujimoto and I. Yamamoto, *Mol. Cryst. Liq. Cryst.*, 1991, **208**, 43; (b) K. Ohta, H. Hasebe, M. Moriya, T. Fujimoto and I. Yamamoto, *J. Mater. Chem.*, 1991, **1**, 831; (c) K. Ohta, M. Moriya, M. Ikejima, H. Hasebe, T. Fujimoto and I. Yamamoto, *Bull. Chem. Soc. Jpn.*, 1993, **66**, 1078; (d) H. Adams, A. C. Albeniz, N. A. Bailey, D. W. Bruce, A. S. Cherodian, R. Dhillon, D. A. Dunmar, P. Espinet, J. L. Feijoo, E. Lalinde, P. M. Maitlis, R. M. Richardson and G. Ungar, *J. Mater. Chem.*, 1991, **1**, 843.

[59] (a) R. Deschenaux, M. Scweissguth, M.-T.-Vilches, A.-M. Levelut, D. Hautot, G. J. Long and D. Luneau, *Organometallics*, 1999, **18**, 5553; (b) A. G. Martin, S. Harms, W. Weigand, D. L. Gin, *Adv. Mater*, 2005, **17**, 602; (c) M.-H. Qi and G.-F. Liu, *J. Mater. Chem.*, 2003, **13**, 2479.

[60] (a) X.-H. Liu, B. Henirich, I. Manners, D. Guillon and D. W. Bruce, *J. Mater. Chem.*, 2000, **10**, 637; (b) M.-A. Guillevic, M. E. Light, S. J. Coles, T. Gelbrich, M. B. Hurthouse and D. W. Bruce, *J. Chem. Soc., Dalton Trans.*, 2000, 1437; (c) S. Coco, P. Espinet and E. Marcos, *J. Mater. Chem.*, 2000, **10**, 1297; (d) S. T. Trzaska, H. Zheng and T. M. Swager, *Chem. Mater.*, 1999, **11**, 130; (e) S. T. Trzasaka, H.-F. Hsu and T. M. Swager, *J. Am. Chem. Soc.*, 1999, **121**, 4518; (f) U. Stebani, G. Lattermann, M. Wittenberg and J. H. Wendorff, *Angew. Chem. Int. Ed. Engl.*, 1996, **35**, 1858; (g) A. B. Blake, J. R. Chipperfield, W. Hussain, R. Paschke and E. Sinn, *Inorg. Chem.*, 1995, **34**,

1125; (h) A. G. Serrette and T. M. Swager, *J. Am. Chem. Soc.*, 1993, **115**, 8879.

[61] (a) C. Bertram, D. W. Bruce, D. A. Dunmar, S. E. Hunt, P. M. Maitlis, M. McCann, *J. Chem. Soc. Chem. Commun.*, 1991, 69; (b) D. W. Bruce, D. A. Dunmur, M. A. Esteruelas, S.E. Hunt, R. Le Lagadec, P. M. Maitlis, J. R. Marsden, E. Sola and J. M. Stacey, *J. Mater. Chem.*, 1991, **1**, 251; (c) J. L. Serrano and T. Sierra, *Chem. Eur. J.*, 2000, **6**, 759.

[62] (a) D. W. Bruce, D. A. Dunmar, P. M. Maitlis, M. M. Manterfield and R Orr, *J. Mater. Chem.*, 1991, **1**, 255; (b) M. Ghedini, M. Longeri and R. Bartolino, *Mol. Cryst. Liq. Cryst.*, 1982, **84**, 207.

[63] (a) M. J. Baena, J. Barberá, P. Espinet, A. Ezcurra, M. B. Ros and J. L. Serrano, *J. Am. Chem. Soc.*, 1994, **116**, 1899; (b) E. Meyer, C. Zucco and H. Gallardo, *J. Mater. Chem.*, 1998, **8**, 1351; (c) L. Plasseraud, L. G. Cuervo, D. Guillon, G. Süss-Fink, R. Deschenaux, D. W. Bruce and B. Donnio, *J. Mater. Chem.*, 2002, **12**, 2653; (d) J. Barberá, E. Cavero, M. Lehmann, J. L. Serrano, T. Sierra and J. T. Vázquez, *J. Am. Chem. Soc.*, 2003, **125**, 4527.

[64] (a) H. Adams, N. A. Bailey, D. W. Bruce, D. A. Dunmur, E. Lalinde, M. Marcos, C. Ridgway, A. J. Smith, and P. M. Maitlis, *Liq. Cryst. 2*, 1987, 381; (b) N. Hoshino, *Coord. Chem. Rev.*, 1998, **174**, 77.

[65] (a) J. Barberá, P. Espinet, E. Lalinde, M. Marcos and J. L. Serrano, *Liq. Cryst.*, 1987, **2**, 833; (b) H. Adams, N. A. Bailey, D. W. Bruce, R. Dhillon, D. A. Dunmar, S. E. Hunt, E. Lalinde, A. A. Maggs, R. Orr, P. Styring, M. S. Wragg and P. M. Maitlis, *Polyhedron*, 1988, **7**, 1861; (c) P. Espinet, E. Lalinde, M. Marcos, J. Péresz and J. L. Serrano, *Organomet.*, 1990, **9**, 555; (d) C. K. Lai, C.-H. Chang and C.-H. Tsai, *J. Mater. Chem.*, 1998, **8**, 599.

[66] D. J. Saccomando, C. Black, G. W. V. Cave, D. P. Lydon and J. P. Rourke, *J. Organomet. Chem.*, 2000, **601**, 305;

[67] (a) J. L. Serrano and T. Sierra, *Chem. Eur. J.*, 2000, **6**, 759; (b) J. Buey, L. Diez, P. Espinet, H.-S. Kitzerow and J. A. Miquel, *Chem. Mater.*, 1996, **8**, 2375.

[68] (a) K. L. Marshall and S. D. Jacobs, *Mol. Cryst. Liq. Cryst.*, 1988, **159**, 181; (b) M. B. Ros, *Metallomesogens*, ed. J. L. Serrano, VCH, Cambridge, 1996, Chapter 11.

[69] (a) C. Piechocki, J. Simon, A. Skoulios, D. Duillon and P. Weber, *J. Am. Chem. Soc.*, 1982, **104**, 5245; (b) B. A. Gregg, M. A. Fox and A. J. Bard, *J. Am. Chem. Soc.*, 1989, **111**, 3024; (c) W. Haase, S. Wrobel and K. Falk, *Pramana, J. Phys.*, 2003, **61**, 189; (d) D. Markovitsi, I. Lécuyer and J. Simon, *J. Phys. Chem.*, 1991, **95**, 3620.

[70] R. Reinitzer, *Monasch. Chem.*, 1888, **9**, 421.

[71] O. Lehmann, *Z. Physik. Chem.*, 1889, **4**, 462.

[72] (a) G. H. Heilmeier, L. A. Zanoni and L. A. Barton, *Appl. Phys. Lett.*, 1968, **13**, 46; (b) G. H. Heilmeier and J. E. Goldmacher, *Appl. Phys. Lett.*, 1968, **13**, 132; (c) G. H. Heilmeier, *Sci. Am.*, 1970, **222**, 100.

[73] G. W. Gray, K. J. Harrison and J. A. Nash, *Electron. Lett.*, 1973, **9**, 130.

[74] (a) G. W. Gray, *Philos. T. Roy. Soc. A*, 1990, **330**, 73; (b) J. A. Castellano, *Mol. Cryst. Liq. Cryst.*, 1988, **165**, 511.

[75] W. Heintz, *J. Prakt. Chem.*, 1855, **66**, 1.

[76] D. Vorländer, *Ber. Dtsch. Chem.*, 1910, **43**, 3120.

[77] For a review of the work carried out by Vorländer and the research that has subsequently followed, see D. Demus, *Mol. Cryst. Liq. Cryst.*, 2001, **364**, 25.

[78] D. Vorländer, *Z. Phys. Chem. Stoechiom., Verwandschaftsl.*, 1923, **105**, 211.

[79] (a) D. Vorländer, *Z. Physik. Chem.*, 1906, **A57**, 357; (b) D. Vorländer. *Ber. Dtsch. Chem. Ges.*, 1907, **40**, 4526.

[80] D. Vorländer, *Ber. Dtsch. Chem. Ges.*, 1907, **40**, 1970.

[81] J. Malthête and J. Billard, *Mol. Cryst. Liq. Cryst.*, 1976, **34**, 117.

[82] A.-M. Giroud and U. T. Müller-Westerhoff, *Mol. Cryst. Liq. Cryst.*, 1977, **41**, 11.

[83] A.-M. Giroud-Godquin and P. M. Maitlis, *Angew. Chem. Int. Ed. Engl.*, 1991, **30**, 375.

[84] (a) D. W. Bruce, D. A. Dunmur, E. Lalinde, P. M. Maitlis and P. Styring, *Liq. Cryst.*, 1988, **3**, 385; (b) D. W. Bruce, D. A. Dunmur, S. A. Hudson, P. M. Maitlis and P. Styring, *Adv. Mater. Opt. Electron*, 1992, **1**, 37; (c) D. W. Bruce, D. A. Dunmur, S. A. Hudson, E. Lalinde, P. M. Maitlis, P. M. McDonald, R. Orr, P. Styring, A. S. Cherodian, R. M. Richardson, J. L. Feijoo and G. Ungar, *Mol. Cryst. Liq. Cryst.*, 1991, **206**, 79; (d) D. W. Bruce, D. A. Dunmur, P. M. Maitlis, P. Styring, M. A. Esteruelas, L. A. Oro, M. B. Ros, J. L. Serrano and E. Sola, *Chem. Mater.*, 1989, **1**, 479.

[85] (a) J. P. Rourke, F. P. Fanizzi, D. W. Bruce, D. A. Dunmur and P. M. Maitlis, *J. Chem. Soc., Dalton Trans.*, 1992, 3009; (b) J. P. Rourke, F. P. Fanizzi, N. J. S. Salt, D. W. Bruce, D. A. Dunmur and P. M. Maitlis, *J. Chem. Soc., Chem. Commun.*, 1990, 229.

[86] (a) D. W. Bruce, D. A. Dunmur, M. A. Esteruelas, S. E. Hunt, R. Le Lagadec, P. M. Maitlis, J. R. Marsden, E. Sola and J. M. Stacey, *J. Mater. Chem.*, 1991, **1**, 251; (b) D. W. Bruce, D. A. Dunmur, M. R. Manterfield, P. M. Maitlis and R. Orr, *J. Mater. Chem.*, 1991, **1**, 255; (c) C. Bertram, D. W.

Bruce, D. A. Dunmur, S. E. Hunt, P. M. Maitlis and M. McCann, *J. Chem. Soc., Chem. Commun.*, 1991, 69.

[87] N. Hoshino, A. Kodama, T. Shibuya, Y. Matsunaga and S. Miyajima, *Inorg. Chem.*, 1991, **30**, 3091.

[88] (a) J. Szydłowska, A. Krówczyński, E. Górecka and D. Pociecha, *Inorg. Chem.*, 2000, **39**, 4879; (b) J. Barberá, A.-M. Levelut, M. Marcos, P. Romero and J. L. Serrano, *Liq. Cryst.*, 1991, **10**, 119.

[89] (a) Y. G. Galyametdinov, G. I. Ivanova and I. V. Ovchinnikov, *Izv. Akad. Nauk SSSR Ser. Khim.*, 1989, 1931; (b) Y. G. Galyametdinov, G. I. Ivanova, K. Griesar, A. Prosvirin, I. Ovchinnikov and W. Haase, *Adv. Mater. 4*, 1992, 739.

[90] R. Paschke, D. Balkow and E. Sinn, *Inorg. Chem.*, 2002, **41**, 1949.

[91] Y. G. Galyametdinov, G. I. Ivanova and I. V. Ovchinnikov, *Zh. Obsch. Khim.*, 1991, **61**, 234.

[92] (a) Y. G. Galyametdinov, G. I. Ivanova and I. V. Ovchinnikov, *Bull. Acad. Sci. USSR, Div. Chem. Sic.*, 1991, **40**, 1109; (b) Y. G. Galyametdinov, G. I. Ivanova, A. V. Prosvirin and O. Kadkin, *Russ. Chem. Bull.*, 1994, **43**, 938; (c) Y. G. Galyametdinov, M. A. Athanassopoulou, K. Griesar, O. Kharitonova, E. A. Soto Bustamante, L. Tinchurina, I. Ovchinnikov and W. Haase, *Chem. Mater.*, 1996, **8**, 922; (c) K. Binnemanns, Y. G. Galyametdinov, S. R. Collinson and D. W. Bruce, *J. Mater. Chem.*, 1998, **8**, 1551; (d) K. Binnemanns, D. W. Bruce, S. R. Collinson, R. Van Deun, Y. G. Galyametdinov and F. Martin, *Phil. Trans. R. Soc. Lond. A*, 1999, **357**, 3063; (e) K. Binnemanns, R. Van Deun, D. W. Bruce and Y. G. Galyametdinov, *Chem. Phys. Lett.*, 1999, **300**, 509; (f) K. Binnemanns, Y. G. Galyametdinov, R. Van Deun, D. W. Bruce, S. R. Collinson, A. P. Polishchunk, I. Bikchantaev,

W. Haase, A. V. Prosvirin, L. Tinchurina, I. Litvinov, A. Gubajdullin, A. Rakhmatullin, K. Uytterhoeven and L. Van Meervelt, *J. Am. Chem. Soc.*, 2000, **122**, 4335; (g) S. R. Collinson, F. Martin, K. Binnemanns, R. Van Deun and D. W. Bruce, *Mol. Cryst. Liq. Cryst.*, 2001, **364**, 745; (h) K. Binnemans, R. Van Deun, C. Göller-Walrand, W. Haase, D. W. Bruce, L. Malykhina and Y. G. Galyametdinov, *Mat. Sci. Eng. C*, 2001, **18**, 247.

[93] A. J. Blake, D. W. Bruce, I. A. Fallis, S. Parsons, H. Richtzenhain, S. A. Ross and M. Schröder, *Phil. T. Roy. Soc. A*, 1996, **354**, 395 and references therein.

[94] (a) H. Richtzenhain, A. J. Blake, D. W. Bruce, I. A. Fallis, W.-S. Li and M. Schröder, *Chem. Commun.*, 2001, 2580; (b) H. Richtzenhain, *Macrocyclic Liquid Crystals*, PhD Thesis, The University of Nottingham, Nottingham, 1997.

[95] C.-W. Chien, K.-T. Liu and C. K. Lai, *J. Mater. Chem.*, 2003, **13**, 1588.

[96] H. Zheng and T. Swager, *J. Am. Chem. Soc.*, 1994, **116**, 761.

[97] M. Ghedini, F. Neve and D. Pucci, *Eur. J. Inorg. Chem.*, 1998, **4**, 501.

[98] P. Espinet, E. Lalinde, M. Marcos, J. Perez and J. L. Serrano, *Organometallics*, 1990, **9**, 555.

[99] P. Espinet, J. Etxebarria, M. Marcos, J. Pérez, A. Remón and J. L. Serrano, *Angew. Chem. Int. Ed. Engl.*, 1989, **28**, 1065.

[100] (a) D. W. Bruce and X.-H. Liu, *J. Chem. Soc., Chem. Comuun.*, 1994, 729; (b) X.-H. Liu, M. N. Abser and D. W. Bruce, *J. Organomet. Chem.*, 1998, **551**, 271.

[101] R. Finn, *Studies on Complexes of Compartmental Imine and Amine Ligands*, PhD Thesis, The University of Nottingham, Nottingham, 2000.

[102] F. Morale, *Metallomesogens Derived From Schiff-Base Chelates and Related Co-ordination Chemistry*, PhD Thesis, The University of Nottingham, Nottingham, 2002.

[103] (a) P. C. Robinson and H. W. Davidson, *Nikon MicroscopyU: Introduction to Polarized Light Microscopy*, 2005.

http://www.microscopyu.com/articles/polarized/polarizedintro.html:

(b) *Section I. Polarized Light and Optical Microscopy*, 1997.

http://acept.la.asu.edu.PiN/rdg/polarize/sectioni.html.

[104] For a more comprehensive account see (a) G. Höhne, W. Hemminger and H.-J. Flammersheim, *Differential Scanning Calorimetry*, Springer, London, 2003; (b) J. L. McNaughton and C. T. Mortimer. *Differential Scanning Calorimetry*, The Perkin-Elmer Corporation, Connecticut, 1975.

[105] For a more detailed account see R. Jenkins and R. L. Snyder, *Introduction to X-Ray Powder Diffractometry*, John Wiley & Sons, Inc., New York, 1996.

[106] A. Beguin, J. Billard, F. Bonamy, J. M. Bustine, P. Curelier, J. C. Dubois and P. Le Barny, *Mol. Cryst. Liq. Cryst.*, 1984, **115**, 1.

CHAPTER 2:

METALLOMESOGENS DERIVED FROM 1,10-PHENANTHROLINE

2.1 INTRODUCTION TO LIQUID CRYSTALS OF 1,10-PHENANTHROLINE

2.1.1 Liquid Crystals of 1,10-Phenanthroline

The synthesis of thermotropic phenanthroline-based liquid crystals is a very recent phenomenon and few examples are reported in the literature. The first liquid crystal of this type was reported by Bruce in 2001.[1] He prepared a linear phenanthroline ligand, based upon disubstitution at the 3,8-postions (Figure 2.1a).

(a)

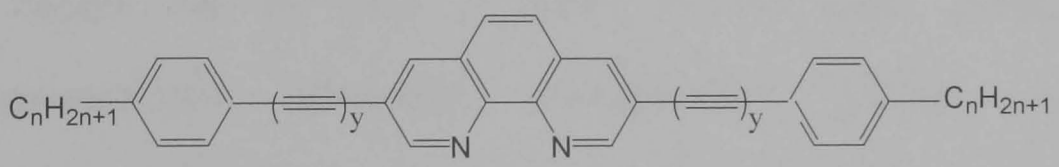

y = 0, 1
n = 5, 8

y = 1, *n* = 5: Cr 158 N >309 decomposed
y = 1, *n* = 8: Cr 144 SmC 232 N 277 I
y = 0, *n* = 5: Cr 188 SmA 229 N 295 I
y = 0, *n* = 8: Cr 122 SmC 272 I

(b)

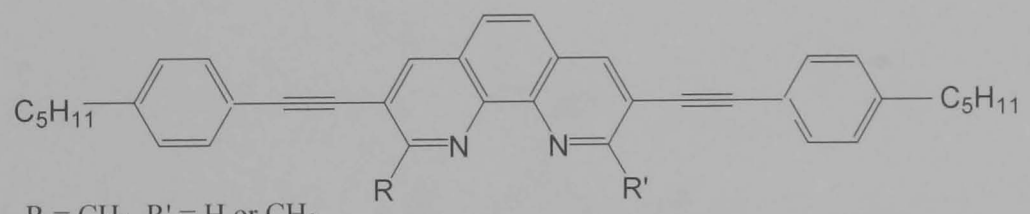

R = CH_3, R' = H or CH_3

R = CH_3, R' = H: Cr 166 N >280 decomposed
R = CH_3, R' = CH_3: Cr 134 N 250 I

Figure 2.1. The first phenanthroline liquid crystals, as reported by Bruce.[1] The corresponding transition temperatures are given with temperatures reported in °C.

The bis(acetylide) molecule (Figure 2.1a, y = 1) displayed a nematic phase, with n = 5, and both nematic and smectic C phases, with n = 8. The diphenyl derivatives (y = 0) displayed nematic and smectic A phases at shorter chain lengths and a smectic C phase at longer chain lengths. However, the melting points were all well above 100°C and the clearing points reached

almost 300°C, often with accompanying decomposition. Therefore, two further phenanthroline liquid crystals were prepared with the intention of lowering the transition temperatures by reducing the molecular anisotropy and/or lowering the symmetry. These molecules incorporated methyl groups at the 2- and/or 9- positions (Figure 2.1b), and although these modifications were successful in lowering the clearing temperature by up to 59°C and preventing decomposition, the effect on the melting temperatures and indeed, the mesomorphism, was negligible.

Ziessel was the next to follow in this field,[2] producing a 2,9-unsymmetrically substituted phenanthroline grafted onto a 1,3-diacylaminobenzene core with four peripheral aliphatic chains to create a pseudo-disc shape (Figure 2.2).

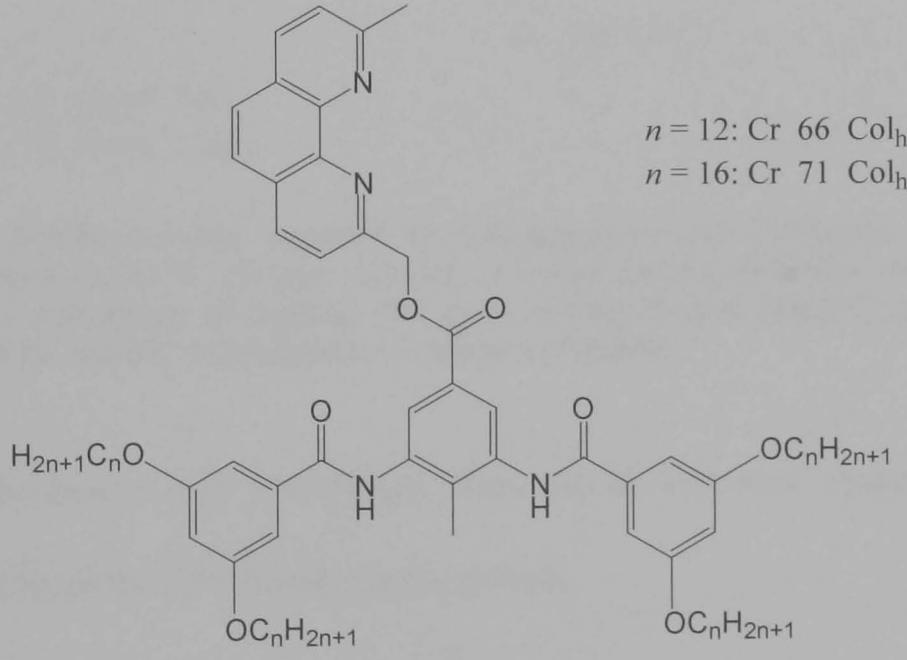

n = 12, 16

n = 12: Cr 66 Col_h 118 I
n = 16: Cr 71 Col_h 119 I

Figure 2.2. Phenanthroline liquid crystals prepared by Ziessel *et al.*, with accompanying transition temperatures in °C.[2]

For n = 12 and 16, the molecules formed columnar hexagonal phases at 66°C and 71°C, respectively, clearing into the isotropic phase at around 118°C. Interestingly, preliminary microscopic and X-ray diffraction measurements

suggested that complexation of the n = 16 ligand to palladium(II) produced a smectic A mesophase at around room temperature.[2]

Finally, Galyametdinov and Binnemans *et al.*[3] prepared tris(β-diketonato)lanthanide(III) complexes using 1,10-phenanthroline as a Lewis-base and a mesomorphic β-diketonate ligand to give monotropic smectic A phases (Figure 2.3).

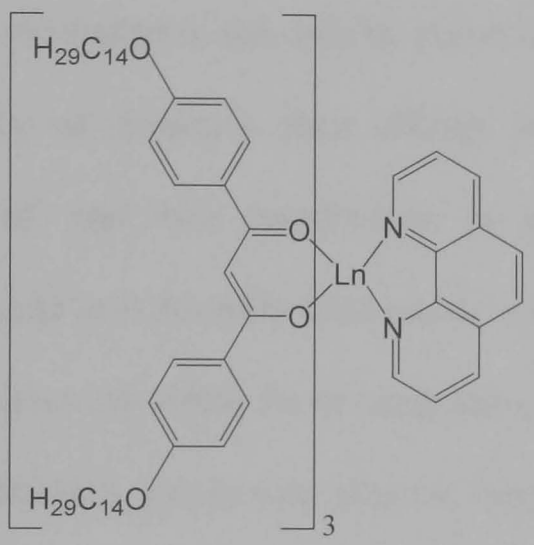

Ln = Tb^{3+}, Eu^{3+}

Ln = Tb^{3+}: Cr 145 (SmA 120) I

Ln = Eu^{3+}: Cr 155 (SmA 138) I

Figure 2.3. Metallomesogens prepared by Galyametdinov and Binnemans *et al.*[3] The transition temperatures, in °C, are also included. To show that the complexes melted without formation of a mesophase on heating, but upon cooling formed smectic A phases, the temperatures of the smectic A mesophases are shown in brackets.

To the best of our knowledge, there are no first-row transition metal-containing phenanthroline-based liquid crystals.

2.1.2 The Design of the 1,10- Phenanthroline-Derived Metallomesogens

The design of our phenanthroline molecule (Figure 2.4) encompassed the necessary features to promote liquid crystalline behaviour. The bent, hemidisk-like ligand based on 2,9-bis-[3',4',5'-tri(alkoxy)phenyliminomethyl]-1,10-phenanthroline comprises a central, rigid 1,10-phenanthroline core, which

is an ideal metallomesogen building block due to favourable N,N'-coordination to transition metal cations.[4] The rigidity and unsaturation of the core, as well as the permanent lateral dipole[5] are also key features, with the bent shape generated by 'arms' symmetrically substituted at the 2,9-positions of the phenanthroline core. Each 'arm' consists of a phenyl ring with three peripheral alkoxy chains of 8, 10, 12, 14, or 16 carbon atoms in length, to promote fluidity. These 'arms' are linked to the core by imine functionalities chosen in particular for their ease of synthesis, their affinity for binding to first-row transition metal cations[6] and their preservation of the conjugation in the system. Hence, the ligand is potentially tetradentate with both phenanthroline and diimine nitrogen donors available for co-ordination. However, the ligands are expected to be tridentate, generating trigonal bipyramidal metal centres with first-row transition metal cations, *i.e.* manganese(II), iron(II), cobalt(II), nickel(II), copper(II) and zinc(II). This is based on the co-ordination geometries of other first-row transition metal ions complexed to related phenanthroline-diimine ligands.[7]

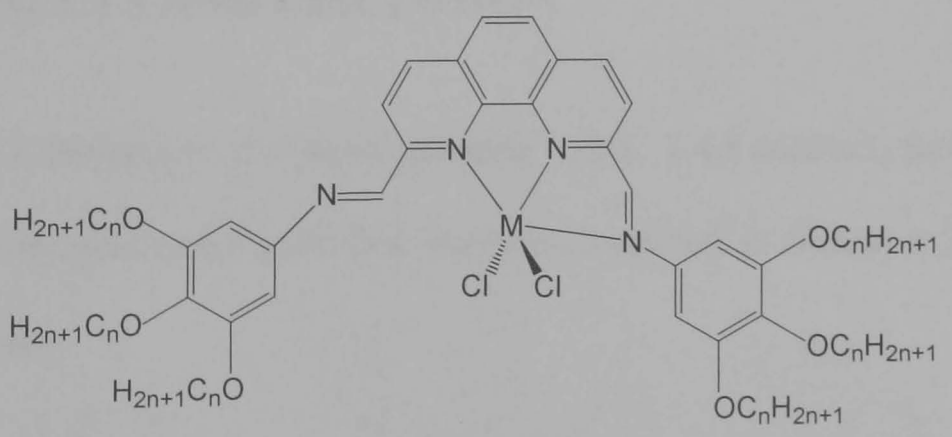

Figure 2.4. The 1,10-phenanthroline-derived complexes, $[MCl_2(L^{Phen\text{-}n})]$ where M = Mn^{2+}, Fe^{2+}, Co^{2+}, Ni^{2+}, Cu^{2+}, Zn^{2+} and n = 8, 10, 12, 14, 16.

As a result of the hemidisk-like shape of the molecules and the core planarity, we expect to generate columnar mesophases on the basis of the *complimentary molecular shape* approach.[8] Using this approach, complexes

with specific molecular interactions are designed that result in correlated structures, and these correlated structures can further organise to form columnar mesophases. For example, two of our hemidisk-shaped complexes could correlate in an anti-parallel manner to form a disk, which can stack in columns (Figure 2.5).

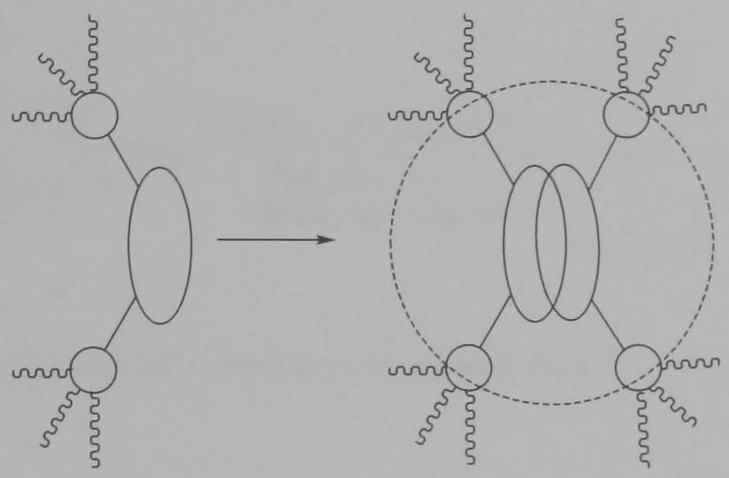

Figure 2.5. The 'disk' formed by two molecules of $[MCl_2(L^{Phen\text{-}n})]$, based on the complimentary molecular shape approach.[8]

We herein report on the synthesis and mesogenic properties of the first thermotropic, phenanthroline first-row transition metal metallomesogens.

2.2 RESULTS AND DISCUSSION

2,9-Diformyl-1,10-phenanthroline[9] and 3,4,5-trialkoxyaniline[10] were prepared by previously published methods, outlined in Schemes 2.1 and 2.2, respectively.

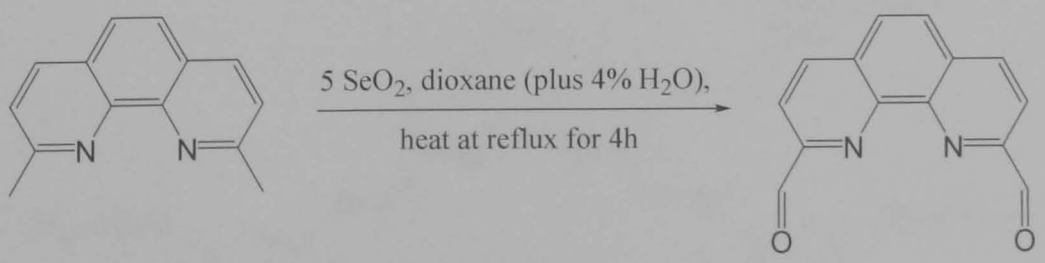

Scheme 2.1. Synthesis of 2,9-diformyl-1,10-phenanthroline.[9]

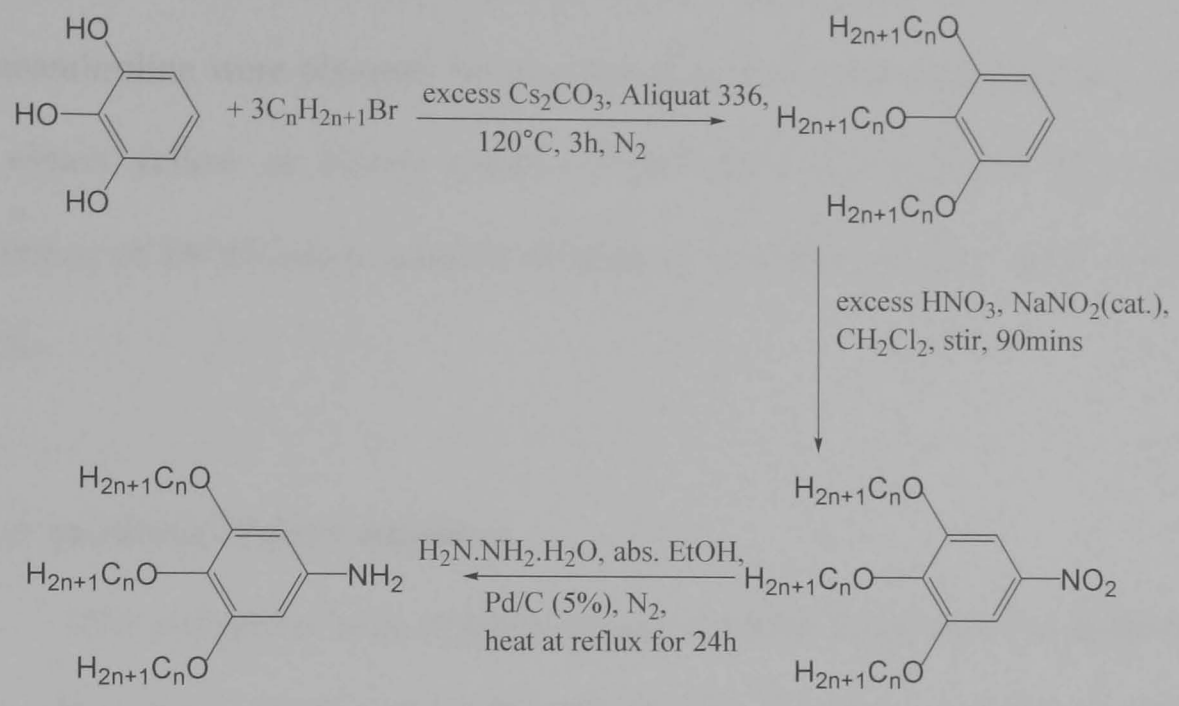

Scheme 2.2. Synthesis of the 3,4,5-trialkoxyaniline compounds.[10]

2.2.1 Synthesis of the Ligands

Six hexacatenar free ligands were prepared with chains of 1, 8, 10, 12, 14 and 16 carbon atoms. The synthetic route is outlined in Scheme 2.3, detailing the synthesis in which 2,9-diformyl-1,10-phenanthroline and two equivalents of the appropriate 3,4,5-trialkoxyaniline undergo Schiff-base condensation under reflux for 24 hours in EtOH.

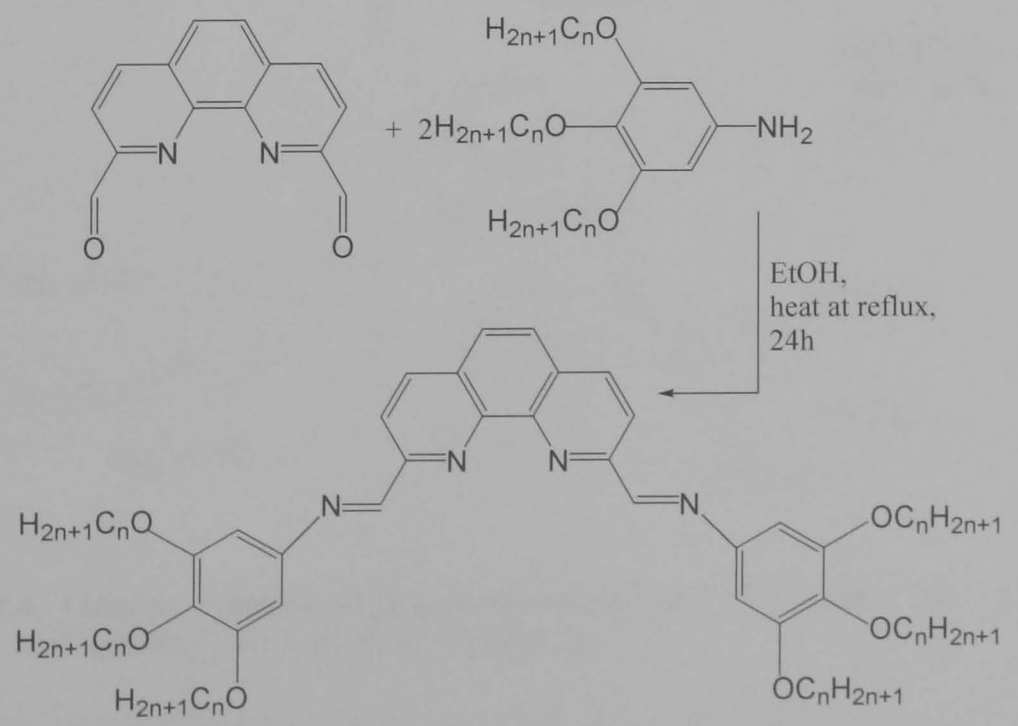

Scheme 2.3. Synthesis of the 2,9-bis-[3',4',5'-tri(alkoxy)phenyliminomethyl]-1,10-phenanthroline ligands, where n = 1, 8, 10, 12, 14 and 16.

The molecules of 2,9-bis-[3',4',5'-tri(alkoxy)phenyliminomethyl]-1,10-phenanthroline were obtained by concentration of the reaction liquor *in vacuo*, to obtain yellow or brown solids. Purification was achieved by solvent diffusion of EtOH into a solution of product in $CHCl_3$ to give yields of 40 – 72%.

2.2.2 Synthesis of the Complexes

The complexes were prepared by the synthetic route outlined in Scheme 2.4. Six series of first-row transition metal complexes of manganese(II), iron(II), cobalt(II), nickel(II), copper(II) and zinc(II) were prepared by template Schiff-base condensation reactions. Each series consisted of alkylated compounds with chain lengths of n = 1, 8, 10, 12, 14, 16 carbon atoms. The n = 1 compounds were synthesised for the purpose of growing single crystals for study by X-ray crystallography.

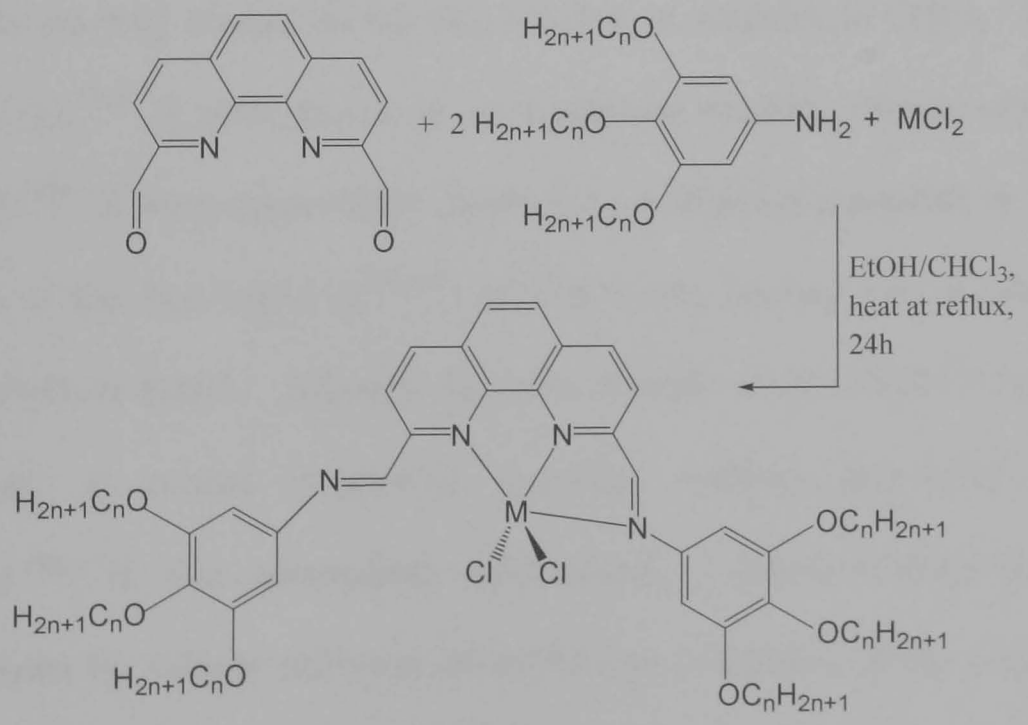

Scheme 2.4. Template synthesis of the complexes $[MCl_2(L^{Phen\text{-}n})]$, where M = Mn^{2+}, Fe^{2+}, Co^{2+}, Ni^{2+}, Cu^{2+} and Zn^{2+}; n = 1, 8, 10, 12, 14 and 16.

The synthetic procedure for each complex was as follows: 2,9-diformyl-1,10-phenanthroline, two equivalents of the appropriate 3,4,5-trialkoxyaniline and one equivalent of metal chloride salt were heated to reflux in EtOH and $CHCl_3$ for 24 hours to produce the 2,9-bis-[3',4',5`-tri(alkoxy)phenyliminomethyl]-1,10-phenanthroline metal(II) chloride complexes, $[MCl_2(L^{Phen\text{-}n})]$. The solid products were obtained either by slow evaporation of the mother liquor or by reduction of solvent volume *in vacuo*. Recrystallisation was achieved by solvent diffusion of either Et_2O or EtOH into a solution of the complex in $CHCl_3$. A template synthesis rather than reaction of the metal salt with the metal-free ligand was selected in order to optimise yields and to avoid the formation of unwanted side products.

Single crystals of the manganese(II), cobalt(II), nickel(II) and zinc(II) methoxy compounds, as well as crystals of the copper(II) complex minus alkoxy chains, $[CuCl_2(L^{Phen\text{-}0})]$, were grown. Crystals of $[MnCl_2(L^{Phen\text{-}1})]$ were grown by layering hexane on top of a solution of complex in $CHCl_3$. Crystals of $[CoCl_2(L^{Phen\text{-}1})]$ were grown in an analogous manner. Single crystals of $[NiCl_2(L^{Phen\text{-}1})]$ were successfully obtained by a different procedure in which a solution of the free ligand ($L^{Phen\text{-}1}$) in $CHCl_3$ was layered over a solution of $NiCl_2.6H_2O$ in EtOH. Attempts to grow crystals of $[CuCl_2(L^{Phen\text{-}1})]$ failed. Therefore, a related copper(II) complex without peripheral chains, $[CuCl_2(L^{Phen\text{-}0})]$, was subsequently synthesised. Crystals of $[CuCl_2(L^{Phen\text{-}0})]$ were grown by solvent diffusion of EtOH into a solution of the complex in $CHCl_3$. Single crystals of $[ZnCl_2(L^{Phen\text{-}1})]$ were grown from slow evaporation of the mother liquor. The poor solubility of $[FeCl_2(L^{Phen\text{-}1})]$ proved an insurmountable issue for crystal growth, so no crystals of the complex were

obtained. Also unsuccessful were the repeated attempts at growing suitably large enough crystals of the free ligand, $L^{Phen\text{-}1}$. Despite numerous attempts, no crystals of suitable quality were obtained for any of the long chain complexes. This is a common problem with liquid crystals,[11] and is ascribed to the fluidity generated by the presence of long alkyl chains inhibiting the growth of single crystals, and the generally weaker intermolecular interactions in liquid crystals compared to crystals.

2.2.3 Characterisation of the Ligands and Complexes

The compounds were all characterised by infrared spectroscopy, mass spectrometry, CHN microanalysis, and, for the ligands and $[ZnCl_2(L^{Phen\text{-}n})]$, by ^1H and ^{13}C NMR spectroscopy.

Evidence for the formation of the Schiff-base products in the infrared spectra was provided by two bands at approximately 1614 and 1586cm^{-1} (the former occasionally obscured by the latter), corresponding to imine stretching vibrations. Further evidence was the absence of any aldehyde or aniline bands associated with the starting materials. There is negligible shift to a lower wavenumber on complexation of the imines to the transition metal ion although, typically, a 10-30cm^{-1} shift is expected.[6(b),12] One possible explanation for this is the highly conjugated nature of the ligands, which would also explain the low frequency of the imine stretches (usually occurring between 1640 and 1690cm^{-1}).[13,12(b)] Therefore, there is no distinct difference between the coordinated and uncoordinated imine stretching vibrations.

^1H NMR spectroscopy of the complexes $[ZnCl_2(L^{Phen\text{-}n})]$ revealed the equivalence of the imine proton environments on the NMR timescale. The

imine proton signal appears in the region δ = 9.49 to 9.42 ppm. with two doublet and one singlet resonances in the aromatic region resulting from the phenanthroline protons, in the regions δ = 8.59 – 8.50, 8.48 – 8.39 and 8.07 – 7.99 ppm, respectively. Comparison of these results with analogous spectra of the uncomplexed ligands shows an expected, albeit slight, downfield shift on complexation to zinc(II) chloride. Most notably, the imine protons are shifted by approximately 0.3ppm and the protons on the lateral phenyl rings are shifted by approximately 0.4ppm. A negligible shift was observed for the phenanthroline protons and no appreciable shift was observed for the alkyl chains.

^{13}C NMR spectroscopy revealed a significant upfield shift of the imine carbon signal of approximately 5 ppm on complexation to zinc(II).

Mass spectrometry provided evidence of the formation of 1:1 metal-ligand complexes and microanalysis gave satisfactory results, usually incorporating one or two molecules of solvents of crystallisation.

2.2.4 Structural Determination by Single Crystal X-Ray Diffractometry

X-ray crystallographic studies on single crystals of $[MnCl_2(L^{Phen\text{-}1})]$, $[CoCl_2(L^{Phen\text{-}1})]$, $[NiCl_2(L^{Phen\text{-}1})]$, $[CuCl_2(L^{Phen\text{-}0})]$ and $[ZnCl_2(L^{Phen\text{-}1})]$ confirmed $[CoCl_2(L^{Phen\text{-}1})]$, $[CuCl_2(L^{Phen\text{-}0})]$ and $[ZnCl_2(L^{Phen\text{-}1})]$ to be monomeric five-coordinate complexes, and $[MnCl_2(L^{Phen\text{-}1})]$ and $[NiCl_2(L^{Phen\text{-}1})]$ to be dimeric octahedral complexes. All compounds crystallise in space group P-1. The metal(II) centres are coordinated to three of the four nitrogen atoms from the diimine ligand and two or three chloride ions, depending on the coordination geometry. The un-coordinated imine nitrogen

points away from the metal(II) cation in order to avoid unfavourable dipolar interactions. The coordination geometries around the metal(II) centres of the five coordinate complexes $[CoCl_2(L^{Phen\text{-}1})]$, $[CuCl_2(L^{Phen\text{-}0})]$ and $[ZnCl_2(L^{Phen\text{-}1})]$ are metal dependent and vary between distorted trigonal bipyramidal and distorted square-based pyramid. The degree of trigonality is defined by the geometric parameter $\tau = (\beta\text{-}\alpha)/60$, where β and α are the largest angles N(10)-M-N(2) and N(1)-M-Cl(1), respectively.[14] A value of $\tau = 0$ indicates perfect tetragonal geometry, whereas unity indicates perfect trigonal bipyramidal geometry.

The lateral phenyl rings on the imine arms are twisted relative to the phenanthroline plane and the cavities created by the presence of these bulky phenyl substituents contain non-interacting molecules of solvent within the unit cell. Further discussion on the interpretation of the crystallographic data for each complex now follows. Selected bond lengths and angles are presented in Tables 2.1 and 2.2 at the end of this section.

2.2.4.1 Structure Determination of $[MnCl_2(L^{Phen\text{-}1})]$

The crystal structure of $[MnCl_2(L^{Phen\text{-}1})]$ (Figure 2.6) revealed that the complex crystallises as a centrosymmetric dimer linked by an asymmetric bridge. The coordination geometry about the manganese(II) centre is distorted octahedral. The axial positions are occupied by the Cl(2) and Cl(1)` ions, whereas the equatorial positions are occupied by N(1), N(2), N(10) and Cl(1). Distortion from ideal octahedral geometry is demonstrated by the bond angles Cl(1)`-Mn(1)-Cl(2) = 177.0(1)°, N(2)-Mn(1)-N(10) = 144.19(9)° and N(1)-

Mn(1)-Cl(1) = 157.18(9)°, which significantly deviate from the ideal angles of 180°.

The bond lengths from manganese(II) cation to the chloride anions are almost identical for Mn(1)-Cl(1) and Mn(1)-Cl(2), which are 2.413(1)Å and 2.411(1)Å, respectively. However, the remaining manganese(II) – chloride bond is elongated relative to Mn(1)-Cl(1) and Mn(1)-Cl(2), hence Mn(1)-Cl(1)' = 2.744(1)Å. The manganese(II) bond lengths to the diimine ligand are similar for Mn(1)-N(2) and Mn(1)-N(10), which have lengths of 2.386(1)Å and 2.388(1)Å, respectively. The Mn(1)-N(1) bond is significantly shorter in comparison, having a bond length of 2.180(1)Å.

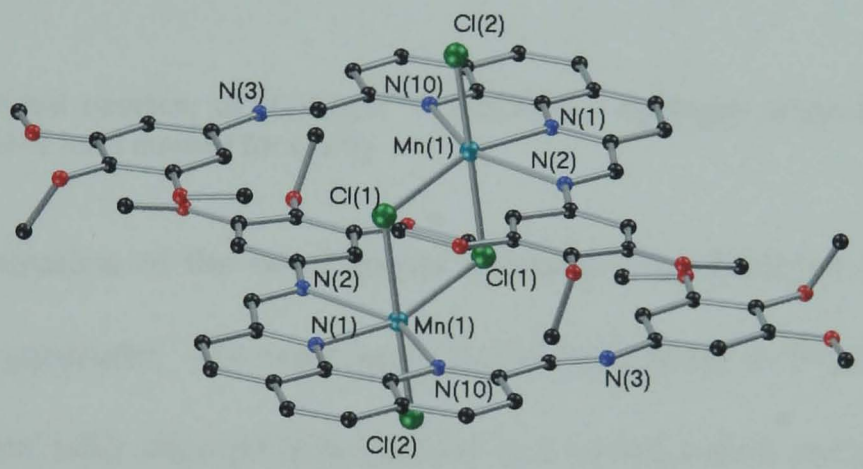

Figure 2.6. Crystal structure of $[MnCl_2(L^{Phen\text{-}1})]_2.2CH_2Cl_2$. Hydrogen atoms and solvents of crystallisation have been omitted for clarity.

In relation to the phenanthroline plane, the manganese(II) cation lies virtually in the plane of the ligand core with a small displacement distance of 0.067Å. The lateral phenyl rings are twisted relative to the phenanthroline plane by angles of 3.032(1)° and 3.603(2)°, hence resulting in a slight deviation in planarity of the ligand backbone.

The manganese cations are separated by 3.9Å, and the ligands are arranged in opposite directions. Thus the complexes exist as a pseudo disk and the structure contains two non-interacting molecules of CH_2Cl_2 per dimer.

2.2.4.2 Structure Determination of $[CoCl_2(L^{Phen\text{-}1})]$

Crystallographic studies of single crystals of $[CoCl_2(L^{Phen\text{-}1})]$ (Figure 2.7) gave a τ parameter of 0.481. This indicates that the coordination geometry of the cobalt(II) centre lies inbetween that of trigonal bipyramidal and square-based pyramid.

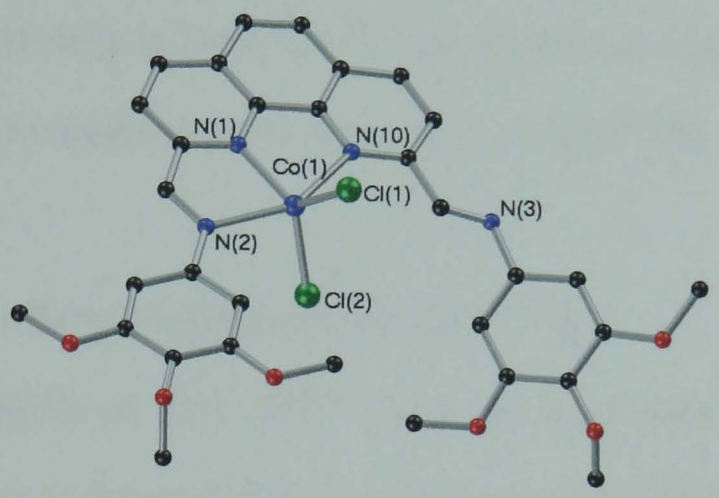

Figure 2.7. Crystal structure of $[CoCl_2(L^{Phen\text{-}1})].2CHCl_3$. Hydrogen atoms and solvents of crystallisation have been omitted for clarity.

Examination of the bond angles illustrated the distorted nature of the coordination geometry. The bond angle N(2)-Co(1)-N(10) is 151.62(12)°. The ideal angle for both trigonal bipyramidal and square-based pyramid is 180°. The angles for N(1)-Co(1)-Cl(1), N(1)-Co(1)-Cl(2) and Cl(2)-Co(1)-Cl(1) are 122.74(10)°, 121.75(10)° and 115.51(5)°. For ideal square-based pyramidal geometry these values should be 180°, 90° and 90°, respectively. For ideal trigonal bipyramidal geometry the values should all be 120°. Hence, the geometry may be regarded as distorted trigonal bipyramidal with a highly distorted axial angle, N(2)-Co(1)-N(10). The equatorial positions are thus occupied by the central nitrogen atom N(1) and both chloride ions.

The bonds from the cobalt(II) cation to the chloride anions are 2.2741(12)Å and 2.2655(12)Å long. Similar bond lengths are observed for the axial bonds Co(1)-N(2) and Co(1)-N(10). These bond lengths are 2.268(3)Å

and 2.284(3)Å, respectively. The remaining equatorial bond for Co(1)-N(1) is at the shorter length of 2.021(3)Å.

The position of the cobalt(II) cation relative to the phenanthroline plane is co-planar. However, the phenyl rings attached to the imine moieties have torsion angles of 10.3(1)° and 27.44(2)°, which are significantly larger than the twist of the phenyl rings in $[MnCl_2(L^{Phen\text{-}1})]$. Contained within the cavities of the structure are two molecules of $CHCl_3$ per $[CoCl_2(L^{Phen\text{-}1})]$.

2.2.4.3 Structure Determination of $[NiCl_2(L^{Phen\text{-}1})]$

Single crystals of $[NiCl_2(L^{Phen\text{-}1})]$ in the solid state (Figure 2.8) are analogous to those of $[MnCl_2(L^{Phen\text{-}1})]_2$. Hence, $[NiCl_2(L^{Phen\text{-}1})]_2$ has distorted octahedral coordination geometry and crystallises as a centrosymmetric dimer, linked by an asymmetric bridge.

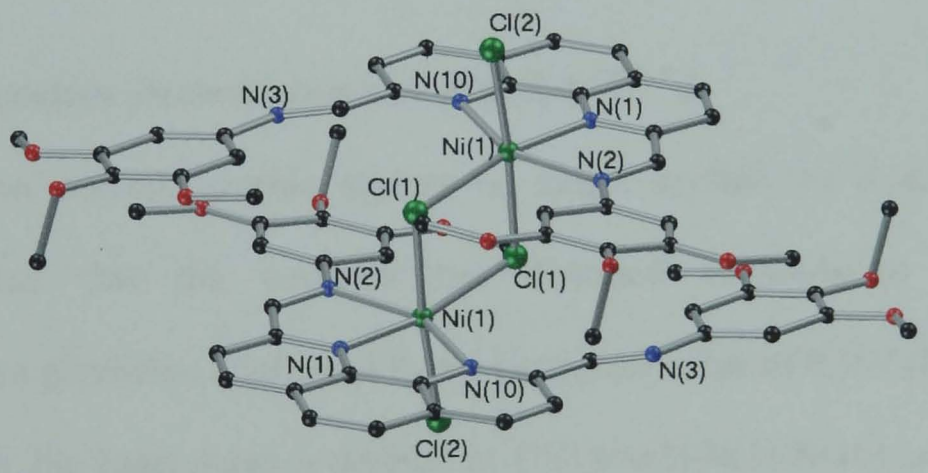

Figure 2.8. Crystal structure of $[NiCl_2(L^{Phen\text{-}1})]_2.2CHCl_3.2.5EtOH$. Hydrogen atoms and solvents of crystallisation have been omitted for clarity.

The equatorial plane is defined by Cl(1)-N(2)-N(1)-N(10) and the axial positions by Cl(2) and Cl(1)'. The deviation from ideal geometry is illustrated by the bond angles Cl(1)'-Ni(1)-Cl(2) = 175.01(4)°, N(2)-Ni(1)-N(10) = 152.90(4)° and N(1)-Ni(1)-Cl(1) = 167.05(4)°, which are significantly different

from the ideal angles of 180°. The nickel(II) cations are separated by a distance of 3.6Å.

The bond length between the axial atom Cl(2) and Ni is 2.3518(6)Å, which is almost identical to the Ni(1)-Cl(1) bond length of 2.3563(6)Å. However, the distance between the manganese(II) cation and the bridging axial chloride ion Cl(1)' is significantly longer at 2.4537(6)Å. The remaining equatorial bond lengths are Ni(1)-N(2) = 2.2974(6)Å, Ni(1)-N(10) = 2.2219(5)Å and Ni(1)-N(1) = 1.9866(5)Å.

With regard to the planarity of the ligand backbone, the phenyl rings are twisted by 5.533(1)° and 8.338(2)° relative to the phenanthroline plane and the nickel(II) cation is displaced by 0.207Å. Each unit cell, which contains one dimer of $[NiCl_2(L^{Phen\text{-}1})]_2$, is also occupied by two non-interacting molecules of $CHCl_3$ and two and a half molecules of EtOH.

2.2.4.4 Structure Determination of $[CuCl_2(L^{Phen\text{-}0})]$

X-ray crystallographic studies on single crystals of $[CuCl_2(L^{Phen\text{-}0})]$ demonstrated that the complex has distorted square-based pyramidal coordination geometry, confirmed by a τ parameter value of 0.167 (Figure 2.9). Once again, the basal plane is defined by Cl(1)-N(2)-N(1)-N(10) and the axial site is occupied by the Cl(2) ion. Instead of ideal angles of 180°, 180° and 90°, the $[CuCl_2(L^{Phen\text{-}0})]$ complex exhibits distorted angles of N(1)-Cu(1)-Cl(1) = 145.50(6)°, N(2)-Cu(1)-N(10) = 155.52(7)° and Cl(1)-Cu(1)-Cl(2) = 108.39(3)°. The copper(II) cation is displaced from the basal plane by 0.428Å toward Cl(2). Interestingly, for this complex the length of the bond Cu(1)-Cl(2) is significantly longer than the Cu(1)-Cl(1) bond. In all of the other

complexes the distances are almost identical, but for $[CuCl_2(L^{Phen\text{-}0})]$ Cu(1)-Cl(2) = 2.3949(7)Å and Cu(1)-Cl(1) = 2.2385(7)Å. The bond lengths Cu(1)-N(2) and Cu(1)-N(10) are 2.153(2)Å and 2.2004(19)Å, respectively. A shorter bond relative to the previous two Cu-N bonds is once again observed for the central nitrogen donor to metal bond, Cu(1)-N(1). This has a bond length of 1.9513(19)Å.

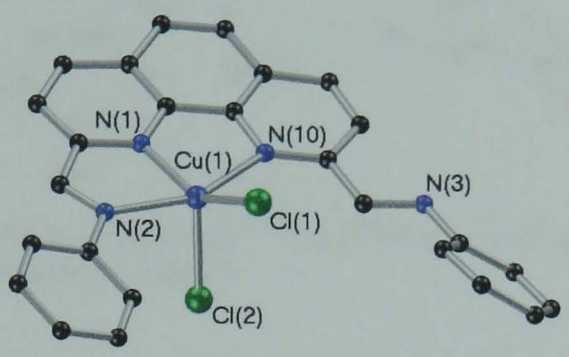

Figure 2.9. Crystal structure of $[CuCl_2(L^{Phen\text{-}0})].2CHCl_3$. Hydrogen atoms and solvents of crystallisation have been omitted for clarity.

The phenyl rings have substantial torsion angles relative to the phenanthroline plane. The rings are twisted at angles of 18.07(2)° and 36.4(1)°, severely disrupting the planarity of the ligand backbone. The copper(II) cation had minimal effect on the perturbation of the planarity of the ligand, with a displacement from the phenanthroline plane of 0.108Å. There are two molecules of $CHCl_3$ per $[CuCl_2(L^{Phen\text{-}0})]$ occupying the cavities in the structure.

2.2.4.5 Structure Determination of $[ZnCl_2(L^{Phen\text{-}1})]$

A structure determination by X-ray crystallography of $[ZnCl_2(L^{Phen\text{-}1})]$ revealed that the coordination geometry of the complex is distorted trigonal bipyramidal (Figure 2.10) and the τ parameter has been calculated as 0.470. The axial angle N(2)-Zn(1)-N(10) = 149.58(11) is much more acute than the ideal angle of 180°. However, the bond angles in the equatorial plane are

much less distorted from the ideal angle of 120° and angles of 121.39°, 121.85(9)° and 116.74(4)° were measured for N(1)-Zn(1)-Cl(1), N(1)-Zn(1)-Cl(2) and Cl(2)-Zn(1)-Cl(1), respectively.

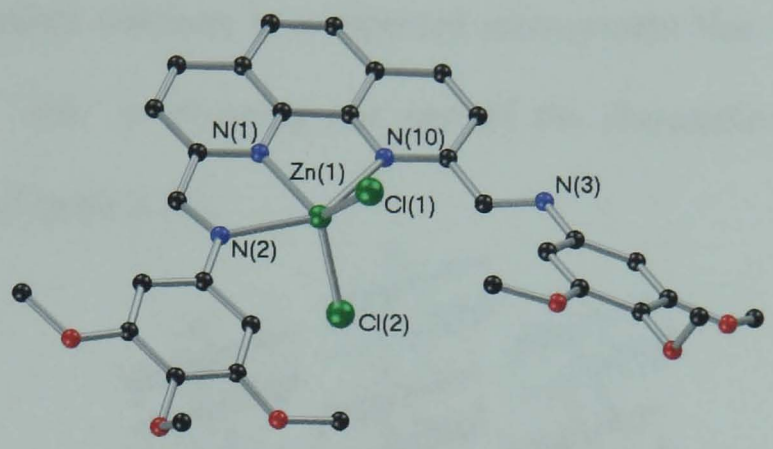

Figure 2.10. Crystal structure of $[ZnCl_2(L^{Phen\text{-}1})].2CHCl_3$. Hydrogen atoms and solvents of crystallisation have been omitted for clarity.

Bonds from the zinc(II) cation to the chloride anions Cl(1) and Cl(2) are almost identical in length being 2.2429(10)Å and 2.2501(10)Å. In accordance with the aforementioned $[MnCl_2(L^{Phen\text{-}1})]_2$, $[CoCl_2(L^{Phen\text{-}1})]$, $[CuCl_2(L^{Phen\text{-}0})]$ and $[NiCl_2(L^{Phen\text{-}1})]_2$ complexes, the Zn(1)-N(1) bond is considerably shorter than the Zn(1)-N(2) and Zn(1)-N(10) bonds. The latter two are 2.302(3)Å and 2.350(3)Å in length, whereas the former is 2.048(3)Å long.

The zinc(II) cation lies in the phenanthroline plane, with the lateral phenyl rings twisted by angles of 18.69(5)° and 26.507(8)°. Two non-interacting molecules of $CHCl_3$ per $[ZnCl_2(L^{Phen\text{-}1})]$ occupy cavities in the structure.

2.2.4.6 Packing Diagrams of the Complexes

In order to ascertain how the complexes self-assemble in the solid state with respect to one another, packing diagrams were produced.

The absence of overlap between the two halves of the asymmetrically bridged 'disk' $[MnCl_2(L^{Phen\text{-}1})]_2$ implies that intermolecular π-π stacking is not present within each 'disk'.[15] However, packing studies show that these pseudo disks stack in tilted columns in a repeated arrangement that sees the phenyl ring from one 'disk' overlapping one part of the phenanthroline ring of an adjacent 'disk' (Figure 2.11).

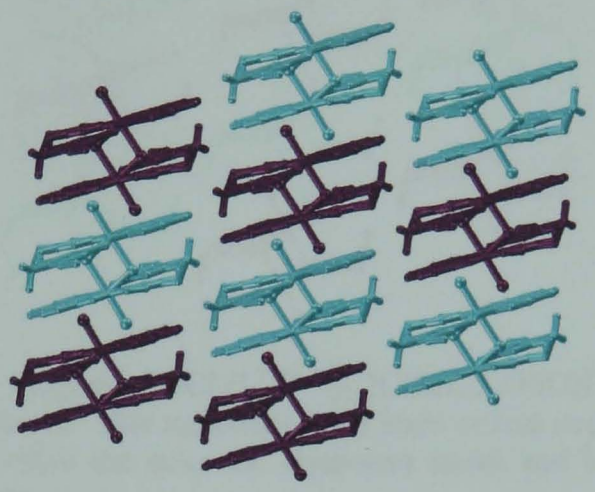

Figure 2.11. Packing diagram of $[MnCl_2(L^{Phen\text{-}1})]_2.2CH_2Cl_2$ showing the columnar arrangement of the complexes. The molecules have been colour coded to show how pairs of molecules are arranged within the columns. Hydrogen atoms and solvents of crystallisation have been omitted for clarity.

The intermolecular distance between the centroid points of the phenanthroline and phenyl rings of each 'disk' is 4.47Å. Due to the twist in the phenyl rings, co-planarity between adjacent 'disks' is offset by an angle of 3.3°. Hence, complexes of $[MnCl_2(L^{Phen\text{-}1})]_2$ self-assemble into columnar-type arrangements in the solid state.

Complexes of $[NiCl_2(L^{Phen\text{-}1})]_2$ pack in an identical manner to complexes of $[MnCl_2(L^{Phen\text{-}1})]_2$ (Figure 2.12). Within each dimer, or 'disk', there is no intra-disk overlap of phenyl and phenanthroline rings. The packing diagram revealed that pairs of molecules stack in tilted columns with alternating overlap of the phenyl ring from one 'disk' with part of the phenanthroline ring from an adjacent 'disk'. Each disk is separated by 4.52Å at the centroid points of the overlapping phenyl and phenanthroline rings.

Negligible π-π interactions are indicated by the long distance between the centroid points and the slight deviation from co-planarity of 5.8° between the phenyl and phenanthroline rings.[15] Hence, $[NiCl_2(L^{Phen\text{-}1})]_2$ complexes also self-assemble into columnar-type arrangements in the solid state.

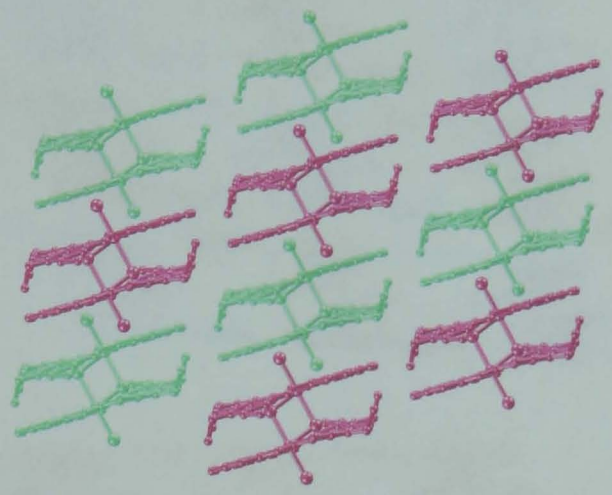

Figure 2.12. Packing diagram $[NiCl_2(L^{Phen\text{-}1})]_2.2CHCl_3.2.5EtOH$ showing the columnar arrangement of the complexes. The molecules have been colour coded to show how pairs of molecules are arranged within the columns. Hydrogen atoms and solvents of crystallisation have been omitted for clarity.

Packing diagrams of $[CoCl_2(L^{Phen\text{-}1})]$ and $[ZnCl_2(L^{Phen\text{-}1})]$ show that the molecules are arranged as pseudo disks which stack, stepwise, in tilted columns (Figures 2.13(a) and 2.13(b)). The arrangement is very similar to the packing diagrams for $[MnCl_2(L^{Phen\text{-}1})]_2$ and $[NiCl_2(L^{Phen\text{-}1})]_2$, except that the molecules are tilted at an angle to allow the phenyl rings to occupy space between the columns.

Thus, pairs of molecules of $[CoCl_2(L^{Phen\text{-}1})]$ and $[ZnCl_2(L^{Phen\text{-}1})]$ are stacked with alternating partial head-to-head overlap of phenanthroline rings, followed by head-to-tail overlap of phenanthroline-phenyl rings (Figures 2.14(a) and 2.14(b)).

The separation between the centroid points in the overlapping phenanthroline rings is 3.51Å for $[ZnCl_2(L^{Phen\text{-}1})]$ and 3.52Å for $[CoCl_2(L^{Phen\text{-}1})]$. In head-to-tail overlap, the separation between the

phenanthroline and phenyl ring centroid points is 4.41Å for $[ZnCl_2(L^{Phen\text{-}1})]$ and 4.50Å for $[CoCl_2(L^{Phen\text{-}1})]$.

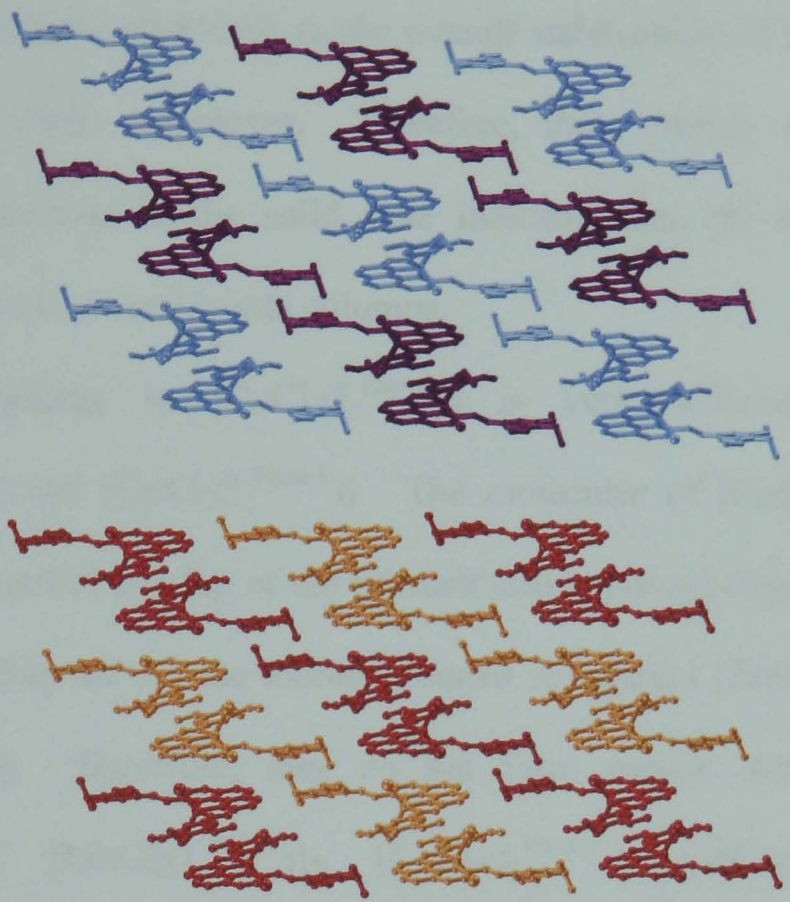

Figure 2.13. Packing diagrams of (a) $[CoCl_2(L^{Phen\text{-}1})].2CHCl_3$ and (b) $[ZnCl_2(L^{Phen\text{-}1})].2CHCl_3$ showing the columnar stacking of the molecules as viewed along the 'b' axis. The molecules have been colour coded to show how pairs of molecules are arranged within the columns. Hydrogen atoms and solvents of crystallisation have been omitted for clarity.

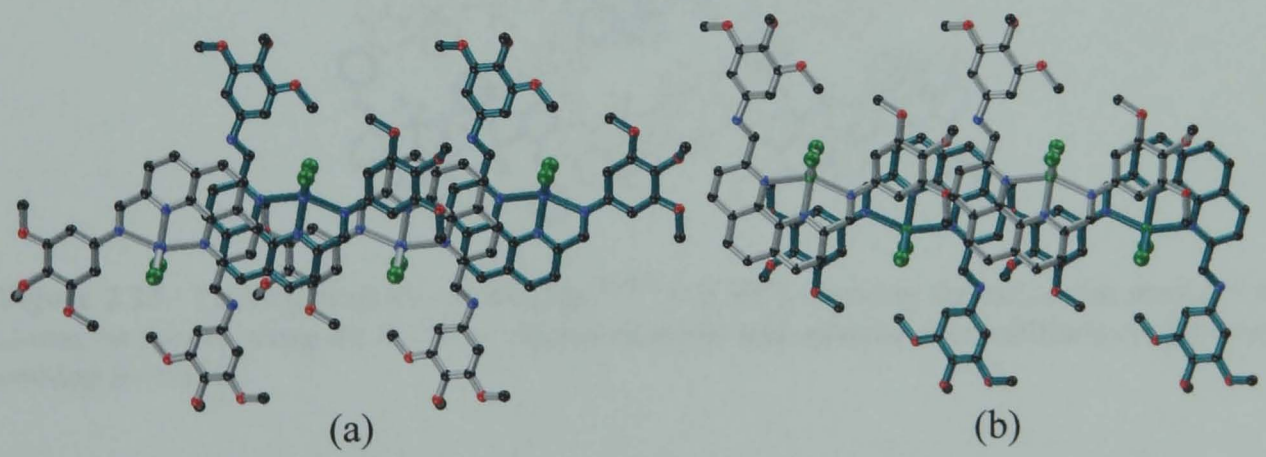

Figure 2.14. Packing diagrams of (a) $[CoCl_2(L^{Phen\text{-}1})].2CHCl_3$ and (b) $[ZnCl_2(L^{Phen\text{-}1})].2CHCl_3$ showing the alternating phenanthroline-phenanthroline and phenanthroline-phenyl ring overlap as viewed along the 'a' axis. Hydrogen atoms and solvents of crystallisation have been omitted for clarity.

Molecules of $[ZnCl_2(L^{Phen\text{-}1})]$ are parallel displaced by 3.09Å, while in $[CoCl_2(L^{Phen\text{-}1})]$ molecules are offset by 3.38Å. The proximity of the co-planar phenanthroline rings implies that there are π-π interactions within the system,[15] and such interactions contribute to the overall stabilisation of the mesophases in the longer chain complexes. Therefore, these studies of zinc(II) and cobalt(II) compounds in the solid state indicated that the molecules were predisposed to self-assemble into columns.

The packing in $[CuCl_2(L^{Phen\text{-}0})]$ is very different to that in $[ZnCl_2(L^{Phen\text{-}1})]$ and $[CoCl_2(L^{Phen\text{-}1})]$. The molecules of $[CuCl_2(L^{Phen\text{-}0})]$ are arranged with partial overlap of the phenanthroline-phenyl rings, but with less overlap than observed for the aforementioned complexes $[ZnCl_2(L^{Phen\text{-}1})]$ and $[CoCl_2(L^{Phen\text{-}1})]$. Therefore, they do not form pseudo disks, unlike the complexes of $[MnCl_2(L^{Phen\text{-}1})]_2$, $[CoCl_2(L^{Phen\text{-}1})]$, $[NiCl_2(L^{Phen\text{-}1})]_2$ and $[ZnCl_2(L^{Phen\text{-}1})]$, but form layers of chains (Figure 2.15).

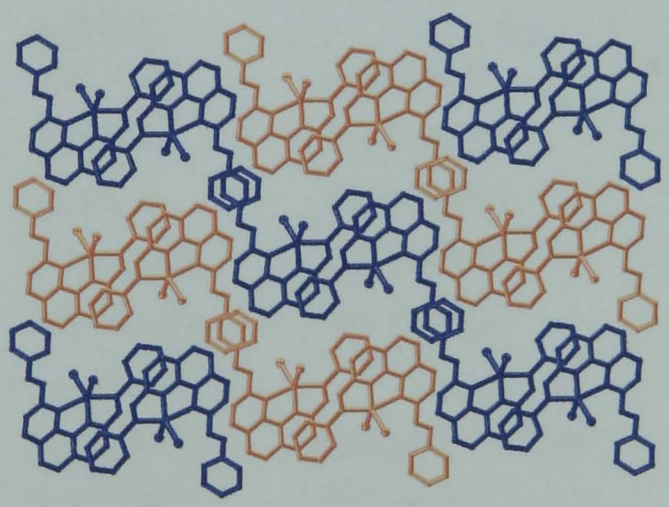

Figure 2.15. Packing diagram of $[CuCl_2(L^{Phen\text{-}0})].2CHCl_3$ showing the molecules arranged in chains, as viewed along the 'b' axis. Hydrogen atoms and solvents of crystallisation have been omitted for clarity.

The overlap between the phenanthroline–phenyl rings in $[CuCl_2(L^{Phen\text{-}0})]$ occurs at an angle of 19.3° and distance of 3.97Å, and we believe that the lack of co-planarity is an obstruction to π-π interactions.[15]

Likewise, the separation of 11.5Å between the layers of chains also rules out the possibility of π-π stacking. This inter-layer distance is far greater than the inter-columnar distances observed for all the other first-row transition metal complexes discussed here.

Table 2.1. Selected bond lengths [Å] and angles [°] for $[MnCl_2(L^{Phen\text{-}1})]_2.2CH_2Cl_2$, $[CoCl_2(L^{Phen\text{-}1})].2CHCl_3$, $[CuCl_2(L^{Phen\text{-}0})].2CHCl_3$, and $[NiCl_2(L^{Phen\text{-}1})]_2.2CHCl_3.2.5EtOH$.

Mn(1)-N(1)	2.180(1)	Ni(1)-N(1)	1.9866(5)
Mn(1)-N(2)	2.386(1)	Ni(1)-N(2)	2.2974(6)
Mn(1)-N(10)	2.388(1)	Ni(1)-N(10)	2.2219(5)
Mn(1)-Cl(2)	2.411 (1)	Ni(1)-Cl(2)	2.3518(6)
Mn(1)-Cl(1)	2.413(1)	Ni(1)-Cl(1)	2.3563(6)
Mn(1)-Cl(1)'	2.744(1)	Ni(1)-Cl(1)'	2.4537(6)
N(2)-Mn(1)-N(10)	144.19(8)	N(2)-Ni(1)-N(10)	152.90(4)
N(1)-Mn(1)-Cl(1)	157.18(9)	N(1)-Ni(1)-Cl(1)	167.05(4)
Cl(2)-Mn(1)-Cl(1)'	177.0(1)	Cl(2)-Ni(1)-Cl(1)'	175.01(4)
N(1)-Mn(1)-Cl(2)	103.13(6)	N(1)-Ni(1)-Cl(2)	94.86(2)
Twist of phenyl rings	3.032(1) 3.603(2)	Twist of phenyl rings	5.533(1) 8.338(2)
Co(1)-N(1)	2.021(3)	Cu(1)-N(1)	1.9513(19)
Co(1)-N(2)	2.268(3)	Cu(1)-N(2)	2.153(2)
Co(1)-N(10)	2.284(3)	Cu(1)-N(10)	2.2004(19)
Co(1)-Cl(2)	2.2655(12)	Cu(1)-Cl(1)	2.2385(7)
Co(1)-Cl(1)	2.2741(12)	Cu(1)-Cl(2)	2.3949(7)
N(2)-Co(1)-N(10)	151.62(12)	N(2)-Cu(1)-N(10)	155.52(7)
N(1)-Co(1)-Cl(1)	122.74(10)	N(1)-Cu(1)-Cl(1)	145.50(6)
N(1)-Co(1)-Cl(2)	121.75(10)	N(1)-Cu(1)-Cl(2)	106.11(6)
Cl(2)-Co(1)-Cl(1)	115.51(5)	Cl(1)-Cu(1)-Cl(2)	108.39(3)
Twist of phenyl rings	10.3(1) 27.44(2)	Twist of phenyl rings	18.07(2) 36.4(1)

Table 2.2. Selected bond lengths [Å] and angles [°] for $[ZnCl_2(L^{Phen\text{-}1})].2CHCl_3$.

Zn(1)-N(1)	2.048(3)
Zn(1)-N(2)	2.302(3)
Zn(1)-N(10)	2.350(3)
Zn(1)-Cl(1)	2.2429(10)
Zn(1)-Cl(2)	2.2501(10)
N(2)-Zn(1)-N(10)	149.58(11)
N(1)-Zn(1)-Cl(1)	121.39(9)
N(1)-Zn(1)-Cl(2)	121.85(9)
Cl(2)-Zn(1)-Cl(1)	116.74(4)
Twist of phenyl rings	18.69(5) 26.507(8)

2.2.5 Liquid Crystalline Properties of $[MCl_2(L^{Phen\text{-}n})]$ and $L^{Phen\text{-}n}$

The liquid crystalline behaviour of the metal-free ligands and complexes was characterised by polarised optical microscopy, differential scanning calorimetry and, where possible, small-angle X-ray diffraction.

Out of the six series of metal complexes, four of the series, plus the free ligands, are liquid crystalline. The $[FeCl_2(L^{Phen\text{-}n})]$ and $[CuCl_2(L^{Phen\text{-}n})]$ series are non-mesomorphic, in common with analogous pyridine complexes prepared by Morale in Nottingham.[16] When heated on the hot stage of a polarised optical microscope, the $[FeCl_2(L^{Phen\text{-}n})]$ and $[CuCl_2(L^{Phen\text{-}n})]$ compounds decompose, since they can undergo redox reaction with oxygen and consequently do not generate liquid crystalline mesophases.

Complexes of $[MnCl_2(L^{Phen\text{-}n})]$, $[CoCl_2(L^{Phen\text{-}n})]$, $[NiCl_2(L^{Phen\text{-}n})]$ and $[ZnCl_2(L^{Phen\text{-}n})]$ are non-liquid crystalline at room temperature, but on heating convert into one or more mesophases (with the exception of $[CoCl_2(L^{Phen\text{-}8})]$, which is non-mesomorphic). The clearing points occur over wide biphasic regions due to decomposition being observed. This reflects a problem often encountered with metallomesogens, that is the tendency to decompose around

the clearing point.[17] As a result of this thermal instability, some transitions were not detectable by DSC and repeated heating-cooling cycles were not possible. Therefore, the DSC traces tended to show either the melting or the clearing transition, but not usually both. As a result of this, a combination of POM and DSC was required to detect all phase transitions.

The mesophases generated were all columnar mesophases, as predicted by use of the complimentary shape approach.[8] This was indicated by the textures observed by POM, which were often dendritic, with regions of fern-like texture and areas of extinction (Figure 2.16). On cooling the compounds, the viscosity of the compounds increased until a glassy texture was observed.

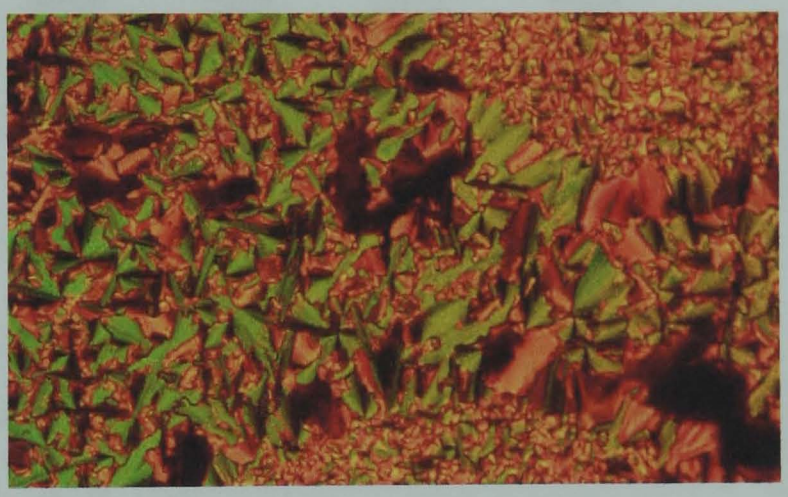

Figures 2.16. Examples of a POM texture for $[CoCl_2(L^{Phen\text{-}12})]$, illustrating the columnar symmetry of the complexes.

The combined data collected from POM and DSC was sufficient to determine the temperature ranges of the columnar mesophases, whereas small-angle X-ray diffraction was required to determine the 2D symmetry of the columnar phases. These combined results are detailed in Tables 2.3 – 2.7.

2.2.5.1 Mesomorphic Properties of $[MnCl_2(L^{Phen\text{-}n})]$

The series of complexes $[MnCl_2(L^{Phen\text{-}n})]$ generated the richest variety of mesophases, which occur between 45 and 201°C (Chart 2.1 and Table 2.3),

and this series had the widest mesomorphic range of all the phenanthroline metallomesogens. The largest range from 55 to 201°C occurred for the $n = 14$ complex, and the shortest range was 50°C for the $n = 16$ complex, which was less than half the range of the other complexes in the series. There was no obvious trend to the change in clearing or melting temperatures with aliphatic chain length, which is most likely due to differing amounts of decomposition.

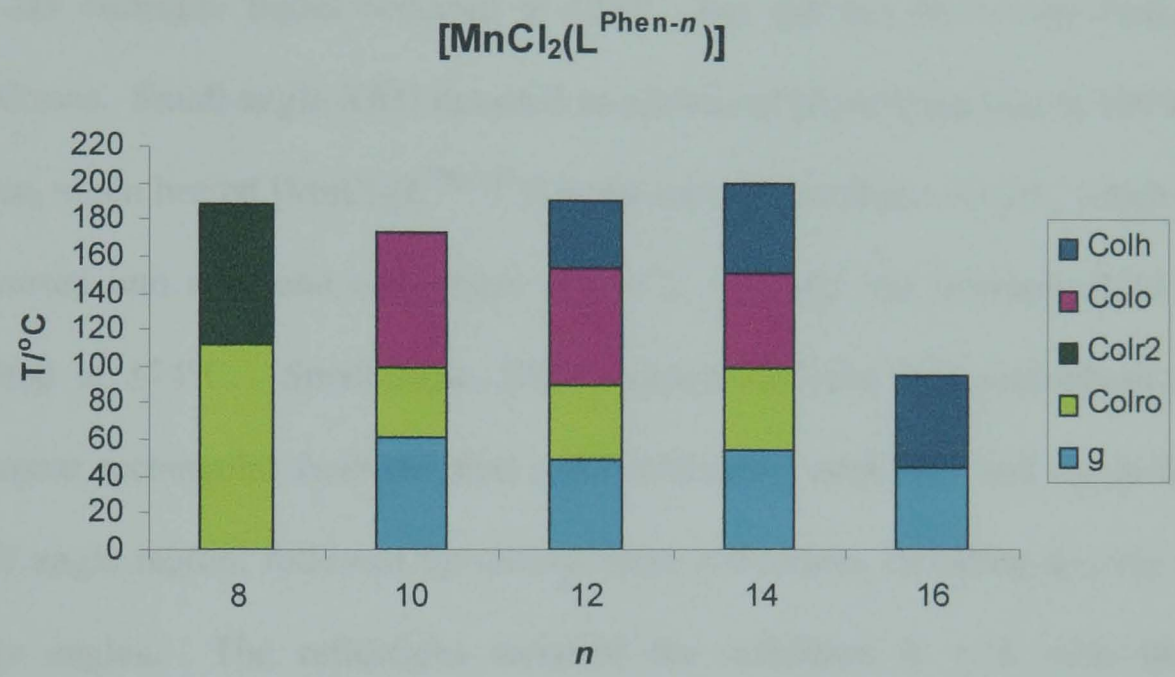

Chart 2.1. Phase diagram representing the transition temperatures of the compounds $[MnCl_2(L^{Phen\text{-}n})]$ (where Col_h, Col_r and Col_o are columnar hexagonal, rectangular and oblique, respectively; Col_{ro} is an ordered columnar rectangular phase; g is the glass transition temperature).

The DSC trace for the $[MnCl_2(L^{Phen\text{-}8})]$ complex displayed two broad, flat peaks at 112°C and 188°C. The smaller peak at 112°C corresponded to a mesophase-mesophase transition and the larger peak at 188°C corresponded to the mesophase-isotropic liquid transition. The solid-to-liquid crystal melting transition was not detected due to decomposition. Small-angle XRD characterised the 2D symmetry of both mesophases as two columnar rectangular phases. These were identified by two first order reflections in the small-angle region corresponding to d_{11} and d_{20}, respectively. Additional second order reflections at wider angles confirmed the characterisation of the

two rectangular columnar phases Col_{r1} and Col_{r2} as *c2mm* lattices, since $h + k = 2n$.

Increasing the chain length to 10 carbon atoms to produce $[MnCl_2(L^{Phen\text{-}10})]$ had the effect of lowering the clearing temperature relative to $[MnCl_2(L^{Phen\text{-}8})]$. POM detected the melting temperature of the solid into the liquid crystalline phase at 62°C. DSC confirmed that the clearing temperature into the isotropic liquid occurred at 174°C, but did not detect any further transitions. Small-angle XRD detected an additional phase transition at 100°C. Hence, when heated $[MnCl_2(L^{Phen\text{-}10})]$ melts into a mesophase at 62°C which is converted into a second mesophase at 100°C. Finally, the isotropic fluid is reached at 174°C. Small-angle XRD characterised the first mesophase as columnar rectangular from the first order diffraction peaks d_{11} and d_{20} in the small angle region, followed by second order reflections including d_{22}, d_{31} at wider angles. The reflections satisfied the condition $h + k = 2n$, thus characterising the space group as *c2mm*. The second mesophase was characterised as columnar oblique from the distinctive appearance of three fundamental reflections in the small angle region corresponding to d_{11}, d_{20} and $d_{1\text{-}1}$.

Characterisation of $[MnCl_2(L^{Phen\text{-}12})]$ by POM confirmed that the solid melted into a mesophase at 49°C and cleared into the isotropic liquid at 191°C. The DSC trace displayed two broad, flat peaks at 154°C and 191°C corresponding to a mesophase that was not detected by POM and the clearing temperature, respectively. In addition to the two mesophases detected by POM and DSC, small-angle XRD confirmed the formation of a third mesophase at 154°C. The first mesophase between 49°C and 90°C was characterised as

columnar rectangular. The diffraction pattern displayed two intense reflections followed by a weaker second order reflection, which corresponded to the spacings d_{11}, d_{20} and d_{22}, respectively. These reflections satisfied the condition $h + k = 2n$, hence the space group was determined as *c2mm*. The second mesophase between 90°C and 154°C was characterised by the occurrence of three fundamental reflections in the small-angle region. The peaks corresponded to the spacings d_{11}, d_{20} and $d_{1\text{-}1}$, which are indicative of a columnar oblique phase. The third mesophase between 154°C and 191°C produced a diffraction pattern that contained a single first order reflection corresponding to d_{10} and was accordingly characterised as columnar hexagonal. Thus, $[MnCl_2(L^{Phen\text{-}12})]$ forms three mesophases, columnar rectangular, oblique and hexagonal. What is particularly interesting about this is the order in which these mesophases are generated. As the compounds are heated, the 2D symmetry changes from columnar rectangular to the more *ordered* columnar oblique phase instead of a more disordered phase, such as columnar hexagonal. At higher temperatures the columnar hexagonal phase is indeed formed before the complex clears into the isotropic liquid.

The complex $[MnCl_2(L^{Phen\text{-}14})]$ has very similar mesomorphic properties to $[MnCl_2(L^{Phen\text{-}12})]$. POM evidenced the melting of the solid to the liquid crystalline phase at 55°C. The DSC trace showed three phase transitions at 100°C, 151°C and 201°C, and characterisation by small-angle XRD confirmed these three mesophases to be columnar rectangular, oblique and hexagonal, respectively. The unusual phase sequence is the same as for $[MnCl_2(L^{Phen\text{-}12})]$, and we can currently offer no explanation for this interesting but curious observation.

The complex $[MnCl_2(L^{Phen\text{-}16})]$ formed a single mesophase. This complex exhibited the lowest melting temperature recorded for any of the $[MnCl_2(L^{Phen\text{-}n})]$ complexes and an unusually low clearing point. POM and DSC confirmed a melting temperature of 45°C and a clearing temperature of 95°C. The diffraction pattern recorded by small-angle XRD characterised the mesophase as columnar hexagonal from the first and second order reflections in the ratio 1:√3, corresponding to d_{10} and d_{11} reflections.

Some general inferences about the influence of the aliphatic chain length on the columnar parameters may be drawn from lattice parameters calculated from the XRD data (shown in Table 2.3). Due to the XRD data being collected at various temperatures and the limited amount of data collected, it should be emphasised that these are inferred rather than absolute conclusions. Examination of the *a* lattice parameters, which refer to the diameter of an individual column, indicate that as the aliphatic chain length is increased the diameter of an individual column also increases. If the *a* lattice parameters of the columnar rectangular mesophases are compared in order of ascending chain length it is apparent that the *a* parameter increases. This is also true for the columnar oblique and columnar hexagonal lattice parameters. Accordingly, as the diameter of an individual column increases with increasing chain length so to does the columnar area, *S*. The only exception to this is for $[MnCl_2(L^{Phen\text{-}14})]$, which has a smaller *S* parameter relative to $n < 14$ resulting from a small *b* parameter. This anomalous result aside, the observation that the diameter and area of an individual column increase with increasing aliphatic chain length is in agreement with our expectations. It follows that as the length of the peripheral chains grows so too does the molecular volume of the

compound, which in turn will increase the diameter and surface area of each column.

Table 2.3. Table showing the combined POM, DSC and XRD data to give the mesophase transition temperatures for $[MnCl_2(L^{Phen\text{-}n})]$. Also included, where possible, are detailed indexation information obtained by XRD studies (where ***n*** = number of carbons in aliphatic chains; **T** = temperature at which data was taken; d_{meas}, and d_{calc} are the measured and calculated diffraction spacings, respectively; ***hk*** is the indexation of the two-dimensional lattice; a, b, and γ are the lattice parameters and S is the lattice area of the hexagonal (Col_h), (ordered) rectangular (Col_{ro}, Col_r) and oblique (Col_o) columnar phases; *p6mm*, *p2gg*, *c2mm* and *p1*are the 2D space groups of the corresponding hexagonal, rectangular and oblique mesophases; I is the isotropic liquid.

n	**T/°C**	$d_{meas.}$/Å	***hk***	$d_{calc.}$/Å	**Mesophase**	**Transitions/°C**
8	80	25.6	11	25.6	Col_r-*c2mm*	Col_{ro} 112 Col_{r2} 188 I
		19.7	20	19.7	a = 39.4Å	
		11.9	31	12.2	b = 33.7Å	
		10.0	40	9.85	S = 1330Å^2	
		4.5	br			
	160	24.5	11	24.5	Col_r-*c2mm*	
		20.9	20	20.9	a = 41.8Å	
		12.3	22	12.25	b = 30.2Å	
		10.3	40	10.45	S = 1265Å^2	
		4.5	br			
10	80	28.4	11	28.4	Col_r-*c2mm*	g 56 Col_{ro} 100 Col_o 174 I
		20.6	20	20.6	a = 41.2Å	
		14.1	22	14.2	b = 39.2Å	
		12.7	31	13.0	S = 1615Å^2	
		10.2	40	10.3		
		9.4	33	9.45		
		4.5	br			
	160	30.2	11	30.2	Col_o-*p1*	
		26.6	20	26.6	a = 56.6Å	
		22.5	1-1	22.54	b = 30.9Å	
		14.5	02	14.55	γ = 70°	
		13.5	40	13.3	S = 1645Å^2	
		13.25	3-1	13.25		
		9.7	03	9.7		
		4.5	br			
12	80	31.2	11	31.2	Col_r-*c2mm*	g 49 Col_{ro} 90 Col_o 154 Col_h 191 I
		21.35	20	21.35	a = 42.7Å	
		15.5	22	15.6	b = 45.7Å	
		4.5	br		S = 1950Å^2	
	140	32.9	11	32.9	Col_o-*p1*	
		28.3	20	28.3	a = 60.7Å	
		23.95	1-1	23.95	b = 33.6Å	
		15.4	02	15.6	γ = 69°	
		14.0	40	14.1	S = 1900Å^2	
		4.5	br			

	160	32.0 4.5	10 br	32.0	Col_h-*p6mm* a = 36.95Å S = 1180Å^2	
14	80	29.5 24.6 16.0 14.8 13.4 10.6 8.4 4.5	20 11 31 40 02 51 33 br	29.5 24.6 15.9 14.75 13.2 10.8 8.2	Col_r-*c2mm* a = 59.0Å b = 27.0Å S = 1600Å^2	g 55 Col_{ro} 100 Col_o 151 Col_h 201 I
	140	33.75 29.9 25.85 16.3 14.7 10.9 4.5	11 20 1-1 02 40 03 br	33.75 29.9 25.85 16.6 14.9 11.05	Col_o-*p1* a = 62.8Å b = 34.9Å γ = 72° S = 2085Å^2	
	160	32.8 18.8 16.2 12.1 11.1 4.5	10 11 20 21 30 br	32.6 18.8 16.3 12.3 10.9	Col_h-*p6mm* a = 37.6Å S = 1230Å^2	
16	80	40.1 23.2 4.5	10 11 br	40.15 23.2	Col_h-*p6mm* a = 46.4Å S = 1860Å^2	g 45 Col_h 95 I

2.2.5.2 Mesomorphic Properties of [$CoCl_2(L^{Phen\text{-}n})$]

The cobalt(II) series was the only series to contain a non-mesomorphic long chain complex, [$CoCl_2(L^{Phen\text{-}8})$]. This complex melted straight from the solid into the isotropic liquid at 160°C. All remaining compounds are mesomorphic (Chart 2.2 and Table 2.4).

The liquid crystalline range for this series was between 56°C and 155°C, and as the length of the aliphatic chains increased from n = 10 to 16 carbon atoms, the clearing temperatures ranged from 155°C to 100°C. The melting temperatures followed no logical order, first decreasing, then increasing and finally decreasing in temperature with increasing chain length. This series had the highest melting temperatures of all the phenanthroline

complexes, with an average of 67°C, compared to 53°C, 57°C and 57°C for the $[MnCl_2(L^{Phen\text{-}n})]$, $[NiCl_2(L^{Phen\text{-}n})]$ and $[ZnCl_2(L^{Phen\text{-}n})]$ series, respectively.

Chart 2.2. Phase diagram representing the transition temperatures of the compounds $[CoCl_2(L^{Phen\text{-}n})]$ (where Col_o is a columnar oblique phase; Col_1 and Col_2 are columnar mesophases whose 2D symmetry has yet to be determined; K is the crystalline phase; g is the glass transition temperature).

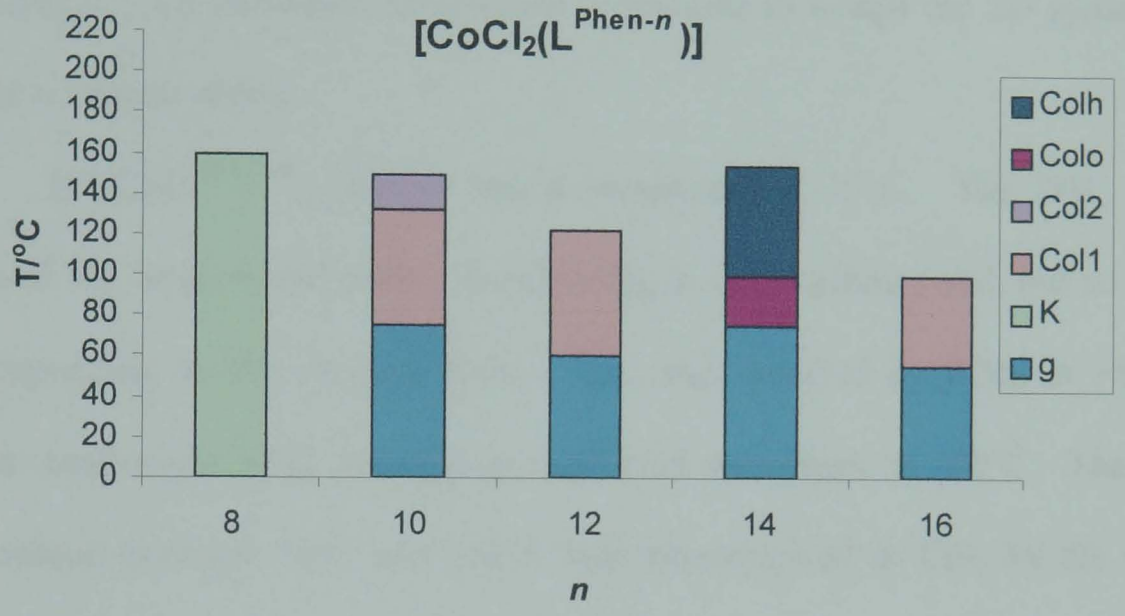

The mesomorphic properties of $[CoCl_2(L^{Phen\text{-}10})]$ were investigated by POM and DSC. DSC indicated that the complex melted into a mesophase at 75°C and this was confirmed by POM. A further two peaks in the DSC trace corresponded to an additional mesophase-mesophase transition at 132°C and mesophase-isotropic liquid transition at 150°C. The platelet texture and areas of extinction observed through crossed polarisers characterised the mesophases as columnar. However, XRD is required for full characterisation of the 2D symmetry.

POM and DSC experiments on $[CoCl_2(L^{Phen\text{-}12})]$ revealed a melting temperature of 69°C and a clearing temperature of 122°C. The platelet texture observed between crossed polarisers was similar to the texture for $[CoCl_2(L^{Phen\text{-}10})]$, indicating that the mesophase was columnar. Characterisation by small-angle XRD indicated that melting into the

mesophase occurred at the slightly lower temperature of 60°C. The discrepancy between characterisation techniques can be explained by the difficulty in assigning the glass transition temperature in POM. due to the increasing viscosity of the sample, and the broad peak in the DSC trace increasing the margin for error. The diffraction pattern generated by $[CoCl_2(L^{Phen\text{-}12})]$ contained insufficient reflections to assign the 2D symmetry of the columnar phase.

$[CoCl_2(L^{Phen\text{-}14})]$ melted into a mesophase at 75°C. The DSC trace showed one large, broad peak corresponding to this melting point, but no peak corresponding to the clearing point. This was detected by POM at 155°C, while small-angle XRD detected an additional mesophase at 100°C. The first mesophase between 75°C and 100°C was characterised as Col_o by the three first-order reflections in the small-angle region of the diffraction pattern, corresponding to d_{11}, $d_{1\text{-}1}$ and d_{20}. The second mesophase between 100°C and 155°C was characterised as columnar hexagonal from growth of the fundamental peak, d_{10}, and the loss of the two smaller peaks relative to the columnar oblique pattern.

Characterisation by POM and DSC of $[CoCl_2(L^{Phen\text{-}16})]$ determined the melting temperature of the solid at 56°C. The DSC trace displayed no further transitions, but POM characterised the isotropic clearing temperature at 100°C. A columnar mesophase was assigned to the complex from the appearance of small platelets in the mesomorphic texture through crossed polarisers. However, the diffraction pattern generated by XRD did not contain sufficient reflections to characterise the phase further.

Currently, the XRD data we have obtained is insufficient to enable us to pass comment on the effect of the length of the aliphatic chains on the structural parameters.

Table 2.4. Table showing the combined POM, DSC and XRD data to give the mesophase transition temperatures for $[CoCl_2(L^{Phen\text{-}n})]$. Also included, where possible, are detailed indexation information obtained by XRD studies (where ***n*** = number of carbons in aliphatic chains; **T** = temperature at which data was taken; d_{meas} and d_{calc} are the measured and calculated diffraction spacings, respectively; ***hk*** is the indexation of the two-dimensional lattice; *a*, *b*, and γ are the lattice parameters and *S* is the lattice area of the oblique (Col_o) columnar phase; *p1* is the 2D space group of the corresponding oblique mesophase; Col_h is a columnar hexagonal mesophase, Col, Col_1 and Col_2 are unidentified columnar mesophases; K is the crystalline phase and I is the isotropic liquid.

n	**T/°C**	$d_{meas.}$/Å	***hk***	$d_{calc.}$/Å	**Mesophase**	**Transitions/°C**
8	-	-	-	-	Non-mesomorphic	K 160 I
10	-	-	-	-	Col_1, Col_2	g 75 Col_1 132 Col_2 150 I
12	80	34.15 24.35 4.5	- - br	-	Col	g 60 Col 122 I
14	80	35.81 30.92 25.26 16.25 4.5	11 1-1 20 31 br	35.81 30.92 25.26 16.25	$Col_o - p1$ a = 51.1 Å b = 44.3 Å γ= 81.5° S =2264Å^2	g 75 Col_o 100 Col_h 155 I
	100	34.48 4.5	10 br	34.48	$Col_h - p6mm$ a = 39.8 Å S = 1373 Å^2	
16	80	39.06 4.5	- br	-	Col	g 56 Col 100 I

2.2.5.3 Mesomorphic Properties of $[NiCl_2(L^{Phen\text{-}n})]$

The five complexes in the nickel(II) series exhibited mesophases in the range 55°C - 151°C (Chart 2.3 and Table 2.5).

$[NiCl_2(L^{Phen\text{-}8})]$ contains the shortest aliphatic chains in the series $[NiCl_2(L^{Phen\text{-}n})]$ and consequently the least amount of liquid-like character. Accordingly, $[NiCl_2(L^{Phen\text{-}8})]$ produced the highest clearing temperature, although the glass transition temperature for this complex was not detected. The remaining clearing temperatures for the complexes $[NiCl_2(L^{Phen\text{-}10})]$,

$[NiCl_2(L^{Phen\text{-}12})]$, $[NiCl_2(L^{Phen\text{-}14})]$ and $[NiCl_2(L^{Phen\text{-}16})]$ were remarkably similar and so did not follow the trend of decreasing in temperature with increased chain length. The glass transition temperatures also remained very similar. Hence for $[NiCl_2(L^{Phen\text{-}n})]$, where n = 10, 12, 14, 16, the length of the aliphatic chains appears to have negligible effect on the transition temperatures.

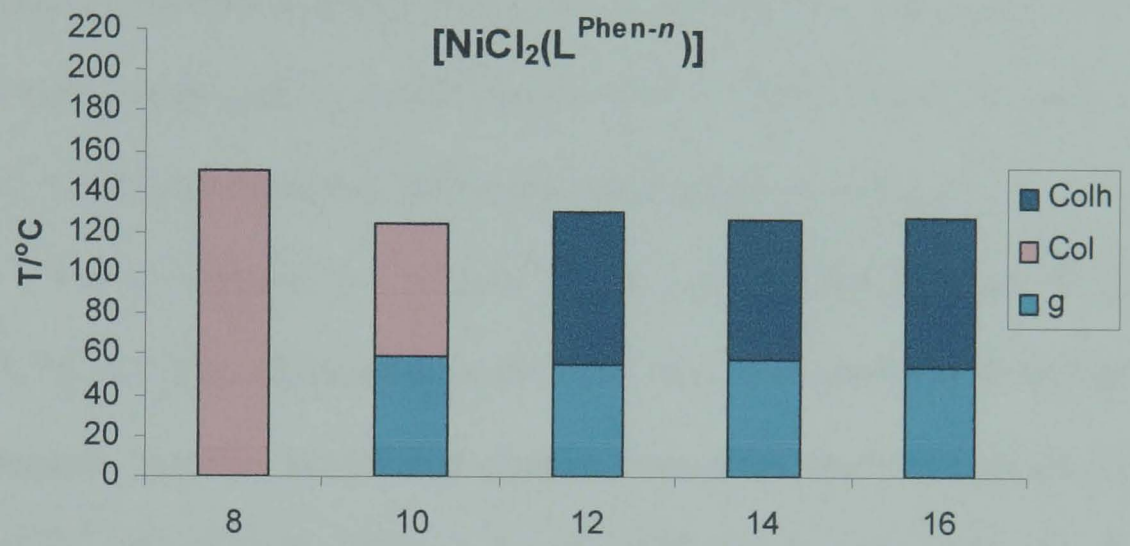

Chart 2.3. Phase diagrams representing the transition temperatures of the compounds $[NiCl_2(L^{Phen\text{-}n})]$ (where Col_h is a columnar hexagonal phase; Col is a columnar mesophase whose 2D symmetry has yet to be determined; g is the glass transition temperature).

The mesomorphic character of $[NiCl_2(L^{Phen\text{-}8})]$ was investigated by POM and DSC. The DSC trace confirmed that the liquid crystal phase cleared at 151°C into the isotropic liquid in agreement with POM observations. However, DSC was unable to detect the initial melting transition into the mesophase, and the cooling of the mesophase to the solid phase was too viscous to determine an accurate temperature with POM. Thus, no melting transition was detected. The generation of a platelet-like texture between crossed polarisers characterised the mesophase as columnar. Further characterisation by XRD is required to establish to 2D symmetry of the columnar phase.

The $[NiCl_2(L^{Phen\text{-}10})]$ complex was also characterised as going through one columnar mesophase by POM and DSC. The DSC trace displayed two broad peaks at 59°C and 125°C in agreement with POM observations.

POM and DSC provided evidence of melting and clearing transitions for $[NiCl_2(L^{Phen\text{-}12})]$ at 56°C and 131°C, respectively. Small-angle XRD confirmed the formation of one columnar phase between these temperatures. The phase was characterised as columnar hexagonal from one intense peak and one much weaker peak in the diffraction pattern. These reflections were in the ratio $1:\sqrt{3}$ and correspond to the hexagonal spacings d_{10} and d_{11}.

The mesophase of $[NiCl_2(L^{Phen\text{-}14})]$ was detected between 58°C and 127°C by one large sharp peak in the DSC trace corresponding to the melting temperature, and the melting and clearing transitions observed through crossed polarisers. Small-angle XRD produced a diffraction pattern with one intense reflection and three weaker reflections in the ratio $1:\sqrt{3}:\sqrt{4}:\sqrt{7}$, which correspond to the columnar hexagonal spacings d_{10}, d_{11}, d_{20} and d_{21}.

$[NiCl_2(L^{Phen\text{-}16})]$ melted into one mesophase at 55°C and cleared into the isotropic liquid at 128°C, as evidenced by POM and the melting transition peak in the DSC trace. Small-angle XRD characterised the mesophase as columnar hexagonal from the one strong and two weak reflections in the diffraction pattern in the ratio $1:\sqrt{3}:\sqrt{4}$, which correspond to the columnar hexagonal spacings d_{10}, d_{11} and d_{20}.

The columnar hexagonal lattice parameters for $[NiCl_2(L^{Phen\text{-}12})]$, $[NiCl_2(L^{Phen\text{-}14})]$ and $[NiCl_2(L^{Phen\text{-}16})]$ confirm the theory that increasing the aliphatic chain length, and hence the molecular volume, results in an increase in columnar diameter and volume.

Table 2.5. Table showing the combined POM, DSC and XRD data to give the mesophase transition temperatures for $[NiCl_2(L^{Phen\text{-}n})]$. Also included, where possible, are detailed indexation information obtained by XRD studies (where ***n*** = number of carbons in aliphatic chains; **T** = temperature at which data was taken; d_{meas} and d_{calc} are the measured and calculated diffraction spacings, respectively; ***hk*** is the indexation of the two-dimensional lattice; *a*, is the lattice parameter and *S* is the lattice area of the hexagonal (Col_h) columnar phase; *p6mm* is the 2D space group of the corresponding hexagonal mesophase; Col is an unidentified columnar mesophase and I is the isotropic liquid.

n	**T/°C**	$d_{meas.}$/Å	***hk***	$d_{calc.}$/Å	**Mesophase**	**Transitions/°C**
8	-	-	-	-	-	Col 151 I
10	-	-	-	-	-	g 59 Col 125 I
12	80	31.47 18.17 4.5	10 11 br	31.47 18.17	Col_h – *p6mm* *a* = 36.3 Å *S* = 1143 Å^2	g 56 Col_h 131 I
14	100	32.67 18.67 16.3 11.78 4.5	10 11 20 21 br	32.54 18.78 16.27 12.30	Col_h – *p6mm* *a* = 37.6 Å *S* =1223Å^2	g 58 Col_h 127 I
16	80	33.6 19.42 16.77 4.5	10 11 20 br	33.6 19.40 16.80	Col_h – *p6mm* *a* = 38.8 Å *S* =1304Å^2	g 55 Col_h 128 I

2.2.5.4 Mesomorphic Properties of $[ZnCl_2(L^{Phen\text{-}n})]$

The mesophases of the complexes $[ZnCl_2(L^{Phen\text{-}n})]$ formed between 50°C and 160°C (Chart 2.4 and Table 2.6). The largest mesomorphic range of 95°C was observed for $[ZnCl_2(L^{Phen\text{-}10})]$, while the smallest range of 45°C corresponded to the complex with the longest aliphatic chain, $[ZnCl_2(L^{Phen\text{-}16})]$. Increasing the length of the aliphatic chains resulted in clearing behaviour typical of many liquid crystals,[18] with the clearing temperature decreasing as the length of the aliphatic chains was increased. This can be explained by the increase in liquid-like character resulting from the additional aliphatic character of the complex. The melting transitions did not however behave in the same manner. Comparison of the glass transition temperatures obtained for $[ZnCl_2(L^{Phen\text{-}10})]$, $[ZnCl_2(L^{Phen\text{-}12})]$, $[ZnCl_2(L^{Phen\text{-}14})]$ and $[ZnCl_2(L^{Phen\text{-}16})]$ confirm a decrease in melting temperature on going from n = 10 to 12, followed by a dramatic increase in melting temperature of 50°C to 70°C from n

= 14 to 16. This indicates that at a certain chain length, in this case n = 14, additional stabilising interactions between the aliphatic chains over-ride the destabilising effect of the long length of the chains.

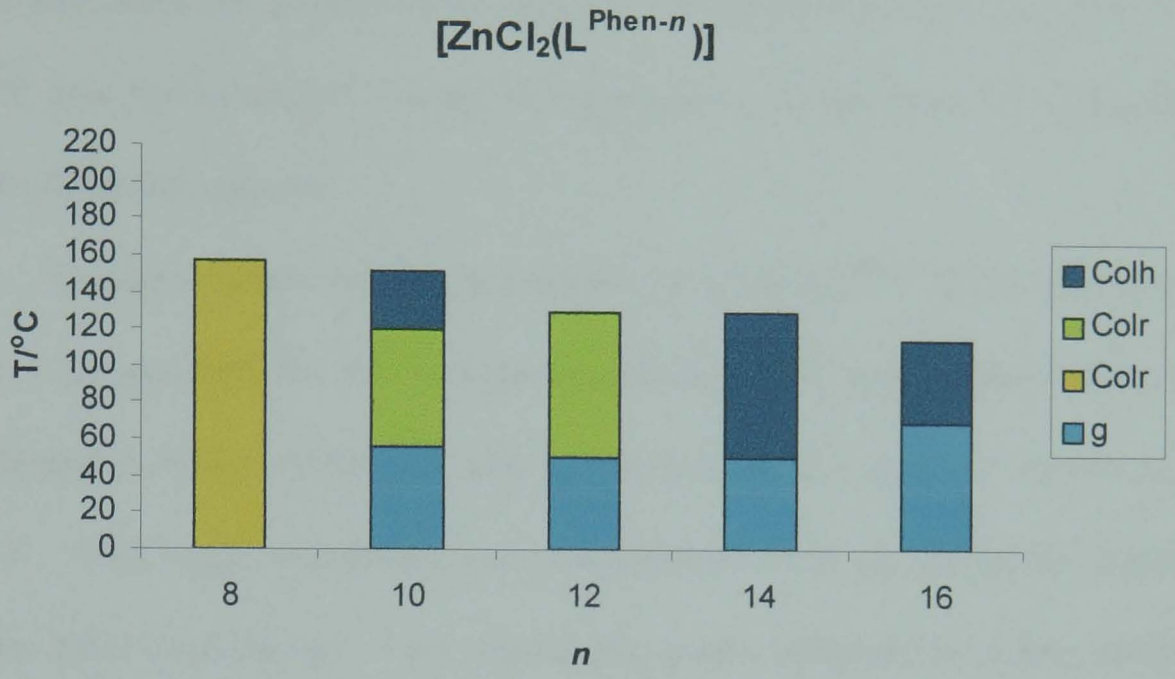

Chart 2.4. Phase diagram representing the transition temperatures of the compounds $[ZnCl_2(L^{Phen\text{-}n})]$ (where Col_h and Col_r are columnar hexagonal and rectangular, respectively; g is the glass transition temperature).

The melting temperature of the complex $[ZnCl_2(L^{Phen\text{-}8})]$ was undetected by POM, DSC and XRD, but the clearing temperature was evidenced at 157°C by a broad peak in the DSC trace. The diffraction pattern from small-angle XRD consisted of two overlapping first order reflections followed by a reflection of less intensity in the small-angle region. The peaks were characterised as the spacings d_{11}/d_{20} and d_{21}. Higher order reflections were present at wider angles, which did not satisfy the condition $h + k = 2n$. On this basis, this phase was characterised as columnar rectangular in the less common space group *p2gg*.

Through crossed polarisers $[ZnCl_2(L^{Phen\text{-}10})]$ melted into a mesophase at 56°C and cleared into the isotropic liquid at 153°C. The clearing temperature was confirmed by a peak at 151°C in the DSC trace. Small-angle XRD

detected a further phase transition at 120°C and characterised both mesophases. The mesophase at 56°C was characterised as columnar rectangular in space group *c2mm* by the twin peaks of d_{11} and d_{20} followed by d_{02} and other higher order reflections in the diffraction pattern. The mesophase between 120°C and 151°C was characterised as columnar hexagonal from the single d_{10} reflection in the diffraction pattern.

Characterisation of the mesophase of $[ZnCl_2(L^{Phen\text{-}12})]$ by DSC only gave a temperature for the melting transition, which along with POM was confirmed at 50°C. POM was able to characterise the isotropic transition at 130°C. This single mesophase was characterised from the diffraction pattern of the XRD experiment. Two overlapping peaks followed by a less intense reflection were characteristic of the d_{11}, d_{20} and d_{02} spacings of a columnar rectangular mesophase. The presence of higher order reflections confirmed that the condition $h + k = 2n$ was satisfied, and hence the space group was derived as *c2mm*.

The complex $[ZnCl_2(L^{Phen\text{-}14})]$ exhibited identical melting and clearing temperatures as $[ZnCl_2(L^{Phen\text{-}12})]$, but whereas $[ZnCl_2(L^{Phen\text{-}12})]$ stabilised the columnar rectangular mesophase $[ZnCl_2(L^{Phen\text{-}14})]$ stabilised the columnar hexagonal phase. The columnar hexagonal mesophase was characterised by the d_{10} and d_{11} reflections in the characteristic ratio of $1:\sqrt{4}$. The d_{20} reflection was not detected in this particular diffraction pattern.

The $[ZnCl_2(L^{Phen\text{-}16})]$ complex also exhibited one columnar hexagonal mesophase, generating an almost identical diffraction pattern to $[ZnCl_2(L^{Phen\text{-}14})]$. However, the mesomorphic range was reduced to between 70°C and 115°C, as characterised by POM. DSC was unable to detect a

measurable peak, due to the broad peaks flattening into the baseline of the DSC trace.

Comparison of the columnar rectangular lattice parameters of $[ZnCl_2(L^{Phen\text{-}8})]$, $[ZnCl_2(L^{Phen\text{-}10})]$ and $[ZnCl_2(L^{Phen\text{-}12})]$ demonstrate that the dimensions of the columns in the mesophase increase with increasing aliphatic chain length (Table 2.6). The lattice parameters of the columnar hexagonal phases of $[ZnCl_2(L^{Phen\text{-}10})]$, $[ZnCl_2(L^{Phen\text{-}14})]$ and $[ZnCl_2(L^{Phen\text{-}16})]$ also evidence the same trend.

Table 2.6. Table showing the combined POM, DSC and XRD data to give the mesophase transition temperatures for $[ZnCl_2(L^{Phen\text{-}n})]$. Also included, where possible, are detailed indexation information obtained by XRD studies (where ***n*** = number of carbons in aliphatic chains; **T** = temperature at which data was taken; $\boldsymbol{d_{meas}}$ and $\boldsymbol{d_{calc}}$ are the measured and calculated diffraction spacings, respectively; ***hk*** is the indexation of the two-dimensional lattice; *a* and *b* are the lattice parameters and *S* is the lattice area of the hexagonal (Col_h) and rectangular (Col_r) columnar phases; *p6mm*, *p2gg* and *c2mm* are the 2D space groups of the corresponding hexagonal and rectangular mesophases; I is the isotropic liquid.

n	**T/°C**	$d_{meas.}$/Å	***hk***	$d_{calc.}$/Å	**Mesophase**	**Transitions/°C**
8	80	25.7	11/20	25.7	Col_r-*p2gg*	Col_r 157 I
		19.5	21	19.4	*a* = 51.4Å	
		12.85	22/40	12.85	*b* = 29.7Å	
		11.4	32	11.2	*S* =1525Å^2	
		10.0	03	9.9		
		8.5	33	8.6		
		4.5	br			
10	80	33.1	11	33.1	Col_r-*c2mm*	g 56 Col_r 120 Col_h 151 I
		28.6	20	28.6	*a* = 57.2Å	
		20.45	02	20.3	*b* = 40.6Å	
		14.2	40	14.3	*S* = 2320Å^2	
		11.9	42	11.7		
		10.9	33	11.0		
		10.1	04	10.1		
		9.4	24	9.6		
		4.5	br			
	140	31.3	10	31.3	Col_h-*p6mm*	
		4.5	br		*a* = 36.1Å	
					S = 1131Å^2	
12	80	35.9	11	35.9	Col_r-*c2mm*	g 50 Col_r 130 I
		31.9	20	31.9	*a* = 63.8Å	
		21.6	02	21.7	*b* = 43.4Å	
		15.9	40	15.95	*S* = 2770Å^2	
		4.5	br			
14	80	37.7	10	37.65	Col_h-*p6mm*	g 50 Col_h 130 I
		21.7	11	21.7	*a* = 43.5Å	
		4.5	br		*S* = 1637Å^2	

16	80	40.3 23.1 4.5	10 11 br	40.15 23.2	Col_h-*p6mm* a = 46.4Å S = 1861Å^2	g 70 Col_h 115 I

From studying the complete data obtained for $[MnCl_2(L^{Phen\text{-}n})]$ and $[ZnCl_2(L^{Phen\text{-}n})]$, it is apparent that the complexes favour the formation of columnar hexagonal over columnar rectangular at longer chain lengths. This mesophase crossover from columnar rectangular to columnar hexagonal has been observed in discotic molecules previously,[18(a),19] and has been attributed to shorter chain complexes favouring the greater core interaction afforded by the formation of a columnar rectangular phase.[20] The tilted columnar rectangular phase reduces the interactions between the bulky aliphatic chains and allows closer contacts between cores. Increasing the number of carbon atoms in the side chains leads to an increase in dispersion forces, which results in the transition to the columnar hexagonal phase with reduced inter-core interactions.

2.2.5.5 Mesomorphic Properties of the Metal-Free Ligands, $L^{Phen\text{-}n}$

The metal-free ligands, $L^{Phen\text{-}n}$, where n = 10, 12, 14 and 16, were also analysed for liquid crystalline behaviour (Chart 2.5 and Table 2.7). These ligands were also found to be mesomorphic.

POM and DSC established that $L^{Phen\text{-}10}$ melted into a liquid crystalline phase at 64°C and cleared into the isotropic liquid at 87°C. Small angle XRD produced a diffraction pattern with reflections in the ratio 1:√3:√4, providing characterisation of the d_{10}, d_{11} and d_{20} reflections of a columnar hexagonal mesophase.

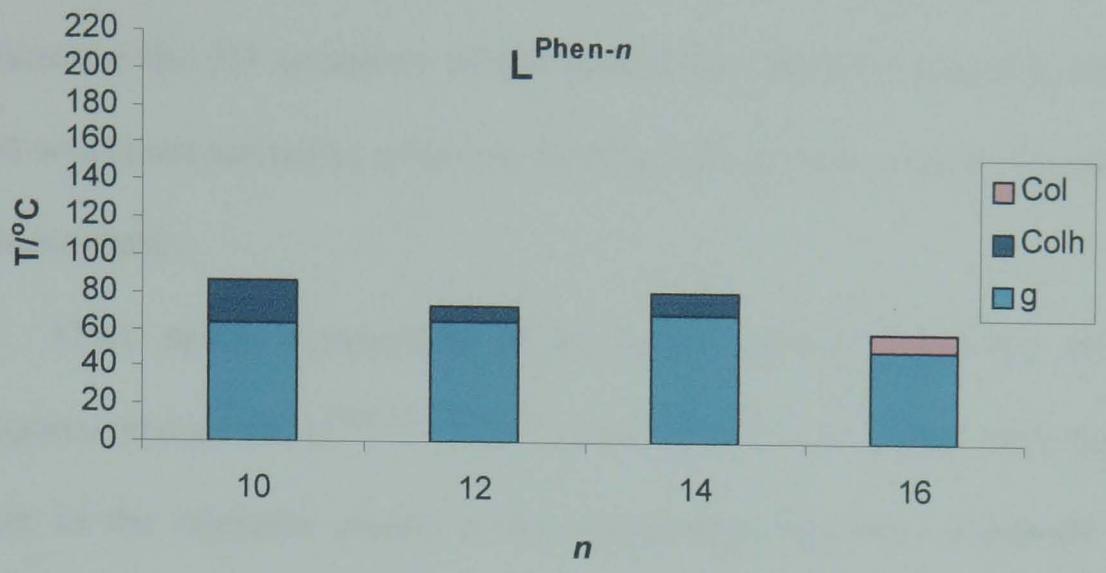

Chart 2.5. Phase diagram representing the transition temperatures of the compounds $L^{Phen\text{-}n}$ (where Col_h is a columnar hexagonal phase; Col is a columnar mesophases whose 2D symmetry has yet to be determined; g is the glass transition temperature).

The DSC trace for $L^{Phen\text{-}12}$ evidenced the melting temperature as a broad peak at 65°C, but did not detect the clearing temperature. POM evidenced the formation of the isotropic liquid at 73°C and confirmed the melting temperature in agreement with DSC measurements. The single mesophase was characterised as columnar hexagonal by the XRD pattern, which showed d_{10}, d_{11} and d_{20} reflections in the ratio $1:\sqrt{3}:\sqrt{4}$.

The mesophase of $L^{Phen\text{-}14}$ was formed at 69°C. The transition was detected in the DSC trace as a large broad peak, but the clearing temperature was not observed by DSC. The transitions were detected through the crossed polarisers of POM. Thus the solid melted into the mesophase at 69°C and cleared into the isotropic fluid at 81°C. The XRD pattern evidenced reflections in the ratio $1:\sqrt{4}$ corresponding to d_{10} and d_{20} peaks. Hence, the mesophase was characterised as columnar hexagonal.

The metal-free ligand $L^{Phen\text{-}16}$ produced the mesophase with the smallest range. The solid melted into the liquid crystalline phase at 50°C and formed

the isotropic liquid at 60°C. DSC was able to detect the melting but not the clearing temperature. Small-angle XRD did not detect sufficient reflections to characterise the 2D symmetry of the mesophase, but the texture observed by POM was characterised as columnar from the dendritic regions in the texture of the mesophase.

Once again, comparison of the lattice parameters of the columnar hexagonal phases of $L^{Phen\text{-}10}$, $L^{Phen\text{-}12}$ and $L^{Phen\text{-}14}$ prove that increasing the length of the aliphatic chains of the compounds increases columnar lattice dimensions.

Table 2.7. Table showing the combined POM, DSC and XRD data to give the mesophase transition temperatures for $L^{Phen\text{-}n}$. Also included, where possible, are detailed indexation information obtained by XRD studies (where $\boldsymbol{n}$ = number of carbons in aliphatic chains; **T** = temperature at which data was taken; $\boldsymbol{d_{meas}}$ and $\boldsymbol{d_{calc}}$ are the measured and calculated diffraction spacings, respectively; ***hk*** is the indexation of the two-dimensional lattice; *a*, is the lattice parameter and *S* is the lattice area of the hexagonal (Col_h) columnar phase; *p6mm* is the 2D space group of the corresponding hexagonal mesophase; Col is an unidentified columnar mesophase and I is the isotropic liquid.

n	**T/°C**	$d_{meas.}$/Å	***hk***	$d_{calc.}$/Å	**Mesophase**	**Transitions/°C**
10	80	38.42 22.21 19.19 4.5	10 11 20 br	38.42 22.18 19.21	Col_h – *p6mm* a = 44.4 Å S =1704Å^2	g 64 Col_h 87 I
12	70	41.55 24.05 20.72 4.5	10 11 20 br	41.55 23.99 20.78	Col_h – *p6mm* a = 48.0 Å S =1994Å^2	g 65 Col_h 73 I
14	80	44.76 22.38 4.5	10 20 br	44.76 22.38	Col_h- *p6mm* a = 51.68Å S = 2313Å^2	g 69 Col_h 81 I
16	-	-	-	-	Col	g 50 Col 60 I

However, the mesophases for $L^{Phen\text{-}n}$ exist over much narrower temperature ranges compared to the corresponding complexes $[MnCl_2(L^{Phen\text{-}n})]$, $[CoCl_2(L^{Phen\text{-}n})]$, $[NiCl_2(L^{Phen\text{-}n})]$ and $[ZnCl_2(L^{Phen\text{-}n})]$, perhaps as a consequence of fewer intermolecular interactions. This mesomorphic range averaged just 13°C, with the observed clearing temperatures in the range 60°C - 87°C, and

melting temperatures in the range 50°C - 69°C. Hence, the clearing temperatures are far lower than any of the metal(II) complexes, which is a trend observed by many complexes and their metal-free analogues.[21] Also of interest is the observation that only the melting temperatures of $[CoCl_2(L^{Phen\text{-}n})]$, where n = 10, 14 and 16, and $[MCl_2(L^{Phen\text{-}16})]$, where M = Co^{2+}, Ni^{2+} and Zn^{2+}, were higher than the melting temperatures of the analogous metal-free ligands $L^{Phen\text{-}n}$. In other words, 11 out of 16 complexes had melting temperatures that were *lower* than their free-metal analogues. From this we can conclude that, in this particular case, incorporating a metal into an organic framework generally *lowers* the melting temperatures and stabilises the liquid crystal phase.

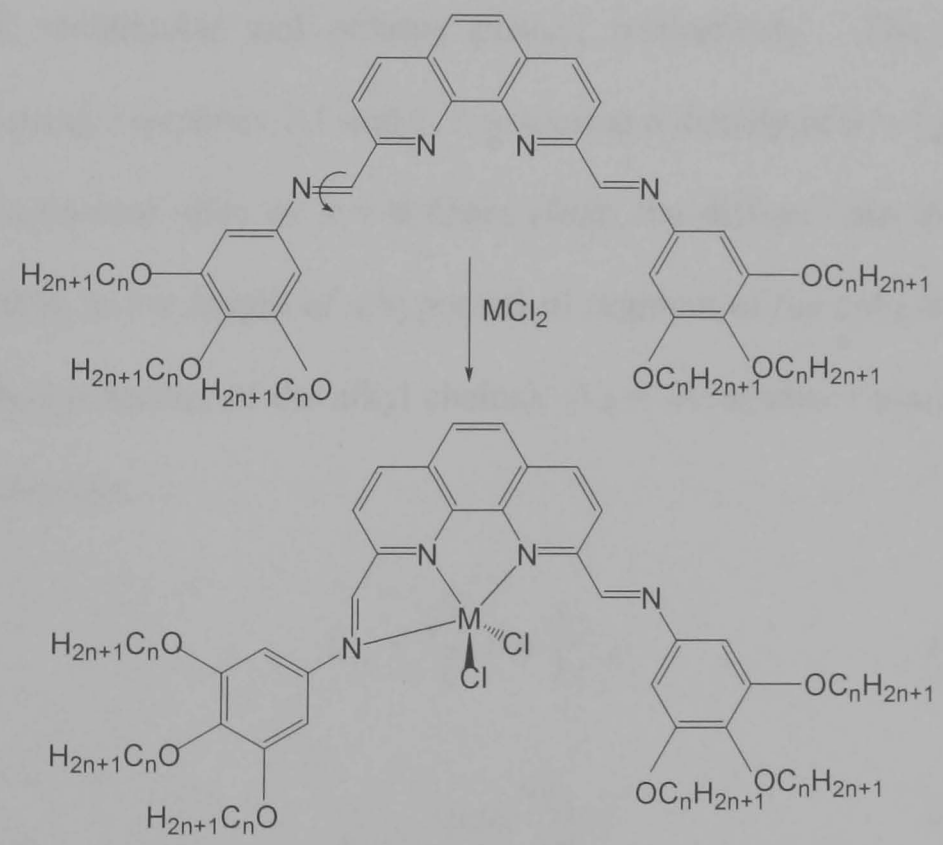

Figure 2.17. The effect of incorporating MCl_2 on the conformation of the organic ligand, $L^{Phen\text{-}n}$.

One possible explanation for this could be that the incorporation of a bis-chloro metal(II) fragment into the ligand lowers melting points because the Cl^- counterions prevent efficient packing of adjacent molecules, hence generating weaker intermolecular interactions and lower melting points. In

addition to the introduction of bulky counterions, the incorporation of a bis-chloro metal(II) fragment is responsible for changing the orientation one of the imines (Figure 2.17). The effect of this is to alter the conformation of the organic ligand, increasing the molecular anisotropy and reducing the symmetry of the molecule on complexation, which in turn may lower the melting temperatures of the complexes relative to the free ligands.

2.2.6 Calculating The Number of Molecules Per Column Cross-Section

The lattice parameters *a* and *b* generated from small angle XRD enable us to make crude approximations about the number of molecules per column cross-section. These values are defined as N_h, N_r and N_o for columnar hexagonal, rectangular and oblique phases, respectively. The values are estimated using Equations 2.1 and 2.2, assuming a density of $\rho = 1 gcm^{-3}$ and a height of columnar slice of h = 0.45nm (from the diffuse halo in the XRD, corresponding to the height of a hypothetical segment of the columns which is required by the density of the alkyl chains). N_A = Avagadro's constant and M = molecular mass.

$$N_h = \frac{\sqrt{3}}{2} a^2 h \frac{N_A}{M} \rho \qquad \text{Equation 2.1}$$

$$N_{r/o} = abh \frac{N_A}{M} \rho \qquad \text{Equation 2.2}$$

Using these equations we can estimate that for $[MnCl_2(L^{Phen\text{-}8})]$ N_{r1} = 2.81 and N_{r2} = 2.67. For $[MnCl_2(L^{Phen\text{-}10})]$ the numbers of molecules per column cross-section are closer to three, with N_r = 3.02 and N_o = 3.27. For $[MnCl_2(L^{Phen\text{-}12})]$ N_r = 1.98, N_o = 3.42 and N_h = 1.98. For $[MnCl_2(L^{Phen\text{-}14})]$ N_r

= 2.42, N_o = 3.33 and N_h = 1.86. Finally for this series, $[MnCl_2(L^{Phen\text{-}16})]$ is calculated as having N_h = 2.62 molecules per column cross section.

For the cobalt(II) series we can calculate that $[CoCl_2(L^{Phen\text{-}14})]$ has N_o = 3.43 and N_h = 2.08. The lattice parameters in the nickel(II) series indicate that $[NiCl_2(L^{Phen\text{-}12})]$ has N_h = 1.91, $[NiCl_2(L^{Phen\text{-}14})]$ has N_h = 1.85 and $[NiCl_2(L^{Phen\text{-}16})]$ has N_h = 1.80.

The values generated for the zinc(II) series indicate that $[ZnCl_2(L^{Phen\text{-}8})]$ has N_r = 3.21, $[ZnCl_2(L^{Phen\text{-}10})]$ has N_r = 4.31 and N_h = 2.09, $[ZnCl_2(L^{Phen\text{-}12})]$ has N_r = 4.61, $[ZnCl_2(L^{Phen\text{-}14})]$ has N_h = 2.57 and $[ZnCl_2(L^{Phen\text{-}16})]$ has N_h = 2.57.

Calculations for the metal-free ligands $L^{Phen\text{-}n}$ gave N_h values of 3.50, 3.62 and 3.77 for n = 10, 12 and 14, respectively.

Assuming these calculations to be correct generates some unexpected results. It was predicted that each cross-section of column, or 'disk', would consist of two hemi-disk shaped molecules. This was supported by single-crystal X-ray diffraction. However, our calculations suggest that for columnar rectangular and oblique phases the number of molecules per column cross-section is anything from about two to over four. For the columnar hexagonal mesophases of the complexes there are approximately two molecules per column cross-section. This increases to over three molecules per column cross-section for the metal-free ligands, perhaps as a consequence of the relatively large Col_h cross-sectional lattice parameter, S.

It is perhaps of no surprise that the tilted symmetry of the columnar rectangular and oblique phases is able to accommodate more than the expected

two molecules per column, or rather that the tilted structure is as a consequence of the increased number of molecules per column.

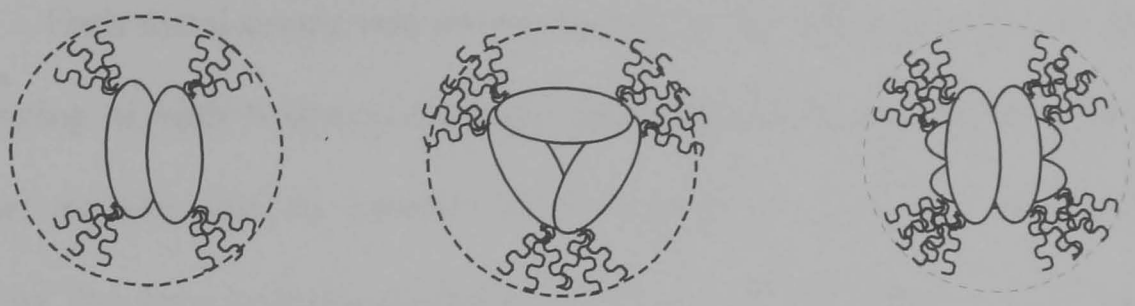

Figure 2.18. Schematic to illustrate (a) the predicted arrangement of molecules in one column, (b) one possible arrangement of three molecules per column cross-section and (c) one possible arrangement of four molecules per column cross-section.

2.3 CONCLUSIONS

To summarise, we have synthesised and studied the liquid crystalline properties of a range of novel first-row transition metal-containing 1,10-phenanthroline derived metallomesogens. These have been prepared via Schiff-base condensation template reactions of manganese(II), cobalt(II), nickel(II) and zinc(II) chlorides with 2,9-diformyl-1,10-phenanthroline and 3,4,5-tri(alkoxy)aniline. The complexes and corresponding 2,9-bis-[3',4',5'-tri(alkoxy)phenyliminomethyl]-1,10-phenanthroline organic ligands were prepared in good yields. Characterisation of the complexes confirmed that they are monomeric 1:1 metal-ligand species.

Structural determination of the analogous methoxy complexes $[MCl_2(L^{Phen\text{-}1})]$, and the complex without any lateral aliphatic groups $[CuCl_2(L^{Phen\text{-}0})]$, by single crystal X-ray diffraction revealed the metal(II) complexes to be either five-coordinate monomeric, with distorted trigonal bipyramidal (for $[CoCl_2(L^{Phen\text{-}1})]$ and $[ZnCl_2(L^{Phen\text{-}1})]$) and distorted square pyramidal (for $[CuCl_2(L^{Phen\text{-}0})]$) coordination geometry, or six–coordinate

dimeric, with octahedral coordination geometry (for $[MnCl_2(L^{Phen\text{-}1})]_2$ and $[NiCl_2(L^{Phen\text{-}1})]_2$).

Each metal centre was coordinated to an N_3-donor set from the ligand consisting of both N-donors from the phenanthroline ring and one imine N-donor, and two chloride ions for the five-coordinate species or three chloride ions for the six-coordinate species. The $[CoCl_2(L^{Phen\text{-}1})]$, $[CuCl_2(L^{Phen\text{-}0})]$ and $[ZnCl_2(L^{Phen\text{-}1})]$ monomers were arranged in offset pairs as 'disks', with partial overlap of the phenanthroline and phenyl rings. The $[MnCl_2(L^{Phen\text{-}1})]_2$ and $[NiCl_2(L^{Phen\text{-}1})]_2$ complexes formed asymmetric bridges through M-Cl-M bonds, producing 'dimeric disks' with the ligands pointed in opposite directions. With the exception of $[CuCl_2(L^{Phen\text{-}0})]$ these disks were arranged as columns in the solid state, akin to their behaviour in the liquid crystalline state.

Four series of complexes, $[MnCl_2(L^{Phen\text{-}n})]$, $[CoCl_2(L^{Phen\text{-}n})]$, $[NiCl_2(L^{Phen\text{-}n})]$ and $[ZnCl_2(L^{Phen\text{-}n})]$, each with aliphatic chain lengths of n = 8, 10, 12, 14 and 16 carbon atoms, and one ligand series, $L^{Phen\text{-}n}$, consisting of chains of n = 10, 12, 14 and 16 carbon atoms, are mesomorphic (with the exception of non-mesomorphic $[CoCl_2(L^{Phen\text{-}8})]$). Each complex or ligand forms one or more columnar mesophases in the regions of 50 - 201°C (for complexes) and 50 - 87°C (for organic ligands). Increasing the length of the aliphatic chains generally decreases the clearing temperatures, although no definite pattern was observed for the effect on the melting temperatures. The length of the chains also influence the 2D symmetry of the mesophases; $[MnCl_2(L^{Phen\text{-}n})]$ and $[ZnCl_2(L^{Phen\text{-}n})]$ illustrated the preference for the formation of columnar hexagonal over columnar rectangular mesophases at longer chain lengths. Variation of the metal centre had the effect of altering

the thermal stability of the mesophases, most notably with the $[MnCl_2(L^{Phen\text{-}n})]$ complexes.

In conclusion, the first thermotropic 1,10-phenanthroline first-row transition metal metallomesogens have been successfully synthesised and studied.

2.4 EXPERIMENTAL

NMR spectra were recorded on either a Bruker DPX300 FT-NMR spectrometer operating at 300.13 MHz for ^1H and 75.48 MHz for broadband proton decoupled ^{13}C, or a Jeol EX270 FT-NMR spectrometer operating at 270.17 MHz for ^1H and 67.93MHz for proton decoupled ^{13}C. Chemical shifts are referenced with respect to residual proton and carbon solvent (with δ_H = 7.26 ppm and δ_C = 77.0 ppm for $CDCl_3$). IR spectra were obtained on a Nicolet AVATAR 360 FT-IR spectrometer as KBr pellets. FAB mass spectra were obtained on a Finnigan MAT TSQ-700 spectrometer at the University of Wales, Swansea, with 3-nitrobenzyl alcohol (NOBA) as matrix. MALDI-TOF mass spectra were obtained on a Voyager-DE-STR spectrometer at the University of Wales, Swansea, with *trans*-2-[3-(4-tert-butylphenyl)-2-methylprop-2-enylidene]malononitrile (DCTB) as matrix. EI and ES mass spectra were recorded by the Mass Spectrometry Service at the University of Nottingham. Elemental analyses (C, H, N) were carried out by the Analytical Department of the University of Nottingham.

Analysis by polarised optical microscopy was carried out using a Zeiss Labpol, or Olympus BH40 microscope equipped with a Link-Am HFS91 hot stage, TMS92 controller and LNP2 cooling unit. Analysis by DSC was carried out on either a Perkin-Elmer DSC7 instrument or a TA DSC 2920 instrument.

using heating and cooling rates of either 5 or 10°C min^{-1}. For analysis by XRD the powdered sample was filled in Lindemann capillaries of 1mm diameter. A linear monochromatic Cu-K_α beam (λ = 1.5405Å) obtained with a sealed-tube generator (900W) and a bent quartz monochromator were used. The diffraction patterns were registered with a curved counter Inel CPS 120, for which the sample temperature was controlled within ± 0.05°C. Periodicidies up to 60Å could be measured. An X-ray pattern was recorded every 20°C for each compound from the crystalline state up to the isotropic liquid.

2.4.1 Aniline Synthesis

2.4.1.1 Synthesis of 1,2,3-trioctyloxybenzene

1,2,3-Trihydroxybenzene (5.01g, 0.0397mol) and 1-bromooctane (23.5g, 0.122mol) were stirred under an atmosphere of N_2. Excess Cs_2CO_3 (50.1g, 0.154mol) and a few drops of Aliquat 336 were added and the cream/brown mixture was stirred and heated to 120°C for 2½ hours. The product was extracted into CH_2Cl_2 (100cm^3) and the excess Cs_2CO_3 was dissolved in H_2O (100cm^3). The aqueous layer was washed with CH_2Cl_2 (7 x 50cm^3), then the organic layers were combined and dried over $MgSO_4$. The solvent was removed under vacuum, leaving a brown oil (15.9g, 86.3%). Microanalysis: Calculated for $C_{30}H_{54}O_3$ C 77.85, H 11.78, N 0.00; found C 77.30, H 11.63, N 0.00. IR (CaF_2 liquid film): ν = 2955vs (C-H), 2854vs (C-H), 1596m (C=C), 1497m (C=C), 1467s (C=C), 1101s (C-O) cm^{-1}. ^{1}H-NMR (300.13MHz, $CDCl_3$, 298K): δ_H 6.87 (1H, t, $^3J_{AX}$ = 8.40Hz, Ar<u>H</u>), 6.54 (2H, d, $^3J_{AX}$ = 8.34Hz, Ar<u>H</u>), 4.09 (2H, t, $^3J_{AX}$ = 6.70Hz, central O<u>CH</u>$_2$), 3.96 (4H, t, $^3J_{AX}$ = 6.41Hz, lateral O<u>CH</u>$_2$), 1.89-1.29 (36H, m, <u>CH</u>$_2$), 0.89 (9H,

2 overlapping triplets, C<u>H</u>$_3$) ppm. ^{13}C-NMR (75.48MHz, $CDCl_3$): δ_C 153.2. 138.3, 123.2, 106.6, 73.0, 69.1, 32.7, 31.7, 28.9, 28.6, 28.0, 22.4, 13.7 ppm. EI MS: m/z = 463 $[C_{30}H_{54}O_3]^+$.

2.4.1.2 Synthesis of 1,2,3-tridecyloxybenzene

Excess Cs_2CO_3 (51.8g, 0.159 mol) and a few drops of Aliquat 336 were added to 1,2,3-trihydroxybenzene (4.99g, 0.0396mol) and 1-bromodecane (26.3g, 0.119mol) under an atmosphere of N_2. The mixture was stirred and heated to 120°C for 3 hours. The product was extracted into CH_2Cl_2 (100cm^3) and the excess Cs_2CO_3 was dissolved in H_2O (100cm^3). The aqueous layer was washed with CH_2Cl_2 (3 x 50cm^3) and the organic layers were collectively dried over $MgSO_4$. The solution was reduced *in vacuo* to give a brown oil (20.3g, 93.9%). Microanalysis: Calculated for $C_{36}H_{66}O_3.0.5H_2O$ C 77.78, H 12.15, N 0.00; found C 77.51, H 12.10, N 0.00. IR (CaF_2 liquid film): ν = 2928vs (C-H), 2856vs (C-H), 1595m (C=C), 1496m (C=C), 1465s (C=C), 1103s (C-O) cm^{-1}. ^{1}H-NMR (300.13MHz, $CDCl_3$, 298K): δ_H 6.91 (1H, t, $^3J_{AX}$ =10.3Hz, Ar<u>H</u>), 6.54 (2H, d, $^3J_{AX}$ = 8.35Hz, Ar<u>H</u>), 4.07 (2H, t, $^3J_{AX}$ =6.72Hz, central OC<u>H</u>$_2$), 3.96 (4H, 2 overlapping triplets, lateral OC<u>H</u>$_2$), 3.37 (6H, m, C<u>H</u>$_2$), 1.90-1.28 (42H, m, C<u>H</u>$_2$), 0.89 (9H, 2 overlapping triplets, C<u>H</u>$_3$) ppm. ^{13}C-NMR (75.48MHz, $CDCl_3$): δ_C 153.3, 138.5, 123.2, 106.6, 72.9, 68.8, 32.8, 31.8, 29.5, 29.4, 29.2, 28.1, 26.0, 22.5, 13.8 ppm. EI MS: m/z = 547 $[C_{36}H_{66}O_3]^+$.

2.4.1.3 Synthesis of 1,2,3-tridodecyloxybenzene

Under an inert atmosphere, excess Cs_2CO_3 (52.0g, 0.160 mol) and a few drops of Aliquat 336 were added to 1,2,3-trihydroxybenzene (5.03g. 0.0399mol) and 1-bromododecane (30.3g, 0.122mol). The mixture was stirred and heated to 120°C for 2½ hours, resulting in a creamy/brown mixture. Addition of CH_2Cl_2 ($100cm^3$) and H_2O ($100cm^3$) followed. The aqueous layer was washed with more CH_2Cl_2 (3 x $50cm^3$) and the organic layers were dried over $MgSO_4$. The solvent was removed under vacuum to produce a brown oil. This solidified on standing and was washed with cold hexane to give a beige solid (21.5g, 85.6%). Microanalysis: Calculated for $C_{42}H_{78}O_3$ C 79.91, H 12.48, N 0.00; found C 80.00, H 12.75, N 0.00. IR (KBr pellet): ν = 2925vs (C-H), 2854vs (C-H), 1502s (C=C), 1467 br,s (C=C), 1116vs (C-O) cm^{-1}. ^{1}H-NMR (300.13MHz, $CDCl_3$, 298K): δ_H 6.90 (1H, t, $^3J_{AX}$ = 8.29Hz, Ar<u>H</u>), 6.53 (2H, d, $^3J_{AX}$ = 8.33Hz, Ar<u>H</u>), 4.05 (2H, t, $^3J_{AX}$ =6.30, central O<u>CH</u>$_2$), 3.96 (4H, 2 overlapping triplets, lateral O<u>CH</u>$_2$), 1.90-1.69 (6H, m, <u>CH</u>$_2$), 1.54-1.27 (54H, m, <u>CH</u>$_2$), 0.88 (9H, 2 overlapping triplets, <u>CH</u>$_3$) ppm. ^{13}C-NMR (75.48MHz, $CDCl_3$, 298K): δ_C 153.4, 138.5, 123.1, 107.0, 73.4, 69.2, 33.9, 32.9, 31.9, 30.4, 29.7, 29.4, 29.4, 28.8, 28.2, 26.1, 14.1 ppm. EI MS: m/z= 631 $[C_{42}H_{78}O_3]^+$.

2.4.1.4 Synthesis of 1,2,3-tritetradecyloxybenzene

1,2,3-Trihydroxybenzene (5.16g, 0.0409mol) and 1-bromotetradecane (34.2g, 0.123 mol) were stirred together under a N_2 atmosphere. To this, excess Cs_2CO_3 (50.0g, 0.153 mol) and a few drops of Aliquat 336 were added. The mixture was heated to 120°C for 3 hours. CH_2Cl_2 ($100cm^3$) and H_2O

($100cm^3$) were added and the aqueous layer was washed with CH_2Cl_2 (6 x $50cm^3$). The organic layers were dried over $MgSO_4$. The solution reduced down to a brown oil, which solidified to brown solid. The solid was recrystallised from $CHCl_3$ and washed with MeOH, resulting in a beige solid (22.5g, 76.9%). Microanalysis: Calculated for $C_{48}H_{90}O_3.H_2O$ C 78.63, H 12.65, N 0.00; found C 78.69, H 12.28, N 0.00. IR (KBr pellet): υ = 2840vs (C-H), 1604s (C=C), 1502s (C=C), 1465s (C=C), 1117s (C-O) cm^{-1}. ^{1}H-NMR (300.13MHz, $CDCl_3$, 298K): δ_H 6.90 (1H, t, $^3J_{AX}$ = 8.31Hz, Ar<u>H</u>), 6.53 (2H, d, $^3J_{AX}$ = 8.34Hz, Ar<u>H</u>), 3.95 (6H, 2 overlapping triplets, O<u>CH</u>$_2$), 1.80 (6H, m, <u>CH</u>$_2$), 1.59-1.26 (66H, m, <u>CH</u>$_2$), 0.88 (9H, 2 overlapping triplets, <u>CH</u>$_3$) ppm. ^{13}C-NMR (75.48MHz, $CDCl_3$, 298K): δ_C 153.5, 138.5, 123.1, 106.9, 73.4, 69.2, 32.9, 31.9, 30.4, 29.7, 29.5, 29.4, 28.8, 26.1, 22.7, 14.1 ppm. ES MS: m/z = 716 $[C_{48}H_{90}O_3]^+$.

2.4.1.5 Synthesis of 1,2,3-trihexadecyloxybenzene

Under an atmosphere of N_2, excess Cs_2CO_3 (51.7g, 0.159mol) and a few drops of Aliquat 336 were added to 1,2,3-trihydroxybenzene (5.01g, 0.0397mol) and 1-bromohexadecane (36.3g, 0.119mol). The brown mixture was heated to 120°C over 3 hours. CH_2Cl_2 ($100cm^3$) and H_2O ($100cm^3$) were added to extract the product and remaining Cs_2CO_3, respectively. The aqueous layer was extracted with further portions of CH_2Cl_2 (3 x $100cm^3$). The combined organic layers were dried over $MgSO_4$. The solution was reduced in volume *in vacuo* to give a cream solid, which was recrystallised from hot EtOH (15.2g, 47.9%). Microanalysis: Calculated for $C_{54}H_{102}O_3.H_2O$ C 79.35, H 12.82, N 0.00; found C 79.13, H 12.44, N 0.00. IR (KBr pellet): υ = 2949vs

(C-H), 2836vs (C-H), 1498s (C=C), 1461br,s (C=C), 1117vs (C-O) cm^{-1}. ^{1}H-NMR (300.13MHz, $CDCl_3$, 298K): δ_H 6.90 (1H, t, $^{3}J_{AX}$ =8.31Hz, Ar<u>H</u>), 6.54 (2H, d, $^{3}J_{AX}$ = 8.34Hz, Ar<u>H</u>), 3.96 (6H, 2 overlapping triplets, OC<u>H</u>$_2$), 1.90-1.26 (84H, m, C<u>H</u>$_2$), 0.88 (9H, 2 overlapping triplets, C<u>H</u>$_3$) ppm. ^{13}C-NMR (75.48MHz, $CDCl_3$, 298K): δ_C 153.5, 134.8, 123.1, 106.8, 73.5, 69.3, 31.9, 30.4, 30.3, 29.7, 29.4, 28.7, 26.1, 26.0, 22.7, 14.1 ppm (five alkyl carbons obscured). ES MS: m/z = 799 $[C_{54}H_{102}O_3]^+$.

2.4.1.6 Synthesis of 3,4,5-trioctyloxynitrobenzene

1,2,3-Trioctyloxybenzene (14.9g, 0.0321mol) was stirred with a catalytic amount of $NaNO_2$ (0.358g, 5.19mmol) and excess concentrated HNO_3 (70%, 0.130g, 0.0973mol) in CH_2Cl_2 (100cm^3) for 60 mins. The solution was neutralised with 2M Na_2CO_3 and the aqueous layer was washed with CH_2Cl_2 (5 x 50cm^3). The organic layers were combined and dried over $MgSO_4$. The brown solution was reduced down to a brown oil (9.87g, 60.7%). Microanalysis: No satisfactory elemental analysis found. IR (CaF_2 liquid film): ν = 2927vs (C-H), 2855s (C-H), 1525m (C-NO_2), 1467m (C=C), 1378w (C-NO_2), 1339m (C-NO_2), 1112m (C-O) cm^{-1}. ^{1}H-NMR (300.13MHz, $CDCl_3$, 298K): δ_H 7.45 (2H, s, Ar<u>H</u>), 4.01 (6H, 2 overlapping triplets, OC<u>H</u>$_2$), 1.88-1.27 (36H, m, C<u>H</u>$_2$), 0.85 (9H, 2 overlapping triplets, C<u>H</u>$_3$) ppm. ^{13}C-NMR (75.48MHz, $CDCl_3$, 298K): δ_C 152.6, 143.8, 143.1, 102.1, 73.6, 69.4, 32.8, 31.7, 29.0, 28.7, 28.1, 22.5, 13.9 ppm. EI MS: m/z = 507 $[C_{30}H_{53}NO_5]^+$.

2.4.1.7 Synthesis of 3,4,5-tridecyloxynitrobenzene

Excess concentrated HNO_3 (70%, 2.53g, 0.0402mol) and a catalytic amount of $NaNO_2$ (0.155g, 2.25mmol) were added to 1,2,3-tridecyloxybenzene (7.95g, 0.0145mol) in CH_2Cl_2 ($100cm^3$) and stirred for 90 mins. The red solution was neutralised with 2M Na_2CO_3 and the aqueous layer was washed with CH_2Cl_2 (4 x $50cm^3$). The organic layers were combined and dried over $MgSO_4$. The solvent was reduced down to a brown oil and EtOH ($20cm^3$) was added, resulting in a beige solid (6.27g, 73.0%). Microanalysis: Calculated for $C_{36}H_{65}NO_5$ C 73.03, H 11.09, N 2.37; found C 72.85, H 10.89, N 2.34. IR (KBr pellet): υ= 2919vs (C-H), 2849vs (C-H), 1614m (C=C), 1513vs (C-NO_2), 1382s (C-NO_2), 1346s (C-NO_2), 1120s (C-O) cm^{-1}. ^{1}H-NMR (300.13MHz, $CDCl_3$, 298K): δ_H 7.47 (2H, s, Ar<u>H</u>), 4.03 (6H, 2 overlapping triplets, OC<u>H_2</u>), 1.83 (4H, t, $^3J_{AX}$ = 6.59Hz, C<u>H_2</u>), 1.74 (2H, t, $^3J_{AX}$ = 6.26Hz, C<u>H_2</u>), 1.48-1.28 (42H, m, C<u>H_2</u>), 0.88 (9H, 2 overlapping triplets, C<u>H_3</u>) ppm. ^{13}C-NMR (75.48MHz, $CDCl_3$, 298K): δ_C 152.7, 143.9, 143.2, 102.2, 73.8, 69.5, 31.9, 30.3, 29.7, 29.6, 29.3, 29.1, 26.0, 22.7, 14.1 ppm. ES MS: m/z= 592 $[C_{36}H_{65}NO_5]^+$.

2.4.1.8 Synthesis of 3,4,5-tridodecyloxynitrobenzene

Over a 90min period, 1,2,3-tridodecyloxybenzene (20.9g, 0.0331mol), excess concentrated HNO_3 (70%, 8.34g, 0.132mol) and a catalytic amount of $NaNO_2$ (0.32g, 4.64mmol) were stirred in CH_2Cl_2 ($50cm^3$). The resulting red solution was neutralised with 2M Na_2CO_3. The aqueous layer was washed with CH_2Cl_2 (4 x $100cm^3$) and the organic layers were combined and dried over $MgSO_4$. Concentration of the orange solution under vacuum resulted in

an orange oil, which solidified over time. Recrystallisation from hot EtOH produced a cream solid (11.4g, 50.9%). Microanalysis: Calculated for $C_{42}H_{77}NO_5$ C 74.62, H 11.48, N 2.07; found C 74.60, H 11.46, N 2.24. IR (KBr pellet): υ = 2919s (C-H), 1615m (C=C), 1514s (C-NO_2), 1384s (C-NO_2), 1349s (C-NO_2), 1121s (C-O) cm^{-1}. ^{1}H-NMR (300.13MHz, $CDCl_3$, 298K): δ_H 7.47 (2H, s, Ar<u>H</u>), 4.05 (6H, 2 overlapping triplets, OC<u>H_2</u>), 1.83 (4H, t, $^3J_{AX}$ = 7.05Hz, C<u>H_2</u>), 1.75 (2H, t, $^3J_{AX}$= 7.25Hz, C<u>H_2</u>), 1.53-1.27 (54H, m, C<u>H_2</u>), 0.88 (9H, 2 overlapping triplets, C<u>H_3</u>) ppm. ^{13}C-NMR (75.48MHz, $CDCl_3$, 298K): δ_C 152.7, 144.1, 143.2, 102.2, 73.8, 69.5, 31.9, 30.3, 29.7, 29.6, 29.5, 29.3, 29.1, 28.2, 26.0, 22.7, 14.1 ppm. EI-MS: m/z= 676 $[C_{42}H_{77}NO_5]^+$.

2.4.1.9 Synthesis of 3,4,5-tritetradecyloxynitrobenzene

1,2,3-Tritetradecyloxybenzene (31.6g, 0.0442 mol), excess concentrated HNO_3 (70%, 8.42g, 0.134 mol) and $NaNO_2$ (0.440g, 6.38mmol) were stirred in CH_2Cl_2 (300cm^3) for 90mins. The dark red/brown solution was neutralised with 2M Na_2CO_3 and the aqueous layer was washed with CH_2Cl_2 (3 x 100cm^3). The organic layers were combined and dried over $MgSO_4$. The solvent was evaporated under reduced pressure, leaving an orange oil. On standing the oil solidified. The solid was recrystallised from EtOH and $CHCl_3$, resulting in a light yellow solid (21.3g, 63.4%). Microanalysis. Calculated for $C_{48}H_{89}NO_5$0.5EtOH C 75.14, H 11.84, N 1.79; found C 75.13, H 11.63, N 1.42. IR (KBr pellet): υ = 2911vs (C-H), 2852vs (C-H), 1616m (C=C), 1513s (C-NO_2), 1379s (C-NO_2), 1347s (C-NO_2), 1122s (C-O) cm^{-1}. ^{1}H-NMR (300.13MHz, $CDCl_3$, 298K): δ_H 7.46 (2H, s, Ar<u>H</u>), 4.05 (6H, 2 overlapping triplets, OC<u>H_2</u>), 1.85-1.27 (72H, m, C<u>H_2</u>), 0.88 (9H, 2 overlapping triplets,

C<u>H</u>$_3$) ppm. ^{13}C-NMR (75.48MHz, $CDCl_3$, 298K): 156.8, 152.7, 107.4, 102.2, 73.8, 69.7, 32.8, 31.9, 30.9, 30.3, 29.7, 29.4, 29.2, 29.1, 28.2, 26.0, 25.8, 22.7, 14.1 ppm (two alkyl carbons obscured). EI MS: m/z = 760 $[C_{48}H_{89}NO_5]^+$.

2.4.1.10 Synthesis of 3,4,5-trihexadecyloxynitrobenzene

$NaNO_2$ (0.183g, 2.65mmol) and concentrated HNO_3 (3.57g, 0.0567mol) were added to a solution of 1,2,3-trihexadecyloxybenzene (15.2g, 0.0189mol) in CH_2Cl_2 (100cm^3) and stirred for 90mins. The solution was neutralised with 2M Na_2CO_3. The aqueous layer was extracted with CH_2Cl_2 (3 x 50cm^3) and the organic layers combined and dried over $MgSO_4$. The solution was reduced in volume, *in vacuo*, to give a beige solid, which was washed with EtOH (10.2g, 63.7%). Microanalysis: Calculated for $C_{54}H_{101}NO_5$ C 76.79 H 12.08, N 1.66; found C 77.39, H 12.13, N 1.50. IR (KBr pellet): ν = 2933vs (C-H), 2843vs (C-H), 1514s (C-NO_2), 1468s (C=C), 1381m (C-NO_2), 1345s (C-NO_2), 1123s (C-O) cm^{-1}. ^{1}H-NMR (300.13MHz, $CDCl_3$, 298K): δ_H 7.46 (2H, s, Ar<u>H</u>), 4.00 (6H, 2 overlapping triplets, OC<u>H</u>$_2$), 1.48-1.27 (84H, m, C<u>H</u>$_2$), 0.87 (9H, 2 overlapping triplets, C<u>H</u>$_3$) ppm. ^{13}C-NMR (75.48MHz, $CDCl_3$, 298K): 156.6, 152.7, 107.4, 102.1, 73.8, 69.6, 32.8, 31.9, 30.4, 30.3, 30.1, 29.7, 29.5, 29.4, 29.2, 29.1, 28.1, 26.1, 25.8, 25.7, 14.1 ppm. EI MS: m/z = 844 $[C_{54}H_{101}NO_5]^+$.

2.4.1.11 Synthesis of 3,4,5-trioctyloxyaniline

Hydrazine monohydrate (4.32g, 0.0863mol) and 1 spatula of palladium (5%) on activated carbon were added to 3,4,5-trioctyloxynitrobenzene (6.08g, 0.0120mol) in absolute EtOH (50cm^3), under an atmosphere of N_2. The black

mixture was heated to reflux for 24 hours and filtered hot. An off-white solid precipitated out of solution. This was recrystallised from hot EtOH. resulting in an off-white solid (4.61g, 80.4%). Microanalysis: Calculated for $C_{30}H_{55}NO_3$ C 75.40, H 11.62, N 2.93; found C 75.37, H 11.48, N 2.81. IR (KBr pellet): υ = 3413s (NH_2), 3331s (NH_2), 2846vs (C-H), 1508s (C=C). 1473s (C=C), 1453s (C=C), 1120vs (C-O) cm^{-1}. ^{1}H-NMR (300.13MHz. $CDCl_3$, 298K): δ_H 5.91 (2H, s, Ar<u>H</u>), 5.60 (2H, br s, N<u>H</u>$_2$), 3.90 (4H, t, $^3J_{AX}$ = 6.52Hz, OC<u>H</u>$_2$), 3.84 (2H, t, $^3J_{AX}$ = 6.63Hz, OC<u>H</u>$_2$), 1.74 (6H, m, C<u>H</u>$_2$), 1.47-1.28 (30H, m, C<u>H</u>$_2$), 0.88 (9H, 2 overlapping triplets, C<u>H</u>$_3$) ppm. ^{13}C-NMR (75.48MHz, $CDCl_3$, 298K): δ_C 153.6, 142.3, 130.9. 94.3, 73.5. 68.8, 31.9. 31.8, 30.2, 29.5, 26.1, 22.6, 14.0 ppm. EI MS: m/z = 477 $[C_{30}H_{55}NO_3]^+$.

2.4.1.12 Synthesis of 3,4,5-tridecyloxyaniline

Under an atmosphere of N_2, 3,4,5-tridecyloxynitrobenzene (1.53g, 2.26mmol) and hydrazine monohydrate (0.800g, 0.0160mol) were stirred in absolute EtOH (40cm^3). One spatula of palladium on activated carbon (5%) was gradually added and the solution was refluxed for 24 hours. The palladium on carbon was filtered off and an off-white precipitate formed as the EtOH solution cooled. The solid was recrystallised from hot EtOH (1.05g, 72.6%). Microanalysis: Calculated for $C_{36}H_{67}NO_3$ C 76.93. H 12.04. N 2.49; found C 76.82. H 11.57, N 2.54. IR (KBr pellet): υ = 3413s (NH_2). 3333s (NH_2), 2846vs (C-H), 1597s (C=C), 1507s (C=C), 1116s (C-O) cm^{-1}. ^{1}H-NMR (300.13MHz. $CDCl_3$. 298K): δ_H 5.91 (2H, s. Ar<u>H</u>). 3.90 (4H. t. $^3J_{AX}$ = 6.52Hz, OC<u>H</u>$_2$). 3.84 (2H, t. $^3J_{AX}$ = 6.61Hz, OC<u>H</u>$_2$), 3.47 (2H, s. N<u>H</u>$_2$). 1.74 (6H, m, C<u>H</u>$_2$). 1.47-1.27 (42H. m, C<u>H</u>$_2$), 0.88 (9H, 2 overlapping triplets. C<u>H</u>$_3$) ppm.

^{13}C-NMR (75.48MHz, $CDCl_3$, 298K): δ_C 153.7, 142.3, 131.2, 94.6, 73.6, 69.0, 31.9, 30.3, 29.7, 29.6, 29.4, 29.4, 26.1, 22.7, 14.1 ppm. EI MS: m/z = 562 $[C_{36}H_{67}NO_3]^+$.

2.4.1.13 Synthesis of 3,4,5-tridodecyloxyaniline

3,4,5-Tridodecyloxynitrobenzene (2.14g, 3.16mmol) and hydrazine monohydrate (1.47g, 0.0456mol), followed by one spatula of palladium (5%) on activated carbon were refluxed in absolute EtOH (50cm^3) for 24 hours under an atmosphere of N_2. The mixture was filtered hot and a white solid precipitated out. This was washed with EtOH and dried (1.50g, 73.6%). Microanalysis: Calculated for $C_{42}H_{79}NO_3$.EtOH C 76.35, H 12.38, N 2.02; found C 76.52, H 12.15, N 2.21. IR (KBr pellet): υ = 3413s (NH_2), 3334s (NH_2), 2871vs (C-H), 1597s (C=C), 1508s (C=C), 1109vs (C-O) cm^{-1}. ^{1}H-NMR (300.13MHz, $CDCl_3$, 298K): δ_H 5.92 (2H, s, Ar$\underline{H}$), 3.90 (4H, t, $^3J_{AX}$= 6.46Hz, OC$\underline{H}_2$), 3.84 (2H, t, $^3J_{AX}$= 6.61Hz, OC$\underline{H}_2$), 3.66 (2H, br s, N$\underline{H}_2$), 1.77 (6H, m, C$\underline{H}_2$), 1.46-1.26 (54H, m, C$\underline{H}_2$), 0.88 (9H, 2 overlapping triplets, C$\underline{H}_3$) ppm. ^{13}C-NMR (75.48MHz, $CDCl_3$, 298K): δ_C 153.8, 140.5, 131.9, 95.3, 73.6, 69.1, 31.9, 30.3, 29.7, 29.4, 26.2, 26.1, 22.7, 14.1 ppm. EI MS: m/z = 646 $[C_{42}H_{79}NO_3]^+$.

2.4.1.14 Synthesis of 3,4,5-tritetradecyloxyaniline

Under inert conditions, 3,4,5-tritetradecyloxynitrobenzene (3.57g, 4.70mmol) and hydrazine monohydrate (2.13g, 0.0664mol) were stirred in absolute EtOH (50cm^3). One spatula of palladium (5%) on activated carbon was added and the mixture was heated to reflux for 24 hours. The mixture was

filtered hot and the resulting white solid from the filtrate was collected. This was recrystallised from hot EtOH (2.72g, 79.2%). Microanalysis: Calculated for $C_{48}H_{91}NO_3$ C 78.95, H 12.56, N 1.92; found C 79.50, H 12.76, N 1.26. IR (KBr pellet): ν = 3411m (NH_2), 3335m (NH_2), 2917vs (C-H), 2850vs (C-H), 1637m (C=C), 1598m (C=C), 1513m (C=C), 1119s (C-O) cm^{-1}. ^{1}H-NMR (300.13MHz, $CDCl_3$, 298K): δ_H 5.91 (2H, s, Ar<u>H</u>), 3.91 (4H, t, $^3J_{AX}$ = 6.51Hz, OC<u>H</u>$_2$), 3.84 (2H, t, $^3J_{AX}$ = 6.52Hz, OC<u>H</u>$_2$), 3.47 (2H, br s, N<u>H</u>$_2$), 1.85-1.26 (72H, m, C<u>H</u>$_2$), 0.88 (9H, 2 overlapping triplets, C<u>H</u>$_3$) ppm. ^{13}C-NMR (75.48MHz, $CDCl_3$, 298K): δ_C 152.7, 140.4, 131.6, 102.2, 73.8, 69.5, 32.8, 31.9, 30.3, 29.7, 29.4, 29.1, 26.0, 25.7, 22.7, 14.1 ppm (three alkyl carbons obscured). EI MS: m/z = 730 $[C_{48}H_{91}NO_3]^+$.

2.4.1.15 Synthesis of 3,4,5-trihexadecyloxyaniline

Absolute EtOH (100cm^3) was added to 3,4,5-trihexadecyloxynitrobenzene (6.47g, 7.66mmol) under an atmosphere of nitrogen. Excess hydrazine hydrate, followed by one spatula of palladium (5%) on activated carbon, was added and the mixture was heated to reflux for 24 hours. The mixture was filtered hot and the resulting white solid was collected and dried (4.52g, 72.5%). Microanalysis: Calculated for $C_{54}H_{103}NO_3$ C 79.63, H 12.65, N 1.72; found C 79.46, H 12.72, N 1.75. IR (KBr pellet): ν = 3414m (NH_2), 3337m (NH_2), 2940vs (C-H), 2844vs (C-H), 1598s (C=C), 1505s (C=C), 1468s (C=C), 1115s (C-O) cm^{-1}. ^{1}H-NMR (300.13MHz, $CDCl_3$, 298K): δ_H 5.90 (2H, s, Ar<u>H</u>), 3.89 (4H, t, $^3J_{AX}$ = 6.50Hz, OC<u>H</u>$_2$), 3.83 (2H, t, $^3J_{AX}$ = 6.60Hz, OC<u>H</u>$_2$), 1.91-1.25 (84H, m, C<u>H</u>$_2$), 0.89 (9H, 2 overlapping triplets, C<u>H</u>$_3$) ppm. ^{13}C-NMR (75.48MHz, $CDCl_3$, 298K): δ_C 153.7, 142.2,

131.1, 94.4, 73.5, 68.9, 31.9, 30.3, 29.7, 29.7, 29.4, 26.2, 26.1, 22.7, 14.1 ppm (six alkyl carbons obscured). EI MS: m/z = 814 $[C_{54}H_{103}NO_3]^+$.

2.4.2 Synthesis of 2,9-Diformyl-1,10-Phenanthroline

2,9-Dimethyl-1,10-phenanthroline (1.28g, 6.15mmol) and excess selenium dioxide (2.72g, 0.0246mol) were heated to reflux for 4 hours in 4% aqueous dioxane ($150cm^3$). The mixture was filtered hot through celite and cotton wool and washed with further portions of hot dioxane. The filtrate was reduced in volume under reduced pressure to give a pale yellow solid (0.665g, 45.8%). Microanalysis: Calculated for $C_{14}H_8N_2O_2.H_2O$ C 66.14, H 3.96, N 11.02; found C 65.93, H 4.09, N 10.81. IR (KBr pellet): ν = 1704s (C=O), 1618w (C=N), 1596m (C=N), 1556m (C=C) cm^{-1}. ^{1}H-NMR (300.13MHz, DMSO, 298K): δ_H 10.35 (2H, s, C<u>H</u>O), 8.79 (2H, d, $^3J_{AB}$ = 8.28Hz, Ar<u>H</u>), 8.31 (2H, d, $^3J_{AB}$ = 8.31Hz, Ar<u>H</u>), 8.29 (2H, s, Ar<u>H</u>) ppm. ^{13}C-NMR (75.48MHz, DMSO, 298K): δ_C 193.7, 152.2, 145.2, 138.4, 131.4, 129.2, 120.1 ppm. ES MS: m/z = 236 $[C_{14}H_8N_2O_2]^+$.

2.4.3 Preparation of 2,9-Bis-[3',4',5'-tri(alkoxy)phenyliminomethyl]-1,10-Phenanthroline, $L^{Phen\text{-}n}$

Similar preparations were used for all ligands (Figure 2.19) and one example is given.

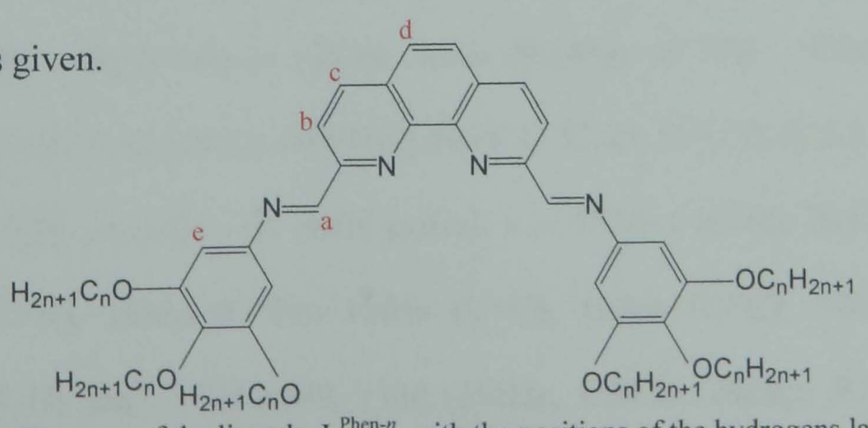

Figure 2.19. Structure of the ligands, $L^{Phen\text{-}n}$, with the positions of the hydrogens labelled a-e.

2.4.3.1 Synthesis of L^{Phen-1}

2,9-Diformyl-1,10-phenanthroline (0.0208g, 0.0880mmol) and 3,4,5-trimethoxyaniline (0.0356g, 0.194mmol) were heated to reflux in EtOH ($25cm^3$) for 4 hours. The yellow solution was concentrated under reduced pressure. The resulting yellow crystals were collected to give the 2.9-bis-[3',4',5'-tri(methoxy)phenyliminomethyl]-1,10-phenanthroline product. Recrystallisation was afforded by the layering of EtOH onto a $CHCl_3$ solution of product. Yield (0.02g, 40.1%). Microanalysis: Calculated for $C_{32}H_{30}N_4O_6$ C 67.83, H 5.34, N 9.89; found C 67.38, H 5.35, N 9.73. IR (KBr pellet): ν = 2992w (C-H), 2936w (C-H), 1681w (C=N), 1585s (C=N), 1502s (C=C), 1453m (C=C), 1419m (C=C), 1118vs (C-O) cm^{-1}. ^{1}H-NMR (300.13MHz, $CDCl_3$, 298K): δ_H 9.20 (2H, s, $\underline{H}_aC$=N), 8.67 (2H, d, $^3J_{AB}$ = 8.41 Hz, $\underline{H}_c$), 8.43 (2H, d, $^3J_{AB}$ = 8.41 Hz, $\underline{H}_b$), 7.96 (2H, s, $\underline{H}_d$), 6.77 (4H, s, $\underline{H}_e$), 3.95 (12H, s, lateral O$C\underline{H}_3$), 3.91 (6H, s, central O$C\underline{H}_3$) ppm. ^{13}C-NMR (75.48MHz, $CDCl_3$, 298K): δ_C 159.9, 155.0, 153.7, 146.1, 145.7, 137.1, 129.9, 127.6, 120.9, 99.0, 61.0, 56.2 ppm. EI MS: m/z = 566 $(L^{Phen-1})^+$.

2.4.3.2 Synthesis of L^{Phen-8}

This ligand was prepared as for L^{Phen-1}, from 2,9-diformyl-1,10-phenanthroline (0.0605g, 0.256mmol) and 3,4,5-trioctyloxyaniline (0.254g, 0.532mmol). Appearance: yellow solid (0.141g, 47.7%). Microanalysis: Calculated for $C_{74}H_{114}N_4O_6.0.5CHCl_3.H_2O$ C 72.55, H 9.52, N 4.54; found C 72.39, H 9.59, N 4.54. IR (KBr pellet): ν = 2920vs (C-H), 2851vs (C-H), 1617m (C=N), 1586s (C=N), 1505s (C=C), 1486s (C=C), 1435s (C=C), 1133vs (C-O) cm^{-1}. ^{1}H-NMR (300.13MHz, $CDCl_3$, 298K): 9.16 (2H, s,

$\underline{H}_aC{=}N$), 8.66 (2H, d, $^3J_{AB}$ = 8.64 Hz, $\underline{H}_c$), 8.40 (2H, d, $^3J_{AB}$ = 8.25 Hz, $\underline{H}_b$), 7.94 (2H, s, $\underline{H}_d$), 6.74 (4H, s, $\underline{H}_e$), 4.04 (12H, m, $OC\underline{H}_2$), 1.88-1.29 (72H, m $C\underline{H}_2$), 0.88 (18H, 2 overlapping triplets, $C\underline{H}_3$) ppm. ^{13}C-NMR (75.48MHz, $CDCl_3$, 298K): δ_C 159.5, 155.1, 153.5, 145.7, 145.6, 137.6, 137.0, 129.8, 127.5, 120.8, 100.2, 73.6, 69.0, 31.9, 31.8, 30.4, 29.4, 26.1, 22.7, 14.1 ppm. MALDI-TOF MS: m/z = 1155 $(L^{Phen\text{-}8})^+$

2.4.3.3 Synthesis of $L^{Phen\text{-}10}$

This ligand was prepared as for $L^{Phen\text{-}1}$, from 2,9-diformyl-1,10-phenanthroline (0.0202g, 0.0855mmol) and 3,4,5-tridecyloxyaniline (0.0959g, 0.171mmol). Appearance: yellow solid (0.0590g, 52.1%). Microanalysis: Calculated for $C_{86}H_{138}N_4O_6.2H_2O$ C 75.95, H 10.52, N 4.12; found C 75.71, H 10.16, N 4.27. IR (KBr pellet): ν = 2907vs (C-H), 1616m (C=N), 1585s (C=N), 1505s (C=C), 1464s (C=C), 1436s (C=C), 1120vs (C-O) cm^{-1}. ^{1}H-NMR (300.13MHz, $CDCl_3$, 298K): δ_H 9.16 (2H, s, $\underline{H}_aC{=}N$), 8.66 (2H, d, $^3J_{AB}$ = 8.15 Hz, $\underline{H}_c$), 8.40 (2H, d, $^3J_{AB}$ = 7.88 Hz, $\underline{H}_b$), 7.94 (2H, s, $\underline{H}_d$), 6.74 (4H, s, $\underline{H}_e$), 4.03 (12H, m, $OC\underline{H}_2$), 1.85-1.28 (96H, m $C\underline{H}_2$), 0.87 (18H, 2 overlapping triplets, $C\underline{H}_3$) ppm. ^{13}C-NMR (75.48MHz, $CDCl_3$, 298K): δ_C 159.5, 155.1, 153.5, 145.6, 145.5, 137.6, 137.0, 130.3, 127.5, 120.8, 100.2, 73.6, 69.0, 31.9, 30.4, 29.6, 29.4, 26.1, 22.7, 14.1 ppm (two alkyl carbons obscured). MALDI-TOF MS: m/z = 1323 $(L^{Phen\text{-}10})^+$

2.4.3.4 Synthesis of $L^{Phen\text{-}12}$

This ligand was prepared as for $L^{Phen\text{-}1}$, from 2,9-diformyl-1,10-phenanthroline (0.0355g, 0.150mmol) and 3,4,5-tridodecyloxyaniline (0.197g,

0.305mmol). Appearance: waxy brown solid (0.137g, 61.1%). Microanalysis: Calculated for $C_{98}H_{162}N_4O_6.0.5CHCl_3$ C 76.23, H 10.55, N 3.61; found C 76.48, H 10.73, N 4.95. IR (KBr pellet): ν = 2913vs (C-H), 2848vs (C-H), 1615m (C=N), 1586s (C=N), 1504s (C=C), 1467s (C=C), 1467s (C=C), 1132vs (C-O) cm^{-1}. ^{1}H-NMR (300.13MHz, $CDCl_3$, 298K): δ_H 9.16 (2H, s, $\underline{H}_aC$=N), 8.65 (2H, d, $^3J_{AB}$ = 8.55 Hz, $\underline{H}_c$), 8.40 (2H, d, $^3J_{AB}$ = 8.38 Hz, $\underline{H}_b$), 7.94 (2H, s, $\underline{H}_d$), 6.74 (4H, s, $\underline{H}_e$), 4.03 (12H, m, O$\underline{CH}_2$), 1.85-1.28 (96H, m $\underline{CH}_2$), 0.87 (18H, 2 overlapping triplets, $\underline{CH}_3$) ppm. ^{13}C-NMR (75.48MHz, $CDCl_3$, 298K): δ_C 159.5, 155.1, 153.5, 145.7, 145.5, 137.7, 137.0, 129.8, 127.5, 120.8, 100.3, 73.6, 69.1, 31.9, 30.4, 29.7, 29.4, 26.1, 22.7, 14.1 ppm (four alkyl carbons obscured). FAB MS: m/z = 1493 $(L^{Phen\text{-}12})^+$.

2.4.3.5 Synthesis of $L^{Phen\text{-}14}$

This ligand was prepared as for $L^{Phen\text{-}1}$, from 2,9-diformyl-1,10-phenanthroline (0.0210g, 0.0889mmol) and 3,4,5-tritetradecyloxyaniline (0.139g, 0.190mmol). Appearance: yellow crystals (0.0876g, 61.4%). Microanalysis: Calculated for $C_{110}H_{186}N_4O_6.2H_2O$ C 77.87, H 11.29, N 3.30; found C 77.72, H 11.24, N 3.59. IR (KBr pellet): ν = 2919vs (C-H), 2850vs (C-H), 1617w (C=N), 1586s (C=N), 1504s (C=C), 1468s (C=C), 1435m (C=C), 1124s (C-O) cm^{-1}. ^{1}H-NMR (300.13MHz, $CDCl_3$, 298K): δ_H 9.16 (2H, s, $\underline{H}_aC$=N), 8.66 (2H, d, $^3J_{AB}$ = 8.38 Hz, $\underline{H}_c$), 8.40 (2H, d, $^3J_{AB}$ = 8.38 Hz, $\underline{H}_b$), 7.94 (2H, s, $\underline{H}_d$), 6.74 (4H, s, $\underline{H}_e$), 4.03 (12H, m, O$\underline{CH}_2$), 1.88-1.26 (144H, m $\underline{CH}_2$), 0.88 (18H, 2 overlapping triplets, $\underline{CH}_3$) ppm. ^{13}C-NMR (75.48MHz, $CDCl_3$, 298K): δ_C 159.5, 155.2, 153.5, 145.7, 145.5, 137.7, 137.0, 129.8,

127.5, 120.8, 100.3, 73.6, 69.1, 31.9, 30.4, 29.7, 29.4, 26.2, 22.7, 14.1ppm (six alkyl carbons obscured). FAB MS: m/z = 1661 $(L^{Phen\text{-}14})^+$.

2.4.3.6 Synthesis of $L^{Phen\text{-}16}$

This ligand was prepared as for $L^{Phen\text{-}1}$, from 2,9-diformyl-1,10-phenanthroline (0.0221g, 0.0935mmol) and 3,4,5-trihexadecyloxyaniline (0.164g, 0.201mmol). Appearance: yellow solid (0.123g, 72.0%). Microanalysis: Calculated for $C_{122}H_{210}N_4O_6.CH_2Cl_2.H_2O$ C 76.47, H 11.16, N 2.90; found C 76.74, H 12.15, N 2.40. IR (KBr pellet): ν = 2917vs (C-H), 2850vs (C-H), 1587m (C=N), 1504m (C=C), 1468s (C=C), 1434w (C=C) cm^{-1}. ^{1}H-NMR (300.13MHz, $CDCl_3$, 298K): δ_H 9.16 (2H, s, $\underline{H}_aC$=N), 8.66 (2H, d, $^3J_{AB}$ = 8.30 Hz, $\underline{H}_c$), 8.40 (2H, d, $^3J_{AB}$ = 8.28 Hz, $\underline{H}_b$), 7.94 (2H, s, $\underline{H}_d$), 6.74 (4H, s, $\underline{H}_e$), 4.03 (12H, m, OC$\underline{H}_2$), 1.85-1.26 (168H, m C$\underline{H}_2$), 0.88 (18H, 2 overlapping triplets, C$\underline{H}_3$) ppm. ^{13}C-NMR (75.48MHz, $CDCl_3$, 298K): δ_C 159.5, 155.2, 153.7, 145.7, 145.5, 137.7, 137.0, 129.8, 127.5, 120.8, 100.3, 73.6, 69.0, 32.8, 31.9, 30.4, 30.3, 29.7, 29.4, 29.37, 26.2, 26.1, 22.7, 14.1 ppm (four alkyl carbons obscured). MALDI-TOF MS: m/z = 1829 $(L^{Phen\text{-}16})^+$.

2.4.4 Preparation of 2,9-Bis-[3',4',5'-tri(alkoxy)phenyliminomethyl]-1,10-Phenanthroline Metal(II) Chloride, $[MCl_2L^{Phen\text{-}n}]$

Similar preparations were used for all compounds (Figure 2.20), so one example for each series of complexes is given.

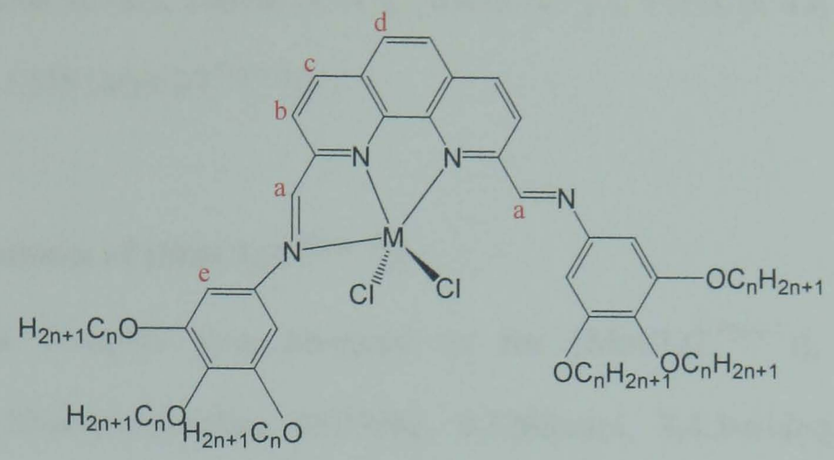

Figure 2.20. Structure of the complexes $[MCl_2(L^{Phen\text{-}n})]$, with selected hydrogen atoms labelled a-e in reference to the NMR spectra of the zinc(II) complexes.

2.4.4.1 Synthesis of $[MnCl_2(L^{Phen\text{-}1})]$

$MnCl_2.4H_2O$ (0.0490g, 0.247mmol), in EtOH ($10cm^3$), was added to a stirred mixture of 2,9-diformyl-1,10-phenanthroline (0.0501g, 0.212 mmol) and 3,4,5-trimethoxyaniline (0.0803g, 0.438mmol) in $CHCl_3$ ($25cm^3$). The red solution was heated to reflux for 24 hours. The solution was left to evaporate slowly at room temperature, affording a red solid (0.0932g, 63.5%). Microanalysis: Calculated for $C_{32}H_{30}Cl_2MnN_4O_6.CHCl_3$ C 52.60, H 4.16, N 7.44; found C 51.96, H 4.25, N 7.25. IR (KBr pellet): ν = 2962m (C-H), 2939m (C-H), 1620w (C=N), 1587s (C=N), 1503s (C=C), 1463m (C=C), 1415m (C=C), 1126s(C-O) cm^{-1}. FAB MS: m/z = 656 $[MnCl(L^{Phen\text{-}1})]^+$.

2.4.4.2 Synthesis of $[MnCl_2(L^{Phen\text{-}8})]$

This complex was prepared as for $[MnCl_2(L^{Phen\text{-}1})]$, from 2,9-diformyl,1,10-phenanthroline (0.0368g, 0.156mmol), 3,4,5-trioctyloxyaniline (0.154g, 0.322mmol) and $MnCl_2.4H_2O$ (0.0358g, 0.181mmol). Appearance: waxy red solid (0.103g, 51.6%). Microanalysis: Calculated for $C_{74}H_{114}Cl_2MnN_4O_6.CHCl_3$ C 64.30, H 8.27, N 4.00; found C 64.99, H 8.77, N 3.81. IR (KBr pellet): ν = 2925vs (C-H), 2854s (C-H), 1622m (C=N), 1587s

(C=N), 1503m (C=C), 1467m (C=C), 1436m (C=C), 1115s (C-O) cm^{-1}. FAB MS: m/z = 1245 $[MnCl(L^{Phen\text{-}8})]^+$.

2.4.4.3 Synthesis of $[MnCl_2(L^{Phen\text{-}10})]$

This complex was prepared as for $[MnCl_2(L^{Phen\text{-}1})]$, from 2,9-diformyl,1,10-phenanthroline (0.0300g, 0.126mmol, 3,4,5-tridecyloxyaniline (0.144g, 0.256mmol) and $MnCl_2.4H_2O$ (0.0251g, 0.126mmol). Appearance: brown solid (0.143g, 77.6%). Microanalysis: Calculated for $C_{86}H_{138}Cl_2MnN_4O_6$ C 71.24, H 9.59, N 3.86; found C 71.02, H 9.60, N 3.84. IR (KBr pellet): ν = 2911br,vs (C-H), 1622m (C=N), 1587s (C=N), 1504s (C=C), 1467s (C=C), 1437m (C=C), 1117vs (C-O) cm^{-1}. MALDI-TOF MS: m/z = 1450 $[MnCl_2(L^{Phen\text{-}10})]^+$.

2.4.4.4 Synthesis of $[MnCl_2(L^{Phen\text{-}12})]$

This complex was prepared as for $[MnCl_2(L^{Phen\text{-}1})]$, from 2,9-diformyl,1,10-phenanthroline (0.0302g, 0.128 mmol), 3,4,5-tridodecyloxyaniline (0.170g, 0.263mmol) and $MnCl_2.4H_2O$ (0.0329g, 0.166mmol). Appearance: waxy orange/yellow solid (0.124g, 62.1%). Microanalysis: Calculated for $C_{98}H_{162}Cl_2MnN_4O_6.CHCl_3$ C 68.43, H 9.46. N 3.22; found C 68.54, H 9.63, N 3.21. IR (KBr pellet): ν = 2858vs (C-H), 1623m (C=N), 1586s (C=N), 1507s (C=C), 1466s (C=C), 1437s (C=C), 1125vs (C-O) cm^{-1}. FAB MS: m/z = 1581 $[MnCl(L^{Phen\text{-}12})]^+$, 1546 $[Mn(L^{Phen\text{-}12})]^+$.

2.4.4.5 Synthesis of $[MnCl_2(L^{Phen\text{-}14})]$

This complex was prepared as for $[MnCl_2(L^{Phen\text{-}1})]$, from 2,9-diformyl,1,10-phenanthroline (0.0339g, 0.143mmol), 3,4,5-tritetradecyloxyaniline (0.211g, 0.289mmol) and $MnCl_2.4H_2O$ (0.0372g, 0.188mmol). Appearance: orange solid (0.152g, 59.4%). Microanalysis: Calculated for $C_{110}H_{186}Cl_2MnN_4O_6.H_2O.0.5CHCl_3$ C 71.19, H 10.19, N 3.01; found C 71.17, H 10.35, N 3.26. IR (KBr pellet): ν = 2911vs (C-H), 1624w (C=N), 1587s (C=N), 1506s (C=C), 1467s (C=C), 1437s (C=C), 1119vs (C-O) cm^{-1}. MALDI-TOF MS: m/z = 1786 $[MnCl_2(L^{Phen\text{-}14})]^+$.

2.4.4.6 Synthesis of $[MnCl_2(L^{Phen\text{-}16})]$

This complex was prepared as for $[MnCl_2(L^{Phen\text{-}1})]$, from 2,9-diformyl,1,10-phenanthroline (0.0306g, 0.130mmol), 3,4,5-trihexadecyloxyaniline (0.219g, 0.269mmol) and $MnCl_2.4H_2O$ (0.0567g, 0.286mmol). Appearance: orange solid (0.242g, 95.2%). Microanalysis: Calculated for $C_{120}H_{210}Cl_2MnN_4O_6.2H_2O$ C 73.58, H 10.97, N 2.85; found C 73.94, H 10.85, N 2.81. IR (KBr pellet): ν = 2919vs (C-H), 2850vs (C-H), 1616w (C=N), 1587m (C=N), 1503s (C=C), 1467s (C=C), 1437m (C=C), 1118vs (C-O) cm^{-1}. FAB MS: m/z = 1917 $[MnCl(L^{Phen\text{-}16})]^+$, 1883 $[Mn(L^{Phen\text{-}16})]^+$.

2.4.4.7 Synthesis of $[FeCl_2(L^{Phen\text{-}1})]$

2,9-Diformyl-1,10-phenanthroline (0.0541g, 0.229mmol) and 3,4,5-trimethoxyaniline (0.0841g, 0.459mmol) were stirred in $CHCl_3$ ($25cm^3$) for 10 mins. $FeCl_2.4H_2O$ (0.0533g, 0.268mmol) in EtOH ($10cm^3$) was added and the

solution underwent a colour change to dark red. The solution was then heated to reflux for 24 hours. The solvent volume was concentrated under reduced pressure to give a brown solid. This was recrystallised from EtOH and $CHCl_3$ (0.112g, 70.3%). Microanalysis: Calculated for $C_{32}H_{30}Cl_2FeN_4O_6$ C 55.43. H 4.36, N 8.08; found C 36.56, H 3.34, N 4.73. IR (KBr pellet): ν = 2935s (C-H), 2827m (C-H), 1627s (C=N), 1588s (C=N), 1504s (C=C), 1464s (C=C), 1420m (C=C), 1126vs (C-O) cm^{-1}. FAB MS: m/z = 657 $[FeCl(L^{Phen\text{-}1})]^+$, 621 $[Fe(L^{Phen\text{-}1})]^+$.

2.4.4.8 Synthesis of $[FeCl_2(L^{Phen\text{-}8})]$

This complex was prepared as for $[FeCl_2(L^{Phen\text{-}1})]$, from 2,9-diformyl,1,10-phenanthroline (0.0502g,0.212mmol), 3,4,5-trioctyloxyaniline (0.211g, 0.442mmol) and $FeCl_2.4H_2O$ (0.0480g, 0.241mmol). Appearance: dark brown solid (0.178g, 65.6%). Microanalysis: Calculated for $C_{74}H_{114}Cl_2FeN_4O_6$ C 69.30, H 8.96, N 4.37; found C 69.21, H 9.34, N 3.64. IR (KBr pellet): ν = 2930vs (C-H), 2855vs (C-H), 1620m (C=N), 1585s (C=N), 1500s (C=C), 1467s (C=C), 1437m (C=C), 1114vs (C-O) cm^{-1}. FAB MS: m/z = 1246 $[FeCl(L^{Phen\text{-}8})]^+$, 1211 $[Fe(L^{Phen\text{-}8})]^+$.

2.4.4.9 Synthesis of $[FeCl_2(L^{Phen\text{-}10})]$

This complex was prepared as for $[FeCl_2(L^{Phen\text{-}1})]$, from 2,9-diformyl,1,10-phenanthroline (0.0520g,0.220mmol), 3,4,5-tridecyloxyaniline (0.252g, 0.448mmol) and $FeCl_2.4H_2O$ (0.0499g, 0.250mmol). Appearance: dark brown solid (0.201g, 63.1%). Microanalysis: Calculated for $C_{86}H_{138}Cl_2FeN_4O_6.CHCl_3.H_2O$ C 68.30, H 9.31, N 3.66; found

C 68.04, H 9.08, N 3.65. IR (KBr pellet): ν = 2926vs (C-H), 2851vs (C-H), 1620w (C=N), 1585s (C=N), 1501s (C=C), 1467s (C=C), 1437m (C=C), 1117vs (C-O) cm^{-1}. FAB MS: m/z = 1414 $[FeCl(L^{Phen\text{-}10})]^+$, 1379 $[Fe(L^{Phen\text{-}10})]^+$.

2.4.4.10 Synthesis of $[FeCl_2(L^{Phen\text{-}12})]$

This complex was prepared as for $[FeCl_2(L^{Phen\text{-}1})]$, from 2,9-diformyl,1,10-phenanthroline (0.0600g,0.254mmol), 3,4,5-tridodecyloxyaniline (0.330g, 0.511mmol) and $FeCl_2.4H_2O$ (0.0578g, 0.291mmol). Appearance: dark brown solid (0.308g, 75.0%). Microanalysis: Calculated for $C_{98}H_{162}Cl_2FeN_4O_6$ C 72.70, H 10.08, N 3.46; found C 62.55, H 7.92, N 4.34. IR (KBr pellet): ν =2955vs (C-H), 2848vs (C-H), 1620m (C=N), 1587s (C=N), 1505s (C=C), 1468s (C=C), 1437s (C=C), 1115vs (C-O) cm^{-1}. FAB MS: m/z = 1582 $[FeCl(L^{Phen\text{-}12})]^+$, 1547 $[Fe(L^{Phen\text{-}12})]^+$.

2.4.4.11 Synthesis of $[FeCl_2(L^{Phen\text{-}14})]$

This complex was prepared as for $[FeCl_2(L^{Phen\text{-}1})]$, from 2,9-diformyl,1,10-phenanthroline (0.0330g,0.140mmol), 3,4,5-tritetradecyloxyaniline (0.202g, 0.277mmol) and $FeCl_2.4H_2O$ (0.0295g, 0.148mmol). Appearance: dark brown solid (0.210g, 83.9%). Microanalysis: Calculated for $C_{110}H_{186}Cl_2FeN_4O_6.CHCl_3.2H_2O$ C 68.65, H 9.91, N 2.88; found C 68.40, H 9.67, N 2.85. IR (KBr pellet): ν = 2950vs (C-H), 2852vs (C-H), 1616m (C=N), 1590s (C=N), 1502s (C=C), 1467s (C=C), 1436m (C=C), 1119vs (C-O) cm^{-1}. FAB MS: m/z = 1750 $[FeCl(L^{Phen\text{-}14})]^+$, 1715 $[Fe(L^{Phen\text{-}14})]^+$.

2.4.4.12 Synthesis of $[FeCl_2(L^{Phen\text{-}16})]$

This complex was prepared as for $[FeCl_2(L^{Phen\text{-}1})]$, from 2,9-diformyl,1,10-phenanthroline (0.0677g,0.287mmol), 3,4,5-trihexadecyloxyaniline (0.469g, 0.576mmol) and $FeCl_2.4H_2O$ (0.0776g, 0.390mmol). Appearance: brown solid (0.474g, 84.4%). Microanalysis: Calculated for $C_{122}H_{210}Cl_2FeN_4O_6.CHCl_3.2H_2O$ C 69.96, H 10.26, N 2.65; found C 69.56, H 10.14, N 2.55. IR (KBr pellet): ν = 2935vs (C-H), 2853vs (C-H), 1620m (C=N), 1586s (C=N), 1501s (C=C), 1468v(C=C), 1437m (C=C), 1118vs (C-O) cm^{-1}. FAB MS: m/z = 1919 $[FeCl(L^{Phen\text{-}16})]^+$, 1883 $[Fe(L^{Phen\text{-}16})]^+$.

2.4.4.13 Synthesis of $[CoCl_2(L^{Phen\text{-}1})]$

2,9-Diformyl-1,10-phenanthroline (0.0499g, 0.211mmol) and 3,4,5-trimethoxyaniline (0.0776g, 0.424mmol) were stirred for 10mins in $CHCl_3$ ($25cm^3$). On addition of $CoCl_2.6H_2O$ (0.0506g, 0.213mmol) in EtOH ($10cm^3$), the mixture became a dark red solution. This was heated to reflux for 24 hours. The solution volume was concentrated under reduced pressure to give a brown/orange solid. This was recrystallised from $CHCl_3$ and EtOH (0.0973g, 66.2%). Microanalysis: Calculated for $C_{32}H_{30}Cl_2CoN_4O_6.H_2O$ C 53.79, H 4.51, N 7.84; found C 53.67, H 4.38, N 7.62. IR (KBr pellet): ν = 2940m (C-H), 1622m (C=N), 1589s (C=N), 1505s (C=C), 1464s (C=C), 1420s (C=C), 1124vs (C-O) cm^{-1}. FAB MS: m/z = 660 $[CoCl(L^{Phen\text{-}1})]^+$, 625 $[Co(L^{Phen\text{-}1})]^+$.

2.4.4.14 Synthesis of $[CoCl_2(L^{Phen\text{-}8})]$

This complex was prepared as for $[CoCl_2(L^{Phen\text{-}1})]$. from 2,9-diformyl,1,10-phenanthroline (0.0623g, 0.264mmol), 3,4,5-trioctyloxyaniline (0.259g, 0.542mmol) and $CoCl_2.6H_2O$ (0.0629g, 0.264mmol). Appearance: waxy, brown solid (0.325g 95.8%). Microanalysis: Calculated for $C_{74}H_{114}Cl_2CoN_4O_6.H_2O$ C 68.18, H 8.97, N 4.30; found C 67.88, H 8.89, N 4.20. IR (KBr pellet): ν = 2927vs (C-H), 2853vs (C-H), 1621m (C=N), 1586s (C=N), 1501s (C=C), 1467s (C=C), 1436m (C=C), 1116br,vs (C-O) cm^{-1}. FAB MS: m/z = 1241 $[Co(L^{Phen\text{-}8})]^+$.

2.4.4.15 Synthesis of $[CoCl_2(L^{Phen\text{-}10})]$

This complex was prepared as for $[CoCl_2(L^{Phen\text{-}1})]$, from 2,9-diformyl,1,10-phenanthroline (0.0509g, 0.215mmol), 3,4,5-tridecyloxyaniline (0.242g, 0.431mmol) and $CoCl_2.6H_2O$ (0.0524g, 0.220mmol). Appearance: dark brown solid (0.234g 74.8%). Microanalysis: Calculated for $C_{86}H_{138}Cl_2CoN_4O_6.H_2O$ C 70.18, H 9.59, N 3.81; found C 69.96, H 9.38, N 3.88. IR (KBr pellet): ν = 2955vs (C-H), 2846vs (C-H), 1621m (C=N), 1585s (C=N), 1499s (C=C), 1461s (C=C), 1429s (C=C), 1119s (C-O) cm^{-1}. FAB MS: m/z = 1380 $[Co(L^{Phen\text{-}10})\text{-}2H]^+$.

2.4.4.16 Synthesis of $[CoCl_2(L^{Phen\text{-}12})]$

This complex was prepared as for $[CoCl_2(L^{Phen\text{-}1})]$, from 2,9-diformyl,1,10-phenanthroline (0.0950g, 0.402mmol), 3,4,5-tridodecyloxyaniline (0.522g, 0.808mmol) and $CoCl_2.6H_2O$ (0.0958g, 0.403mmol). Appearance: waxy, brown solid (0.484g 74.1%). Microanalysis:

Calculated for $C_{98}H_{162}Cl_2CoN_4O_6.H_2O$ C 71.76, H 10.08, N 3.42: found C 71.93, H 10.05, N 3.28. IR (KBr pellet): ν = 2930vs (C-H), 2853vs (C-H), 1614m (C=N), 1587s (C=N), 1502s (C=C), 1467s (C=C), 1438m (C=C), 1118vs (C-O) cm^{-1}. FAB MS: m/z = 1551 $[Co(L^{Phen\text{-}12})]^+$.

2.4.4.17 Synthesis of $[CoCl_2(L^{Phen\text{-}14})]$

This complex was prepared as for $[CoCl_2(L^{Phen\text{-}1})]$, from 2,9-diformyl,1,10-phenanthroline (0.0295g, 0.124mmol), 3,4,5-tritetradecyloxyaniline (0.181g, 0.248mmol) and $CoCl_2.6H_2O$ (0.0307g, 0.129mmol). Appearance: orange solid (0.150g 67.3%). Microanalysis: Calculated for $C_{110}H_{186}Cl_2CoN_4O_6.CHCl_3$ C 69.80, H 9.87, N 2.93; found C 69.66, H 10.01, N 2.55. IR (KBr pellet): ν = 2917vs (C-H), 2849vs (C-H), 1611m (C=N), 1590m (C=N), 1500m (C=C), 1467m (C=C), 1437w (C=C), 1118m (C-O) cm^{-1}. FAB MS: m/z = 1719 $[Co(L^{Phen\text{-}14})]^+$.

2.4.4.18 Synthesis of $[CoCl_2(L^{Phen\text{-}16})]$

This complex was prepared as for $[CoCl_2(L^{Phen\text{-}1})]$, from 2,9-diformyl,1,10-phenanthroline (0.108g, 0.456mmol), 3,4,5-trihexadecyloxyaniline (0.748g, 0.918mmol) and $CoCl_2.6H_2O$ (0.114g, 0.479mmol). Appearance: brown/orange solid (0.774g, 86.6%). Microanalysis: Calculated for $C_{122}H_{210}Cl_2CoN_4O_6.CHCl_3$ C 73.12, H 10.55, N 2.77; found C 72.98, H 10.73, N 3.15. IR (KBr pellet): ν = 2920vs (C-H), 2849vs (C-H), 1614m (C=N), 1588m (C=N), 1502m (C=C), 1468s (C=C), 1437m (C=C), 1118s (C-O) cm^{-1}. FAB MS: m/z = 1923 $[CoCl(L^{Phen\text{-}16})]^+$, 1888 $[Co(L^{Phen\text{-}16})]^+$.

2.4.4.19 Synthesis of $[NiCl_2(L^{Phen\text{-}1})]$

In a solution of $CHCl_3$, 2,9-diformyl-1,10-phenanthroline (0.0392g,0.139mmol) was added to 3,4,5-trimethoxyaniline (0.0539g, 0.294mmol) and stirred for 10 mins. $NiCl_2.6H_2O$ (0.0424g, 0.178mmol) in EtOH ($10cm^3$) was added and the yellow mixture became an orange/brown solution. The solution was heated to reflux for 24 hours and then allowed to cool, producing a yellow solid (0.0266g, 27.5%). Microanalysis: Calculated for $C_{32}H_{30}Cl_2N_4NiO_6.2CHCl_3$ C 48.43, H 3.83, N 6.85; found C 49.06, H 4.10, N 7.16. IR (KBr pellet): ν = 2991w (C-H), 2941w (C-H), 1622w (C=N), 1588s (C=N), 1505s (C=C), 1453m (C=C), 1420m (C=C), 1125s (C-O) cm^{-1}. FAB MS: m/z = 659 $[NiCl(L^{Phen\text{-}1})]^+$.

2.4.4.20 Synthesis of $[NiCl_2(L^{Phen\text{-}8})]$

This complex was prepared as for $[NiCl_2(L^{Phen\text{-}1})]$, from 2,9-diformyl,1,10-phenanthroline (0.0374g, 0.158mmol), 3,4,5-trioctyloxyaniline (0.165g, 0.345mmol) and $NiCl_2.6H_2O$ (0.0452g, 0.190mmol). Appearance: orange/ brown solid (0.0741g 36.5%). Microanalysis: Calculated for $C_{74}H_{114}Cl_2N_4NiO_6.3CHCl_3$ C 62.97, H 8.05, N 3.82; found C 62.22, H 8.79, N 3.64. IR (KBr pellet): ν = 2925vs (C-H), 2855vs (C-H), 1622w (C=N), 1585s (C=N), 1502s (C=C), 1467s (C=C), 1435m (C=C), 1114vs (C-O) cm^{-1}. FAB MS: m/z = 1252 $[NiCl(L^{Phen\text{-}8})]^+$. 1217 $[Ni(L^{Phen\text{-}8})]^+$.

2.4.4.21 Synthesis of $[NiCl_2(L^{Phen\text{-}10})]$

This complex was prepared as for $[NiCl_2(L^{Phen\text{-}1})]$, from 2,9-diformyl,1,10-phenanthroline (0.0740g, 0.313mmol), 3,4,5-tridecyloxyaniline (0.390g, 0.604mmol) and $NiCl_2.6H_2O$ (0.0780g, 0.328mmol). Appearance: dark brown, waxy solid (0.322g 70.8%). Microanalysis: Calculated for $C_{86}H_{138}Cl_2N_4NiO_6.CHCl_3$ C 66.43, H 8.91, N 3.56; found C 66.43, H 8.91, N 3.56. IR (KBr pellet): ν = 2921s (C-H), 1587s (C=N), 1501s (C=C), 1466s (C=C), 1427m (C=C), 1119vs (C-O) cm^{-1}. MALDI-TOF MS: m/z = 1453 $[NiCl_2(L^{Phen\text{-}10})]^+$.

2.4.4.22 Synthesis of $[NiCl_2(L^{Phen\text{-}12})]$

This complex was prepared as for $[NiCl_2(L^{Phen\text{-}1})]$, from 2,9-diformyl,1,10-phenanthroline (0.0291g, 0.123mmol), 3,4,5-tridodecyloxyaniline (0.164g, 0.254mmol) and $NiCl_2.6H_2O$ (0.0301g, 0.127mmol). Appearance: waxy, brown solid (0.155g 77.7%). Microanalysis: Calculated for $C_{98}H_{162}Cl_2N_4NiO_6.2H_2O$ C 70.99, H 10.09, N 3.38; found C 70.59, H 9.92, N 3.32. IR (KBr pellet): ν = 2920vs (C-H), 2853vs (C-H), 1614w (C=N), 1586m (C=N), 1502s (C=C), 1467s (C-H), 1436m (C-H), 1116vs (C-O) cm^{-1}. FAB MS: m/z = 1585 $[NiCl(L^{Phen\text{-}12})]^+$, 1549 $[Ni(L^{Phen\text{-}12})]^+$.

2.4.4.23 Synthesis of $[NiCl_2(L^{Phen\text{-}14})]$

This complex was prepared as for $[NiCl_2(L^{Phen\text{-}1})]$, from 2,9-diformyl,1,10-phenanthroline (0.0121g,0.0512mmol), 3,4,5-tritetradecyloxyaniline (0.0750g, 0.103mmol) and $NiCl_2.6H_2O$ (0.0124g,

0.0522mmol). Appearance: orange solid (0.0534g, 58.2%). Microanalysis: Calculated for $C_{110}H_{186}Cl_2N_4NiO_6.2CHCl_3$ C 70.33, H 9.93, N 2.93; found C 69.47, H 10.29, N 2.89. IR (KBr pellet): ν = 2924vs (C-H), 2852vs (C-H), 1602w (C=N), 1588m (C=N), 1502m (C=C), 1467m (C=C), 1437w (C=C), 1118s (C-O) cm^{-1}. FAB MS: m/z = 1754 $[NiCl(L^{Phen\text{-}14})]^+$, 1717 $[Ni(L^{Phen\text{-}14})]^+$.

2.4.4.24 Synthesis of $[NiCl_2(L^{Phen\text{-}16})]$

This complex was prepared as for $[NiCl_2(L^{Phen\text{-}1})]$, from 2,9-diformyl,1,10-phenanthroline (0.0241g,0.102mmol), 3,4,5-trihexadecyloxyaniline (0.168g, 0.206mmol) and $NiCl_2.6H_2O$ (0.0256g, 0.108mmol). Appearance: orange solid (0.183g, 91.9%). Microanalysis: Calculated for $C_{122}H_{210}Cl_2N_4NiO_6.CHCl_3$ C 71.09, H 10.23, N 2.70; found C 71.12, H 10.75, N 2.79. IR (KBr pellet): ν = 2911s (C-H), 2854s (C-H), 1614w (C=N), 1586s (C=N), 1503s (C=C), 1468s (C=C), 1436m (C=C), 1117vs (C-O) cm^{-1}. FAB MS: m/z = 1921 $[NiCl(L^{Phen\text{-}16})]^+$, 1886 $[Ni(L^{Phen\text{-}16})]^+$.

2.4.4.25 Synthesis of $[CuCl_2(L^{Phen\text{-}1})]$

2,9-Diformyl-1,10-phenanthroline (0.0504g, 0.213mmol) and 3,4,5-trimethoxyaniline (0.0786g, 0.429mmol) were stirred in $CHCl_3$ ($25cm^3$) for 10 mins. $CuCl_2$ (0.0400g, 0.298mmol) in EtOH ($10cm^3$) was added and the solution underwent a colour change to dark red. The solution was then heated to reflux for 24 hours. The solvent volume was concentrated under reduced pressure to give a dark brown solid (0.0912g, 61.1%). Microanalysis: Calculated for $C_{32}H_{30}Cl_2CuN_4O_6.CHCl_3.3H_2O$ C 45.32, H 4.26, N 6.41; found

C 45.38, H 3.79, N 6.83. IR (KBr pellet): ν = 2965m (C-H), 1616m (C=N), 1588m (C=N), 1502m (C=C), 1465m (C=C), 1105vs (C-O) cm^{-1}.

2.4.4.26 Synthesis of $[CuCl_2(L^{Phen\text{-}8})]$

This complex was prepared as for $[CuCl_2(L^{Phen\text{-}1})]$, from 2,9-diformyl,1,10-phenanthroline (0.0572g,0.242mmol), 3,4,5-trioctyloxyaniline (0.234g, 0.490mmol) and $CuCl_2$ (0.0344g, 0.256mmol). Appearance: brown solid (0.214g, 68.6%). Microanalysis: Calculated for $C_{74}H_{114}Cl_2CuN_4O_6.3CHCl_3$ C 62.77, H 8.02, N 3.80; found C 62.68, H 7.99, N 4.43. IR (KBr pellet): ν = 2926vs (C-H), 2855vs (C-H), 1620m (C=N), 1589s (C=N), 1501s (C=C), 1467s (C=C), 1437m (C=C), 1102vs (C-O) cm^{-1}. FAB MS: m/z = 1219 $[Cu(L^{Phen\text{-}8})]^+$.

2.4.4.27 Synthesis of $[CuCl_2(L^{Phen\text{-}10})]$

This complex was prepared $[CuCl_2(L^{Phen\text{-}1})]$, from 2,9-diformyl,1,10-phenanthroline (0.0531g,0.225mmol), 3,4,5-tridecyloxyaniline (0.253g, 0.450mmol) and $CuCl_2$ (0.0315g, 0.234mmol). Appearance: brown solid (0.148g, 45.4%). Microanalysis: Calculated for $C_{86}H_{138}Cl_2CuN_4O_6 4CHCl_3$ C 55.83, H 7.39, N 2.89; found C 55.97, H 7.13, N 3.06. IR (KBr pellet): ν = 2955vs (C-H), 2914vs (C-H), 1614m (C=N), 1586s (C=N), 1500s (C=C), 1467s (C=C), 1433s (C=C), 1113vs (C-O) cm^{-1}. FAB MS: m/z = 1387 $[Cu(L^{Phen\text{-}10})]^+$.

2.4.4.28 Synthesis of $[CuCl_2(L^{Phen\text{-}12})]$

This complex was prepared $[CuCl_2(L^{Phen\text{-}1})]$, from 2,9-diformyl,1,10-phenanthroline (0.0386g,0.163mmol), 3,4,5-tridodecyloxyaniline (0.208g, 0.322mmol) and $CuCl_2$ (0.0399g, 0.168mmol). Appearance: dark brown solid (0.202g, 76.3%). Microanalysis: Calculated for $C_{98}H_{162}Cl_2CuN_4O_6.CHCl_3$ C 68.09, H 9.41, N 3.21; found C 67.92, H 9.75, N 2.98. IR (KBr pellet): ν = 2926vs (C-H), 2853vs (C-H), 1621w (C=N), 1587m (C=N), 1501s (C=C), 1467s (C=C), 1436m (C=C), 1116vs (C-O) cm^{-1}. FAB MS: m/z = 1554 $[Cu(L^{Phen\text{-}12})]^+$.

2.4.4.29 Synthesis of $[CuCl_2(L^{Phen\text{-}14})]$

This complex was prepared $[CuCl_2(L^{Phen\text{-}1})]$, from 2,9-diformyl,1,10-phenanthroline (0.0120g,0.0508mmol), 3,4,5-tritetradecyloxyaniline (0.0767g, 0.0103mmol) and $CuCl_2$ (0.0113g, 0.0840mmol). Appearance: dark brown/red solid (0.0517g, 56.7%). Microanalysis: Calculated for $C_{110}H_{186}Cl_2CuN_4O_6.CHCl_3.2H_2O$ C 68.35, H 9.87, N 2.87; found C 68.27, H 9.92, N 2.47. IR (KBr pellet): ν = 2919vs (C-H), 2851vs (C-H), 1623w (C=N), 1592m (C=N), 1502w (C=C), 1467m (C=C), 1102s (C-O) cm^{-1}. FAB MS: Expected ions not found.

2.4.4.30 Synthesis of $[CuCl_2(L^{Phen\text{-}16})]$

This complex was prepared $[CuCl_2(L^{Phen\text{-}1})]$, from 2,9-diformyl,1,10-phenanthroline (0.0435g, 0.184mmol), 3,4,5-trihexadecyloxyaniline (0.302g, 0.371mmol) and $CuCl_2$ (0.0321g, 0.239mmol). Appearance: dark brown/red solid (0.251g, 67.5%). Microanalysis: Calculated for

$C_{122}H_{210}Cl_2CuN_4O_6.2CHCl_3$ C 71.41, H 10.27, N 2.69; found C 71.75, H 10.26, N 2.80. IR (KBr pellet): ν = 2937vs (C-H), 2844vs (C-H), 1617m (C=N), 1589s (C=N), 1499m (C=C), 1467s (C=C), 1111vs (C-O) cm^{-1}. FAB MS: Expected ions not found

2.4.4.31 Synthesis of $[ZnCl_2(L^{Phen\text{-}1})]$

2,9-Diformyl-1,10-phenanthroline (0.0507g, 0.215mmol) and 3,4,5-trimethoxyaniline (0.0847g, 0.462mmol) were stirred in chloroform ($25cm^3$) for 10 mins. $ZnCl_2$ (0.0512g, 0.376mmol) in EtOH ($10cm^3$) was added and the solution underwent a colour change from yellow to orange. This was then heated at reflux for 24 hours. The solution was concentrated under reduced pressure and an orange solid precipitated out. The solid was recrystallised from EtOH and $CHCl_3$. Yield (0.111g, 73.4%). Microanalysis: Calculated for $C_{32}H_{30}Cl_2N_4O_6Zn.2H_2O$ C 52.01, H 4.64, N 7.58; found C 52.79, H 4.11, N 7.53. IR (KBr pellet): ν = 2940w (C-H), 1624m (C=N), 1590s (C=N), 1505s (C=C), 1464m (C=C), 1420m (C=C), 1126vs (C-O) cm^{-1}. ^{1}H-NMR (300.13MHz, $CDCl_3$, 298K): δ_H 9.49 (2H, s, $\underline{H}_aC$=N), 8.60 (2H, d, $^3J_{AB}$ = 8.43Hz, $\underline{H}_c$), 8.50 (2H, d, $^3J_{AB}$ = 7.85 Hz, $\underline{H}_b$), 8.06 (2H, s, $\underline{H}_d$), 7.20 (4H, s, $\underline{H}_e$), 3.91 (12H, s, lateral OC$\underline{H}_3$), 3.84 (6H, s, central OC$\underline{H}_3$) ppm. ^{13}C-NMR (75.48MHz, $CDCl_3$, 298K): δ_C 154.4, 153.3, 151.1, 142.7, 140.7, 139.5, 138.8, 130.0, 127.5, 124.8, 101.0, 60.9, 56.2 ppm. FAB MS: m/z = 667 $[ZnCl(L^{Phen\text{-}1})]^+$, 702 $[ZnCl_2(L^{Phen\text{-}1})]^+$.

2.4.4.32 Synthesis of $[ZnCl_2(L^{Phen\text{-}8})]$

This complex was prepared as for $[ZnCl_2(L^{Phen\text{-}1})]$, from 2,9-diformyl-1,10-phenanthroline (0.0429g, 0.182mmol), 3,4,5-trioctyloxyaniline (0.0299g, 0.219mmol) and $ZnCl_2$ (0.0188g, 0.393mmol). Appearance: orange solid (0.162g, 69.0%). Microanalysis: Calculated for $C_{74}H_{114}Cl_2N_4O_6Zn.CH_2Cl_2$ C 65.52, H 8.50, N 4.07; found C 64.80, H 8.67, N 4.00. IR (KBr pellet): ν = 2917vs (C-H), 2855vs (C-H), 1624m (C=N), 1585s (C=N), 1502s (C=C), 1468s (C=C), 1435s (C=C), 1115vs (C-O) cm^{-1}. ^{1}H-NMR (300.13MHz, $CDCl_3$, 298K): δ_H 9.49 (2H, s, $\underline{H}_aC$=N), 8.50 (2H, d, $^3J_{AB}$ = 8.26 Hz, $\underline{H}_c$), 8.39 (2H, d, $^3J_{AB}$ = 8.20 Hz, $\underline{H}_b$), 7.99 (2H, s, $\underline{H}_d$), 7.10 (4H, s, $\underline{H}_e$), 3.96 (12H, m, OC$\underline{H}_2$), 1.77-1.27 (72H, m, C$\underline{H}_2$), 0.87 (18H, 2 overlapping triplets, C$\underline{H}_3$) ppm. ^{13}C-NMR (75.48MHz, $CDCl_3$, 298K): δ_C 152.8, 152.3, 150.4, 141.8, 139.9, 138.3, 129.0, 126.4, 123.6, 101.2, 72.5, 68.2, 31.0, 30.9, 29.5, 28.3, 25.2, 21.7, 13.0 ppm. FAB MS: m/z = 1255 $[ZnCl(L^{Phen\text{-}8})]^+$.

2.4.4.33 Synthesis of $[ZnCl_2(L^{Phen\text{-}10})]$

This complex was prepared as for $[ZnCl_2(L^{Phen\text{-}1})]$, from 2,9-diformyl-1,10-phenanthroline (0.0268g, 0.113mmol), 3,4,5-tridecyloxyaniline (0.127g, 0.227mmol) and $ZnCl_2$ (0.0108g, 0.132mmol). Appearance: red solid (0.117g, 71.0%). Microanalysis: Calculated for $C_{86}H_{138}Cl_2N_4O_6Zn.H_2O.CHCl_3$ C 65.40, H 8.90, N 3.51; found C 65.24, H 9.09, N 3.56. IR (KBr pellet): ν = 2919vs (C-H), 2853vs (C-H),1622m (C=N), 1586vs (C=N), 1501s (C=C), 1467s (C=C), 1436s (C=C), 1117vs (C-O) cm^{-1}. ^{1}H-NMR (300.13MHz, $CDCl_3$, 298K): δ_H 9.43 (2H, s, $\underline{H}_aC$=N), 8.55 (2H, d, $^3J_{AB}$ = 6.00 Hz, $\underline{H}_c$), 8.45 (2H, d, $^3J_{AB}$ = 7.50 Hz, $\underline{H}_b$), 8.02 (2H, s, $\underline{H}_d$), 7.13 (4H, s, $\underline{H}_e$), 4.04 (8H, t, $^3J_{AB}$

= 6.18 Hz, lateral OC$\underline{H}_2$), 3.97 (4H, t, $^3J_{AB}$ = 6.75 Hz, central OC$\underline{H}_2$), 1.79-1.27 (96H, m, C$\underline{H}_2$), 0.88 (18H, 2 overlapping triplets, C$\underline{H}_3$) ppm. ^{13}C-NMR (75.48MHz, $CDCl_3$, 298K): δ_C 153.1, 151.1, 145.3, 142.5, 140.6, 139.3, 138.7, 129.8, 127.4, 124.5, 101.8, 73.4, 68.9, 31.9, 30.4, 29.8, 29.6, 29.4, 26.2, 26.1, 22.7, 14.1 ppm. FAB-MS: m/z = 1423 $[ZnCl(L^{Phen\text{-}10})]^+$.

2.4.4.34 Synthesis of $[ZnCl_2(L^{Phen\text{-}12})]$

This complex was prepared as for $[ZnCl_2(L^{Phen\text{-}1})]$, from 2,9-diformyl-1,10-phenanthroline (0.0300g, 0.127mmol), 3,4,5-tridodecyloxyaniline (0.166g, 0.257mmol) and $ZnCl_2$ (0.0184g, 0.135mmol). Appearance: orange solid (0.178g, 86.0%). Microanalysis: Calculated for $C_{98}H_{162}Cl_2N_4O_6Zn.2CHCl_3$ C 64.32, H 8.85, N 3.00; found C 65.49, H 9.27, N 3.00. IR (KBr pellet): ν = 2923vs (C-H), 2852vs (C-H), 1622w (C=N), 1586m (C=N), 1503s (C=C), 1467m (C=C), 1436w (C=C), 1116vs (C-O) cm^{-1}. ^{1}H-NMR (300.13MHz, $CDCl_3$, 298K): δ_H 9.43 (2H, s, $\underline{H}_aC$=N), 8.55 (2H, d, $^3J_{AB}$ = 8.18 Hz, $\underline{H}_c$), 8.45 (2H, d, $^3J_{AB}$ = 8.50 Hz, $\underline{H}_b$), 8.02 (2H, s, $\underline{H}_d$), 7.13 (4H, s, $\underline{H}_e$), 4.04 (8H, t, $^3J_{AX}$ = 6.17 Hz, lateral OC$\underline{H}_2$), 3.98 (4H, t, $^3J_{AX}$ = 6.42 Hz, central OC$\underline{H}_2$), 1.79-1.26 (120H, m, C$\underline{H}_2$), 0.88 (18H, 2 overlapping triplets, C$\underline{H}_3$) ppm. ^{13}C-NMR (75.48MHz, $CDCl_3$, 298K): δ_C 153.9, 153.1, 151.1, 142.5, 140.6, 139.2, 138.7, 129.8, 127.4, 124.5, 101.8, 73.4, 69.0, 31.9, 30.4, 29.7, 29.6, 29.4, 26.2, 26.14, 22.7, 14.1 ppm (two alkyl carbons obscured). FAB MS: m/z = 1591 $[ZnCl(L^{Phen\text{-}12})]^+$.

2.4.4.35 Synthesis of $[ZnCl_2(L^{Phen\text{-}14})]$

This complex was prepared as for $[ZnCl_2(L^{Phen\text{-}1})]$. from 2,9-diformyl-1,10-phenanthroline (0.0326g, 0.138mmol), 3,4,5-tritetradecyloxyaniline (0.227g, 0.311mmol) and $ZnCl_2$ (0.0223g, 0.164mmol). Appearance: red solid (0.182g, 73.2%). Microanalysis: Calculated for $C_{110}H_{186}Cl_2N_4O_6.H_2O$ C 72.79, H 10.44, N 3.09; found C 72.35, H 10.51, N 3.24. IR (KBr pellet): ν = 1622w (C=N), 1586s (C=N) cm^{-1}. ^{1}H-NMR (300.13MHz, $CDCl_3$, 298K): δ_H 9.42 (2H, s, $\underline{H}_aC$=N), 8.56 (2H, d, $^3J_{AB}$ = 8.24 Hz, $\underline{H}_c$), 8.46 (2H, d, $^3J_{AB}$ = 8.37 Hz, $\underline{H}_b$), 8.02 (2H, s, $\underline{H}_d$), 7.13 (4H, s, $\underline{H}_e$), 4.05 (8H, t, $^3J_{AX}$ = 6.36 Hz, lateral O$C\underline{H}_2$), 3.98 (4H, t, $^3J_{AX}$ =6.48 Hz, central O$C\underline{H}_2$), 1.76-1.26 (144H, m, $C\underline{H}_2$), 0.88 (18H, 2 overlapping triplets, $C\underline{H}_3$) ppm. ^{13}C-NMR (75.48MHz, $CDCl_3$, 298K): δ_C 154.2, 153.4, 153.1, 142.7, 140.5, 140.6, 138.7, 129.8, 127.4, 124.7, 101.8, 73.4, 69.0, 31.9, 30.4, 29.8, 29.4, 26.2, 22.7, 14.1 ppm (six alkyl carbons obscured). FAB MS: m/z = 1761 $[ZnCl(L^{Phen\text{-}14})]^+$.

2.4.4.36 Synthesis of $[ZnCl_2(L^{Phen\text{-}16})]$

This complex was prepared as for $[ZnCl_2(L^{Phen\text{-}1})]$, from 2,9-diformyl-1,10-phenanthroline (0.0607g, 0.257mmol), 3,4,5-trihexadecyloxyaniline (0.420g, 0.516mmol) and $ZnCl_2$ (0.0388g, 0.285mmol). Appearance: red solid (0.0427g, 84.5%). Microanalysis: Calculated for $C_{122}H_{210}Cl_2N_4O_6Zn.2H_2O$ C 73.22, H 10.78, N 2.80; found C 73.07, H 10.55, N 2.80. IR (KBr pellet): ν = 2839vs (C-H), 1616w (C=N), 1586s (C=N), 1503s (C=C), 1468s (C=C), 1420s (C=C), 1120vs (C-O) cm^{-1}. ^{1}H-NMR (300.13MHz, $CDCl_3$, 298K): δ_H 9.45 (2H, s, $\underline{H}_aC$=N), 8.53 (2H, d, $^3J_{AB}$ = 9.00Hz, $\underline{H}_c$), 8.43 (2H, d, $^3J_{AB}$ = 9.00 Hz, $\underline{H}_b$), 8.01 (2H, s, $\underline{H}_d$), 7.12 (4H, s, $\underline{H}_e$), 4.02 (8H, t, $^3J_{AX}$ = 6.82 Hz, lateral

$OC\underline{H}_2$), 3.96 (4H, t, $^3J_{AX}$ = 6.00 Hz central $OC\underline{H}_2$), 1.74-1.25 (168H, m, $C\underline{H}_2$), 0.88 (18H, 2 overlapping triplets, $C\underline{H}_3$) ppm. ^{13}C-NMR (75.48MHz, $CDCl_3$, 298K): δ_C 154.0, 153.1, 151.1, 142.5, 140.6, 139.3, 138.7, 129.8, 127.4, 124.7, 101.7, 73.4, 68.9, 31.9, 30.4, 30.3, 29.8, 29.6, 29.4, 29.3, 26.2, 25.7, 22.7, 14.1 ppm (four alkyl carbons obscured). MALDI-TOF MS: m/z = 1966 $[ZnCl_2(L^{Phen\text{-}16})]^+$.

2.5 REFERENCES

[1] S. J. P. Bousquet and D. W. Bruce, *J. Mater. Chem.*, 2001, **11**, 1769.

[2] G. Pickaert, L. Douce, R. Ziessel and D. Guillon, *Chem. Commun.*, 2002, 1584.

[3] Y. G. Galyametdinov, L. Malykhina, W. Haase, K. Drisen and K. Binnemans, *Liq. Cryst.*, 2002, **29**, 1581.

[4] (a) M. A. Masood and D. J. Hodgson, *Inorg. Chem.*, 1992, **32**, 4839; (b) A. Angeloff, J.-C. Daran, J. Bernadou and B. Meunier, *Eur. J. Inorg. Chem.*, 2000, 1985; (c) C. W. G. Ansell, J. Lewis, M. C. Liptrot, P. R. Raithby and M. Schröder, *J. Chem. Soc. Dalton Trans.*, 1982, 1593; (d) C. Dietrich-Buchecker, J.-P. Sauvage and J.-M. Kern, *J. Am. Chem. Soc.*, 1989, **111**, 7791.

[5] For a review of non-liquid crystalline 1,10-phenanthroline chemistry see P. G. Sammes and G. Yahioglu, *Chem. Soc. Rev.*, 1994, **23**, 327.

[6] (a) D. L. de Murillas, R. Piñol, M. B. Ros, J. L. Serrano, T. Sierra and M. R. de la Fuente, *J. Mater. Chem.*, 2004, **14**, 1117; (b) R. Inglesias, M. Marcos, J. L. Serrano and T. Sierra, *Chem. Mater.*, 1996, **8**, 2611.

[7] (a) L. Wang, W.-H. Sun, L. Han, H. Yang, Y. Hu and X. Jin, *J. Organomet. Chem.*, 2002, **658**, 62; (b) G. J. P. Britovsek, S. P. D. Baugh, O. Hoarau, V. C.

Gibson, D. F. Wass, A. J. P. White and D. J. Williams, *Inorg. Chim. Acta*, 2003, **345**, 279; (c) A. Angeloff, J.-C. Daran, J. Bernadou and B. Meunier, *Eur. J. Inorg. Chem.*, 2000, 1985.

[8] (a) C. K. Lai, A. G. Serrete, T. M. Swager, *J. Am. Chem. Soc.*, 1992, **114**, 7948; (b) A. G. Serrete and T. M. Swager, *J. Am. Chem. Soc.*, 1993, **115**, 8879.

[9] C. J. Chandler, L. W. Deady and J. A. Reiss, *J. Heterocyclic Chem.*, 1981, **18**, 599.

[10] (a) M. Veber, H. Strzelecka and C. Jallabert, *Mol. Cryst. Liq. Cryst. Inc. Nomlin. Opt.*, 1988, **156**, 347; (b) A. Zinsou, M. Veber, H. Strzelecka, C. Jallabert and P. Fourré, *New J. Chem.*, 1993, **17**, 309.

[11] (a) F. Morale, R. W. Date, D. Guillon, D. W. Bruce, R. L. Finn, C. Wilson, A. J. Blake, M. Schröder and B. Donnio, *Chem. Eur. J.*, 2003, **9**, 2484; (b) L. Douce, A. El-ghayoury, A. Skoulios and R. Ziessel, *Chem. Commun.*, 1999, 2033; (c) E. Terazzi, S. Torelli, G. Bernardinelli, J.-P. Rivera, J.-M. Bénech, C. Bourgogne, B. Donnio, D. Guillon, D. Imbert, J.-C. G. Bünzli, A. Pinto, D. Jeannerat and C. Piguet, *J. Am .Chem. Soc.*, 2005, **127**, 888; (d) G. Barberio, A. Bellusci, A. Crispini, M. Ghedini, A. Golemme, P. Prus and D. Pucci, *Eur. J. Inorg. Chem.*, 2005, 181.

[12] (a) S. Ameeruniska and P. S. Zacharias, *Polyhedron*, 1994, **13**, 15/16, 2327; (b) A. Toth, C. Floriani, M. Pasquali, A. Chiesi-Villa, A. Gaetani-Manfredotti and C. Guastini, *Inorg. Chem.*, 1985, **24**, 648; (c) M. Marcos, J. L. Serrano, T. Sierra and M. J. Giménez, *Chem. Mater.*, 1993, **5**, 1332.

[13] D. H. Williams and I. Fleming, *Spectroscopic Methods in Organic Chemistry*, 4th edition, McGraw-Hill International (UK) Limited, Maidenhead, 1989.

[14] A. W. Addison, T. N. Rao, A. Reedijik, J. van Rijn and G. C. Verschoor, *J. Chem. Soc. Dalton Trans.*, 1984, 1349.

[15] C. Janiak, *J. Chem. Soc., Dalton Trans.*, 2000, 3885.

[16] F. Morale, *Metallomesogens Derived From Schiff-Base Chelates and Related Co-ordination Chemistry*, PhD Thesis, The University of Nottingham, Nottingham, 2002.

[17] (a) M. A. Esteruelas, E. Sola, L. A. Oro, M. B. Ros, M. Marcos and J. L. Serrano, *J. Organomet. Chem.*, 1990, **387**, 103; (b) S. Suarez, D. Imbert, F. Gumy, C. Piguet and J. C. G. Bunzli, *Chem. Mater.*, 2004, **16**, 3257; (c) K. Binnemans, R. Van Deun, B. Thijs, I. Vanwelkenhuysen, I. Geuens, *Chem. Mater.*, 2004, **16**, 2021; (d) S. Coco, P. Espinet, E. Marcos, *J. Mater. Chem.*, 2000, **10**, 1297; (e) P. Alejos, S. Coco, P. Espinet, *New. J. Chem.*, 1995, **19**, 799; (f) J. A. R. Cheda, M. V. G. Pérez, M. I. R. Yélamos and A. S. Arenas, *J. Therm. Anal. Calorim.*, 2004, **76**, 7.

[18] (a) H. Zheng, C. K. Lai and T. M. Swager, *Chem. Mater.*, 1995, **7**, 2067; (b) K. Binnemans, J. Sleven, S. De Feyter, F. C. De Scryver, B. Donnio and D. Guillon, *Chem. Mater.*, 2003, **15**, 3930; (c) K. Ohta, H. Akimoto, T. Fujimoto and I. Yamamoto, *J. Mater. Chem.*, 1994, **4**, 61.

[19] C. K. Lai, C.-H. Tsai and Y.-S. Pang, *J. Mater. Chem.*, 1998, **8**, 1355.

[20] C. R. Safinya, K. S. Liang, W. A. Varady, N. A. Clark and G. Andersson, *Phys. Rev. Lett.*, 1984, **53**, 1172.

[21] (a) M. J. Cook, M. F. Daniel, K. J. Harrison, N. B. McKeown and A. J. Thomson, *J. Chem. Soc., Chem. Commun.*, 1987, 1086; (b) O. Fernández, G. de la Torre, F. Fernández-Lázaro, J. Barberá and T. Torres, *Chem. Mater.*, 1997, **9**, 3017; (c) J. Barberá, *Metallomesogens: Symthesis, Properites and Applications*, ed. J. L. Serrano, VCH:Weinheim, 1996, Chapter 4; (d) B. Donnio, D. Guillon, R. Deschenaux and D. W. Bruce, *Comprehensive Coord. Chem. II*, ed. J. A. McCleverty and T. J. Meyer, Oxford: Elsevier, 2004, **7**, 357.

CHAPTER 3:

METALLOMESOGENS DERIVED FROM 2,2'-BIPYRIDINE

3.1 INTRODUCTION TO LIQUID CRYSTALS OF 2,2' BIPYRIDINE

3.1.1 Liquid Crystals of 2,2'-Bipyridine

The use of 2,2'-bipyridine motifs in the design of thermotropic liquid crystals has been established for over a decade longer than the use of 1,10-phenanthroline moieties. The first 2,2'-bipyridines of this type were synthesised in the late 1980's, when Hanabusa *et al.* designed homopolyesters (Figure 3.1) and copolyesters (Figure 3.2) with 5,5'-disubstituted-2,2'-bipyridine units.[1]

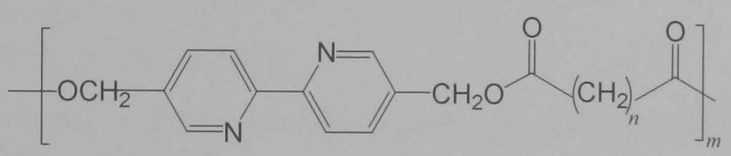

L^1

Cr 120 Sm 142 I

Figure 3.1. Mesomorphic homopolyester containing 2,2'-bipyridine, where n = 10 (L^{1a}) and 11 (L^{1b}).[1] Transition temperatures are given in °C.

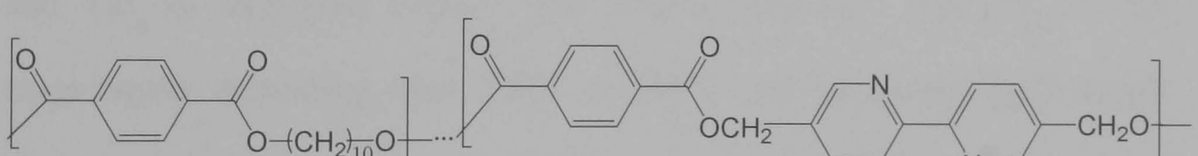

L^2

Cr 114 N 135 I

Figure 3.2. Mesomorphic copolyester containing 2,2'-bipyridine, where p/q = 9/1 (L^{2a}) and p/q =4/1 (L^{2b}).[1] Transition temperatures are given in °C.

The Hanabusa group were also the first to prepare thermotropic 2,2'-bipyridine metallomesogens with the binding of transition metal salts $FeCl_2$ and $CuCl_2$ into the polyesters L^1 and L^2. The homopolyester ligands L^1 (Figure 3.1) and their complexes at low concentrations of metal ions displayed smectic phases, whereas the copolyesters L^2 (Figure 3.2) and their complexes displayed nematic phases. Since this initial discovery of mesomorphic 2,2'-

bipyridines, there have been two groups who have dominated this field, namely Bruce[2] and Ziessel.[3] Their principal findings are reviewed below.

Bruce and Rowe prepared 5,5'-disubstitued-2,2'-bipyridine diesters of the type displayed in Figure 3.3.

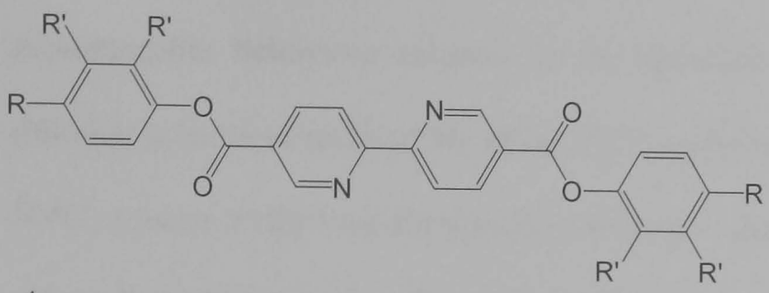

$R = OCH_3$, $R' = H$ L^4
$R = OC_4H_9$, $R' = H$
$R = OC_8H_{17}$, $R' = H$
$R = OC_{12}H_{25}$, $R' = H$
$R = OC_8H_{17}$, $R' = F$ L^5

L^4 $n = 1$: Cr 220 SmA 241 N 428 I
$n = 4$: Cr 194 SmC 256 SmA 299 N 370 I
$n = 8$: Cr 135 Cryst J 155 SmC 275 SmA 280 N 290 I
$n = 12$: Cr 140 SmC 260 N 265 I
L^5 $n = 8$: Cr 206 SmC 232 N 259 I

Figure 3.3. 5,5'-Disubstituted-2,2'-bipyridine diesters prepared by Bruce and Rowe.[2(a),2(b),2(d)] Transition temperatures are given in °C.

The dicatenar species with R' = H and $R = OC_nH_{2n+1}$ (where n = 1, 4, 8 and 12) all displayed nematic and smectic phases,[2(a)] with the melting temperatures decreasing from 220°C to 140°C with increasing chain length. This was a trend also observed by the clearing temperatures, which decreased from 428°C to 265°C. In the longer chain compounds the stability of the smectic C phase was dominant over both that of the smectic A and nematic mesophases.

Attempts to incorporate transition metal cations into the ligands whilst retaining liquid crystalline behaviour were unsuccessful. Complexation of $W(CO)_4$, $PdCl_2$, $NiCl_2$, $CoCl_2$ and $Cu(NO_3)_2$ to the ligands L^4 with n = 8 in Figure 3.3, or of $Mo(CO)_4$ to L^4 with n = 12, resulted in decomposition of the complexes on heating. Complexation of $[ReBr(CO)_5]$ to L^4 with n = 8 resulted in a thermally stable complex, although the complex displayed no mesomorphic behaviour and melted into the isotropic liquid at 253°C.[2(b)]

The effect of dipolar atoms as lateral substituents in 2,2'-bipyridine-derived compounds was investigated by fluorination of the 5,5'-disubstitued-2,2'-bipyridine diester ligand in Figure 3.3. The compound L^5 had R' = F and R = OC_8H_{17} (Figure 3.3).[2(d)] The effect of fluorination was to destabilise the mesomorphic behaviour relative to the non-fluorinated analogue, L^4. The clearing point was reduced by about 30°C and the melting point increased by 70°C, relative to the non-fluorinated analogue. The mesophase types were also affected, so that the crystal smectic J and smectic A phases that were present in the phase transition sequence for L^4 with n = 8 were omitted from the phase sequence for the fluorinated analogue, L^5. Hence, L^5 generated smectic C and nematic mesophases only.

Fluorination had little effect on the transition metal complex $[Re(CO)_3Br(L^5)]$ relative to $[Re(CO)_3Br(L^4)]$, as both had similar melting temperatures and neither displayed any mesomorphic character.[2(d)]

Non-fluorinated ligands with carboxylate groups at the 4,4'- positions of 2,2'-bipyridine (Figure 3.4) were also studied to examine the relationship between structure and mesomorphism in these systems.[2(a)]

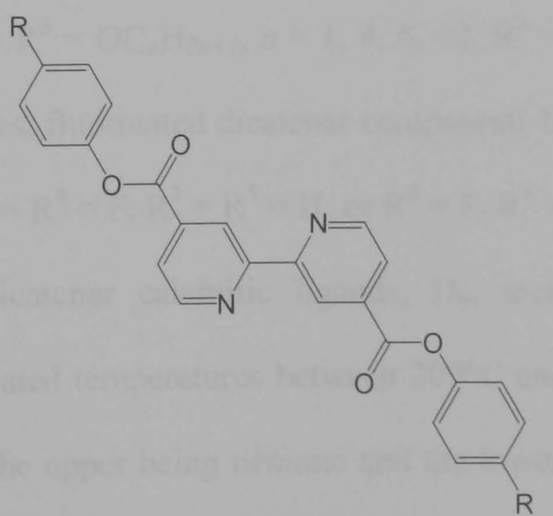

L^6: R = OC_nH_{2n+1}
n = 1: Cr 208 N 210 I
n = 4: Cr 199 (N 195) I
n = 8: Cr 169 I

Figure 3.4. Bis(alkoxyphenyl)-2,2'-bipyridine-4,4'-dicarboxylate ligands prepared by Bruce and Rowe, with R = OC_nH_{2n+1} (where n = 1, 4, 8).[2(a)] Transition temperatures are given in °C.

The 4,4'-diesters exhibited much lower clearing points than their 5,5'-analogues, but the melting temperatures remained similar. The smectic character exhibited by the 5,5'-diesters was completely lost in the 4,4'-ligands, which showed an enantiotropic nematic phase for $n = 1$, a monotropic nematic phase for $n = 4$, and no mesomorphic character for $n = 8$. These observations can be explained by the reduction in shape anisotropy of the 4,4'-diesters, which is no longer able to stabilise the formation of smectic phases.

As part of continuing investigations into the mesomorphic properties of 2,2'-bipyridine ligands and complexes, Bruce and Rowe focussed on 5,5'-disubstituted compounds. In an effort to prepare bipyridine metallomesogens, highly anisotropic ligands were prepared to compensate for any perturbation of anisotropy (and subsequent loss of liquid crystalline behaviour) prompted by metal complexation. Hence, the new ligand design incorporated the bipyridine core along with four phenyl rings (Figure 3.5).

These ligands were prepared as dicatenar species, D_n ($R^2 = OC_nH_{2n+1}$, $n = 1, 4, 8, 12, 14$, $R^1 = R^3 = R^4 = R^5 = H$), a full series of tetracatenar ligands, T_n ($R^1 = R^2 = OC_nH_{2n+1}$, $n = 1$-14, $R^3 = R^4 = R^5 = H$) and hexacatenar compounds, H_n ($R^1 = R^2 = R^3 = OC_nH_{2n+1}$, $n = 1, 4, 8, 12$, $R^4 = R^5 = H$).[2(c)] In addition to these molecules, fluorinated dicatenar compounds L^8 were also synthesised ($R^2 = OC_8H_{17}$, $R^1 = R^4 = F$, $R^3 = R^5 = H$; or $R^5 = F$, $R^1 = R^3 = R^4 = H$).[2(d)]

The dicatenar calamitic ligands, D_n, melted into liquid crystalline phases at elevated temperatures between 209°C and 269°C. D_1 exhibited two mesophases, the upper being nematic and the lower an unidentified phase. D_4 went though a nematic phase only, whereas the longer chain molecules of D_8, D_{12} and D_{14} exhibited smectic C and nematic mesophases.

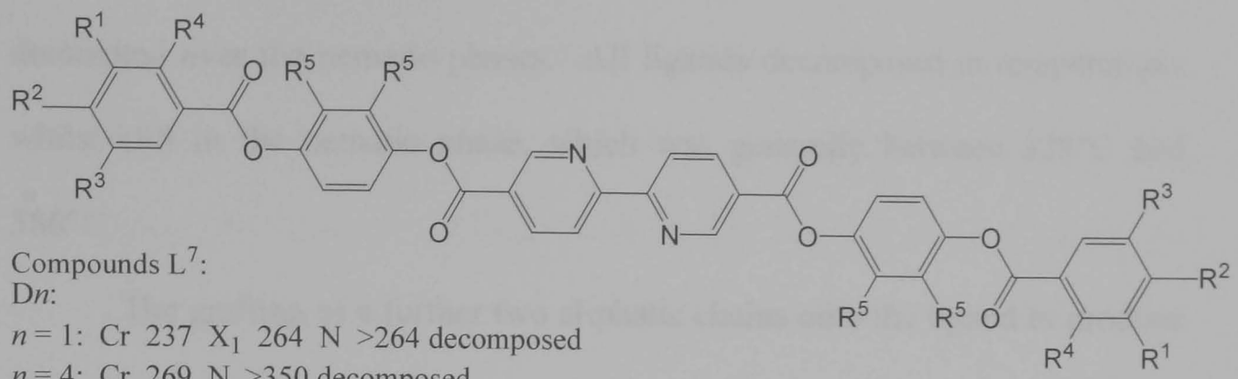

Compounds L^7:
D*n*:
n = 1: Cr 237 X_1 264 N >264 decomposed
n = 4: Cr 269 N >350 decomposed
n = 8: Cr 231 SmC 328 N >328 decomposed
n = 12: Cr 210 X_2 212 SmC 341 N >341 decomposed
n = 14: Cr 209 X_2 211 SmC 355 N 368 I decomposed

T*n*:
n = 1: Cr 259 N >300 decomposed
n = 2: Cr 262 N >300 decomposed
n = 3: Cr 263 N 345 I
n = 4: Cr 242 N 325 I
n = 5: Cr 221 SmC 229 N 294 I
n = 6: Cr 196 SmC 220 Cub 239 N 272 I
n = 7: Cr 184 SmC 197 Cub 239 I
n = 8: Cr 173 SmC 188 Cub 229 Col_h 237 I
n = 9: Cr 171 Col_h 238 I
n = 10: Cr 166 Col_h 237 I
n = 11: Cr 165 Col_h 236 I
n = 12: Cr 161 Col_h 234 I
n = 13: Cr 161 Col_h 229 I
n = 14: Cr 161 Col_h 230 I

H_n:
n = 1: Cr 203 Cub 211 SmA 217 N 292 I
n = 4: Cr 143 Col 176 I
n = 8: Cr 85 Col_1 157 Col_2 165 I
n = 12: Cr 54 Col_1 142 Col_2 151 I

$Re(CO)_3Br(D_4)$: Cr 275 N 315 I
$Re(CO)_3Br(D_8)$: Cr 224 N 315 I
$Re(CO)_3Br(D_{12})$: Cr 238 SmC 267 N 296 I
$Re(CO)_3Br(T_{10})$: Cr 128 Col_h 170 I
$Re(CO)_3Br(T_{12})$: Cr 125 Cub 158 Col_h 177 I
$Re(CO)_3Br(T_{14})$: Cr 122 Col_r 157 Cub 168 Col_h 198 I

Compounds L^8:
L^{8a}: Cr 174 Cr' 239 SmC 360 N decomposed
L^{8b}: Cr 219 SmC 256 N decomposed
$Re(CO)_3Br(L^{8b})$: Cr 224 SmC 259 N 304 I decomposed

Figure 3.5. Di-, tetra- and hexacatenar ligands synthesised by Bruce and Rowe.[2(c)-(f)] Compounds L^7: D_n has $R^2 = OC_nH_{2n+1}$, *n* = 1, 4, 8, 12, 14, $R^1 = R^3 = R^4 = R^5 = H$; T_n has $R^1 = R^2 = OC_nH_{2n+1}$, *n* = 1-14, $R^3 = R^4 = R^5 = H$); and H_n has $R^1 = R^2 = R^3 = OC_nH_{2n+1}$, *n* = 1, 4, 8, 12, $R^4 = R^5 = H$. Compounds L^8: L^{8a} has $R^2 = OC_8H_{17}$, $R^1 = R^4 = F$, $R^3 = R^5 = H$; L^{8b} has $R^2 = OC_8H_{17}$, $R^5 = F$, $R^1 = R^3 = R^4 = H$. Transition temperatures are given in °C.

D_{12} and D_{14} displayed an additional short-range phase between the crystal and smectic C phases, which was tentatively assigned as a crystal smectic phase.

The smectic C temperature range increased with increasing chain length. and dominated over the nematic phases. All ligands decomposed at temperatures whilst still in the nematic phase, which was generally between 328°C and 386°C.

The grafting of a further two aliphatic chains onto the ligand to produce tetracatenar, T_n, compounds was expected to strongly influence the types of mesophases produced as the length of the chains were increased. Therefore, a complete homologous series from n = 1-14 was synthesised. Compared to the melting and clearing temperatures of the analogous n = 4, 8, 12 and 14 dicatenar ligands, the tetracatenar compounds showed much lower transition temperatures as is expected of ligands of increased liquid-like character. These melting and clearing temperatures progressively decreased with increasing n, and the T_n series exhibited phase behaviour typical of tetracatenar species. At short chain lengths nematic and smectic C phases were observed and at long chain lengths columnar hexagonal phases appeared. The crossover from calamitic-like behaviour to discotic-like behaviour occurred at intermediate chain lengths and was accompanied by the appearance of a cubic phase.

To complete the study of the effects of increasing the number of aliphatic chains on the mesomorphic character of the 2,2'-bipyridine ligand in Figure 3.5, Bruce and Rowe prepared the hexacatenar compounds, H_n, with n = 1, 4, 8 and 12. Once again, the incorporation of additional chains served to lower the melting and clearing temperatures relative to the di- and tetracatenar species. Both melting and clearing transitions for H_n decreased with increasing n. The melting temperatures decreased steadily from 203°C to 54°C. The compounds cleared into the isotropic liquid between 176°C and 151°C for n =

4, 8, 12, and at 292°C for n = 1. Typical hexacatenar phase behaviour was exhibited by the n = 4, 8, and 12 compounds, which formed columnar mesophases. The n = 1 derivative showed the unusual phase sequence Cr – *Cub* – *SmA* – *N* – I, which is thought to be the first time this exact sequence has been observed. It is more usual to observe either the phase sequence Cub – SmA - I or Cub – N - I.[4]

To test whether the increased anisotropy of the ligands prevented the loss of mesomorphism on complexation, the ligands D_4, D_8, D_{12}, T_{10}, T_{12} and T_{14} were reacted with $[ReBr(CO)_5]$.[2(e),2(f)] No loss in mesomorphism was observed. Both $[Re(CO)_3Br(D_4)]$ and $[Re(CO)_3Br(D_{12})]$ retained the respective nematic and smectic C phases seen in the free ligands. $[Re(CO)_3Br(D_8)]$ formed a single nematic phase, but did not form the smectic C phase that was displayed by the metal-free analogue. The effect of complexation on the transition temperatures was to decrease clearing temperatures relative to the metal-free ligands. The melting temperatures for $[Re(CO)_3Br(D_4)]$ and $[Re(CO)_3Br(D_{12})]$ were higher than D_4 and D_{12}, whereas the melting temperature for $[Re(CO)_3Br(D_8)]$ was lower than D_8. The overall result of complexation of the dicatenar ligands to rhenium(I) was to decrease the mesomorphic temperature range.

As well as preserving the columnar phases seen in the tetracatenar ligands, the Re(I) tetracatenar complexes of T_{12} and T_{14} displayed an additional cubic phase. The clearing temperatures of the T*n* complexes increased with increasing chain length, whereas the opposite trend was observed for the melting points. Hence, mesomorphism was stabilised as the length of the aliphatic chains was increased. In comparison to the metal-free tetracatenar

ligands, the complexes exhibited much lower melting and clearing temperatures. Thus, the mesophase temperature ranges for $[Re(CO)_3Br(T_{10})]$ and $[Re(CO)_3Br(T_{12})]$ were smaller than those for T_{10} and T_{12}, whereas $[Re(CO)_3Br(T_{14})]$ had a larger mesomorphic range than T_{14}.

As with the aforementioned two phenyl-ring bipyridine molecules L^6, the effects of fluorination were investigated on the dicatenar $n = 8$ compound.[2(d)] The two sites of fluorination were either on the outer (L^{8a}: $R^1 = R^4 = F$) or inner (L^{8b}: $R^5 = F$) phenyl rings (Figure 3.5). In comparison to the non-fluorinated analogue, all three molecules displayed identical smectic C and nematic mesophases, and fluorination affected only the extent of stabilisation of each particular phase. Substitution at the inner rings (L^{8b}) resulted in destabilisation of the smectic C phase, and reducing the transition temperature from smectic C to nematic by about 70°C. The melting temperature was also reduced though less significantly. Substitution at the outer rings (L^{8a}) produced an additional crystal phase and stabilised the smectic C phase by over 30°C, relative to the non-fluorinated analogue D_8. The accompanying decomposition in the nematic phases hindered the measurement of clearing temperatures for L^{8a} and L^{8b}. Complexation of the molecule L^{8b} to $Re(CO)_5Br$ to give $[Re(CO)_3Br(L^{8b})]$ resulted in a large reduction in the stability of the smectic C phase, along with destabilisation of the nematic phase.

Bruce and Rowe tweaked the design of the four phenyl-ring ligand one further time by reversing the direction of the outer ester groups (Figure 3.6), thus arranging the dipoles as a kind of 'outboard' dipole in the hope of promoting smectic phases.[2(c)]

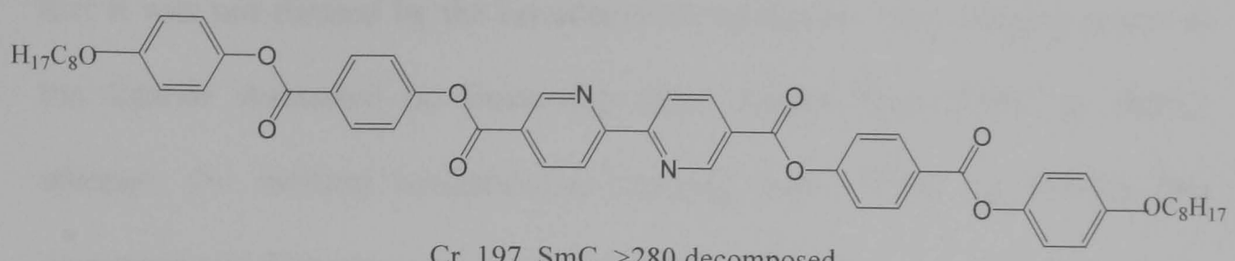

Cr 197 SmC >280 decomposed

L^9

Figure 3.6. Bruce and Rowe ligand with 'reversed' outer diesters.[2(c)] Transition temperatures are given in °C.

The result was to stabilise the smectic phase by destabilising the crystal and nematic phases compared to the original ligand D_8 (Figure 3.5). The nematic phase was suppressed completely and the melting temperature was reduced by 34°C to 197°C. Above 280°C the smectic C phase decomposed.

The research carried out by Ziessel *et al.* on 2,2'-bipyridine moieties has been predominantly centred on the study of asymmetric 5,5'-disubstituted-2,2'-bipyridines. Initial work in this field was on the synthesis and characterisation of the liquid crystalline properties of the mono-substituted 5-methyl-5'-(4-*n*-alkoxyphenylvinyl)-2,2'-bipyridine (Figure 3.7).[3(a),3(b)]

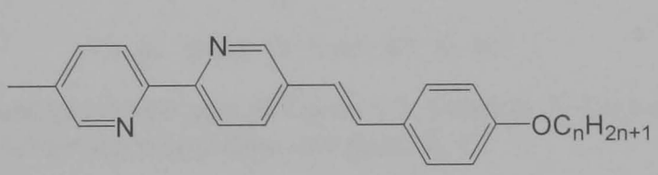

L^{10}:

n = 8: Cr 130 SmB 143 SmA 165 N 210 I
n = 10: Cr 110 SmB 145 SmA 178 N 202 I
n = 12: Cr 115 SmB 145 SmA 185 N 198 I
n = 14: Cr 118 SmB 142 SmA 182 N 190 I
n = 16: Cr 120 SmB 140 SmA 180 I

Figure 3.7. 5-Methyl-5'-(4-*n*-alkoxyphenylvinyl)-2,2'-bipyridine, where *n* = 8, 10, 12, 14, 16.[3(a),3(b)] Transition temperatures are given in °C.

These calamitic molecules displayed successive smectic B, smectic A and nematic phases on increasing temperature. As the length of the chain was increased the smectic phases were stabilised at the expense of the nematic phases. The nematic phase was sufficiently destabilised at long chain lengths

that it was not formed by the hexadecyloxy molecule. The clearing points of the ligands decreased on increasing chain length from 210°C to 180°C, whereas the melting temperatures (ranging from 130°C to 115°C) first decreased and then increased on going from $n = 8$ to 16.

Removal of the polar conjugated linkage and replacement with a more flexible non-polar connecting group (Figure 3.8) resulted in a narrower mesomorphic temperature range. However, the mesophase types remained the same, but the melting and clearing temperatures were significantly reduced compared to the conjugated version. These findings were rationalised by considering 5-methyl-5'-[2-(4-decyloxyphenyl)ethyl]-2,2'-bipyridine having a shorter conjugation length, a smaller polarisability, and less-planar structure. All of these factors served to destabilise the mesomorphic character of the molecule.[3(g)]

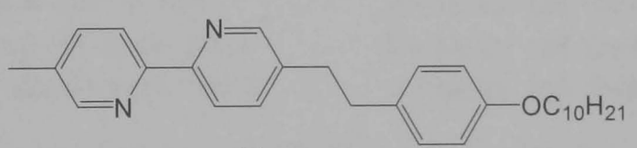

L^{11}

Cr 61 SmB 73 SmA 87 N 107 I

Figure 3.8. Non-conjugated analogue of Figure 3.7, 5-methyl-5'-[2-(4-decyloxyphenyl)ethyl]-2,2'-bipyridine.[3(g)] Transition temperatures are given in °C.

In an effort to induce mesophases through hydrogen-bonding the Ziessel group equipped the ligand 5-methyl-5'-[2-(4-decyloxyphenyl)ethyl]-2,2'-bipyridine (Figure 3.8) with an alcohol fragment (Figure 3.9).[3(g)]

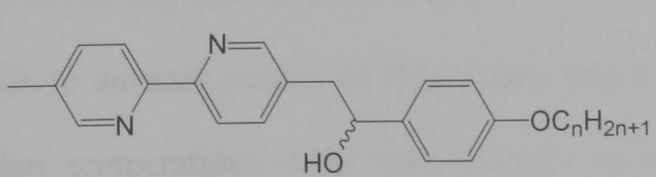

L^{12}

$n = 6$: Cr 98 SmA 123 N 143 I
$n = 8$: Cr 80 SmA 138 N 147 I
$n = 10$: Cr 64 SmA 129 I
$n = 12$: Cr 82 SmA 140 I

Figure 3.9. Chiral ligand 5-methyl-5'-[2-(4-alkyloxyphenyl)-2-hydroxyethyl]-2,2'-bipyridine, where $n = 6$, 8, 10 and 12.[3(g)] Transition temperatures are given in °C.

The racemic compounds with a branching hydroxy function and an aliphatic chain of length n = 6, 8, 10 and 12 carbon atoms, stabilised smectic A phases. The nematic phases were destabilised and were only observed alongside the smectic A phase for n = 6 and 8. The mesomorphic phases were formed in the temperature range of 64°C and 147°C.

Another family of 5,5'-substitued 2,2'-bipyridine ligands studied by Ziessel *et al.* contained ethynyl rather than ethyl linkage groups (Figure 3.10).[3(h)]

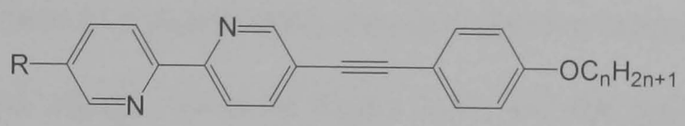

L^{13}:
R = H, n = 6: Cr 84 N 98 I
n = 8: Cr 81 N 106 I
n = 10: Cr 82 SmA 97 N 108 I
n = 12: Cr 87 SmA 101 N 107 I
n = 14: Cr 80 SmB 89 SmA 105 I
n = 16: Cr 85 SmB 89 SmA 106 I

L^{14}:
R = Br, n = 6: Cr 140 SmA 187 N 215 I
n = 8: Cr 129 SmA 192 N 202 I
n = 10: Cr 116 SmA 189 I
n = 12: Cr 120 SmA 188 I
n = 14: Cr 118 SmA 185 I
n = 16: Cr 110 SmB 120 SmA 176 I

Figure 3.10. Unsymmetrical 5,5'-substituted 2,2'-bipyridine, with 4-*n*-alkoxyphenylethynyl function.[3(h)] R = Br or H, n = 6, 8, 10, 12, 14, 16. Transition temperatures are given in °C.

Two series of compounds were produced with R = Br or H, both with n = 6, 8, 10, 12, 14 and 16 carbon atoms. The mesomorphic compounds with R = H, L^{13}, are unusual in that they have a terminal hydrogen. The mesomorphic character of this system varied with increasing number of carbon atoms in the aliphatic chain, crossing over from a nematic phase at short chain lengths to smectic phases at long chain lengths. However, the melting and clearing temperatures were not strongly influenced by the length of the aliphatic chain, with the melting transitions occurring between 80°C and 85°C and the isotropic transitions between 98°C and 108°C, regardless of chain length.

The series with R = Br, L^{14}, experienced similar stabilisation of the smectic phases with increasing chain length. However, the melting and clearing temperatures were more dependent on the aliphatic chain length than the previous series L^{13}. The clearing temperatures decreased from 215°C to 176°C as the chain length went from 6 to 16 carbon atoms. Likewise, the melting temperatures decreased from 140°C to 110°C.

The Ziessel group also synthesised a symmetrical 2,2'-bipyridine molecule with 4-*n*-hexadecyloxyphenylethynyl functions, L^{15} (Figure 3.11).[3(c)] The ligand experienced a significantly elevated clearing temperature relative to the unsymmetrical ligand shown in Figure 3.10, and the melting temperature was raised by approximately 30°C. The symmetrical ligand displayed a richer variety of smectic mesophases than the asymmetric analogues, and instead of going through smectic A and B phases below the isotropic liquid, the ligand L^{15} showed smectic C, I, and F phases in addition to an unidentified mesophase X.

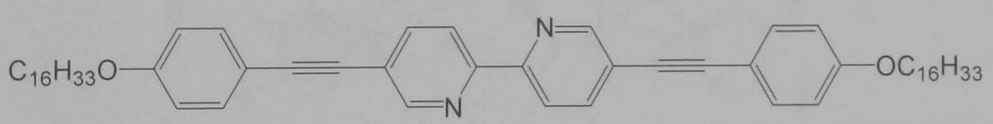

L^{15}

Cr 113 X 125 SmF 149 SmI 168 SmC 237 I

Figure 3.11. 5,5'-[(4-Hexadecyloxyphenyl)ethynyl]-2,2'-bipyridine, prepared by Ziessel *et al.*[3(c)] Transition temperatures are given in °C.

Ziessel *et al.* have also developed two bipyridine metallomesogens. The first was a cationic palladium(II) complex with alkylsulfate counterion, L^{16} (Figure 3.12).[3(d)] The metal-free ligand was itself non-mesomorphic, whereas the complex melted at 131°C into a columnar mesophase. Subsequent heating resulted in the formation of a smectic A phase at 168°C followed by the

isotropic liquid at 216°C. This complex was the first reported example of a 2,2'-bipyridine metallomesogen to display a columnar mesophase.

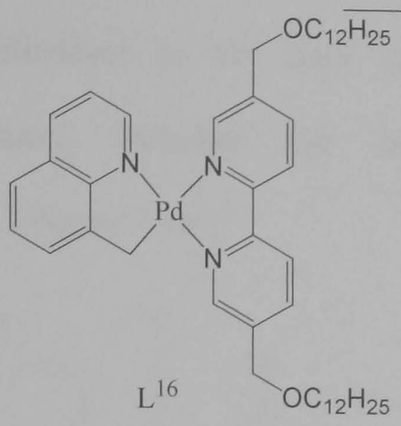

Cr 131 Col 168 SmA 216 I

L^{16}

Figure 3.12. The first 2,2'-bipyridine metallomesogen to display a columnar mesophase, $X^- = {}^-O_3SOC_{12}H_{25}$.[3(d)] Transition temperatures are given in °C.

The second 2,2'-bipyridine metallomesogen to originate from the Ziessel group was based on a 2,2'-bipyridine fragment symmetrically substituted at the 6,6'-positions bearing functionalised imino groups (Figure 3.13).[3(f)]

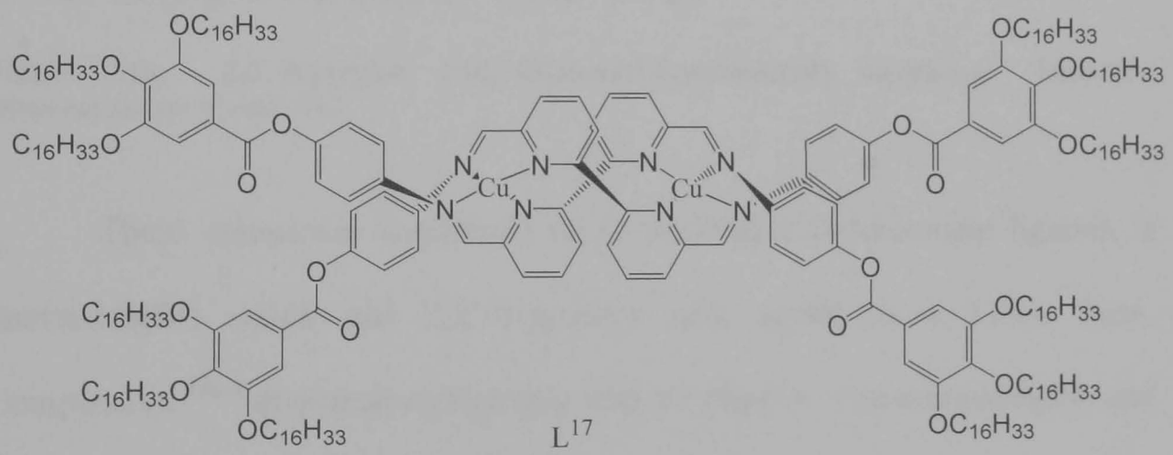

L^{17}

Cr 25 Col 181 I

Figure 3.13. Mesomorphic copper(I) complex $[Cu_2L_2](BF_4)_2$ (anions omitted for clarity).[3(f)] Transition temperatures are given in °C.

The metal-free ligand was once again non-mesomorphic, but complexation to $[Cu(CH_3CN)_4]BF_4$ resulted in a mesomorphic binuclear copper(I) complex $[Cu_2L_2](BF_4)_2$, L^{17} (Figure 3.13). The helical complex formed a viscous columnar phase at 25°C before clearing into the isotropic liquid at 181°C. This copper(I) complex was the first liquid crystalline metallohelicate and is

especially significant because of its ability to form a columnar mesophase at room temperature.

Recent contributions to the field of thermotropic 2,2'-bipyridine metallomesogens have included the lanthanide(III) complexes by Galyametdinov *et al.* (Figure 3.14).[5]

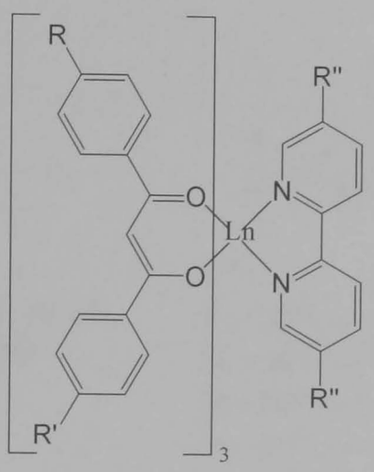

L^{18a}: Cr 133 (SmA 115) I
L^{18b}: Cr 166 (SmX 149) I
L^{18c}: Cr 162 (SmX 143) I
L^{18d}: Cr 95 SmX 130 I

L^{18a}: R = R' = $OC_{14}H_{29}$, R'' = H, Ln = Eu^{3+}
L^{18b}: R = R' = $OC_{14}H_{29}$, R'' = $CO(O)C_{11}H_{23}$, Ln = Eu^{3+}
L^{18c}: R = R' = $OC_{14}H_{29}$, R'' = $CO(O)C_{11}H_{23}$, Ln = Tb^{3+}
L^{18d}: R = $OC_{12}H_{25}$, R' = $OC_{16}H_{33}$, R'' = $C_{17}H_{35}$, Ln = Eu^{3+}

Figure 3.14. 2,2'-Bipyridine tris(β-diketonato)lanthanide(III) complexes.[5] Transition temperatures are given in °C.

These complexes comprised of mesomorphic β-diketonate ligands, a lanthanide(III) cation and 2,2'-bipyridine unit acting as a Lewis base. Complexes L^{18a-c} displayed monotropic smectic phases. The europium(III) and terbium(III) complexes, L^{18b} and L^{18c}, formed the smectic phase at 149°C and 143°C, respectively, whereas the europium(III) complex with the unsubstituted bipyridine unit L^{18a} formed a smectic A phase at a lower temperature. Initial characterisation of the complex L^{18d} revealed an enantiotropic liquid crystalline phase between 95°C and 130°C. POM observations indicated that the phase was probably smectic. These complexes represent a new class of

metallomesogen with coordination number eight, in which mesomorphism is introduced via a β-diketonate ligand.

Finally in this review of 2,2'-bipyridine thermotropic liquid crystals, our attention is drawn to the recent research by Pucci and co-workers (Figure 3.15).[6]

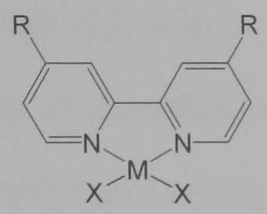

L^{19}:
R = $COOC_nH_{2n+1}$, n = 16, 22;
X = Cl^-; M = Ni, Pd, Pt

L^{19}:
M = Ni^{2+}, n = 16: Cr 226 Sm 234 I
M = Ni^{2+}, n = 22: Cr 229 Sm 251 I decomposed
M = Pd^{2+}, n = 16: Cr 97 Cr' 130 SmA 156 I
M = Pd^{2+}, n = 22: Cr 87 Cr' 98 SmA 140 I
M = Pt^{2+}, n = 16: Cr 58 Cr' 76 Sm 170 I
M = Pt^{2+}, n = 22: Cr 34 Cr' 72 Sm 145 I

L^{20}:
R = $COOC_{16}H_{33}$; M = Pd, Pt;
X = I^-, Br^-, N_3^-

L^{20}:
X = I^-, M = Pd^{2+}: Cr 75 Cr' 117 Cr'' 125 Sm 186 I
X = I^-, M = Pt^{2+}: Cr 37 Cr' 67 Sm 212 I
X = Br^-, M = Pd^{2+}: Cr 39 Cr' 80 Sm 179 I
X = Br^-, M = Pt^{2+}: Cr 39 Sm 179 I
X = N_3^-, M = Pd^{2+}: Cr 55 Cr' 103 Sm 146 SmA 159 I
X = N_3^-, M = Pt^{2+}: Cr 39 Cr' 59 Sm 165 SmA 170 I

L^{21}:
n = 12, 16; X = Cl^-, M = Zn, Pd
R = 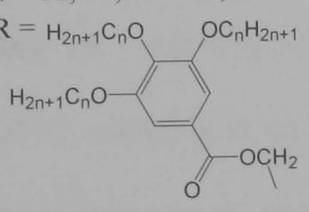

L^{21}:
M = Zn^{2+}, n = 12: Cr 46 Col_{h1} 123 Col_{h2} 132 I
M = Zn^{2+}, n = 16: Cr 59 Cr' 91 Col_h 111 I
M = Pd^{2+}, n = 12: Cr 76 Col_{h1} 136 Col_{h2} 145 I
M = Pd^{2+}, n = 16: Cr 49 Col_h 128 I

Figure 3.15. Mesomorphic 4,4'-disubstituted 2,2'bipyridines, prepared by Pucci *et al.*[6] Transition temperatures are given in °C.

Smectic phases were formed by all of the complexes in the series L^{19} and L^{20}.[6(a),6(b)] The nickel(II) complexes in the series L^{19} displayed a lamellar phase at temperatures higher than for the palladium(II) and platinum(II)

homologues, and cleared into the isotropic liquid at elevated temperatures in excess of 230°C. The platinum(II) complexes of L^{19} displayed clearing temperatures slightly higher than those of the palladium(II) homologues, and the platinum(II) complexes also had the lowest melting temperatures. giving them the largest mesomorphic range. Complexes with $n = 8$ and M = zinc(II) were also synthesised but none were found to be mesomorphic.

Through replacement of the chloride groups with iodide, bromide and azide ligands, the thermal behaviour of the complexes in the series L^{20} could be varied. For the platinum(II) complexes of L^{20} the melting temperatures were reduced relative to $X = Cl^-$ when $X = I^-$ and Br^-, but the melting temperatures increased for $X = N_3^-$. The clearing temperatures increased significantly for $X = I^-$, slightly for $X = Br^-$ and remained the same for $X = N_3^-$. For the palladium(II) complexes the melting temperatures were reduced and the clearing temperatures increased for all three substitutions relative to $X = Cl^-$.

Most recently the mesomorphic properties of the polycatenar complexes L^{21} have been studied (Figure 3.15).[6(c)] These species produced columnar mesophases for all zinc(II) and palladium(II) complexes with $n = 12$ and 16. All had relatively low melting temperatures of between 46°C and 91°C, clearing in the region 111°C to 145°C. The metal-free ligands of these complexes were non-mesomorphic. These compounds are rare examples of mesomorphic materials derived from tetrahedral zinc(II) complexes.[6(c),7]

3.1.2 The Design of the 2,2'-Bipyridine-Derived Metallomesogens

The design for our bipyridine molecules was analogous to the approach for the phenanthroline system (Chapter 2), but with a 6,6'-disubstituted-2,2-bipyridine core (Figure 3.16).

The core of the molecule was modified from 1,10-phenanthroline to the more flexible bipyridine derivative in order to observe its effect on the mesomorphic behaviour. We postulated that a more flexible core would lower transition temperatures as a result of a less ordered packing arrangement, with the possibility of generating alternative mesophases. However, it was vital to strike the correct balance between rigidity and fluidity in order to preserve mesomorphic character.

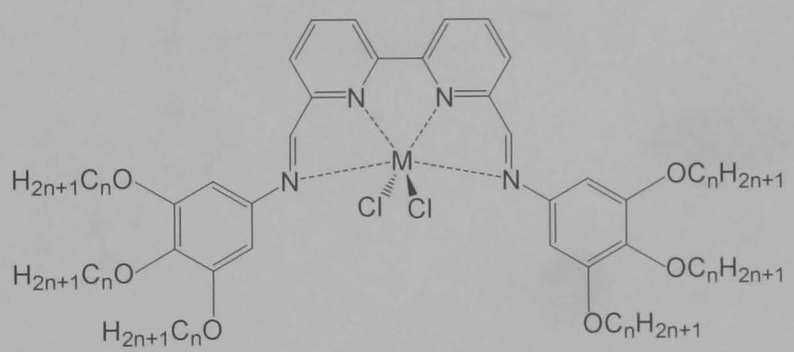

Figure 3.16. The 2,2'-bipyridine-derived complexes, $[MCl_2(L^{Bipy\text{-}n})]$ where M = Mn^{2+}, Fe^{2+}, Co^{2+}, Ni^{2+}, Cu^{2+}, Zn^{2+} and n = 16. For M = Ni^{2+} and Zn^{2+} n = 10, 12, 14, 16.

Any changes in mesophase symmetry were likely to result from deviations in planarity at the core of the ligand. We expected that out-of-plane rotation about the central exocyclic C-C bond would effect the packing of the molecules in the liquid crystalline state and hence the types of mesophase formed. In the absence of a planar core the formation of columnar mesophases is expected to be less favourable.

Another consideration regarding the effect of a 2,2'-bipyridyl core on the liquid crystalline character of a complex is the mode of coordination of the

bipyridine ligand to the metal cation. There are two main possibilities. The first is coordination to both core bipyridine nitrogens in 1:1 metal : ligand stoichiometry, in common with the phenanthroline complexes (Figure 3.16). The second is coordination to one core bipyridine nitrogen and one imine nitrogen as a result of free rotation around exocyclic C-C bond. This would give rise to 2:1 metal : ligand stoichiometry, and would result in an elongated rod-shaped molecule (Figure 3.17a). However, using the complimentary molecular shape approach the formation of pseudo-disks would still be possible, although possibly disfavoured by the presence of the coordinating chloride anions (Figure 3.17b).

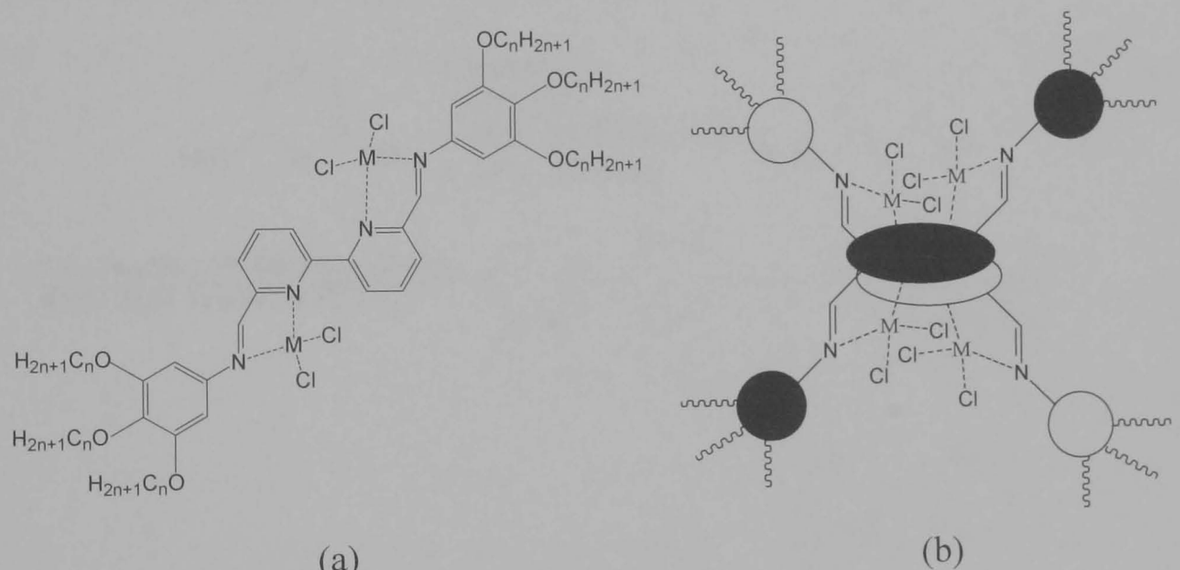

(a) (b)

Figure 3.17. (a) Alternative mode of coordination for 2,2'-bipyridine-derived complexes, (b) possible pseudo-disk formation of two molecules of (a).

We report herein on the synthesis and mesogenic properties of the first mononuclear octahedral and trigonal bipyramidal 6,6'-disubstituted-2,2'-bipyridine metallomesogens, $[MCl_2(L^{Bipy\text{-}n})]$.

3.2 RESULTS AND DISCUSSION

3.2.1 Synthesis of 6,6'-Diformyl-2,2'-Bipyridine

The dialdehyde 6,6'diformyl-2,2'-bipyridine was prepared by the previously published methods,[8] as outlined in Scheme 3.1 below. The three-step process first involved bromination of commercially available 2-aminopicoline.[8(a)] This was followed by a catalytic modification of the Ullmann synthesis employing $Pd(OAc)_2$ for the homocoupling of 6-bromopicoline to produce 6,6'-dimethyl-2,2'-bipyridine.[8(b)] The dimethyl product was oxidised with selenium dioxide in glacial acetic acid to give 6,6'-diformyl-2,2'-bipyridine in overall low yield.[8(c)]

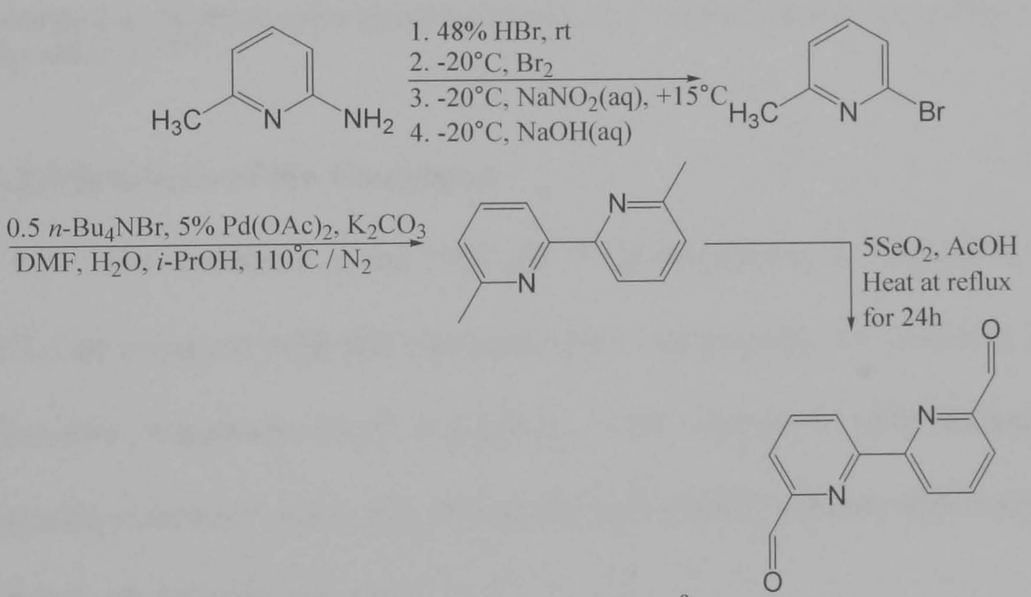

Scheme 3.1. Synthesis of 6,6'-diformyl-2,2'-bipyridine.[8]

3.2.2 Synthesis of the Ligand

The ligand $L^{Bipy\text{-}1}$ was prepared by a Schiff-base condensation reaction of 6,6'-diformyl-2,2'-bipyridine with 3,4,5-trimethoxyaniline in EtOH and $CHCl_3$ (Scheme 3.2).

The mixture was heated to reflux, at which point it became a yellow solution. Reflux temperature was maintained for 24 hours, and the solution

volume was reduced *in vacuo* to give a pale yellow solid, which was collected. The product was recrystallised by solvent diffusion of hexane into a solution of the product in $CHCl_3$ to give the ligand 6,6'-bis-[3',4',5'-tri(methoxy)phenyliminomethyl]-2,2'-bipyridine in 89.0% yield.

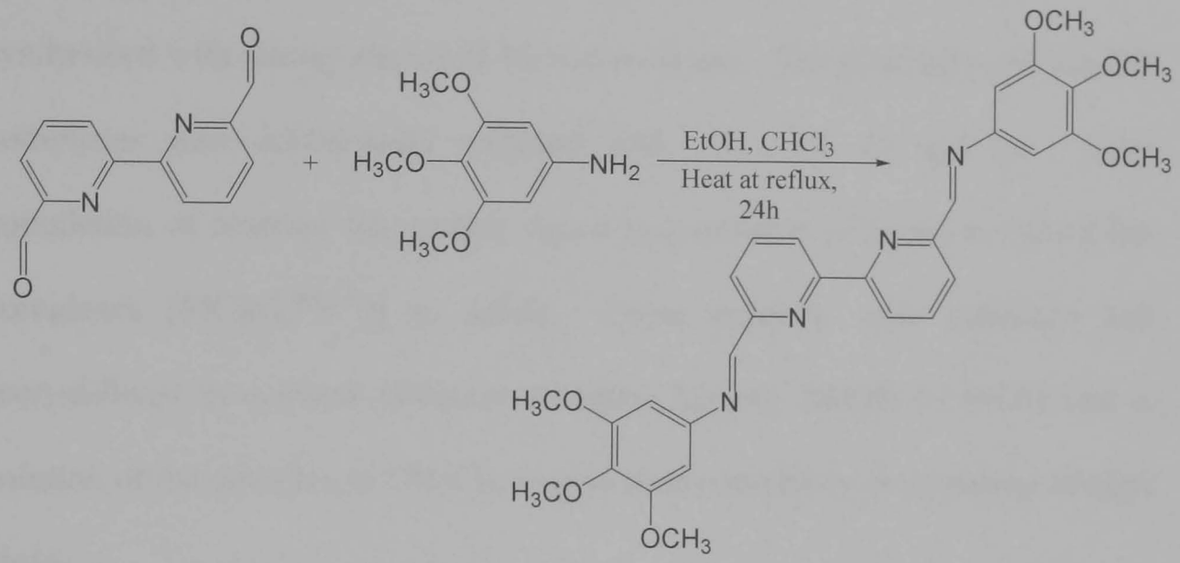

Scheme 3.2. Synthesis of the ligand 6,6'-bis-[3',4',5'-tri(alkoxy)phenyliminomethyl]-2,2'-bipyridine, $L^{Bipy\text{-}1}$.

3.2.3 Synthesis of the Complexes

The synthesis of the $[MCl_2(L^{Bipy\text{-}n})]$ complexes is outlined in Scheme 3.3. In common with the phenanthroline compounds, six different series of first-row transition metal complexes were prepared with manganese(II), iron(II), cobalt(II), nickel(II), copper(II) and zinc(II) cations, and chains of n = 10, 12, 14, 16 carbon atoms.

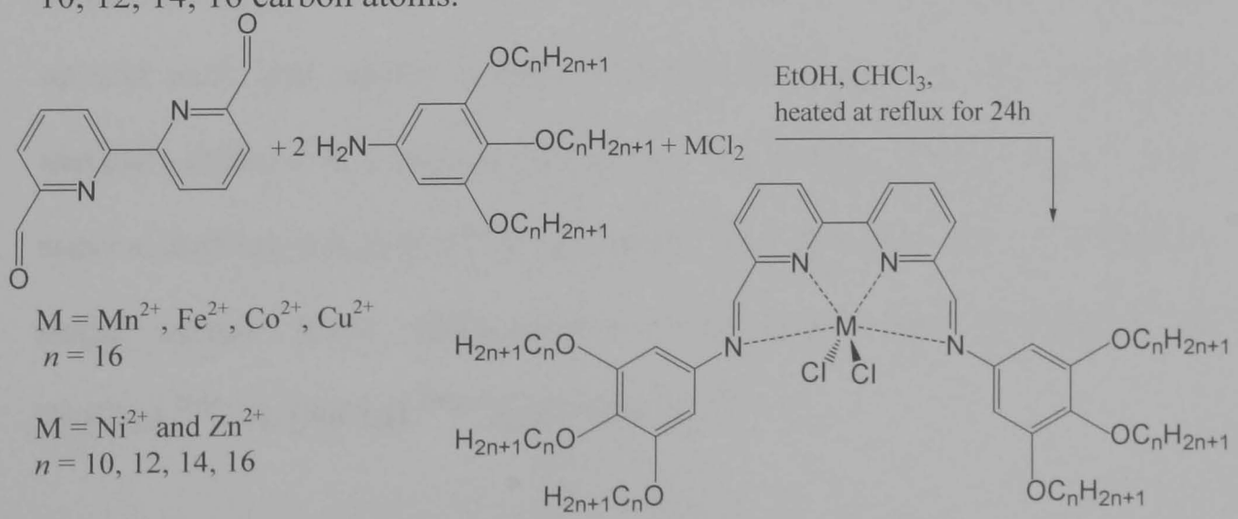

Scheme 3.3. Template synthesis of the complexes $[MCl_2(L^{Bipy\text{-}n})]$, 6,6'-bis-[3',4',5'-tri(alkoxy)phenyliminomethyl]-2,2'-bipyridine metal(II) chloride.

The long chain complexes were prepared by template Schiff-base condensation reactions of 6,6'-diformyl-2,2'-bipyridine with two equivalents of 3,4,5-trialkoxyaniline, in the presence of the appropriate metal chloride salt under reflux for 24 hours in EtOH and $CHCl_3$. Each compound was synthesised with alkoxy chains of 16 carbon atoms. The nickel(II) and zinc(II) complexes were additionally prepared with n = 10, 12 and 14. After completion of reaction the mother liquor was reduced *in vacuo* to afford the complexes $[MCl_2(L^{Bipy\text{-}n})]$ as solids. These products were collected and recrystallised by solvent diffusion of either hexane, MeOH or EtOH into a solution of the complex in CH_2Cl_2, to give pure complexes in moderate-to-high yields.

The methoxy complexes $[MnCl_2(L^{Bipy\text{-}1})]$, $[FeCl_2(L^{Bipy\text{-}1})]$, $[CoCl_2(L^{Bipy\text{-}1})]$, $[NiCl_2(L^{Bipy\text{-}1})]$, $[CuCl_2(L^{Bipy\text{-}1})]$ and $[ZnCl_2(L^{Bipy\text{-}1})]$ were prepared for the purpose of growing single crystals, for study by X-ray crystallography. The method of preparation differed from the syntheses of the long chain complexes outlined above. In the case of the methoxy compounds the free ligand $L^{Bipy\text{-}1}$ was initially prepared by the Schiff-base method mentioned earlier (Scheme 3.2). Five solutions of $L^{Bipy\text{-}1}$ in $CHCl_3$ were made up and each was layered with a stoichiometric amount of the appropriate metal(II) chloride in a solution of EtOH. The layered solutions were left to stand at ambient temperature for three days. Over this time crystals suitable for single crystal X-ray diffractometry were grown for $[MnCl_2(L^{Bipy\text{-}1})]$, $[CoCl_2(L^{Bipy\text{-}1})]$, $[NiCl_2(L^{Bipy\text{-}1})]$ and $[ZnCl_2(L^{Bipy\text{-}1})]$.

3.2.4 Characterisation of the Ligands and Complexes

All compounds were characterised by infrared spectroscopy, mass spectrometry, CHN microanalysis and, for the diamagnetic zinc(II) compounds and for ligands, by ^{1}H and ^{13}C NMR spectroscopy.

The infrared spectra of the ligand $L^{Bipy\text{-}1}$ and complexes $[MCl_2(L^{Bipy\text{-}n})]$ confirmed the completion of the Schiff-base condensation reaction, by the presence of the strong $\nu_{C=N}$ stretching vibrations at around 1588cm^{-1}. The second, weaker, $\nu_{C=N}$ stretching vibration occurred between 1610 and 1658cm^{-1}, depending on the transition metal ion. The absence of carbonyl and amine absorption bands associated with the dialdehyde and amine starting materials, confirmed that reaction was complete. Very strong absorption bands near 1120cm^{-1} are attributed to the C-O ether stretch. These were accompanied by strong absorptions in the C-H region between 2850 and 2920cm^{-1} resulting from the aliphatic chains.

MALDI-TOF and electron ionisation mass spectrometry provided evidence of 1:1 metal:ligand complexes by displaying peaks assigned to $[MCl(L^{Bipy\text{-}n})]^{+}$, and for occasionally $[M(L^{Bipy\text{-}n})]^{+}$ and $[MCl_2(L^{Bipy\text{-}n})]^{+}$. EI MS confirmed the successful formation of the free ligand. Microanalytical data were consistent with the successful formation of ligands and complexes, accompanied by usually one or two solvent molecules of H_2O or CH_2Cl_2.

The ^{1}H-NMR spectra of the complexes $[ZnCl_2(L^{Bipy\text{-}n})]$ confirmed the completion of the condensation reaction with an imine proton resonance in the region of 9.33-9.38ppm. The single imine peak provided evidence of equivalent imine proton environments on the NMR timescale, implying the formation of either symmetrical or fluxional species. Two doublets and a

triplet were observed further upfield at around 8.22, 8.16 and 8.09ppm. respectively, assigned to the bipyridine protons. Protons attributed to the phenyl rings occurred around 7.07ppm. The complicated resonances attributed to the protons on the long alkyl chains occurred furthest upfield at between 3.99 and 0.87ppm.

The corresponding ^{13}C-NMR spectra revealed the expected ten peaks between 154 and 102ppm for the imine and aryl carbon resonances. The remaining carbon resonances corresponding to the alkyl chains were observed in the region 74 – 14ppm. Many of the resonances for the alkyl chains overlapped, and individual peaks for each carbon in the alkyl chains were not always observed.

^{1}H-NMR spectroscopy of the free ligand $L^{Bipy\text{-}1}$ revealed that the resonances of the protons in the ligand were shifted relative to $[ZnCl_2(L^{Bipy\text{-}n})]$. Complexation to $ZnCl_2$ resulted in a downfield shift for the imine protons by up to 0.62ppm. Similarly the protons *para* to the nitrogens in the bipyridine fragment were shifted downfield by 0.10ppm and the phenyl ring protons were shifted by 0.43ppm. Conversely, the protons *meta* to the nitrogens in the bipyridine fragment were shifted upfield by 0.42ppm and 0.13ppm, respectively.

3.2.5 Structure Determination by Single Crystal X-Ray Diffractometry

Single crystal X-ray diffractometry of $[MnCl_2(L^{Bipy\text{-}1})]$, $[CoCl_2(L^{Bipy\text{-}1})]$, $[NiCl_2(L^{Bipy\text{-}1})]$ and $[ZnCl_2(L^{Bipy\text{-}1})]$ revealed the structural geometry of the molecules in the solid state. All complexes are monomeric with chelating rather than bridging ligands. The complexes $[MnCl_2(L^{Bipy\text{-}1})]$, $[CoCl_2(L^{Bipy\text{-}1})]$

and $[NiCl_2(L^{Bipy\text{-}1})]$ show metal centres with distorted octahedral coordination geometries. The complex $[ZnCl_2(L^{Bipy\text{-}1})]$, with its relatively small zinc(II) centre, shows a distorted trigonal bipyramidal coordination geometry. Selected bond lengths and angles are shown in Tables 3.1 and 3.2. Thus, for the distorted octahedral complexes $[MnCl_2(L^{Bipy\text{-}1})]$, $[CoCl_2(L^{Bipy\text{-}1})]$ and $[NiCl_2(L^{Bipy\text{-}1})]$, the bipyridine ligand acts as a 4N-donor with four nitrogen donors in the equatorial plane and the chloride ions in the axial plane (Figures 3.18-3.20). For the distorted trigonal bipyramidal complex $[ZnCl_2(L^{Bipy\text{-}1})]$ (Figure 3.21), the metal is coordinated to three of the four nitrogens in the bipyridine ligand and both chloride ions. Further discussion of the crystallographic data for each individual complex now follows.

3.2.5.1 Structure determination of $[MnCl_2(L^{Bipy\text{-}1})]$

The crystal structure of $[MnCl_2(L^{Bipy\text{-}1})]$ revealed the complex crystallised in the monoclinic space group I2/a, with a distorted octahedrally-coordinated metal centre (Figure 3.18). The significant deviation from ideal octahedral geometry is demonstrated by the bond angles Cl(1)-Mn-Cl(2) = 144.1(1)°, N(1)-Mn-N(8') = 139.0(1)°, N(1')-Mn-N(8) = 139.4(1)° and Cl(1)-Mn-N(1) = 110.75(8)°.

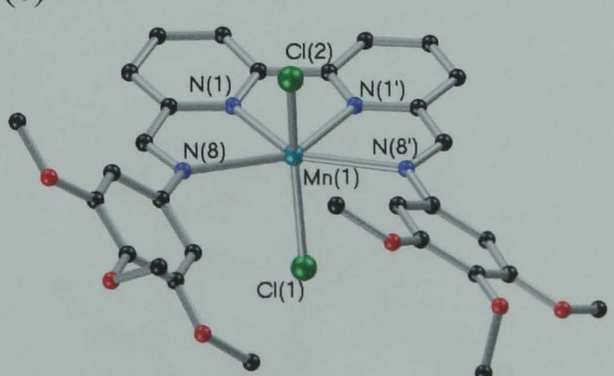

Figure 3.18. Crystal structure of $[MnCl_2(L^{Bipy\text{-}1})].0.5EtOH$. Hydrogen atoms and solvents of crystallisation have been omitted for clarity.

The manganese(II) cation lies in the equatorial plane with the bond lengths Mn-N(1) = 2.274Å, Mn-N(1') = 2.269(1)Å, Mn-N(8) = 2.418(1)Å and Mn-N(8') = 2.466(1)Å. The axial bond lengths are 2.416(1)Å for both Mn-Cl(1) and Mn-Cl(2). In relation to the average plane defined by the bipyridine rings, the manganese(II) cation is displaced out of plane by 0.08Å.

Rotation about the exocyclic carbon-carbon bond in the bipyridine core allows a slight deviation from co-planarity of the pyridine rings. Hence, the rings are twisted relative to each other by 4.959(3)°. The phenyl rings exhibit substantial twists relative to the bipyridine plane of 39.64(2)° and 33.44(2)°, resulting in cavities that contain half a non-interacting molecule of EtOH per $[MnCl_2(L^{Bipy\text{-}1})]$.

3.2.5.2 Structure Determination of $[CoCl_2(L^{Bipy\text{-}1})]$

The crystal structure of the complex $[CoCl_2(L^{Bipy\text{-}1})]$ confirmed that the compound crystallises in the triclinic space group P-1 and the coordination geometry is distorted octahedral (Figure 3.19). Deviation from ideal octahedral geometry is not as extreme as for $[MnCl_2(L^{Bipy\text{-}1})]$, but is significant nonetheless. The bond angles about the cobalt(II) centre are Cl(2)-Co-Cl(2) = 164.88(3)°, N(1)-Co-N(8') = 148.35(9)°, N(1')-Co-N(8) = 148.47° and Cl(1)-Co-N(1) = 95.02(7)°.

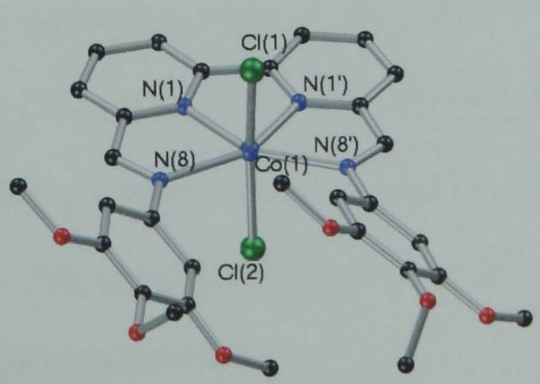

Figure 3.19. Crystal structure of $[CoCl_2(L^{Bipy\text{-}1})].5CHCl_3$. Hydrogen atoms and solvents of crystallisation have been omitted for clarity.

The equatorial plane contains the cobalt(II) cation, which lies virtually co-planar with the bipyridine core, displaced by 0.035Å. The bond lengths from the cobalt(II) centre are Co-N(1) = Co-N(1') = 2.099(2)Å, Co-N(8) = 2.206(2)Å, Co-N(8') = 2.209(2)Å and Co-Cl(1) = Co-Cl(2) = 2.408(8)Å.

The pyridine rings in the core of the molecule are slightly twisted relative to each other by 3.101(2)°. The phenyl rings are significantly twisted relative to the bipyridine plane by 38.28(2)° and 39.12(2)°. Within the large cavities found in the network of $[CoCl_2(L^{Bipy\text{-}1})]$ are five non-interacting molecules of $CHCl_3$ per $[CoCl_2(L^{Bipy\text{-}1})]$.

Table 3.1. Selected bond lengths [Å] and angles [°] for $[MnCl_2(L^{Bipy\text{-}1})].0.5C_2H_5OH$ and $[CoCl_2(L^{Bipy\text{-}1})].5CHCl_3$.

Mn-N(1)	2.274(1)	Co-N(1)	2.099(2)
Mn-N(8)	2.418(1)	Co-N(8)	2.206(2)
Mn-N(1')	2.269(1)	Co-N(1')	2.099(2)
Mn-N(8')	2.466(1)	Co-N(8')	2.209(2)
Mn-Cl(1)	2.416(1)	Co-Cl(1)	2.408(8)
Mn-Cl(2)	2.416(1)	Co-Cl(2)	2.408(8)
Cl(1) – Mn – Cl(2)	144.1(1)	Cl(1) – Co – Cl(2)	164.88(3)
N(1) – Mn – N(8')	139.0(1)	N(1) – Co – N(8')	148.35(9)
N(1') – Mn – N(8)	139.4(1)	N(1') – Co – N(8)	148.47(9)
Cl(1) – Mn – N(1)	110.75(8)	Cl(1) – Co – N(1)	95.02(7)
Twist of bipyridine rings	4.959(3)	Twist of bipyridine rings	3.101(2)
Twist of phenyl rings	39.64(2) 33.44(2)	Twist of phenyl rings	38.28(2) 39.12(2)

3.2.5.3 Structure Determination of $[NiCl_2(L^{Bipy\text{-}1})]$

The distorted octahedral complex $[NiCl_2(L^{Bipy\text{-}1})]$ also crystallises in triclinic space group P-1 (Figure 3.20). This complex has the least distorted octahedral coordination geometry relative to the complexes $[MnCl_2(L^{Bipy\text{-}1})]$ and $[CoCl_2(L^{Bipy\text{-}1})]$. The equatorial angles are 153.87(13)° and 153.29(13)°. whereas the axial angle is 167.80(4)°.

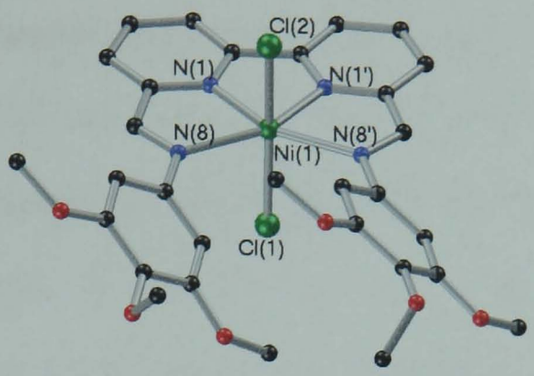

Figure 3.20. Crystal structure of $[NiCl_2(L^{Bipy\text{-}1})].5CHCl_3$. Hydrogen atoms and solvents of crystallisation have been omitted for clarity.

The nickel(II) cation lies in the equatorial plane, co-planar with the plane of the bipyridine core, and the bond lengths within the plane are Ni-N(1) = Ni-N(1') = 2.015(3)Å, Ni-N(8) = 2.209(3)Å and Ni-N(8') = 2.216(4)Å. The axial bond lengths are Ni-Cl(1) = 2.3886(14)Å and Ni-Cl(2) = 2.3825(14)Å.

As well as having the least distorted octahedral coordination geometry of the bipyridine-derived complexes, $[NiCl_2(L^{Bipy\text{-}1})]$ also has the bipyridine core with the smallest deviation from co-planarity. The pyridine rings are twisted 3.002(9)° relative to each other, whereas the phenyl rings have large deviations from the plane of the bipyridine core and are twisted by 38.5(1)° and 39.4(1)°. Cavities within the structure accommodate five non-interacting molecules of $CHCl_3$ per $[NiCl_2(L^{Bipy\text{-}1})]$.

3.2.5.4 Structure Determination of $[ZnCl_2(L^{Bipy\text{-}1})]$

Single crystal X-ray diffraction revealed that the complex $[ZnCl_2(L^{Bipy\text{-}1})]$ is a five-coordinate highly distorted trigonal bipyramidal compound in triclinic space group P-1 (Figure 3.21).

The geometric parameter defining the degree of trigonality, τ, was measured as 0.35. Despite this value being closer to zero than one the

geometry is described as trigonal bipyramidal rather than square-based pyramidal as a consequence of the overall bond angles. The angles N(1)-Zn-Cl(2) = 119.8(4)°, Cl(1)-Zn-Cl(2) = 113.6° and Cl(1)-Zn-N(1) = 126.5° are far closer to the ideal trigonal bipyramidal angles of 120° than the ideal square-based pyramidal angles of 90°, 90° and 180°, respectively. Thus, the coordination geometry can be regarded as distorted trigonal bipyramidal in which the equatorial positions are occupied by two chloride ions and one bipyridine nitrogen donor. The axial positions are occupied by the remaining bipyridine nitrogen and one of the imine nitrogens at an angle of N(1')-Zn-N(8) = 148.1(5)°. The remaining imine nitrogen points away from the zinc(II) centre. The inequivalence of the imines in the solid state and the symmetrical structure inferred by the ^{1}H- and ^{13}C-NMR spectroscopy in $CDCl_3$, reveals that in solution the complex is fluxionally dynamic on the NMR timescale.

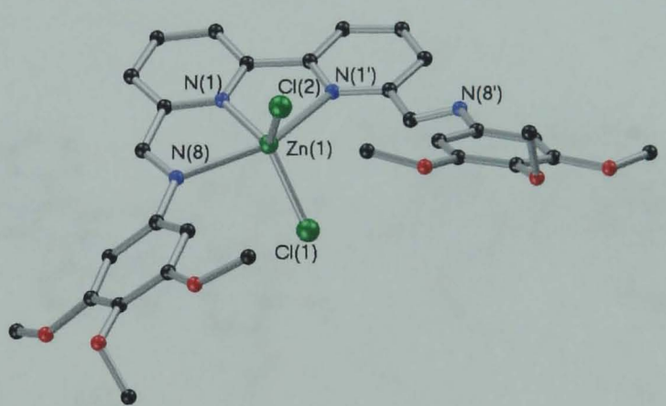

Figure 3.21. Crystal structure of $[ZnCl_2(L^{Bipy\text{-}1})].CHCl_3$. Hydrogen atoms and solvent molecules have been omitted for clarity.

The bonds extending from the zinc(II) centre are Zn-N(1) = 2.080(8)Å, Zn-N(1') = 2.265(8)Å, Zn-N(8) = 2.311(9)Å, Zn-Cl(1) = 2.240(8)Å and Zn-Cl(2) = 2.276(9)Å. The core of the molecule has the greatest deviation from planarity of all the bipyridine complexes, as the pyridine rings are twisted 5.79(2)° relative to each other to allow coordination to the small zinc(II) cation. The cation lies just 0.046Å out of the plane averaged by the bipyridine core,

whereas the phenyl rings are twisted 31.4(1)° and 27.0(6)° relative to the bipyridine plane. The cavities in the $[ZnCl_2(L^{Bipy\text{-}1})]$ network accommodate one non-interacting molecule of $CHCl_3$ per complex.

Table 3.2. Selected bond lengths [Å] and angles [°] for $[NiCl_2(L^{Bipy\text{-}1})]$. $5CHCl_3$ and $[ZnCl_2(L^{Bipy\text{-}1})].CHCl_3$.

Ni-N(1)	2.015(3)	Zn-N(1)	2.080(8)
Ni-N(8)	2.209(3)	Zn-N(8)	2.311(9)
Ni-N(1')	2.015(3)	Zn-N(1')	2.265(8)
Ni-N(8')	2.216(4)	Zn-N(8')	-
Ni-Cl(1)	2.3886(14)	Zn-Cl(1)	2.240(8)
Ni-Cl(2)	2.3825(14)	Zn-Cl(2)	2.276(9)
Cl(1) – Ni – Cl(2)	167.80(4)	Cl(1) – Zn – Cl(2)	113.6(4)
N(1) – Ni – N(8')	153.87(13)	N(1) – Zn – Cl(2)	119.8(4)
N(1') – Ni – N(8)	153.29(13)	N(1') – Zn – N(8)	148.1(5)
Cl(1) – Ni – N(1)	95.78(10)	Cl(1) – Zn – N(1)	126.5(5)
Twist of bipyridine rings	3.002(9)	Twist of bipyridine rings	5.79(2)
Twist of phenyl rings	38.5(1)	Twist of phenyl rings	31.4(1)
	39.4(1)		27.0(6)

3.2.5.5 Packing Diagrams of the Complexes

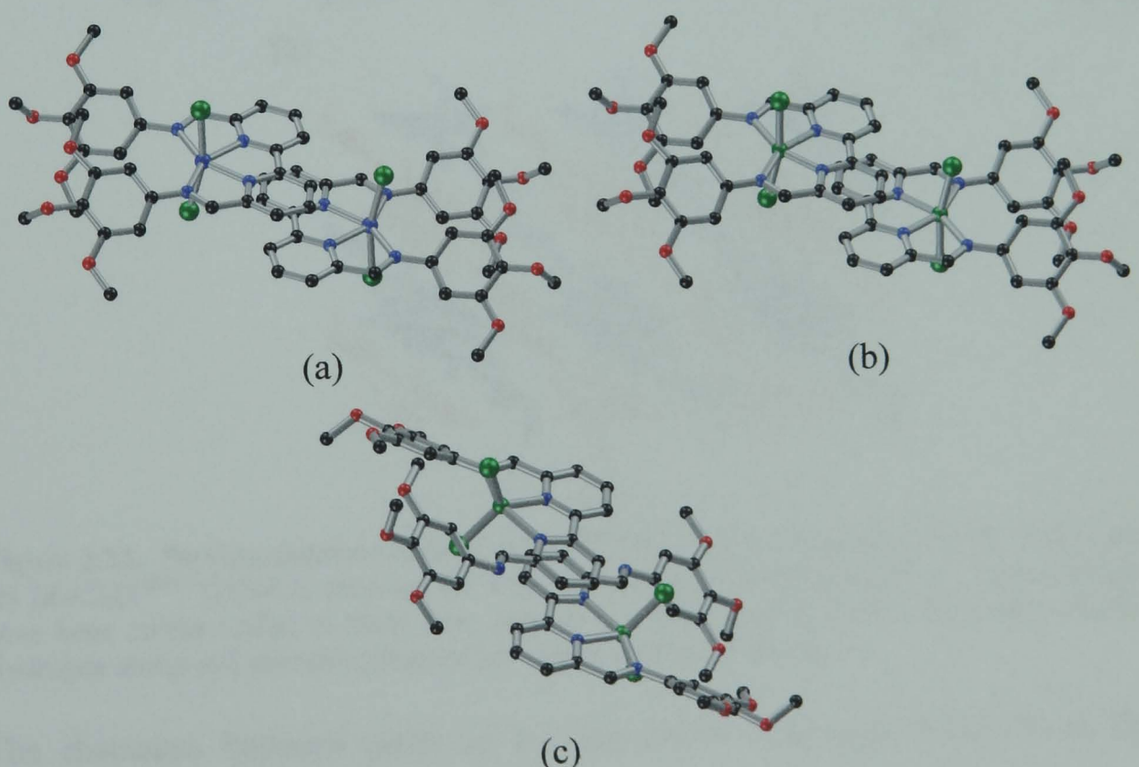

Figure 3.22. Packing diagrams to show how pairs of (a) $[CoCl_2(L^{Bipy\text{-}1})]$, (b) $[NiCl_2(L^{Bipy\text{-}1})]$ and (c) $[ZnCl_2(L^{Bipy\text{-}1})]$ are arranged in the solid state. Hydrogen atoms and solvent molecules have been omitted for clarity.

Packing diagrams of the complexes were produced to determine how the complexes assemble in the solid sate. The diagrams reveal that $[CoCl_2(L^{Bipy\text{-}1})]$, $[NiCl_2(L^{Bipy\text{-}1})]$ and $[ZnCl_2(L^{Bipy\text{-}1})]$ pack in similar arrangements, whereas packing in $[MnCl_2(L^{Bipy\text{-}1})]$ is significantly different. The most common packing arrangement for the bipyridine compounds is for the molecules to assemble into pairs, or 'disks', with overlapping coplanar bipyridine units (Figure 3.22).

These pairs of molecules are arranged in distinct tilted columns with solvent molecules occupying the inter-columnar voids (Figure 3.23).

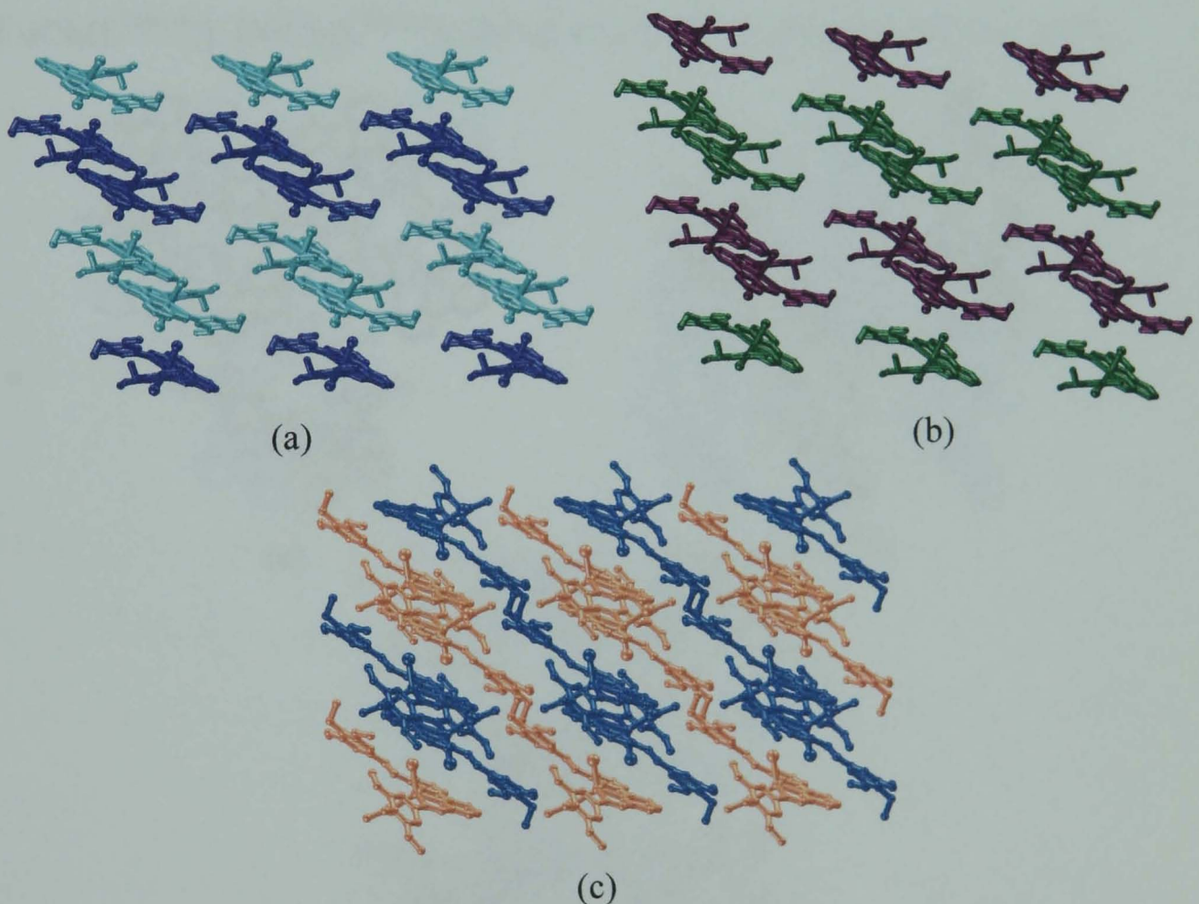

Figure 3.23. Packing diagrams of (a) $[CoCl_2(L^{Bipy\text{-}1})].5CHCl_3$, (b) $[NiCl_2(L^{Bipy\text{-}1})].5CHCl_3$ and (c) $[ZnCl_2(L^{Bipy\text{-}1})].CHCl_3$ showing the columnar stacking of the molecules. The molecules have been colour coded to show how pairs of molecules are arranged within the columns. Hydrogen atoms and solvent molecules have been omitted for clarity.

The distances between pairs of the bipyridine fragments taken from the centroid points of each fragment are 3.82Å for $[CoCl_2(L^{Bipy\text{-}1})]$, 3.83Å for $[NiCl_2(L^{Bipy\text{-}1})]$ and 3.56Å for $[ZnCl_2(L^{Bipy\text{-}1})]$. This gives bipyridine plane-

plane distances of 3.76Å, 3.78Å and 3.43Å, respectively. The pairs of bipyridine units are slightly parallel displaced with respect to each other by 0.667Å, 0.606Å and 0.951Å for the $[CoCl_2(L^{Bipy\text{-}1})]$, $[NiCl_2(L^{Bipy\text{-}1})]$ and $[ZnCl_2(L^{Bipy\text{-}1})]$, respectively. The proximity of the bipyridine cores is indicative of π-π interactions.[9] Each complex exhibits metal-metal distances of Co-Co = 7.72 Å, Ni-Ni = 7.60 Å and Zn-Zn = 7.02 Å. Hence, these complexes appear to be predisposed to assemble into columnar arrangements in the solid state.

The complex $[MnCl_2(L^{Bipy\text{-}1})]$ has a different packing arrangement to its $[CoCl_2(L^{Bipy\text{-}1})]$, $[NiCl_2(L^{Bipy\text{-}1})]$ and $[ZnCl_2(L^{Bipy\text{-}1})]$ analogues (Figure 3.24).

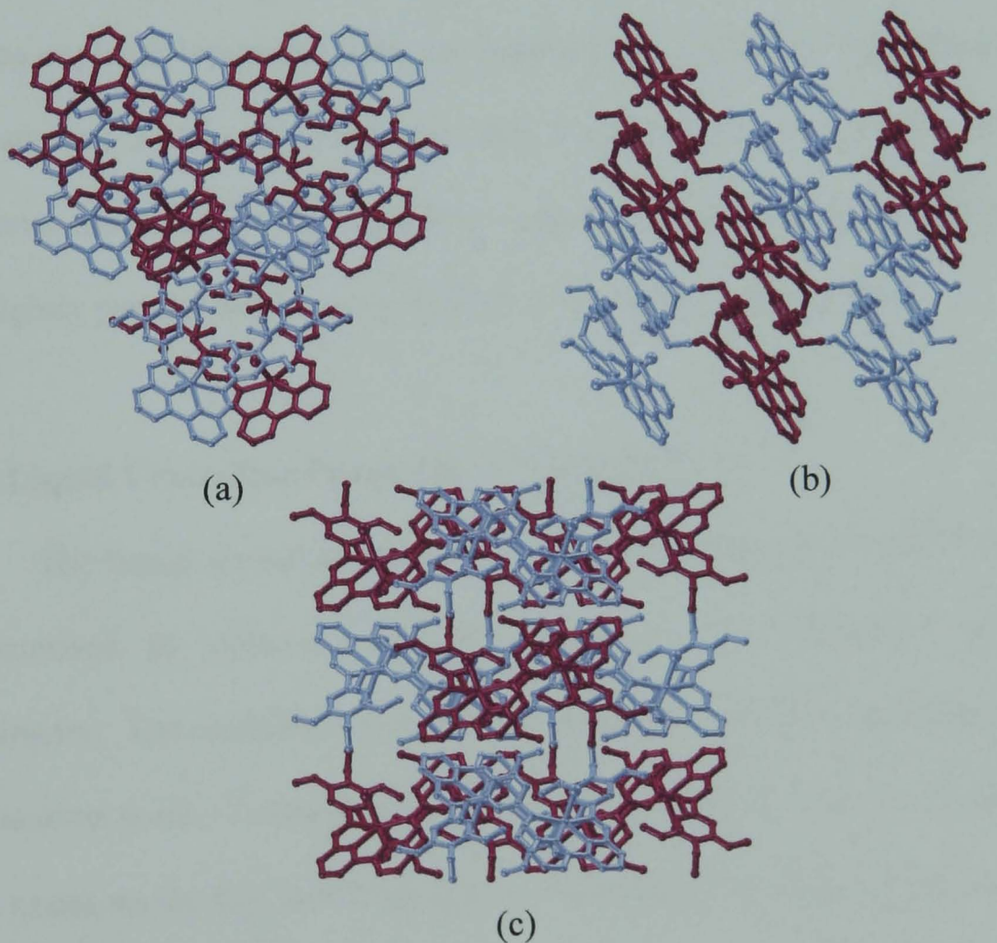

Figure 3.24. Packing diagrams of $[MnCl_2(L^{Bipy\text{-}1})].0.5EtOH$, as viewed along the a, b and c axes, respectively. Coplanar molecules are the same colour; molecules of different colour are twisted 42° relative to each other. Hydrogen atoms and solvent molecules have been omitted for clarity.

Although pairs of molecules are assembled as pseudo disks, the arrangement of these disks with respect to each other differs. Unlike the complexes $[CoCl_2(L^{Bipy\text{-}1})]$, $[NiCl_2(L^{Bipy\text{-}1})]$ and $[ZnCl_2(L^{Bipy\text{-}1})]$, which are arranged in discrete columns with each complex having molecules at a uniform angle of tilt, the complex $[MnCl_2(L^{Bipy\text{-}1})]$ has columns at one tilt angle that are interposed with columns at another tilt angle to form zig-zagged layers of molecules (Figures 3.24a and 3.24c). The relative angle of tilt between non-coplanar molecules is 42.2°. Half a solvent molecule of EtOH per complex resides between the layers.

The metal-metal distance between pairs of $[MnCl_2(L^{Bipy\text{-}1})]$ is 7.76Å and the coplanar bipyridine units are separated by 3.83Å, giving a plane-plane separation of 3.61Å. This indicates that π-π interactions are present between co-planar molecules.[9] The bipyridine fragments in each $[MnCl_2(L^{Bipy\text{-}1})]$ pair are slightly parallel displaced by 0.465Å, with respect to each other.

3.2.6 Liquid Crystalline Properties of $[MCl_2(L^{Bipy\text{-}n})]$

The liquid crystalline behaviour of the complexes $[MCl_2(L^{Bipy\text{-}n})]$ was characterised by polarised optical microscopy and differential scanning calorimetry. The complexes were often accompanied by decomposition around the clearing point. Consequently, it was common to only obtain informative DSC traces on the first heat-cool cycle. Often these traces would not show all phase transitions and so complimentary characterisation by POM was also performed. In addition to DSC and POM, small-angle X-ray diffractometry was used to verify the 2D symmetry of the mesophases of $[MCl_2(L^{Bipy\text{-}n})]$ (M = nickel(II) and zinc(II), n = 10 and 12; M = manganese(II) and cobalt(II), n =

16). However, sufficient peaks were not detected to characterise the symmetry of neither $[MnCl_2(L^{Bipy\text{-}16})]$ nor $[CoCl_2(L^{Bipy\text{-}16})]$.

The combined POM, DSC and XRD results are reported in Tables 3.4-3.6.

3.2.6.1 Mesomorphic Properties of $[MCl_2(L^{Bipy\text{-}16})]$

Six complexes $[MnCl_2(L^{Bipy\text{-}16})]$, $[FeCl_2(L^{Bipy\text{-}16})]$, $[CoCl_2(L^{Bipy\text{-}16})]$, $[NiCl_2(L^{Bipy\text{-}16})]$, $[CuCl_2(L^{Bipy\text{-}16})]$ and $[ZnCl_2(L^{Bipy\text{-}16})]$ were characterised by POM and DSC. In accordance with the analogous phenanthroline complexes, complexes of $[FeCl_2(L^{Bipy\text{-}16})]$ and $[CuCl_2(L^{Bipy\text{-}16})]$ are non-mesomorphic and melted into the isotropic liquid at 80°C and 72°C, respectively (for further discussion on these findings the reader is referred to Chapter 2, Section 2.2.5). The liquid crystalline properties of the complexes $[MCl_2(L^{Bipy\text{-}16})]$ (M = manganese(II), cobalt(II), nickel(II) and zinc(II)) are presented in Chart 3.1.

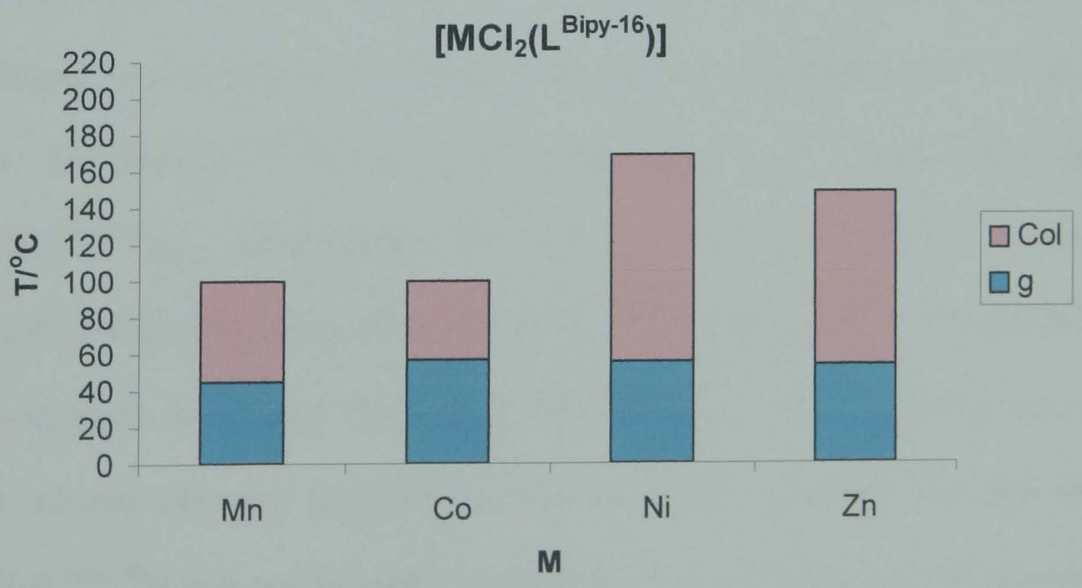

Chart 3.1. Phase diagram representing the transition temperatures of the compounds $[MCl_2(L^{Bipy\text{-}16})]$ (where Col is a columnar phase, whose 2D symmetry has yet to be determined; g is the glass transition temperature).

Through crossed polarisers $[MnCl_2(L^{Bipy\text{-}16})]$ melted into a columnar mesophase at 45°C and cleared into the isotropic liquid at 100°C. DSC detected the glass transition temperature as one peak only at 45°C. The clearing temperature of $[CoCl_2(L^{Bipy\text{-}16})]$ also occurred at 100°C, whereas the columnar mesophase range was shortened relative to $[MnCl_2(L^{Bipy\text{-}16})]$ by a higher glass transition temperature of 57°C. DSC detected one broad peak at 66°C, although XRD confirmed the melting transition to occur between 40 and 60°C, in agreement with the POM measurement.

The complexes $[NiCl_2(L^{Bipy\text{-}16})]$ and $[ZnCl_2(L^{Bipy\text{-}16})]$ both experienced similar melting temperatures to $[MnCl_2(L^{Bipy\text{-}16})]$ and $[CoCl_2(L^{Bipy\text{-}16})]$ of 56°C and 53°C, respectively. Columnar mesophases were characterised by small platelets observed by POM. The mesophases for $[NiCl_2(L^{Bipy\text{-}16})]$ and $[ZnCl_2(L^{Bipy\text{-}16})]$ were stabilised relative to $[MnCl_2(L^{Bipy\text{-}16})]$ and $[CoCl_2(L^{Bipy\text{-}16})]$, as the clearing temperatures of $[NiCl_2(L^{Bipy\text{-}16})]$ and $[ZnCl_2(L^{Bipy\text{-}16})]$ were significantly higher. $[NiCl_2(L^{Bipy\text{-}16})]$ cleared to the isotropic liquid at 170°C and $[ZnCl_2(L^{Bipy\text{-}16})]$ at 150°C, by POM. These transitions were confirmed by the DSC traces as two sharp peaks at 56°C and 169°C for $[NiCl_2(L^{Bipy\text{-}16})]$, and two broad peaks at 54°C and 149°C for $[ZnCl_2(L^{Bipy\text{-}16})]$. Interestingly, the DSC trace for $[NiCl_2(L^{Bipy\text{-}16})]$ was repeatable, displaying sharp peaks for all phase transitions observed by POM. Encouraged by this display of stability, additional $[NiCl_2(L^{Bipy\text{-}n})]$ complexes (n = 10, 12 and 14) were prepared and characterised. Although the trace for $[ZnCl_2(L^{Bipy\text{-}16})]$ was not repeatable, both melting and clearing transitions were detected by DSC on the first heating cycle and so $[ZnCl_2(L^{Bipy\text{-}n})]$ (n = 10, 12 and 14) were also studied. The results of these studies are discussed below.

Table 3.4. Table showing the combined POM, DSC and XRD data to give the mesophase transition temperatures for $[MCl_2(L^{Bipy\text{-}16})]$. Also included, where possible, are detailed indexation information obtained by XRD studies (where **M** = central metal cation; **T** = temperature at which data was taken; d_{meas}, and d_{calc} are the measured and calculated diffraction spacings, respectively; ***hk*** is the indexation of the two-dimensional lattice; Col is an unidentified columnar mesophase and I is the isotropic liquid).

M	T/°C	$d_{meas.}$/Å	*hk*	$d_{calc.}$/Å	Mesophase	Transitions/°C
Mn	80	41.16 28.57 4.5	- - br	-	Col	g 45 Col 100 I
Co	80	41.54 28.75 4.5	- - br	-	Col	g 57 Col 100 I
Ni	-	-	-	-	Col	g 56 Col 169 I
Zn	-	-	-	-	Col	g 54 Col 149 I

3.2.6.2 Mesomorphic Properties of $[NiCl_2(L^{Bipy\text{-}n})]$

The liquid crystalline behaviour of the complexes $[NiCl_2(L^{Bipy\text{-}n})]$ is presented below, in Chart 3.2.

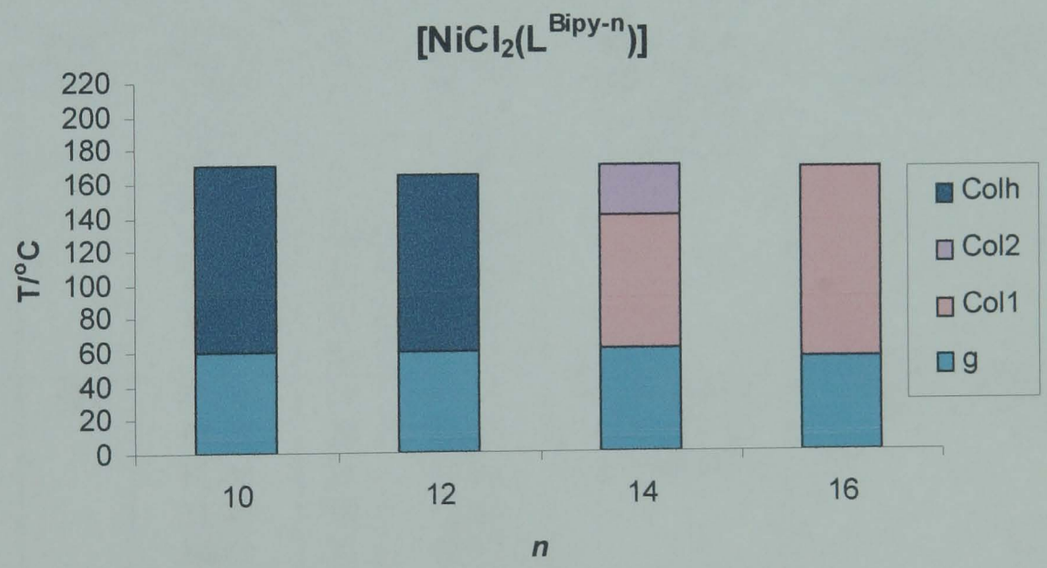

Chart 3.2. Phase diagram representing the transition temperatures of the compounds $[NiCl_2(L^{Bipy\text{-}n})]$ (where Col_h is a columnar hexagonal phase; Col_1 and Col_2* are columnar mesophases whose 2D symmetry have yet to be determined;* Col_2 is a monotropic phase; g is the glass transition temperature).

The glass transition temperatures of $[NiCl_2(L^{Bipy\text{-}10})]$ and $[NiCl_2(L^{Bipy\text{-}12})]$ were not observed by POM due to the highly viscous nature of the compounds making the transition from mesophase to solid difficult to detect. However, all transitions were repeatedly detected by DSC. The DSC

traces for $[NiCl_2(L^{Bipy\text{-}10})]$ showed a broad peak at 75°C followed by a sharp peak at 170°C. The traces for $[NiCl_2(L^{Bipy\text{-}12})]$ and $[NiCl_2(L^{Bipy\text{-}14})]$ showed peaks corresponding to the melting transitions at 60°C and 62°C. both of which were sharper than the corresponding melting peak for $[NiCl_2(L^{Bipy\text{-}10})]$. The traces also displayed a sharp peak for the clearing points at 164°C and 171°C, respectively. These temperatures were in agreement with the POM measurements. The complex of $[NiCl_2(L^{Bipy\text{-}14})]$ also displayed a monotropic phase at 141°C, which was observed repeatedly by DSC but not by POM.

Table 3.5. Table showing the combined POM, DSC and XRD data to give the mesophase transition temperatures for $[NiCl_2(L^{Bipy\text{-}n})]$. Also included, where possible, are detailed indexation information obtained by XRD studies (where ***n*** = number of carbons in aliphatic chains; **T** = temperature at which data was taken; d_{meas}, and d_{calc} are the measured and calculated diffraction spacings, respectively; ***hk*** is the indexation of the two-dimensional lattice; *a* is the lattice parameter and *S* is the lattice area of the hexagonal (Col_h) columnar phase; *p6mm* is the 2D space group of the corresponding hexagonal mesophase; Col, Col_1 and Col_2 are unidentified columnar mesophases and I is the isotropic liquid).

n	**T/°C**	$d_{meas.}$/Å	***hk***	$d_{calc.}$/Å	**Mesophase**	**Transitions/°C**
10	160	35.06	10	35.06	$Col_h - p6mm$	g 60 Col_h 171 I
		20.34	11	20.24	$a = 40.5$ Å	
		17.45	20	17.8	$S = 1419Å^2$	
		13.17	21	13.25		
		11.63	30	11.69		
		10.11	22	10.12		
		9.68	31	9.72		
		4.5	br			
12	120	37.33	10	37.33	$Col_h - p6mm$	g 60 Col_h 164 I
		18.71	20	18.67	$a = 43.1$ Å	
		14.08	21	14.01	$S = 1609Å^2$	
		12.47	30	12.44		
		10.83	31	10.77		
		10.34	22	10.35		
		4.5	br			
14	-	-	-	-	Col_1, Col_2	g 61 Col_1 (Col_2 141) 171 I
16	-	-	-	-	Col	g 56 Col 169 I

The two compounds $[NiCl_2(L^{Bipy\text{-}10})]$ and $[NiCl_2(L^{Bipy\text{-}12})]$ were additionally studied by XRD. The mesophases from both complexes were characterised as columnar hexagonal phases by the presence of one very strong and six weak diffraction peaks in the small-angle region, occurring in the ratio

1:√3:√4:√7:√9:√12:√13. Therefore, it appears that in the $[NiCl_2(L^{Bipy\text{-}n})]$ series the complexes go through one columnar mesophase on heating (and two for $[NiCl_2(L^{Bipy\text{-}14})]$ on cooling). The length of the aliphatic chains does not appear to have an appreciable effect on the melting and clearing transition temperatures, which remain similar regardless of chain length. However, the chain lengths do have an effect on the lattice parameters of the columnar hexagonal mesophases. The XRD data collected for $[NiCl_2(L^{Bipy\text{-}10})]$ and $[NiCl_2(L^{Bipy\text{-}12})]$ indicate that an increase in chain length results in an increase in the lattice parameters *a* and *S*. This translates to an increase in the dimensions of each column in the mesophase, which is what we would expect from compounds of increasing molecular volume.

We have been able to estimate the number of molecules per column cross-section for $[NiCl_2(L^{Bipy\text{-}10})]$ and $[NiCl_2(L^{Bipy\text{-}12})]$, as described in Chapter 2, Section 2.2.5.6. The N_h value for $[NiCl_2(L^{Bipy\text{-}10})]$ is 2.69. For $[NiCl_2(L^{Bipy\text{-}12})]$ this value is very similar, with N_h = 2.73. These numbers indicate that there are more than the expected two molecules per column cross-section.

3.2.6.3 Mesomorphic Properties of $[ZnCl_2(L^{Bipy\text{-}n})]$

The liquid crystalline behaviour of the final metal in this series of complexes, $[ZnCl_2(L^{Bipy\text{-}n})]$, is presented below, in Chart 3.3.

The melting temperatures of $[ZnCl_2(L^{Bipy\text{-}10})]$ and $[ZnCl_2(L^{Bipy\text{-}12})]$ were not detected by DSC, but were confirmed by POM and XRD as occurring at 60°C for both complexes. The melting temperatures of $[ZnCl_2(L^{Bipy\text{-}14})]$ and $[ZnCl_2(L^{Bipy\text{-}16})]$ were observed by DSC and POM as occurring at 36°C and

54°C, respectively. All mesophases were characterised as columnar by POM from the platelets and crosses appearing in the textures.

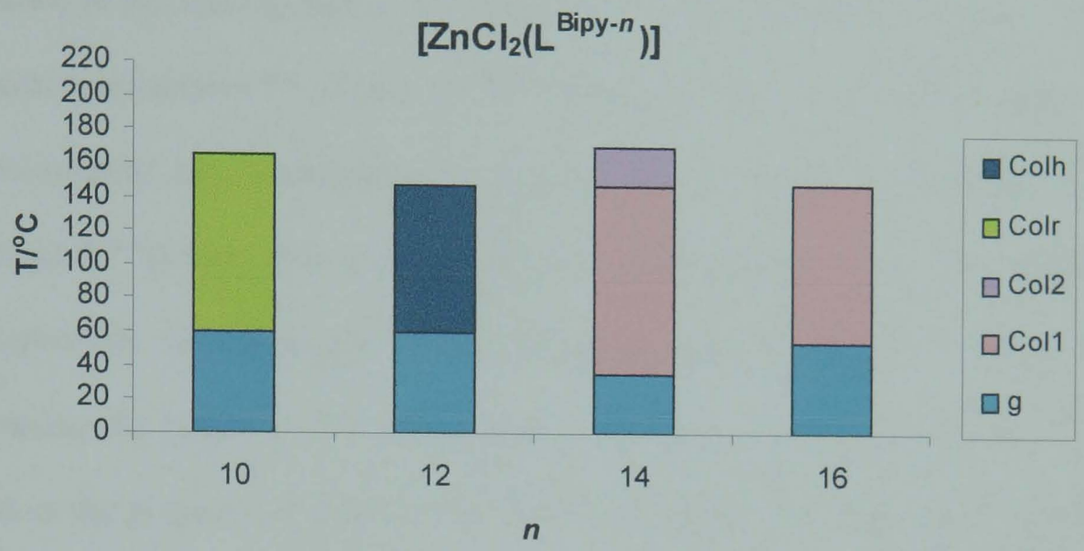

Chart 3.3. Phase diagrams representing the transition temperatures of the compounds $[ZnCl_2(L^{Bipy\text{-}n})]$ (where Col_h and Col_r are columnar hexagonal and rectangular phases, respectively; Col_1 and Col_2 are columnar mesophases whose 2D symmetry have yet to be determined; g is the glass transition temperature).

The clearing temperatures appeared as broad peaks in the DSC traces at 165°C, 157°C, 171°C and 149°C for $[ZnCl_2(L^{Bipy\text{-}10})]$, $[ZnCl_2(L^{Bipy\text{-}12})]$, $[ZnCl_2(L^{Bipy\text{-}14})]$ and $[ZnCl_2(L^{Bipy\text{-}16})]$, respectively. All were in agreement with the POM observations, except for $[ZnCl_2(L^{Bipy\text{-}14})]$ which appeared to clear at 164°C. The broadness of the DSC peak could have attributed to this error. Another feature of $[ZnCl_2(L^{Bipy\text{-}14})]$ was that DSC showed the appearance of a second mesophase at 147°C, whereas all other $[ZnCl_2(L^{Bipy\text{-}n})]$ formed one mesophase only. Hence, mesomorphism is most stable for $[ZnCl_2(L^{Bipy\text{-}14})]$, which also displayed the greatest number of mesophases.

Small-angle XRD was additionally used to characterise the phases for $[ZnCl_2(L^{Bipy\text{-}10})]$ and $[ZnCl_2(L^{Bipy\text{-}12})]$. For $[ZnCl_2(L^{Bipy\text{-}10})]$ a columnar rectangular mesophase was detected by the presence of one very strong, one strong and one medium diffraction peak in the small angle region,

corresponding to d_{20}, d_{11} and $d_{1\text{-}1}$, respectively. These reflections satisfied the condition $h + k = 2n$, hence the space group was determined as *c2mm*. For $[ZnCl_2(L^{Bipy\text{-}12})]$ a columnar hexagonal mesophase was detected by the presence of d_{10} and d_{20} bands in the ratio $1:\sqrt{4}$. The number of molecules per column cross-section for $[ZnCl_2(L^{Bipy\text{-}12})]$ was calculated as $N_h = 1.89$, which is approximately two molecules. Therefore, the temperatures at which the $[ZnCl_2(L^{Bipy\text{-}n})]$ form columnar mesophases and subsequently isotropic liquids is dependent on the length of the peripheral aliphatic chains. However, increasing the length of the chains from $n = 10$ to 16 carbon atoms does not result in the progressive reduction of melting and clearing temperatures. At the present time it is not possible to establish the precise correlation between chain length and lattice parameters without further XRD characterisation.

Comparison of the complexes $[NiCl_2(L^{Bipy\text{-}n})]$ and $[ZnCl_2(L^{Bipy\text{-}n})]$ reveals that both series generally have melting temperatures of around 60°C. The exception to this is $[ZnCl_2(L^{Bipy\text{-}14})]$ which melted at 36°C. The $[NiCl_2(L^{Bipy\text{-}n})]$ series generally has higher clearing temperatures than their $[ZnCl_2(L^{Bipy\text{-}n})]$ analogues, ranging from 164°C to 171°C for $[NiCl_2(L^{Bipy\text{-}n})]$ and 147°C to 171°C for $[ZnCl_2(L^{Bipy\text{-}n})]$. This is possibly as a consequence of the different coordination geometries of the complexes. As mentioned previously, $[NiCl_2(L^{Bipy\text{-}n})]$ complexes are six-coordinate and have distorted octahedral coordination geometry. Conversely, $[ZnCl_2(L^{Bipy\text{-}n})]$ complexes are five-coordinate distorted trigonal bipyramidal species. Therefore, the lower clearing temperatures of $[ZnCl_2(L^{Bipy\text{-}n})]$ could result from the presence of the flexible, non-coordinated imine arm. However, $[ZnCl_2(L^{Bipy\text{-}16})]$ has far higher clearing temperatures than both $[MnCl_2(L^{Bipy\text{-}16})]$ and $[CoCl_2(L^{Bipy\text{-}16})]$, which

have octahedral coordination geometries. Thus, the influence of coordination geometry on the mesomorphic character of the bipyridine complexes is not fully determined.

But one absolute conclusion that can be drawn from mesomorphic data collated for $[MCl_2(L^{Bipy\text{-}n})]$ is that the slight deviation from coplanarity at the core of the bipyridine complexes is not a barrier to columnar mesophase formation.

Table 3.6. Table showing the combined POM, DSC and XRD data to give the mesophase transition temperatures for $[ZnCl_2(L^{Bipy\text{-}n})]$. Also included, where possible, are detailed indexation information obtained by XRD studies (where ***n*** = number of carbons in aliphatic chains; **T** = temperature at which data was taken; d_{meas}, and d_{calc} are the measured and calculated diffraction spacings, respectively; ***hk*** is the indexation of the two-dimensional lattice; Col_r and Col_h are rectangular and hexagonal columnar mesophases, respectively; *a* is the lattice parameter and *S* is the lattice area of the hexagonal (Col_h) columnar phase; *p6mm* is the 2D space group of the corresponding hexagonal mesophase; Col, Col_1 and Col_2 are unidentified columnar mesophases and I is the isotropic liquid).

n	**T/°C**	$d_{meas.}$/Å	***hk***	$d_{calc.}$/Å	**Mesophase**	**Transitions/°C**
10	140	29.67	d_{20}	-	Col_r – *c2mm*	g 60 Col_r 165 I
		24.62	d_{11}	-		
		14.68	$d_{1\text{-}1}$	-		
		10.13		-		
		4.5	br			
12	120	31.06	d_{10}	31.06	Col_h – *p6mm*	g 60 Col_h 147 I
		15.53	d_{20}	15.53	a = 35.9Å	
		4.5	br		S = 1114 Å^2	
14	-	-	-	-	Col_1, Col_2	g 36 Col_1 147 Col_2 171 I
16	-	-	-	-	Col	g 54 Col 149 I

3.2.7 Comparison of the Bipyridine *vs.* the Phenanthroline Complexes

The effect of substituting the 1,10-phenanthroline core with a 2,2'-bipyridine one was to overwhelmingly stabilise columnar mesomorphism. As demonstrated by the phase diagram in Chart 3.4 the clearing temperatures of the bipyridine complexes were elevated often significantly relative to the phenanthroline complexes. The exception is $[CoCl_2(L^{Bipy\text{-}16})]$, which had the same isotropic point as $[CoCl_2(L^{Phen\text{-}16})]$. All melting temperatures generally remained at similar temperatures. Consequently, the columnar mesophase

range was increased for $[MCl_2(L^{Bipy\text{-}n})]$. It can be concluded that a more flexible bipyridine core serves to increase the isotropic transition temperatures overall without having as significant an effect on the melting temperatures.

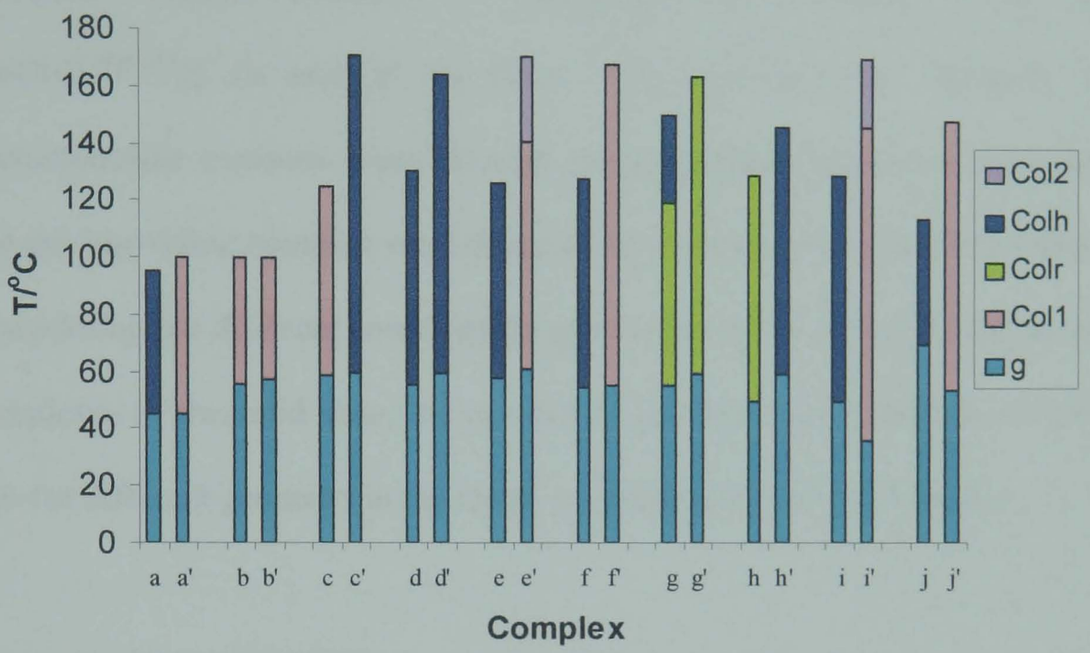

a = $[MnCl_2(L^{Phen\text{-}16})]$, a' = $[MnCl_2(L^{Bipy\text{-}16})]$, b = $[CoCl_2(L^{Phen\text{-}16})]$, b' = $[CoCl_2(L^{Bipy\text{-}16})]$,
c = $[NiCl_2(L^{Phen\text{-}10})]$, c' = $[NiCl_2(L^{Bipy\text{-}10})]$, d = $[NiCl_2(L^{Phen\text{-}12})]$, d' = $[NiCl_2(L^{Bipy\text{-}12})]$,
e = $[NiCl_2(L^{Phen\text{-}14})]$, e' = $[NiCl_2(L^{Bipy\text{-}14})]$, f = $[NiCl_2(L^{Phen\text{-}16})]$, f' = $[NiCl_2(L^{Bipy\text{-}16})]$,
g = $[ZnCl_2(L^{Phen\text{-}10})]$, g' = $[ZnCl_2(L^{Bipy\text{-}10})]$, h = $[ZnCl_2(L^{Phen\text{-}12})]$, h' = $[ZnCl_2(L^{Bipy\text{-}12})]$,
i = $[ZnCl_2(L^{Phen\text{-}14})]$, i' = $[ZnCl_2(L^{Bipy\text{-}14})]$, j = $[ZnCl_2(L^{Phen\text{-}16})]$, j' = $[ZnCl_2(L^{Bipy\text{-}16})]$.

Chart 3.4. Phase diagram comparing the liquid crystalline phase behaviour of the related phenanthroline and bipyridine complexes, where Col_r and Col_h are columnar rectangular and hexagonal mesophases, respectively; Col_1 and Col_2 are columnar phases whose 2D symmetry is currently unidentified; and g is the glass transition temperature.

At the present time it is only possible to make direct comparisons between the types of columnar mesophase preferentially formed by the phenanthroline and bipyridine complexes of $[NiCl_2(L^{12})]$, $[ZnCl_2(L^{10})]$ and $[ZnCl_2(L^{12})]$ (d,d', g,g' and h,h' in Chart 3.4).

Both $[NiCl_2(L^{Phen\text{-}12})]$ and $[NiCl_2(L^{Bipy\text{-}12})]$ (d and d' in Chart 3.4) form one columnar hexagonal mesophase below the isotropic liquid. However, $[ZnCl_2(L^{Phen\text{-}10})]$ and $[ZnCl_2(L^{Bipy\text{-}10})]$ (g and g' in Chart 3.4) showed different transitions. $[ZnCl_2(L^{Phen\text{-}10})]$ melted into a columnar rectangular mesophase, then a columnar hexagonal mesophase followed by the isotropic liquid,

whereas $[ZnCl_2(L^{Bipy\text{-}10})]$ exhibited a columnar rectangular mesophase only. This suggests that the bipyridine core stabilises the formation of the columnar rectangular phase at the expense of the columnar hexagonal phase for this particular zinc(II) complex. Comparison of $[ZnCl_2(L^{Phen\text{-}12})]$ with $[ZnCl_2(L^{Bipy\text{-}12})]$ (h and h' in Chart 3.4) suggested the opposite: the phenanthroline complex went through one columnar rectangular mesophase and the bipyridine complex went through one columnar hexagonal mesophase. Considering the different coordination geometries of the nickel(II) and zinc(II) complexes in the solid state, the occurrence of this opposite sequence implies that the different geometry at the metal is maintained in the mesophase.

3.3 CONCLUSIONS

To conclude, the first mononuclear octahedral and trigonal bipyramidal 6,6'-disubstituted-2,2'-bipyridine metallomesogens $[MCl_2(L^{Bipy\text{-}n})]$ have been successfully synthesised and studied. These compounds were synthesised using similar procedures to the phenanthroline analogues. The complexes $[MCl_2(L^{Bipy\text{-}n})]$ were prepared in good yields from Schiff-base condensation template reactions of manganese(II), cobalt(II), nickel(II) and zinc(II) chlorides with 6,6'-diformyl-2,2'-bipyridine and 3,4,5-tri(alkoxy)aniline. Characterisation of the complexes confirmed that they are monomeric 1:1 metal-ligand compounds.

Single crystal X-ray diffraction provided further structural characterisation of the complexes $[MCl_2(L^{Bipy\text{-}1})]$. The compounds $[MnCl_2(L^{Bipy\text{-}1})]$, $[CoCl_2(L^{Bipy\text{-}1})]$ and $[NiCl_2(L^{Bipy\text{-}1})]$ have six-coordinate distorted octahedral coordination geometry, whereas $[ZnCl_2(L^{Bipy\text{-}1})]$ has five-

coordinate distorted trigonal bipyramidal coordination geometry, as a consequence of the small size of the zinc(II) cation. A major difference between the bipyridine and phenanthroline compounds is ligand coordination to the metal centres, as the rigidity of the phenanthroline core prevents coordination of the second imine arm to the metals.

The packing arrangements of $[MCl_2(L^{Bipy\text{-}1})]$, where M = cobalt(II), nickel(II) and zinc(II), are very similar to $[MCl_2(L^{Phen\text{-}1})]$, where M = manganese(II) cobalt(II), nickel(II) and zinc(II), with pairs of molecules arranged as pseudo disks in tilted columns, in space group P-1. The one anomalous packing network is of $[MnCl_2(L^{Bipy\text{-}1})]$, which is in the alternative space group I2/a. Although pairs of molecules are correlated as pseudo disks, they are arranged in zig-zagged layers rather than discrete columns. One common feature of the packing diagrams is that all bipyridine complexes have a greater intermolecular bipyridine - bipyridine plane separation relative to the intermolecular phenanthroline - phenanthroline plane distances of the corresponding phenanthroline analogues. This is unsurprising considering octahedral geometry of $[MnCl_2(L^{Bipy\text{-}1})]$, $[CoCl_2(L^{Bipy\text{-}1})]$ and $[NiCl_2(L^{Bipy\text{-}1})]$ and the resulting dominating presence of the chloride anions. Consequently, the intermolecular distances between bipyridine complexes are greater than the corresponding phenanthroline complexes, with the exception of $[ZnCl_2(L^{Bipy\text{-}1})]$.

Investigation of the liquid crystalline properties of the complexes $[MCl_2(L^{Bipy\text{-}n})]$ revealed that $[MnCl_2(L^{Bipy\text{-}16})]$, $[NiCl_2(L^{Bipy\text{-}n})]$, $[CoCl_2(L^{Bipy\text{-}16})]$ and $[ZnCl_2(L^{Bipy\text{-}n})]$ (n = 10, 12, 14, 16) are mesomorphic.

The complexes all form at least one columnar mesophase, with compounds $[NiCl_2(L^{Bipy\text{-}14})]$ and $[ZnCl_2(L^{Bipy\text{-}14})]$ both forming two columnar mesophases.

The liquid crystalline properties of $[NiCl_2(L^{Bipy\text{-}16})]$ and $[ZnCl_2(L^{Bipy\text{-}16})]$ are stabilised relative to other $n = 16$ compounds, $[MnCl_2(L^{Bipy\text{-}16})]$ and $[CoCl_2(L^{Bipy\text{-}16})]$. All four compounds melt into the mesophase at around 50°C, but $[NiCl_2(L^{Bipy\text{-}16})]$ and $[ZnCl_2(L^{Bipy\text{-}16})]$ clear into the isotropic liquid at 169°C and 149°C, respectively, whereas $[MnCl_2(L^{Bipy\text{-}16})]$ and $[CoCl_2(L^{Bipy\text{-}16})]$ clear at 100°C.

Investigation of the mesomorphic behaviour of $[NiCl_2(L^{Bipy\text{-}n})]$ (n = 10, 12, 14, 16) revealed that the length of the aliphatic chain had negligible influence on melting and clearing temperatures. The complexes melted in the range 56°C – 61°C and cleared between 164°C and 171°C.

With the exception of $[ZnCl_2(L^{Bipy\text{-}14})]$ which melts at 36°C, the complexes $[ZnCl_2(L^{Bipy\text{-}n})]$ have near-identical melting temperatures to the $[NiCl_2(L^{Bipy\text{-}n})]$ compounds. The range of the clearing temperatures for $[ZnCl_2(L^{Bipy\text{-}n})]$ is from 147°C to 171°C and consequently indicates that the columnar mesophases of the $[NiCl_2(L^{Bipy\text{-}n})]$ are stabilised relative to $[ZnCl_2(L^{Bipy\text{-}n})]$. Once again the solitary exception to this is $[ZnCl_2(L^{Bipy\text{-}14})]$. With the low melting temperature of 36°C the columnar mesophases of $[ZnCl_2(L^{Bipy\text{-}14})]$ exist over 135°C, compared to 110°C for the mesophases of $[NiCl_2(L^{Bipy\text{-}14})]$. Thus, variation of the length of the aliphatic chains appears to have only a small effect on the melting temperatures of the complexes $[MCl_2(L^{Bipy\text{-}n})]$. The effect on the clearing temperatures, however, is far less predictable. Changing the metal(II) centre dramatically reduces the thermal stability of $[MnCl_2(L^{Bipy\text{-}16})]$ and $[CoCl_2(L^{Bipy\text{-}16})]$ relative to $[NiCl_2(L^{Bipy\text{-}16})]$

and $[ZnCl_2(L^{Bipy\text{-}16})]$. The series with the greatest thermal stability of all is $[NiCl_2(L^{Bipy\text{-}n})]$.

3.4 EXPERIMENTAL

NMR spectra were recorded on either a Bruker DPX300 FT-NMR spectrometer operating at 300.13 MHz for ^1H and 75.48 MHz for broadband proton decoupled ^{13}C, or a Jeol EX270 FT-NMR spectrometer operating at 270.17 MHz for ^1H and 67.93MHz for broadband proton decoupled ^{13}C. Chemical shifts are referenced with respect to residual proton and carbon solvent (with δ_H = 7.26 ppm and δ_C = 77.0 ppm for $CDCl_3$). IR spectra were obtained on a Nicolet AVATAR 360 FT-IR spectrometer as KBr pellets. FAB mass spectra were obtained on a Finnigan MAT TSQ-700 spectrometer at the University of Wales, Swansea, with 3-nitrobenzyl alcohol (NOBA) as matrix. MALDI-TOF mass spectra were obtained on a Voyager-DE-STR spectrometer at the University of Wales, Swansea, with *trans*-2-[3-(4-tert-butylphenyl)-2-methylprop-2-enylidene]malononitrile (DCTB) as matrix. EI and ES mass spectra were recorded by the Mass Spectrometry Service at the University of Nottingham. Elemental analyses (C, H, N) were carried out by the Analytical Department of the University of Nottingham.

Analysis by polarised optical microscopy was carried out using a Zeiss Labpol, or Olympus BH40 microscope equipped with a Link-Am HFS91 hot stage, TMS92 controller and LNP2 cooling unit. Analysis by DSC was carried out on either a Perkin-Elmer DSC7 instrument or a TA DSC 2920 instrument, using heating and cooling rates of either 5 or 10°C min^{-1}. For analysis by XRD the powdered sample was filled in Lindemann capillaries of 1mm diameter. A

linear monochromatic Cu-K_α beam (λ = 1.5405Å) obtained with a sealed-tube generator (900W) and a bent quartz monochromator were used. The diffraction patterns were registered with a curved counter Inel CPS 120, for which the sample temperature was controlled within ± 0.05°C. Periodicidies up to 60Å could be measured. An X-ray pattern was recorded every 20°C for each compound from the crystalline state up to the isotropic liquid.

3.4.1 Synthesis of the Anilines

See Chapter 2, section 2.4.1.

3.4.2 Synthesis of 6,6'-Diformyl-2,2'-Bipyridine

3.4.2.1 Synthesis of 6-Bromopicoline

2-Aminopicoline (37.0g, 0.342mol) was added in portions under vigorous stirring to 48% HBr (185cm^3) at 20 to 30°C. Once the solid had dissolved, the solution was cooled to -20°C. Cooled Br_2 (48cm^3, 0.958mol) was added dropwise over 30 mins, maintaining the temperature at -20°C and the resulting paste was stirred at this temperature for 90 mins. Aqueous $NaNO_2$ (63g, 0.913mol, 93cm^3 H_2O) was then added dropwise and the red/brown reaction mixture was allowed to warm to room temperature over 1 hour and was then stirred for an additional 45 mins. On cooling to -20°C, the red mixture became a thick orange paste. This was treated with cooled, aqueous NaOH (247g, 370cm^3 H_2O), ensuring the temperature did not exceed -10°C. The yellow suspension was allowed to warm to room temperature and stirred for 1 hour. The mixture was extracted with EtOAc (4 x 500cm^3) and the organic phases were collectively dried over Na_2SO_4. The solvent was removed

in vacuo to give 6-bromopicoline as a brown oil (48.0g, 81.6%). Microanalysis: Calculated for C_6H_6BrN C 41.89, H 3.52, N 8.14: found C 39.54, H 3.18, N 7.85. IR (CaF_2 liquid film): ν = 2959w (CH_3), 1585s (C=N), 1557s (C=C), 1436s (C=C) cm^{-1}. ^{1}H-NMR (300.13MHz, $CDCl_3$, 298K): δ_H 7.39 (1H, t, $^3J_{AB}$ = 7.68Hz, Ar<u>H</u>), 7.25 (1H, d, $^3J_{AB}$ = 7.85Hz, Ar<u>H</u>), 7.07 (1H, d, $^3J_{AB}$ = 7.50Hz, Ar<u>H</u>), 2.50 (3H, s, C<u>H</u>$_3$) ppm. ^{13}C-NMR (75.48MHz, $CDCl_3$, 298K): δ_C 159.6, 140.9, 138.3, 124.7, 121.8, 23.9 ppm. EI MS: m/z = 171 $[C_6H_6BrN]^+$.

3.4.2.2 Synthesis of 6,6'-Dimethyl-2,2'-Bipyridine

A mixture of 6-bromopicoline (8.09g, 0.0470mol), tetra *n*-butylammonium bromide (7.58g, 0.0235mol), $Pd(OAc)_2$ (0.528g, 2.35 x 10^{-3}mol) and K_2CO_3 (6.50g, 0.0470mol) in DMF and H_2O (2.4:1, 6.5cm^3: 2.7cm^3) was heated to 110°C under N_2. Isopropyl alcohol (5cm^3) was added and the stirring was continued at 110°C for 2 days. The cooled mixture was diluted with H_2O (200cm^3) and the product extracted with EtOAc (5 x 100cm^3). The combined organic phases were dried over $MgSO_4$ and the solvent was removed *in vacuo* to give a thick brown oil. The residue was dissolved in hexane, resulting in white crystals of 6,6'-dimethyl-2,2'-bipyridine (1.54g, 35.6%). Microanalysis: Calculated for $C_{12}H_{12}N_2$ C 78.22, H 6.58, N 15.21; found C 77.78, H 6.12, N 15.31. ^{1}H-NMR (300.13MHz, $CDCl_3$, 298K): δ_H 8.18 (2H, d, $^3J_{AX}$ = 7.82Hz, Ar<u>H</u>), 7.67 (2H, t, $^3J_{AX}$ = 7.73Hz, Ar<u>H</u>), 7.14 (2H, d, $^3J_{AX}$ = 7.60Hz, Ar<u>H</u>), 2.62 (6H, s, C<u>H</u>$_3$) ppm. ^{13}C-NMR (75.48MHz, $CDCl_3$, 298K): δ_C 157.4, 154.7, 137.3, 123.3, 117.5, 24.2 ppm. EI MS: m/z = 184 $[C_{12}H_{12}N_2]^+$.

3.4.2.3 Synthesis of 6,6'-Diformyl-2,2'-Bipyridine

6,6'-Dimethyl-2,2'-bipyridine (1.54g, 8.38 x 10^{-3}mol) and excess selenium dioxide (4.65g, 0.0419mol) were heated to reflux for 24 hours in glacial AcOH (150cm^3). The mixture was filtered hot through celite and cotton wool and washed with hot AcOH. The solvent was reduced in volume *in vacuo* and a white solid was collected. This was washed with H_2O and EtOH and dried, to give 6,6'-diformyl-2,2'-bipyridine (0.650g, 36.6%). Micoranalysis: Calculated for $C_{12}H_8N_2O_2.0.5H_2O$ C 65.15, H 4.10, N 12.66; found C 65.00, H 3.76, N 12.46. IR (KBr pellet): ν = 1707vs (C=O), 1578s (C=C), 1561m (C=N) cm^{-1}. ^{1}H-NMR (300.13MHz, $CDCl_3$, 298K): δ_H 10.11 (2H, s, C<u>H</u>O), 8.77 (2H, dd, $^3J_{AM}$ = 7.89Hz, $^4J_{AX}$ = 0.93Hz, Ar<u>H</u>), 8.28 (2H, t, $^3J_{AX}$ = 7.79Hz, Ar<u>H</u>), 8.06 (2H, dd, $^3J_{AM}$ = 7.65Hz, $^4J_{AX}$ = 0.93Hz, Ar<u>H</u>) ppm. ^{13}C-NMR (75.48MHz, $CDCl_3$, 298K): δ_C 193.4, 154.8, 152.1, 139.3, 125.1, 122.5 ppm. EI MS: m/z = 212 $[C_{12}H_8N_2O_2]^+$.

3.4.3 Synthesis of 6,6'-Bis-[3',4',5'-tri(methoxy)phenyliminomethyl]-2,2'-Bipyridine, L^{Bipy-1}

6,6'-Diformyl-2,2'-bipyridine (0.578g, 2.72 x 10^{-3} mol) and 3,4,5-trimethoxyaniline were heated to reflux in EtOH (100cm^3) and $CHCl_3$ (15cm^3) for 4 hours. The solvent volume was reduced *in vacuo* to give a pale yellow solid, which was filtered off, washed with EtOH and dried to give L^{Bipy-1} (Figure 3.25). This was recrystallised from hexane and $CHCl_3$ (1.31g, 89.0%). Microanalysis: Calculated for $C_{30}H_{30}N_4O_6.2H_2O$ C 62.27, H 5.92, N 9.68; found C 62.82, H 5.55, N 9.35. IR (KBr pellet): υ = 2942w (C-H), 2836w (C-H), 1623w (C=N), 1588vs (C=N), 1504s (C=C), 1468s (C=C), 1438s

(C=C), 1132vs (C-O) cm^{-1}. ^{1}H-NMR (300.13MHz, $CDCl_3$, 298K): δ_H 8.76 (2H, s, $\underline{H}_aC{=}N$), 8.58 (2H, d, $^3J_{AX}$ = 7.62Hz, $\underline{H}_d$), 8.29 (2H, d, $^3J_{AX}$ = 7.52Hz, $\underline{H}_b$), 7.99 (2H, t, $^3J_{AX}$ = 7.82Hz, $\underline{H}_c$), 6.64 (4H, s, $\underline{H}_e$), 3.94 (18H, s, $OC\underline{H}_3$) ppm. ^{13}C-NMR (67.93MHz, $CDCl_3$, 298K): δ_C 161, 156, 155, 154, 153, 147, 138, 123, 122, 98.6, 61.5, 56.3 ppm. EI MS: m/z = 542 $[L^{Bipy\text{-}1}]^+$.

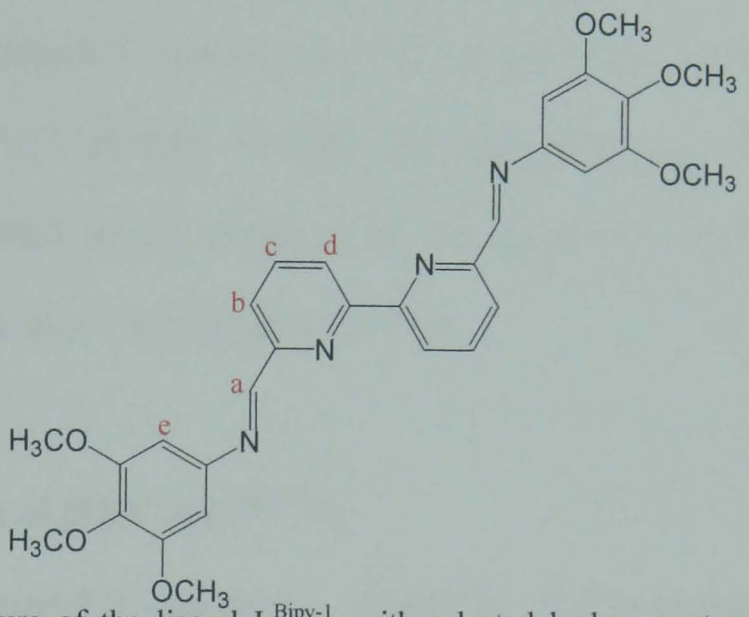

Figure 3.25. Structure of the ligand $L^{Bipy\text{-}1}$, with selected hydrogen atoms labelled a-e in reference to the NMR spectral assignments.

3.4.4 Synthesis of 6,6'-Bis-[3',4',5'-tri(alkoxy)phenyliminomethyl]-2,2'-Bipyridine Metal(II) Chloride, $[MCl_2(L^{Bipy\text{-}n})]$

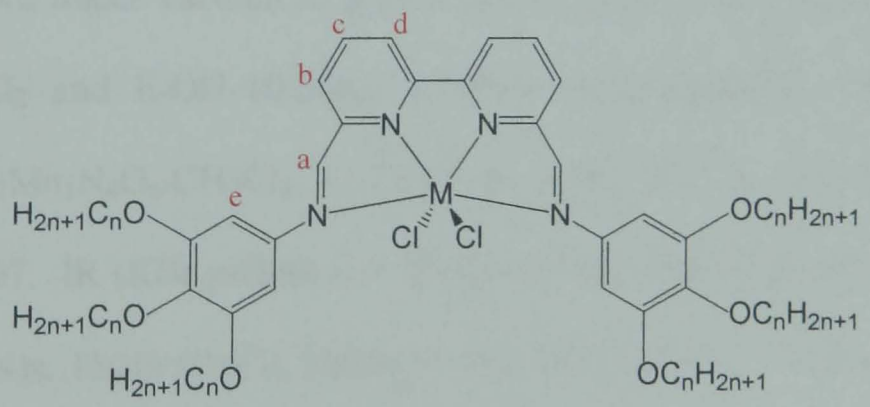

Figure 3.26. Structure of the complexes $[MCl_2(L^{Bipy\text{-}n})]$, with selected hydrogen atoms labelled a-e in reference to the NMR spectral assignments of the zinc(II) complexes.

Similar preparations were used for all nickel(II) and zinc(II) compounds, with n = 10, 12, 14, 16 (Figure 3.26), so one example for each series of complexes is given.

3.4.4.1 Synthesis of $[MnCl_2(L^{Bipy\text{-}1})]$

A solution of $MnCl_2.4H_2O$ (0.0304g, 1.54 x 10^{-4}mol) in EtOH (8cm^3) was layered on top of a solution of $L^{Bipy\text{-}1}$ (0.0795g, 1.47 x 10^{-4}mol) in $CHCl_3$ (8cm^3) and left to stand for two days. Red crystals of $[MnCl_2(L^{Bipy\text{-}1})]$ were produced. These were filtered off, washed with EtOH and dried (0.0684g, 68.8%). Microanalysis: Calculated for $C_{30}H_{30}Cl_2MnN_4O_6$ C 53.91, H 4.52, N 8.38; found C 53.27, H 4.79, N 7.82. IR (KBr pellet): υ = 1618m (C=N), 1578s (C=N), 1508m (C=C), 1499s (C=C), 1491s (C=C), 1128vs (C-O) cm^{-1}. MALDI-TOF MS: m/z = 632 $[MnCl(L^{Bipy\text{-}1})]^+$.

3.4.4.2 Synthesis of $[MnCl_2(L^{Bipy\text{-}16})]$

6,6'-Diformyl-2,2'-bipyridine (0.0497g, 0.234mmol) and 3,4,5-trihexadecyloxyaniline (0.0391g, 1.98mmol) were stirred in $CHCl_3$ (75cm^3) for 10 mins. $MnCl_2.4H_2O$ (0.0472g, 0.238mmol) in EtOH (25cm^3) was added and the solution was heated to reflux for 24 hours. The solvent volume was reduced down under vacuum to give a yellow solid, which was recrystallised from CH_2Cl_2 and EtOH (0.386g, 85.4%). Microanalysis: Calculated for $C_{120}H_{210}\ Cl_2Mn_1N_4O_6.CH_2Cl_2$ C 72.10, H 10.60, N 2.78; found C 72.08, H 10.74, N 2.97. IR (KBr pellet): υ = 2918vs (C-H), 2847vs (C-H), 1619(C=N), 1588w (C=N)s, 1501s (C=C), 1468s (C=C), 1437s (C=C), 1118vs (C-O) cm^{-1}. MALDI-TOF MS: m/z = 1896 $[MnCl(L^{Bipy\text{-}16})]^+$.

3.4.4.3 Synthesis of $[FeCl_2(L^{Bipy\text{-}1})]$

A solution of $FeCl_2.4H_2O$ (0.0305g, 1.53 x 10^{-4}mol) in EtOH (8cm^3) was layered on top of a solution of $L^{Bipy\text{-}1}$ (0.0795g, 1.47 x 10^{-4} mol) in $CHCl_3$

($8cm^3$) and left to stand for two days. Small dark green crystals of $[FeCl_2(L^{Bipy\text{-}1})]$ were produced. These were filtered off, washed with EtOH and dried (0.0488g, 47.7%). Microanalysis: Calculated for $C_{30}H_{30}Cl_2FeN_4O_6.0.5CHCl_3$ C 50.25, H 4.22, N 7.69; found C 49.58, H 4.25, N 7.52. MALDI-TOF MS: m/z = 669 $[FeCl_2(L^{Bipy\text{-}1})]^+$.

3.4.4.4 Synthesis of $[FeCl_2(L^{Bipy\text{-}16})]$

6,6'-Diformyl-2,2'-bipyridine (0.0460g, 0.217mmol) and 3,4,5-trihexadecyloxyaniline (0.363g, 0.446mmol) were stirred in $CHCl_3$ ($75cm^3$) under an atmosphere of N_2 for 10 mins. $FeCl_2.4H_2O$ (0.0455g, 0.229mmol) in EtOH ($25cm^3$) was added and the solution was heated to reflux for 24 hours. The solution was reduced in volume under vacuum to give a brown solid, which was recrystallised from $CHCl_3$ and EtOH (0.304g, 72.5%). Microanalysis: Calculated for $C_{120}H_{210}Cl_2Fe_1N_4O_6.CHCl_3$ C 70.85, H 10.37, N 2.73; found C 70.94, H 10.61, N 3.11. IR (KBr pellet): υ = 2915vs (C-H), 2850vs (C-H), 1638w (C=N), 1589s (C=N), 1503m (C=C), 1469s (C=C), 1437m (C=C), 1120vs (C-O) cm^{-1}. MALDI-TOF MS: m/z = 1896 $[FeCl(L^{Bipy\text{-}16})]^+$.

3.4.4.5 Synthesis of $[CoCl_2(L^{Bipy\text{-}1})]$

A solution of $CoCl_2.6H_2O$ (0.0357g, 1.50×10^{-4}mol) in EtOH ($8cm^3$) was layered on top of a solution of $L^{Bipy\text{-}1}$ (0.0808g, 1.49×10^{-4} mol) in $CHCl_3$ ($8cm^3$) and left to stand for two days. Orange crystals of $[CoCl_2(L^{Bipy\text{-}1})]$ were produced. These were filtered off, washed with EtOH and dried (0.096g, 95.8%). Microanalysis: Calculated for $C_{30}H_{30}Cl_2CoN_4O_6.2CHCl_3$ C 42.18, H

3.54, N 6.15; found C 42.67, H 3.68, N 6.36. IR (KBr pellet): υ = 2941w (C-H), 2839w (C-H), 1614m (C=N), 1589s (C=N), 1503s (C=C), 1466s (C=C), 1422s (C=C), 1123vs (C-O) cm^{-1}. MALDI-TOF MS: m/z = 636 $[CoCl(L^{Bipy\text{-}1})]^+$.

3.4.4.6 Synthesis of $[CoCl_2(L^{Bipy\text{-}16})]$

6,6'-Diformyl-2,2'-bipyridine (0.0515g, 0.243mmol) and 3,4,5-trihexadecyloxyaniline (0.401g, 0.492mmol) were stirred in $CHCl_3$ ($75cm^3$) for 10 mins. $CoCl_2.6H_2O$ (0.0586g, 0.246mmol) in EtOH ($25cm^3$) was added and the solution was heated to reflux for 24 hours. The solvent was reduced in volume *in vacuo* to give a brown solid, which was recrystallised from CH_2Cl_2 and EtOH (0.386g, 82.1%). Microanalysis: Calculated for $C_{120}H_{210}Cl_2Co_1N_4O_6.CH_2Cl_2$ C 71.95, H 10.58, N 2.77; found C 71.82, H 10.54, N 2.78. IR (KBr pellet): υ = 2914vs (C-H), 2848vs (C-H), 1614w (C=N), 1588s (C=N), 1502m (C=C), 1469s (C=C), 1437m (C=C), 1120vs (C-O) cm^{-1}. MALDI-TOF MS: m/z = 1899 $[CoCl(L^{Bipy\text{-}16})]^+$.

3.4.4.7 Synthesis of $[NiCl_2(L^{Bipy\text{-}1})]$

A solution of $NiCl_2.6H_2O$ (0.0352g, 1.48 x 10^{-4}mol) in EtOH ($8cm^3$) was layered on top of a solution of $L^{Bipy\text{-}1}$ (0.0798g, 1.47 x 10^{-4} mol) in $CHCl_3$ ($8cm^3$) and left to stand for two days. Orange crystals of $[NiCl_2(L^{Bipy\text{-}1})]$ were produced. These were filtered off, washed with EtOH and dried (0.097g, 98.2%). Microanalysis: Calculated for $C_{30}H_{30}Cl_2N_4NiO_6.3CHCl_3$ C 38.47, H 3.23, N 5.44; found C 37.61, H 3.21, N 5.55. IR (KBr pellet): υ = 2942w (C-H), 2839w (C-H), 1613m (C=N), 1589s (C=N), 1505s (C=C), 1464s (C=C),

1423s (C=C), 1126vs (C-O) cm^{-1}. MALDI-TOF MS: m/z = 635 $[NiCl(L^{Bipy\text{-}1})]^+$.

3.4.4.8 Synthesis of $[NiCl_2(L^{Bipy\text{-}10})]$

6,6-Diformyl-2,2'-bipyridine (0.0188g, 0.0886mmol) and 3,4,5-tridecyloxyaniline (0.0992g, 0.176mmol) were stirred in $CHCl_3$ ($25cm^3$) for 10 mins. $NiCl_2.6H_2O$ (0.0217g, 0.0913mmol) in EtOH ($8cm^3$) was added and the red/orange solution was heated to reflux for 24 hours. The solvent volume was reduced down *in vacuo* to give a brown solid, which was recrystallised from CH_2Cl_2 and MeOH (0.0723g, 57.1%). Microanalysis: Calculated for $C_{84}H_{138}Cl_2N_4Ni_1O_6.2H_2O$ C 68.84, H 9.77, N 3.82; found 68.93, H 9.57, N 3.94. IR (KBr pellet): υ = 2924vs (C-H), 2853vs (C-H), 1611w (C=N), 1587s (C=N), 1501(C=C)s, 1468s (C=C), 1437m (C=C), 1117vs (C-O) cm^{-1}. MALDI-TOF MS: m/z = 1394 $[NiCl(L^{Bipy\text{-}10})]^+$.

3.4.4.9 Synthesis of $[NiCl_2(L^{Bipy\text{-}12})]$

This compound was prepared as for $[NiCl_2(L^{Bipy\text{-}10})]$, from 6,6'-diformyl-2,2'-bipyridine (0.0330g, 0.155mmol), 3,4,5-tridodecyloxyaniline (0.199g, 0.308mmol) and $NiCl_2.6H_2O$ (0.0376g, 0.158mmol). Appearance: yellow microcrystals (0.169g, 68.2%). Microanalysis: Calculated for $C_{96}H_{162}Cl_2N_4Ni_1O_6.CH_2Cl_2$ C 69.23, H 9.82, N 3.33; found C 69.08, H 9.80, N 3.35. IR (KBr pellet): υ = 2922vs (C-H), 2851vs (C-H), 1610w (C=N), 1588s (C=N), 1502s (C=C), 1468s (C=C), 1437m (C=C), 1118vs (C-O) cm^{-1}. MALDI-TOF MS: m/z = 1562 $[NiCl(L^{Bipy\text{-}12})]^+$.

3.4.4.10 Synthesis of $[NiCl_2(L^{Bipy\text{-}14})]$

This compound was prepared as for $[NiCl_2(L^{Bipy\text{-}10})]$. from 6,6'-diformyl-2,2'-bipyridine (0.0388g, 0.183mmol), 3,4,5'-tritetradecyloxyaniline (0.267g, 0.366mmol) and $NiCl_2.6H_2O$ (0.0452g, 0.190mmol). Appearance: orange solid (0.224g, 69.3%). Microanalysis: Calculated for $C_{108}H_{186}Cl_2N_4Ni_1O_6.CH_2Cl_2$ C 70.72, H 10.24, N 3.03; found C 70.69, H 10.63, N 5.60. IR (KBr pellet): υ = 2920vs (C-H), 2850vs (C-H), 1614w (C=N), 1588s (C=N), 1503m (C=C), 1469s (C=C), 1437m (C=C), 1121vs (C-O) cm^{-1}. MALDI-TOF MS: m/z = 1730 $[NiCl(L^{Bipy\text{-}14})]^+$.

3.4.4.11 Synthesis of $[NiCl_2(L^{Bipy\text{-}16})]$

This compound was prepared as for $[NiCl_2(L^{Bipy\text{-}10})]$. from 6,6'-diformyl-2,2'-bipyridine (0.0670g, 0.316mmol), 3,4,5-trihexadecyloxyaniline (0.519g, 0.637mmol) and $NiCl_2.6H_2O$ (0.116g, 0.488mmol). Appearance: yellow solid (0.403g, 65.9%). Microanalysis: Calculated for $C_{120}H_{210}Cl_2N_4Ni_1O_6.CH_2Cl_2$ C 71.96, H 10.58, N 2.77; found C 72.60, H 10.63, N 2.67. IR (KBr pellet): υ = 2929vs (C-H), 2853vs (C-H), 1614w (C=N), 1587s (C=N), 1503s (C=C), 1470s (C=C), 1437s (C=C), 1122vs (C-O) cm^{-1}. MALDI-TOF MS: m/z = 1863 $[Ni(L^{Bipy\text{-}16})]^+$, 1899 $[NiCl(L^{Bipy\text{-}16})]^+$.

3.4.4.12 Synthesis of $[CuCl_2(L^{Bipy\text{-}1})]$

A solution of $CuCl_2$ (0.0221g, 1.64 x 10^{-4}mol) in EtOH (8cm^3) was layered on top of a solution of $L^{Bipy\text{-}1}$ (0.0810g, 1.49 x 10^{-4} mol) in $CHCl_3$ (8cm^3) and left to stand for five days. A brown precipitate crashed out and

would not crystallise despite repeated attempts. The precipitate was filtered off, washed with EtOH and dried (0.0473g, 42.6%). Microanalysis: Calculated for $C_{30}H_{30}Cl_2CuN_4O_6.CHCl_3EtOH$ C 47.05, H 4.43, N 6.65; found C 47.70, H 4.30, N 7.28. MALDI-TOF MS: m/z = 640 $[CuCl(L^{Bipy\text{-}1})]^+$.

3.4.4.13 Synthesis of $[CuCl_2(L^{Bipy\text{-}16})]$

6,6'-Diformyl-2,2'-bipyridine (0.0557g, 0.262mmol) and 3.4.5-trihexadecyloxyaniline (0.432g, 0.530mmol) were stirred in $CHCl_3$ ($75cm^3$) for 10 mins. $CuCl_2$ (0.0365g, 0.271mmol) in EtOH ($25cm^3$) was added and the solution was heated to reflux for 24 hours. The solvent volume was reduced *in vacuo*, giving a dark brown solid, which was recrystallised from CH_2Cl_2 and EtOH (0.310g, 61.0%). Microanalysis: Calculated for $C_{120}H_{210}Cl_2Cu_1N_4O_6.CH_2Cl_2$ C 71.79, H 10.56, N 2.77; found C 71.81, H 10.45, N 2.86. IR (KBr pellet): υ = 2843vs (C-H), 1658m (C=N), 1589s (C=N), 1498m (C=C), 1467s (C=C), 1437m (C=C), 1114vs (C-O) cm^{-1}. MALDI-TOF MS: m/z = 1868 $[Cu(L^{Bipy\text{-}16})]^+$.

3.4.4.14 Synthesis of $[ZnCl_2(L^{Bipy\text{-}1})]$

A solution of $ZnCl_2$ (0.0161g, 1.18 x 10^{-4}mol) in EtOH ($8cm^3$) was layered on top of a solution of $L^{Bipy\text{-}1}$ (0.0482g, 8.88 x 10^{-5} mol) in $CHCl_3$ ($8cm^3$) and left to stand for two days. Yellow crystals of $[ZnCl_2(L^{Bipy\text{-}1})]$ were produced. These were filtered off, washed with EtOH and dried (0.0536g, 89.0%). Microanalysis: Calculated for $C_{30}H_{30}Cl_2N_4O_6Zn_1.0.5H_2O$ C 52.38, H 4.54, N 8.14: found C 52.24, H 4.32, N 8.26. IR (KBr pellet): υ = 2939m (C-H), 2835w (C-H), 1622w (C=N), 1589s (C=N), 1503s (C=C), 1466s (C=C),

1424s (C=C), 1127vs (C-O) cm^{-1}. ^{1}H-NMR (300.13MHz, $CDCl_3$, 298K): δ_H 9.43 (2H, s, $\underline{H}_aC=N$), 8.29 (2H, d, $^3J_{AB}$ = 6.83Hz, $\underline{H}_d$), 8.22 (2H, d, $^3J_{AB}$ = 7.18Hz, $\underline{H}_b$), 8.17 (2H, t, $^3J_{AB}$ = 7.66Hz, $\underline{H}_c$), 7.14 (4H, s, $\underline{H}_e$), 3.87 (18H, s, $OC\underline{H}_3$) ppm. ^{13}C-NMR (75.48MHz, $CDCl_3$, 298K): δ_C 154.0, 153.3, 151.6, 148.5, 145.0, 143.0, 138.4, 126.5, 123.0, 100.8, 61.0, 56.2 ppm. LSI MS: m/z = 641 $[ZnCl(L^{Bipy\text{-}1})]^+$.

3.4.4.15 Synthesis of $[ZnCl_2(L^{Bipy\text{-}10})]$

6,6'-Diformyl-2,2'-bipyridine (0.0901g, 0.425mmol) and 3,4,5-tridecyloxyaniline (0.484g, 0.861mmol) were stirred together in $CHCl_3$ ($75cm^3$) for 10 mins. A solution of $ZnCl_2$ (0.0641g, 0.470mmol) in EtOH ($25cm^3$) was added and the orange solution was heated to reflux for 24 hours. The solvent volume was reduced *in vacuo* to give an orange solid, which was recrystallised from CH_2Cl_2 and EtOH and dried (0.332g, 54.4%). Microanalysis: Calculated for $C_{84}H_{138}Cl_2N_4O_6Zn_1.2H_2O$ C 68.52, H 9.72, N 3.81; found C 68.29, H 9.26, N 3.66. IR (KBr pellet): υ = 2917vs (C-H), 2854vs (C-H), 1621w (C=N), 1588s (C=N), 1500s (C=C), 1467s (C=C), 1437m (C=C), 1116vs (C-O) cm^{-1}. ^{1}H-NMR (300.13MHz, $CDCl_3$, 298K): δ_H 9.38 (2H, s, $\underline{H}_aC=N$), 8.21 (2H, d, $^3J_{AB}$ = 7.74Hz, $\underline{H}_d$), 8.12 (2H, d, $^3J_{AB}$ = 7.43Hz, $\underline{H}_b$), 8.03 (2H, t, $^3J_{AB}$ = 7.61Hz, $\underline{H}_c$), 7.06 (4H, s, $\underline{H}_e$), 3.98 (12H, m, $OC\underline{H}_2$), 1.79-1.26 (96H, m, $C\underline{H}_2$), 0.87 (18H, 2 overlapping triplets, $C\underline{H}_3$) ppm. ^{13}C-NMR (75.48MHz, $CDCl_3$, 298K): δ_C 154.2, 153.2, 151.7, 148.5, 142.6, 140.8, 138.4, 126.3, 122.8, 101.7, 73.5, 69.0, 31.9, 30.4, 29.8, 29.7, 29.6, 29.4, 26.2, 22.7, 14.1 ppm. MALDI-TOF MS: m/z = 1400 $[ZnCl(L^{Bipy\text{-}10})]^+$.

3.4.4.16 Synthesis of $[ZnCl_2(L^{Bipy\text{-}12})]$

This compound was prepared as for $[ZnCl_2(L^{Bipy\text{-}10})]$. from 6,6'-diformyl-2,2'-bipyridine (0.0901g, 0.425mmol), 3,4,5-tridodecyloxyaniline (0.551g, 0.853mmol) and $ZnCl_2$ (0.0584g, 0.429mmol). Appearance: brown, waxy solid (0.528g, 77.4%). Microanalysis: Calculated for $C_{96}H_{162}Cl_2N_4O_6Zn_1.2H_2O$ C 70.28, H 10.20, N 3.41; found C 70.08, H 9.81, N 3.24. IR (KBr pellet): υ = 2921vs (C-H), 1620w (C=N), 1589s (C=N), 1505s (C=C), 1464s (C=C), 1436m (C=C), 1118vs (C-O) cm^{-1}. ^{1}H-NMR (300.13MHz, $CDCl_3$, 298K): δ_H 9.36 (2H, s, $\underline{H}_aC$=N), 8.22 (2H, d, $^3J_{AB}$ = 7.77Hz, $\underline{H}_d$), 8.14 (2H, d, $^3J_{AB}$ = 7.41Hz, $\underline{H}_b$), 8.05 (2H, t, $^3J_{AB}$ = 7.44Hz, $\underline{H}_c$), 7.06 (4H, s, $\underline{H}_e$), 3.99 (12H, m, OC$\underline{H}_2$), 1.79-1.26 (120H, m, C$\underline{H}_2$), 0.89 (18H, 2 overlapping triplets, C$\underline{H}_3$) ppm. ^{13}C-NMR (75.48MHz, $CDCl_3$, 298K): δ_C 154.2, 153.2, 151.7, 148.5, 142.6, 140.8, 138.5, 126.3, 122.8, 101.7, 73.5, 69.0, 32.0, 30.4, 29.7, 29.6, 29.4, 26.2, 22.7, 14.1 ppm (three alkyl carbons obscured). MALDI-TOF MS: m/z = 1568 $[ZnCl(L^{Bipy\text{-}12})]^+$.

3.4.4.17 Synthesis of $[ZnCl_2(L^{Bipy\text{-}14})]$

This compound was prepared as for $[ZnCl_2(L^{Bipy\text{-}10})]$, from 6,6'-diformyl-2,2'-bipyridine (0.0919g, 0.433mmol), 3,4,5-tritetradecyloxyaniline (0.827g, 1.13mmol) and $ZnCl_2$ (0.0616g, 0.452mmol). Appearance: yellow solid (0.635g, 82.7%). Microanalysis: Calculated for $C_{108}H_{186}Cl_2N_4O_6Zn_1$ C 73.16, H 10.57, N 3.16; found C 73.34, H 10.84, N 2.44. IR (KBr pellet): υ = 2919vs (C-H), 2850vs (C-H), 1588s (C=N), 1501m (C=C), 1469s (C=C), 1437m (C=C), 1118vs (C-O) cm^{-1}. ^{1}H-NMR (300.13MHz, $CDCl_3$, 298K): δ_H 9.33 (2H, s, $\underline{H}_aC$=N), 8.24 (2H, d, $^3J_{AB}$ =

7.75Hz, $\underline{H}_d$), 8.17 (2H, d, $^3J_{AB}$ = 7.49Hz, $\underline{H}_b$), 8.10 (2H, t, $^3J_{AB}$ = 7.46Hz, $\underline{H}_c$), 7.07 (4H, s, $\underline{H}_e$), 3.98 (12H, m, OC$\underline{H}_2$), 1.84-1.26 (144H, m, C$\underline{H}_2$), 0.88 (18H, 2 overlapping triplets, C$\underline{H}_3$) ppm. ^{13}C-NMR (75.48MHz, $CDCl_3$, 298K): δ_C 154.2, 153.4, 151.6, 148.4, 142.6, 140.7, 138.5, 126.3, 122.8, 101.7, 73.5, 69.1, 31.9, 30.4, 29.8, 29.7, 29.4, 26.2, 26.1, 22.7, 14.1 ppm (four alkyl carbons obscured). MALDI-TOF MS: m/z = 1737 $[ZnCl(L^{Bipy\text{-}14})]^+$.

3.4.4.18 Synthesis of $[ZnCl_2(L^{Bipy\text{-}16})]$

This compound was prepared as for $[ZnCl_2(L^{Bipy\text{-}10})]$, from 6,6'-diformyl-2,2'-bipyridine (0.0907g, 0.427mmol), 3,4,5-trihexadecyloxyaniline (0.0698g, 0.857mmol) and $ZnCl_2$ (0.0588g, 0.432mmol). Appearance: yellow solid (0.588g, 70.9%). Microanalysis: Calculated for $C_{120}H_{210}Cl_2N_4O_6Zn_1.H_2O$ C 73.56, H 10.91, N 2.86; found C 73.41, H 10.45, N 2.57. IR (KBr pellet): υ = 2920vs (C-H), 2850vs (C-H), 1621w (C=N), 1587s (C=N), 1501m (C=C), 1468s (C=C), 1436m (C=C), 1117vs (C-O) cm^{-1}. ^{1}H-NMR (300.13MHz, $CDCl_3$, 298K): δ_H 9.34 (2H, s, $\underline{H}_aC$=N), 8.24 (2H, d, $^3J_{AB}$ = 7.44Hz, $\underline{H}_d$), 8.19 (2H, d, $^3J_{AB}$ = 7.21Hz, $\underline{H}_b$), 8.09 (2H, t, $^3J_{AB}$ = 7.34Hz, $\underline{H}_c$), 7.07 (4H, s, $\underline{H}_e$), 3.97 (12H, m, OC$\underline{H}_2$), 1.78-1.25 (168H, m, C$\underline{H}_2$), 0.88 (18H, 2 overlapping triplets, C$\underline{H}_3$) ppm. ^{13}C-NMR (75.48MHz, $CDCl_3$, 298K): δ_C 154.2, 153.1, 151.7, 148.5, 142.6, 140.8, 138.4, 126.3, 122.8, 101.7, 73.5, 69.0, 31.9, 30.4, 29.8, 29.6, 29.4, 26.2, 22.7, 14.1 ppm (seven alkyl carbons obscured). MALDI-TOF MS: m/z = 1909 $[ZnCl(L^{Bipy\text{-}16})]^+$.

3.5 REFERENCES

[1] K. Hanabusa, J. Higashi, T. Koyama and H. Shirai, *Makromol. Chem.*, 1989, **190**, 1.

[2] (a) K. E. Rowe and D. W. Bruce, *Liq. Cryst.*, 1995, **18**, 161; (b) K. E. Rowe and D. W. Bruce, *Liq. Cryst.*, 1996, **20**, 183; (c) K. E. Rowe and D. W. Bruce, *J. Mater. Chem.*, 1998, **8**, 331; (d) K. E. Rowe and D. W. Bruce, *Mol. Cryst. Liq. Cryst.*, 1999, **326**, 15; (e) K. E. Rowe and D. W. Bruce, *J. Chem. Soc., Dalton Trans.*, 1996, 3913; (f) R. W. Date, E. F. Iglesias, K. E. Rowe, J. M. Elliott and D. W. Bruce, *Dalton Trans.*, 2003, 1914.

[3] (a) L. Douce, R. Ziessel, R. Seghrouchni, A. Skoulios, E. Campillos and R. Deschemaux, *Liq. Cryst.*, 1995, **18**, 157; (b) L. Douce, R. Ziessel, R. Seghrouchni, A. Skoulios, E. Campillos and R. Deschemaux, *Liq. Cryst.*, 1996, **20**, 235; (c) A. El-ghayoury, L. Douce, R. Ziessel, R. Seghrouchni and A. Skoulios, *Liq. Cryst.*, 1996, **21**, 143; (d) A. El-ghayoury, L. Douce, A. Skoulios and R. Ziessel, *Angew. Chem. Int. Ed.*, 1998, **37**, 1255; (e) A. El-ghayoury, L. Douce, A. Skoulios and R. Ziessel, *Angew. Chem.*, 1998, **37**, 1303; (f) A. El-ghayoury, L. Douce, A. Skoulios and R. Ziessel, *Angew. Chem. Int. Ed.*, 1998, **37**, 2205; (g) L. Douce, R. Ziessel, H.-H. Lai and H.-C. Lin, *Liq. Cryst.*, 1999, **26**, 1797; (h) A. El-ghayoury, L. Douce, R. Ziessel and A. Skoulios, *Liq. Cryst.*, 2000, **27**, 1653; (i) R. Ziessel, *Coord. Chem. Rev.*, 2001, **216-217**, 195.

[4] M. Lee, N.-K. Oh, H.-K. Lin and W.-C. Zin, *Macromolecules*, 1996, **29**, 5567.

[5] (a) Y. G. Galyametdinov, L. V. Malykhina, W. Haase, K. Driesen and K. Binnemans, *Liq. Cryst.*, 2002, **29**, 1581; (b) A. A. Knyazev , V. S. Lobkov and Y. G. Galyametinov, *Russ. Chem. Bull., Int. Ed.*, 2004, **53**, 942.

[6] (a) D. Pucci, G. Barberio, A. Crispini, M. Ghedini and O. Francescangeli, *Mol.Cryst. Liq. Cryst.*, 2003, **395**, 325; (b) D. Pucci, G. Barberio, A. Crispini, O. Francescangeli, M. Ghedini and M. La Deda, *Eur. J. Inorg. Chem.*. 2003, 3649; (c) G. Barberio, A. Bellusci, A. Crispini, M. Ghedini, A. Golemme, P. Prus and D. Pucci, *Eur. J. Inorg. Chem.*, 2005, 181.

[7] (a) R. Giménez, A. B. Manrique, S. Uriel, J. Barberá and J. L. Serrano, *Chem. Commun.*, 2004, 2064; (b) C. K. Lee, M. J. Ling and I. J. B. Lin, *Dalton Trans.*, 2003, **24**, 4731.

[8] (a) U. S. Schubert, C. Eschbaumer and M. Heller, *Org. Lett.*, 2000, **2**, 21, 3373. (b) T. M. Cassol, F. W. J. Demnitz, M. Navarro and E. A. d. Neves, *Tetrahedron. Lett.*, 2000, **41**, 8203. (c) G. R. Newkome and H.-W. Lee, *J. Am. Chem. Soc*, 1983, **105**, 5956.

[9] C. Janiak, *J. Chem. Soc., Dalton Trans.*, 2000, 3885.

CHAPTER 4:

METALLOMESOGENS DERIVED FROM 5,5'-DIMETHYLDIPYRROMETHANE

4.1 INTRODUCTION TO PYRROLE LIQUID CRYSTALS

4.1.1 Pyrrole-Derived Liquid Crystals

Thermotropic liquid crystalline compounds containing pyrrole moieties can be broadly categorised into two groups. The first are the discotic macrocyclic-derived compounds with phthalocyanine or porphyrin rings,[2-13] and the second are the calamitic monomeric N-substituted pyrroles that are subsequently polymerised to form polypyrrole backbones.[14-16] There are naturally a few exceptions that fall outside of these two categories, such as derivatives of diketopyrrolopyrrole (*DPPD*)[17,18] as well as 2- substituted monomeric pyrroles[19,20] and these compounds will also form part of the discussion. To the best of our knowledge there are no bent-core mesomorphic compounds derived from derivatives of dipyrromethane in the literature.

The discotic shapes of phthalocyanine and porphyrin macrocycles are ideal cores for the generation of columnar mesophases, and the magnetic conductivity properties of some of the complexes make them suitable for use as one-dimensional conductors. Consequently, their mesomorphic properties have been extensively studied. Given the breadth of investigation into these types of mesomorphic macrocycles and the excellent review covering this topic,[1] a few key examples have been chosen to illustrate the properties of these macrocycles.

Phthalocyanine compounds were the first inherently disk-like metallomesogens to show columnar mesophases.[2] The first reported liquid-crystalline phthalocyanine metallomesogen was published in 1982 by Simon *et al.* (Figure 4.1).[2] The copper(II) complex of L^{22} was substituted with eight peripheral dodecyloxymethyl chains, and one columnar hexagonal phase was

generated between 53°C to 300°C, at which temperature it started to decompose without clearing into the isotropic liquid. The metal-free ligand generated a columnar hexagonal mesophase over a narrower temperature range, whereby the compound melted at the higher temperature of 79°C and cleared at the lower temperature of 260°C, relative to the copper(II) complex.[3]

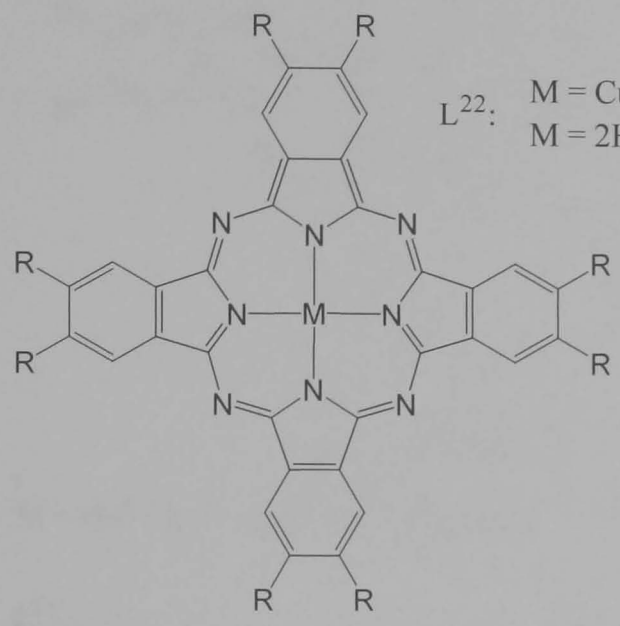

L^{22}: $M = Cu^{2+}$, $R = OCH_2OC_{12}H_{25}$: Cr 53 Col_h >300 I
$M = 2H$, $R = OCH_2OC_{12}H_{25}$: Cr 79 Col_h ~260 I

Figure 4.1. Phthalocyanine compounds forming columnar hexagonal mesophases.[2,3] Transition temperatures are given in °C.

Subsequent variation of the metal(II) centre and peripheral chain length, including M = zinc(II), manganese(II), lead(II), nickel(II), tin(II), cobalt(II), and R = $CH_2OC_nH_{2n+1}$,[4] persistently resulted in columnar hexagonal mesophases with high thermal stability.

Expanded phthalocyanine complexes with polycatenar pendent arms have also been developed (Figure 4.2). The effect of incorporating bulky side arms with two alkoxy chains per phenyl ring[5] (Figure 4.2, L^{23}) was to generate rich mesomorphism. The copper(II) complexes with chain lengths of n = 9, 10, 11, 12, 13 and 14 carbon atoms generated a low temperature columnar hexagonal phase. This was accompanied by either three columnar rectangular phases (n = 9, 10), or two (n = 11, 12) or one (n = 13, 14) columnar rectangular phases plus one columnar tetragonal and one cubic phase at higher

temperatures. The mesomorphic temperature range existed over 100°C, with clearing temperatures around 200°C.

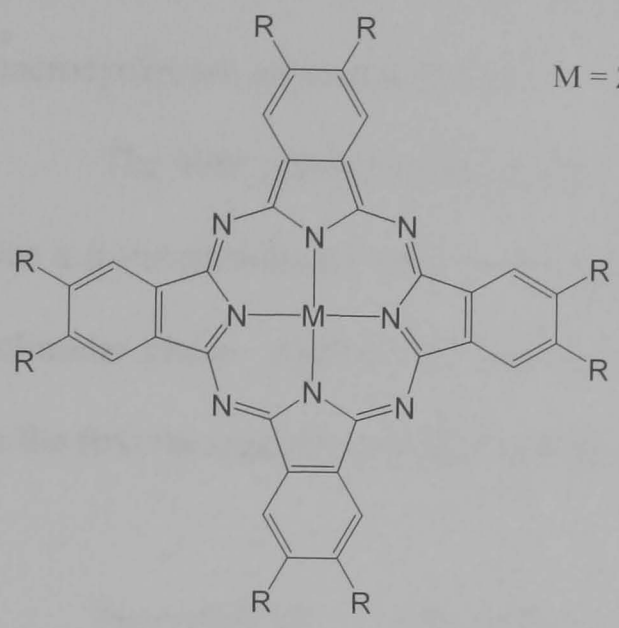

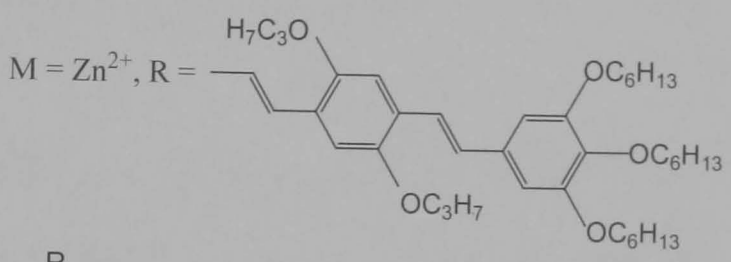

L^{24}: Cr 16 Col_h 220 I

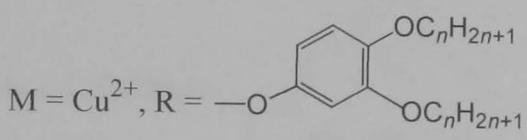

n = 9, 10, 11, 12, 13, 14

L^{23}:
n = 9: Col_h 94 Col_{r1} 128 Col_{r2} 151 Col_{r3} 217 I
n = 10: Col_h 104 Col_{r1} 131 Col_{r2} 142 Col_{r3} 202 I
n = 11: Col_h 106 Col_{r1} 136 Col_{r2} 176 Col_{tet} 190 Cub 202 I
n = 12: Col_h 106 Col_{r1} 132 Col_{r2} 149 Col_{tet} 188 Cub 195 I
n = 13: Col_h 105 Col_{r1} 126 Col_{tet} 174 Cub 184 I
n = 14: Col_h 111 Col_{r1} 126 Col_{tet} 176 Cub 181 I

Figure 4.2. Expanded phthalocyanine complexes with polycatenar chains.[5,6] Transition temperatures are given in °C.

The further extended phthalocyanine L^{24} (Figure 4.2) with additional aliphatic chains generated a room temperature columnar hexagonal phase that was stable up to 220°C.[6]

Porphyrin macrocycles have a smaller ring size than phthalocyanine rings. Consequently, their mesomorphic properties have been investigated to determine whether the predicted decrease in mesophase viscosity relative to the phthalocyanine compounds would result in enhancement of the orientational and alignment properties.

Porphyrin liquid crystals can be categorised into two groups depending on the position of the substituents around the macrocyclic core. Either functionalisation occurs at the β-positions of the pyrrole rings, or the macrocycles are *meso*-substituted.

The first mesomorphic porphyrin reported in 1980 by Goodby *et al.*[7] was a β-octasubstituted ester of uroporphyrin and this generated a monotropic columnar phase. Further investigation into this class of liquid crystal resulted in the first mesogenic metalloporphyrin in 1987 (Figure 4.3, L^{25}).[8]

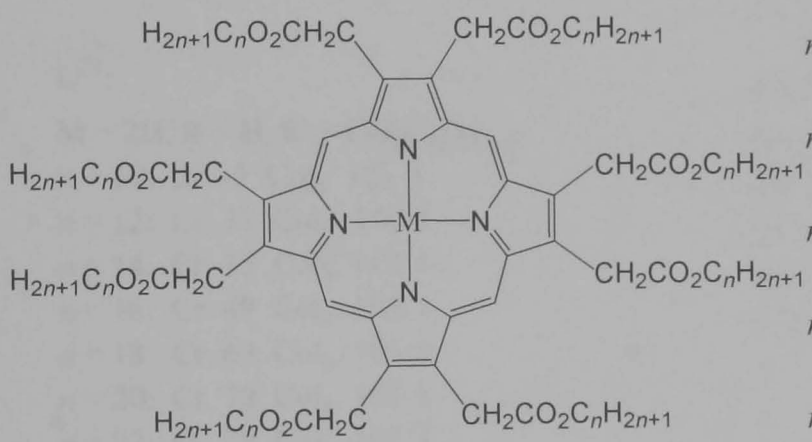

L^{25}

$n = 6$, M = 2H: Cr 122 Col_r 177 I
$n = 6$, M = Zn^{2+}: Cr 124 Col_r 218 I
$n = 8$, M = 2H: Cr 104 Col_r 160 I
$n = 8$, M = Zn^{2+}: Cr 105 Col_r 201 I
$n = 10$, M = 2H: Cr 90 Col_r 149 I
$n = 10$, M = Zn^{2+}: Cr 91 Col_r 183 I
$n = 11$, M = 2H: Cr 83 Col_r 149 I
$n = 11$, M = Zn^{2+}: Cr 79 Col_r 167 I
$n = 12$, M = 2H: Cr 90 Col_r 151 I
$n = 12$, M = Zn^{2+}: Cr 91 Col_r 182 I
$n = 14$, M = 2H: Cr 93 Col_r 131 I
$n = 14$, M = Zn^{2+}: Cr 87 Col_r 167 I

Figure 4.3. β-Octasubstituted metallopophyrins.[8,9] Transition temperatures are given in °C.

Initial[8] and subsequent[9] synthesis and study of the zinc(II) and the metal-free base compounds with n = 6, 8, 10, 11, 12, 14, revealed that the compounds form one columnar rectangular mesophase. Both zinc(II) complexes and the corresponding metal-free base compounds had near-identical melting temperatures, which decreased with increasing aliphatic chain length. The clearing temperatures on complexation to zinc(II) were significantly higher than the metal-free analogues, leading to a stabilisation of the liquid crystalline phase. However, the clearing temperatures of both sets of compounds decreased on increasing chain length. Variation of the metal centre

with M = platinum(II), palladium(II), cadmium(II), zinc(II), copper(II) and nickel(II) and n = 10, resulted in similar transition temperatures for all complexes and an identical columnar rectangular mesophase.[9]

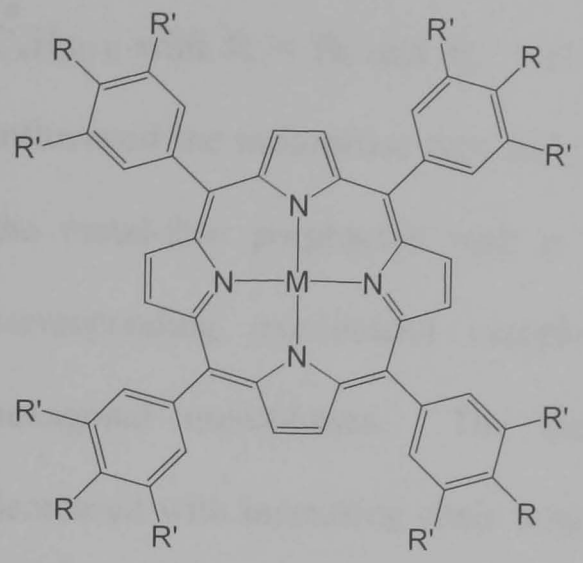

L^{27}:

M = 2H, R = H, R' = $CO_2C_nH_{2n+1}$:
n = 10: Cr -3 Col_h 121 I
n = 12: Cr 17 Col_h 114 I
n = 14: Cr 36 Col_h 113 I
n = 16: Cr 49 Col_h 103 I
n = 18: Cr 63 Col_h 106 I
n = 20: Cr 70 Col_h 103 I
n = 22: Cr 78 Col_h 101 I

M = VO, R = H, R' = $CO_2C_nH_{2n+1}$:
n = 12: Cr 13 Col_h 233 I

L^{26}:

M = 2H, R' = H, R = C_nH_{2n+1}:
n = 6: Cr 190 D_L 263 I
n = 7: Cr 145 D_L 237 I
n = 8: Cr 126 D_L 209 I
n = 9: Cr 107 D_L 187 I
n = 10: Cr 52 D_L 173 I
n = 11: Cr 23 D_{L1} 55 D_{L2} 162 I
n = 12: Cr 31 D_{L1} 52 D_{L2} 155 I
n = 13: Cr 37 D_{L1} 60 D_{L2} 148 I
n = 14: Cr 52 D_{L1} 57 D_{L2} 141 I
n = 15: Cr 56 D_{L1} 66 D_{L2} 135 I
n = 16: Cr 65 D_{L1} 71 D_{L2} 129 I

R = $C_{12}H_{25}$, R' = H:
M = Co^{2+}: Cr 28 D_{L1} 50 D_{L2} 161 I
M = Ni^{2+}: Cr 44 D_L 129 I
M = Cu^{2+}: Cr 32 D_{L1} 56 D_{L2} 188 I
M = Zn^{2+}: Cr 37 D_{L1} 52 D_{L2} 220 I
M = Pd^{2+}: Cr 30 D_{L1} 60 D_{L2} 186 I

Figure 4.4. *Meso*-substituted metalloporphyrins.[10,11,12] Transition temperatures are given in °C.

Meso-substituted porphyrins were found to have mesomorphic properties that were dependent on the nature of the side chains (Figure 4.4). Alkoxyphenyl chains with n = 5-14, 18 and M = 2H[10] or n = 10 and M = Zn^{2+},[11] were not sufficient to induce mesophases. However, the analogous metal-free tetrakis(alkylphenyl)porphyrins[10(b)] generated a lamellar-type arrangement of disks, D_L, from n = 6 – 16 (Figure 4.4, L^{26}). Each compound exhibited either one ($6 \leq n \leq 10$) or two ($n \geq 11$) discotic lamellar mesophases. Divalent metal complexes of M = cobalt(II), nickel(II), copper(II), zinc(II) and

palladium(II) with $n = 12$[10(b)] also exhibited discotic lamellar phases (Figure 4.4, L^{26}).

Doubling the side-chain density of the porphyrins by replacing R = C_nH_{2n+1} with R = H, and R' = H with R' = $CO_2C_nH_{2n+1}$ (Figure 4.4, L^{27}) influenced the mesophase type and stability. Patel and Suslick[12] reported that the metal-free porphyrins with n = 10, 12, 14, 16, 18, 20, 22, and the corresponding oxovanadyl complex with n = 12, generated columnar hexagonal mesophases. The mesophase stability of these compounds decreased with increasing chain length, but was increased by the incorporation of the oxovanadyl ion.

The molecular shape of porphyrin mesogens has been extended to include rod-like moieties (Figure 4.5, L^{28}).[13]

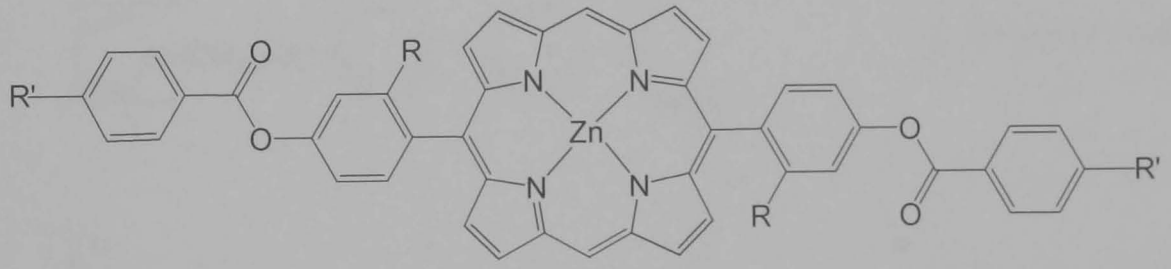

L^{28}

R = H, R' = OC_7H_{15}: Cr 309 N 433 I
R = OC_8H_{17}, R' = OC_7H_{15}: Cr 141 N 189 I

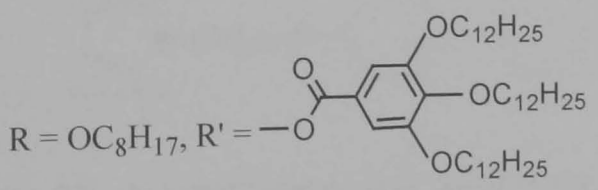

: Cr 50 N 153 I

Figure 4.5. Elongated 5,15-disubstituted metalloporphyrins.[13] Transition temperatures are given in °C.

Bruce and Wang substituted the porphyrin ring at the 5- and 15- positions, producing a dramatic effect on the mesomorphic behaviour of the compounds. Instead of generating columnar mesophases the elongation of the porphyrin fragment was significant enough to produce nematic phases. The incorporation

of the chains at R was also found to be important with regard to destabilising the columnar aggregation of the porphyrin cores.

Along with macrocyclic pyrrole-derived mesogens the other most commonly studied pyrrolic liquid crystals are the N-substituted pyrroles.

L^{29}:

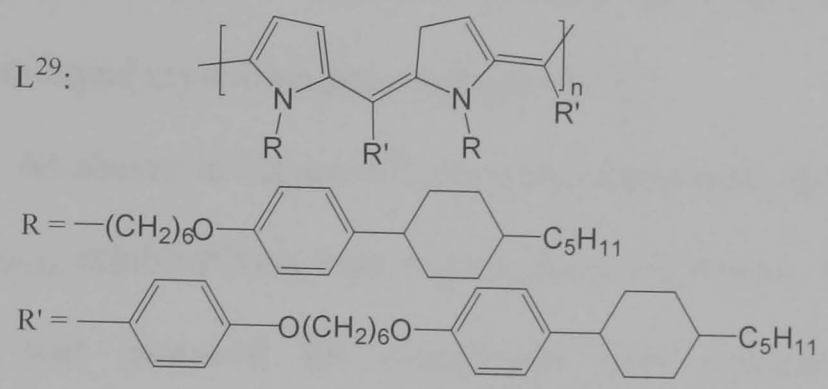

g 57 SmA 128 I

L^{30}:

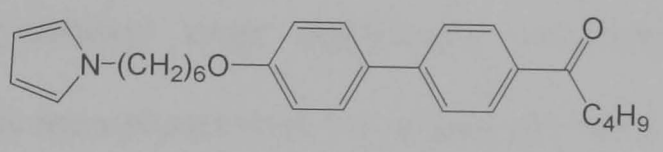

Cr 84 SmX 85 SmA 94 I

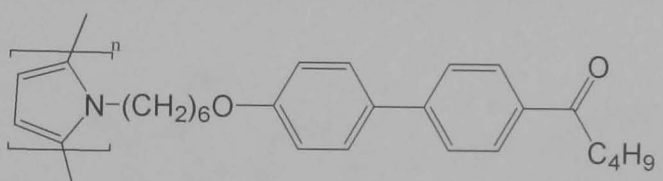

g 190 (SmX 168) I

L^{31}:

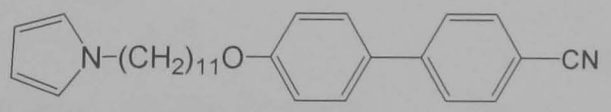

Cr 86 (N 56) I

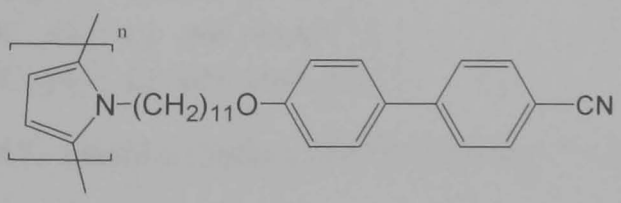

g 92 SmA 154 I

Figure 4.6. N-Substituted pyrrole moieties for liquid crystalline polymers, L^{29},[14] L^{30},[15] L^{31}.[16] Transition temperatures are given in °C.

N-Substituted pyrroles are employed in the synthesis of liquid crystalline polymers as the backbone of the polymer with N-substituted mesogenic side groups. N-Substituted pyrroles are used to ensure regioregularity of the polymer. A few recent examples of monomers and polymers are given in Figure 4.6 to demonstrate the liquid crystalline behaviour of the polymers. As

expected of these rod-like compounds, nematic and smectic mesophases dominate.

Diketopyrrolopyrrole (*DPPD*) derivatives are stable fluorescent molecules that have found application as photostable and weatherproof pigments and dyes.[17] However, suitably functionalised DPPD molecules generate liquid crystalline phases (Figure 4.7).[18]

As shown in Figure 4.7, the compounds with alkoxy substituents, R = OC_nH_{2n+1}, exhibited very narrow mesophase temperature ranges. As the chain length was increased the mesophases were increasingly stabilised and smectic A phases were dominant over the nematic phase. Additional phenyl and cyclohexyl rings significantly stabilised the generated mesophases. Nematic mesophases were formed around 200°C and persisted at over 300°C.

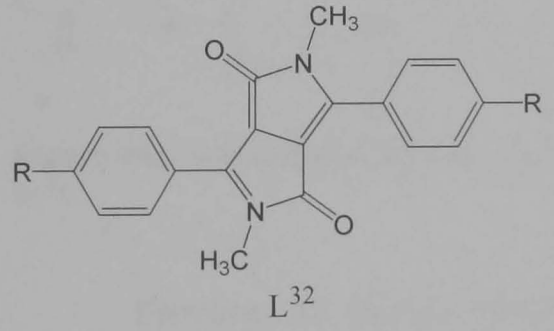

L^{32}

$R = OC_8H_{17}$: Cr 106 N 114 I
$R = OC_{10}H_{21}$: Cr 106 SmA 119 I
$R = OC_{12}H_{25}$: Cr 109 SmA 123 I

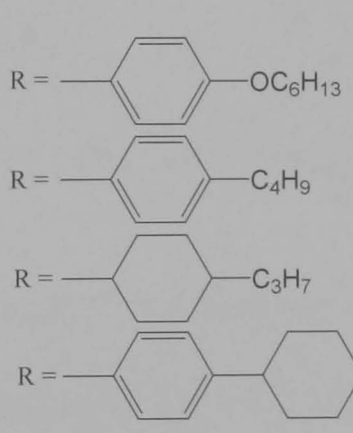

Figure 4.7. Liquid crystalline DPPD derivatives.[18] Transition temperatures are given in °C.

2-Substituted pyrrole derivatives have been synthesised as suitable ligands for metallomesogens (Figures 4.8 and 4.9).[19,20] These ligands are particularly suitable for coordination to transition metal ions due to their N,N donor set.

Bruce *et al.*[19] synthesised rod-like ligands that ended in either alkoxybenzoate esters (L^{33}) or alkylcyclohexanoate esters (L^{34}). All

compounds generated a single nematic mesophase. The melting temperatures of the alkoxybenzoate ester compounds decreased on increasing aliphatic chain length, with the exception of the $n = 10$ molecule. The clearing temperatures of the compounds decreased with increasing chain length in accordance with the odd-even effect. The alkylcyclohexanoate ester compounds also exhibited nematic mesophases, even at short chain lengths ($n = 3$). Comparing L^{33} with $n = 6$ and L^{34} with $n = 7$, it is apparent that the latter has a slightly greater stabilising effect on the nematic phase than the former. There are currently no published results on the complexation of these ligands to metal cations.

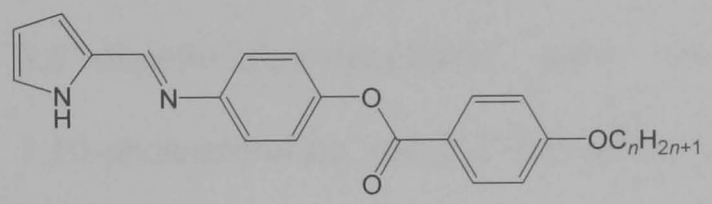

$n = 6$: Cr 123 N 150 I
$n = 7$: Cr 110 N 133 I
$n = 8$: Cr 103 N 140 I
$n = 9$: Cr 92 N 128 I
$n = 10$: Cr 96 N 138 I

L^{33}

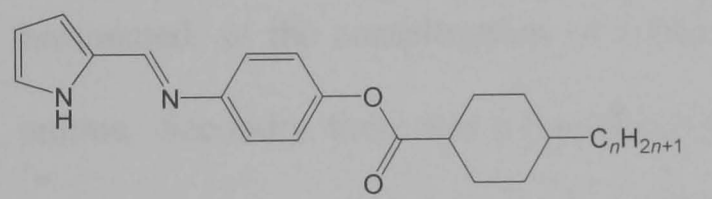

$n = 3$: Cr 132 N 157 I
$n = 5$: Cr 113 N 163 I
$n = 7$: Cr 118 N 155 I

L^{34}

Figure 4.8. 2-Substituted pyrroles studied by Bruce *et al.*[19] Transition temperatures are given in °C.

Previous to Bruce, Pyżuk *et al.*[20] synthesised the first non-discotic metallomesogens to possess four chelating N atoms (Figure 4.9).

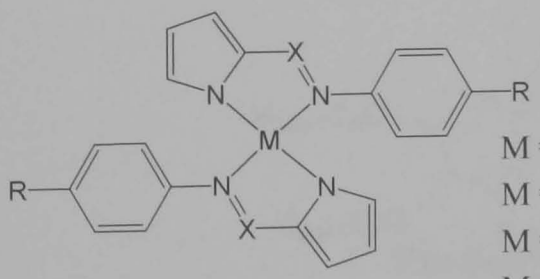

L^{35}

M = 2H, X = N, R = N=N-C_6H_4-OC_6H_{13}: Cr 126 N 185 I
M = Ni^{2+}, X = N, R = N=N-C_6H_4-OC_6H_{13}: Cr 208 N 222 I
M = 2H, X = N, R = C_6H_{10}-C_6H_{13}: Cr 128 (N 109) I
M = Ni^{2+}, X = N, R = C_6H_{10}-C_6H_{13}: Cr 174 N 201 I
M = 2H, X = CH, R = C_6H_{10}-C_6H_{13}: Cr 93 N 128 I
M = Ni^{2+}, X = CH, R = C_6H_{10}-C_6H_{13}: Cr 222 (N 205) I
M = Cu^{2+}, X = CH, R = C_6H_{10}-C_6H_{13}: Cr 130 N 168 I

Figure 4.9. 2-Substituted pyrroles studied by Pyżuk *et al.*[20] Transition temperatures are given in °C.

Metal-free rod-like compounds and complexes of nickel(II) and copper(II) with disk-like cores were studied, and all compounds generated

nematic mesophases. Complexation to nickel(II) resulted in higher transition temperatures, possibly as a result of increased π-π interactions between the planar cores. The low transition temperatures of the copper(II) complex relative to the nickel(II) complexes could be as a result of imperfect planarity of the chelate core.

4.1.2 The Design of the 5,5'-Dimethyldipyrromethane-Derived Metallomesogens

The core of our molecule was modified one final time to that of a 5,5'-dimethyldipyrromethane fragment (Figure 4.10). This 2,2'-disubstituted-5,5'-dimethyldipyrromethane core was markedly different to the 1,10-phenanthroline and 2,2'-bipyridine cores. Firstly, the core was doubly protonated, so the complexation of metal(II) cations required no coordinating anions. Secondly, there was a loss of conjugation at the quaternary carbon, and thirdly the planarity at the core was lost by the presence of methyl groups at the quaternary carbon.

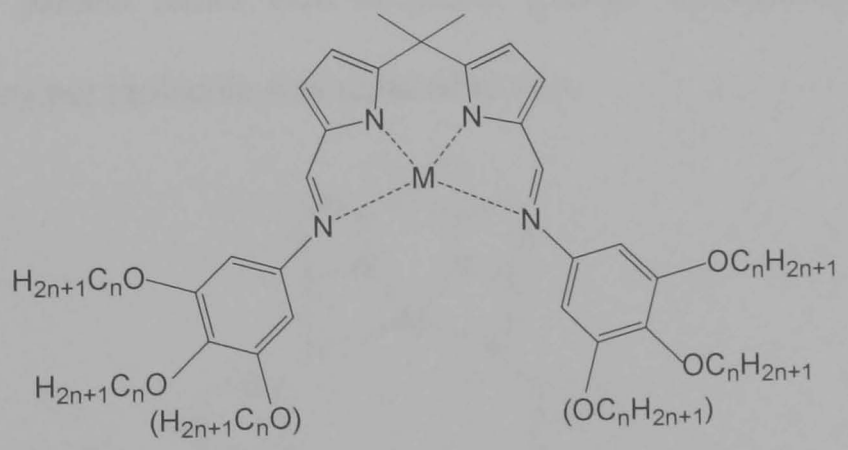

Figure 4.10. The dipyrrole complexes, (tc)-$[M(L^{Dipy\text{-}n})]_x$, where M = Zn^{2+}, Pd^{2+} and x = 1, 2; n = 1, 10, 12, 14, 16 for $[M(L^{Dipy\text{-}n})]_x$ and n = 1, 16 for tc-$[M(L^{Dipy\text{-}n})]_x$.

The 1,10-phenanthroline- and 2,2'-bipyridine-derived complexes allowed us to observe the mesomorphic behaviour related to (amongst other things) the length of the peripheral alkyl chains. One feature of the dipyrrole

compounds is that both hexacatenar ($[M(L^{Dipy\text{-}n})]_x$) and tetracatenar ($tc\text{-}[M(L^{Dipy\text{-}n})]_x$) metal-free ligands and complexes were synthesised for direct comparison of the mesomorphic properties with aliphatic chain density. The removal of two chains eradicated one third of the molecule's fluid character. Hence, not only did we expect a rise in transition temperatures, but we also anticipated a possible change in mesophase type since the formation of columnar mesophases is dependent on the ratio of the percentage core area to the percentage of chain area.[21]

One further modification made to the dipyrrole-derived molecule was the introduction of longer arms in the guise of additional phenyl rings with ester linkers (Figure 4.11). The intention behind this was to elongate the molecule in order to generate banana liquid crystal phases. As mentioned in Chapter 1, banana molecules generally require between five and seven aromatic rings.[22] Therefore with the introduction of a further two rings into the system, $ex\text{-}H_2L^{Dipy\text{-}n}$ contained six aromatic rings. To help promote the formation of banana rather than columnar phases, the number of terminal aliphatic chains per molecule was reduced to two.

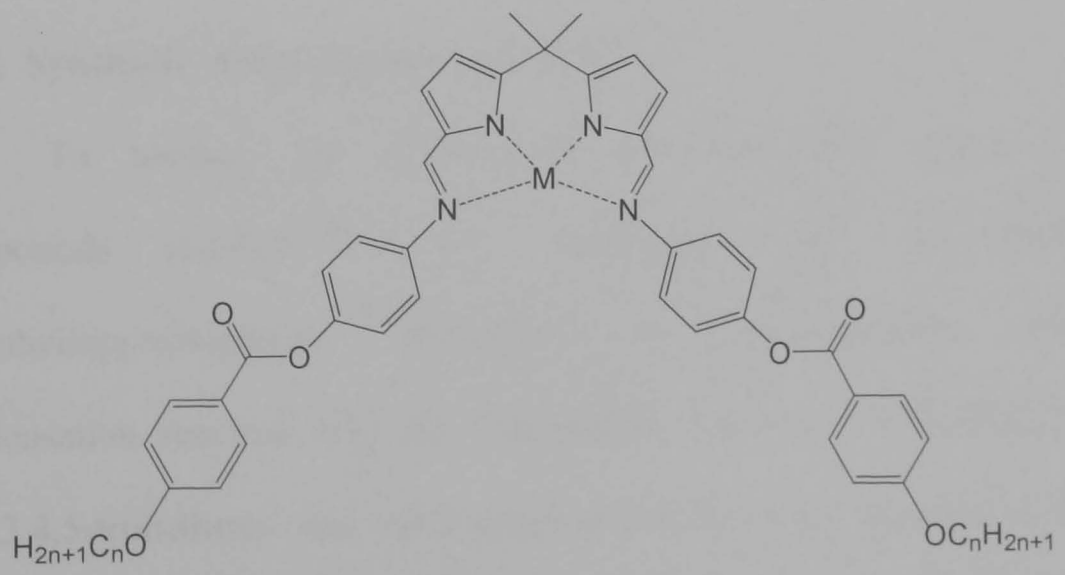

Figure 4.11. Extended dipyrrole complexes, ex-$[M(L^{Dipy\text{-}n})]_x$, where M = Zn^{2+}, Pd^{2+}, x = 1, 2, and n = 1, 16.

We herein report on the synthesis and mesogenic properties of the first reported liquid crystalline bent-core compounds derived from dimethyldipyrromethane, $[M(L^{Dipy\text{-}n})]_x$, tc-$[M(L^{Dipy\text{-}n})]_x$ and ex-$[M(L^{Dipy\text{-}n})]_x$.

4.2 RESULTS AND DISCUSSION

4.2.1 Synthesis of 2,2'-Diformyl-5,5'-dimethyldipyrromethane

The total ligand synthesis is shown below in Scheme 4.1. The 5,5'-dimethyldipyrromethane core of the ligand was prepared by previously published methods.[23] The acid-catalysed condensation reaction between a large excess of pyrrole and acetone reacted in 5 mins, and was followed by neutralisation on the addition of a weak base. Purification was afforded by Kugelrohr distillation to give colourless crystals of 5,5'-dimethyldipyrromethane in moderate yield. 5,5'-Dimethyldipyrromethane was reacted further in a Vilsmeier-Haack reaction with $POCl_3$ and DMF to produce the dialdehyde 2,2'-diformyl-5,5'-dimethyldipyrromethane in high yield (72%).

4.2.2 Synthesis of the Ligands, (tc)-$H_2L^{Dipy\text{-}n}$

To produce the hexacatenar and tetracatenar dipyrrole-derived compounds (tc)-$H_2L^{Dipy\text{-}n}$, the dialdehyde core, 2,2'-diformyl-5,5'-dimethyldipyrromethane, underwent an acid-catalysed Schiff-base condensation reaction with the appropriate 3,4-di-or 3,4,5-trialkoxyaniline. The 3,4,5-trimethoxy- and trihexadecyloxyanilines were prepared as described in Chapter 2, whereas the analogous 3,4-dialkoxyanilines were prepared in an identical manner but starting from 1,2-dihydroxybenzene. The resulting

yellow ligands of (tc)-$H_2L^{Dipy\text{-}n}$ were recrystallised in high yield from solvent layering of EtOH onto a solution of the product in $CHCl_3$. Despite repeated attempts no suitable quality single crystals of the free ligands were prepared.

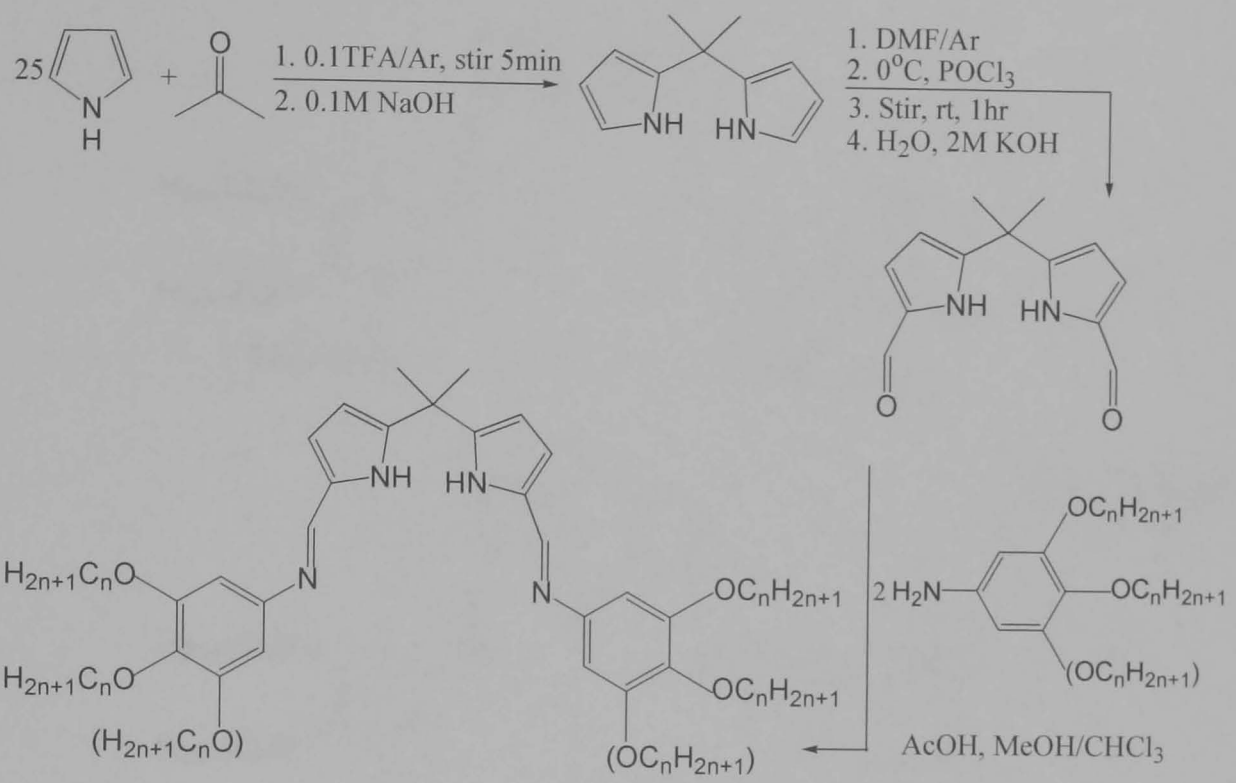

Scheme 4.1. Synthetic scheme for the synthesis of (tc)-$H_2L^{Dipy\text{-}n}$, where n = 1, 10,12,14, 16 for $H_2L^{Dipy\text{-}n}$ and n = 1, 16 for tc-$H_2L^{Dipy\text{-}n}$.[23]

4.2.3 Synthesis of the Complexes, (tc)-$[M(L^{Dipy\text{-}n})]_x$

The complexes (tc)-$[Pd(L^{Dipy\text{-}n})]$ were synthesised by deprotonation of (tc)-$H_2L^{Dipy\text{-}n}$ with NEt_3 and reaction with $Pd(OAc)_2$ in a solution of CH_2Cl_2. The complexes (tc)-$[Zn(L^{Dipy\text{-}n})]_2$ were prepared by dissolving $Zn(OAc)_2.2H_2O$ in MeOH and adding the methanolic solution to a solution of (tc)-$[L^{Dipy\text{-}n}]^{2-}$ in CH_2Cl_2. Overnight stirring at room temperature of the compounds produced (tc)-$[Pd(L^{Dipy\text{-}n})]$ and (tc)-$[Zn(L^{Dipy\text{-}n})]_2$, as outlined in Scheme 4.2. The complexes $[Pd(L^{Dipy\text{-}n})]$ and $[Zn(L^{Dipy\text{-}n})]_2$ where n = 1, 10, 12, 14, 16, and tc-$[Pd(L^{Dipy\text{-}n})]$ and tc-$[Zn(L^{Dipy\text{-}n})]_2$ where n = 1 and 16, were recrystallised from solvent diffusion of either Et_2O or EtOH into $CHCl_3$, affording the products in yields of 50-99%. Single crystals of $[Zn(L^{Dipy\text{-}1})]_2$ were grown by

vapour diffusion of Et_2O into a $CHCl_3$ solution of $[Zn(L^{Dipy\text{-}1})]_2$. No suitable single crystals of $[Pd(L^{Dipy\text{-}1})]$, tc-$[Zn(L^{Dipy\text{-}1})]_2$ or tc-$[Pd(L^{Dipy\text{-}1})]$ could be grown.

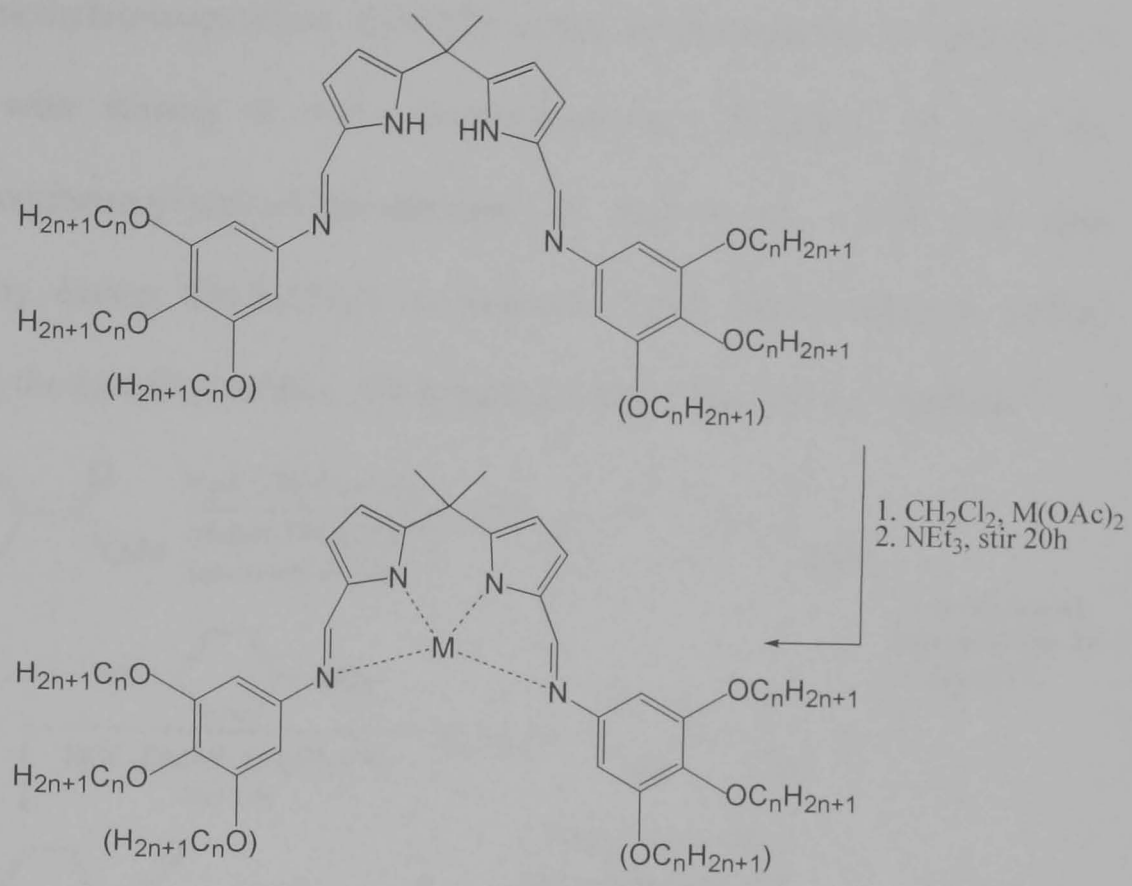

Scheme 4.2. Synthesis of the complexes (tc)-$[M(L^{Dipy\text{-}n})]_x$ where M = Pd^{2+}, x = 1 and M = Zn^{2+}, x = 2; n = 1, 10, 12, 14, 16 for $[M(L^{Dipy\text{-}n})]_x$ and n = 1, 16 for tc-$[M(L^{Dipy\text{-}n})]_x$.

4.2.4 Synthesis of the Extended Dipyrrole Ligands, ex-$H_2L^{Dipy\text{-}n}$

The synthetic route to the extended aniline ((4-hexadecyloxy)benzoyl)oxy)-4-aniline is outlined in Scheme 4.3. The hexadecyloxy- product was synthesised from commercially available methyl 4-hydroxybenzoate, whereas the methoxy- product was synthesised from commercially available *p*-anisic acid. Hence, Scheme 4.3 shows the preparation of the hexadecyloxy- product, and the route to the methoxy- product is applicable from step three of the Scheme.

A modified literature procedure[24] used in the preparation of the 3,4,5-trialkoxyanilines was used to alkylate methyl 4-hydroxybenzoate.

Saponification[25] with KOH in EtOH and heating to reflux gave 4-hexadecyloxybenzoic acid in high yield (98%). Following this, the benzoic acid was reacted with 4-nitrophenol, N,N'-dicyclohexylcarbodiimide (DCC) and 4-dimethylaminopyridine (DMAP) under an atmosphere of nitrogen in CH_2Cl_2, with stirring at room temperature for 19 hours[26] to give the (4-(methoxy)benzoyl)oxy)-4-nitrobenzene in high yield. This was then reduced by excess $SnCl_2.2H_2O$ in absolute EtOH with heating to reflux, producing the extended aniline, ((4-hexadecyloxy)benzoyl)oxy)-4-aniline.[25]

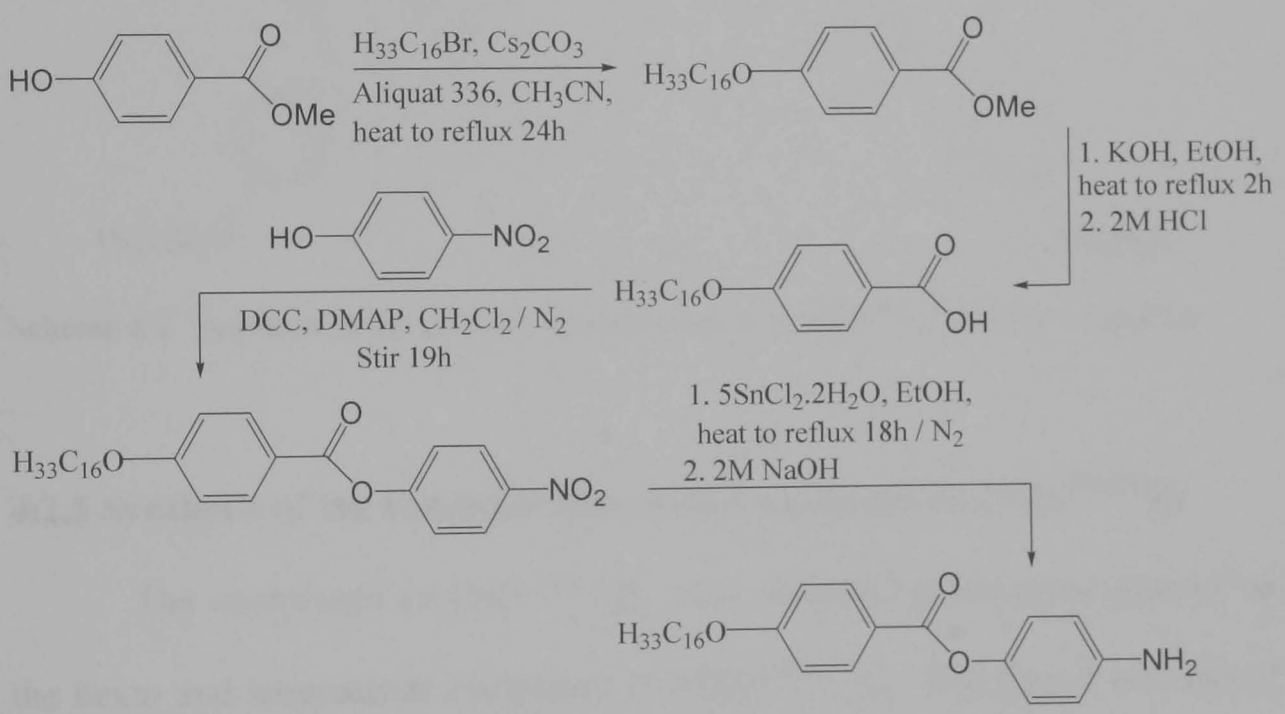

Scheme 4.3. Synthesis of extended aniline ((4-hexadecyloxy)benzoyl)oxy)-4-aniline.[24,25,26]

The extended ligands ex-$H_2(L^{Dipy\text{-}1})$ and ex-$H_2(L^{Dipy\text{-}16})$ were prepared by acid-catalysed Schiff-base condensation reactions of 2,2'-diformyl-5,5'-dimethyldipyrromethane with two equivalents of extended aniline in EtOH and THF, with stirring at room temperature for 4 hours. Purification was afforded by solvent diffusion of MeOH into a solution of the product in $CHCl_3$. The yellow products were produced in yields of 73 and 79%, respectively (Scheme 4.4). In accordance with the contracted metal-free ligand analogues,

(tc)-$H_2L^{Dipy\text{-}1}$, crystals suitable for study by single crystal X-ray diffractometry were not obtained.

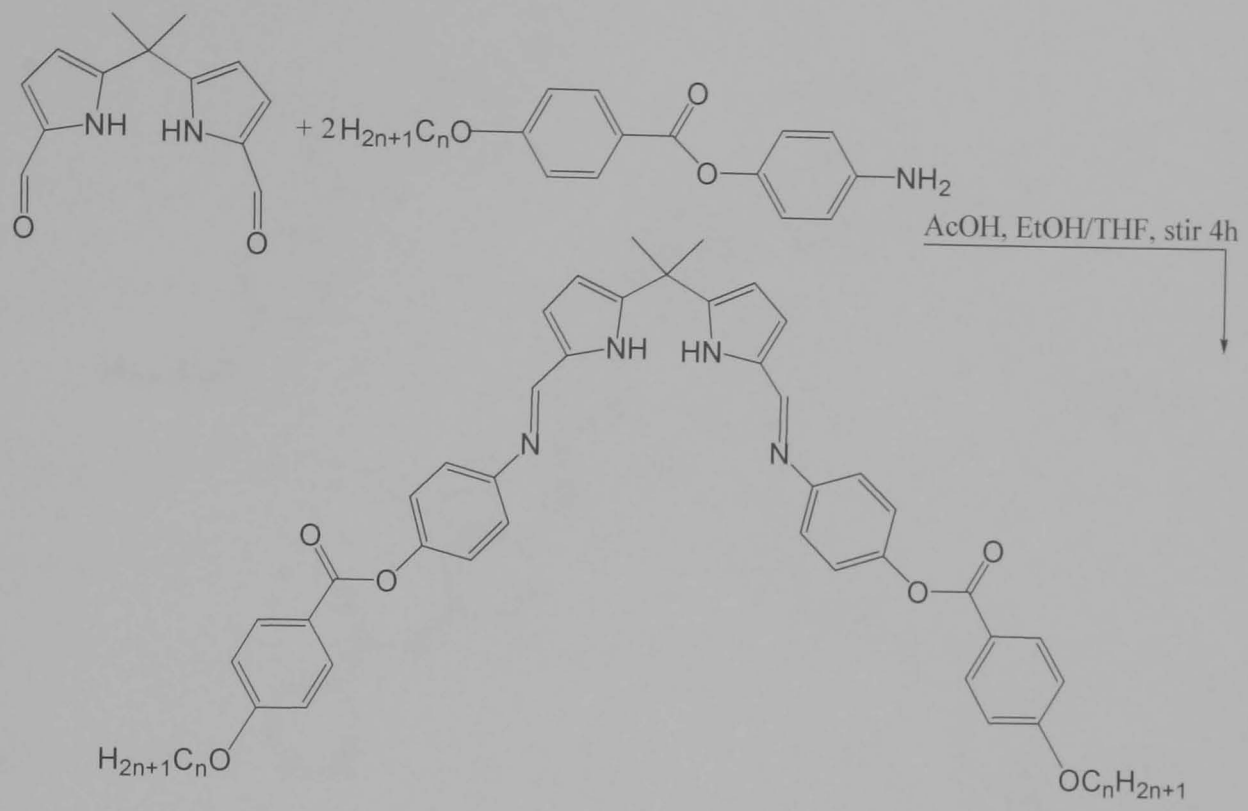

Scheme 4.4. Synthesis of the extended dipyrrole ligand, ex-$H_2L^{Dipy\text{-}n}$, where n = 1 and 16.

4.2.5 Synthesis of the Extended Dipyrrole Complexes, ex-$[M(L^{Dipy\text{-}n})]_x$

The complexes ex-$[M(L^{Dipy\text{-}n})]_x$ were prepared in the same manner as the hexa- and tetracatenar complexes (tc)-$[M(L^{Dipy\text{-}n})]_x$. The ligand was stirred with base in CH_2Cl_2 and this was followed by the addition of either $Pd(OAc)_2$ in CH_2Cl_2, or $Zn(OAc)_2.2H_2O$ in MeOH. The solutions were subsequently stirred for 20 hours (Scheme 4.5). The products were recrystallised by solvent diffusion of alcohol into a solution of the product in $CHCl_3$, and yellow complexes of ex-$[Pd(L^{Dipy\text{-}n})]$ and ex-$[Zn(L^{Dipy\text{-}n})]_2$ were obtained in yields ranging from 52-77%. Single crystals of ex-$[Zn(L^{Dipy\text{-}1})]$ and ex-$[Pd(L^{Dipy\text{-}1})]$ were successfully obtained by solvent diffusion of hexane into a solution of the product in CH_2Cl_2.

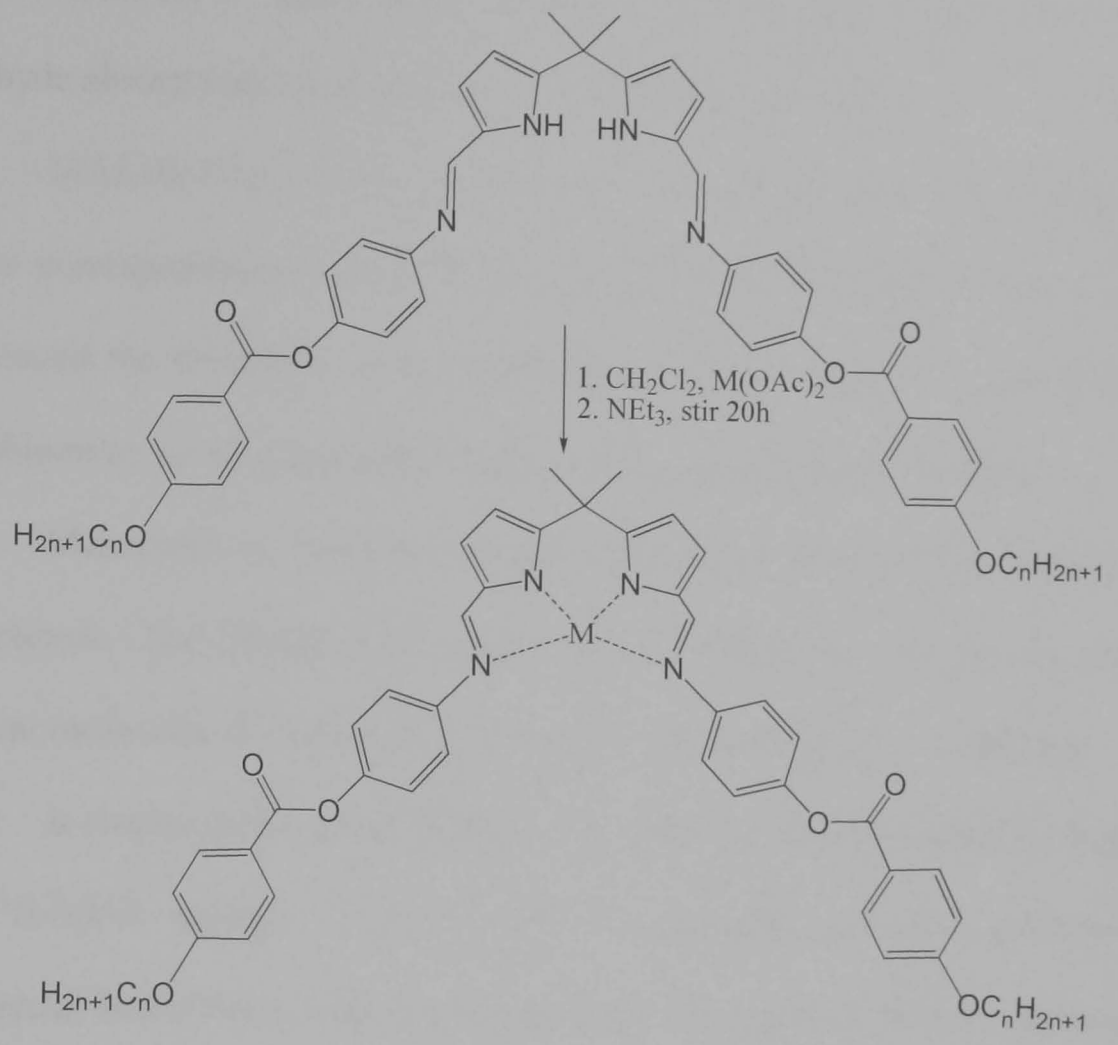

Scheme 4.5. Synthesis of the extended dipyrrole complexes, $[M(L^{Dipy\text{-}n})]_x$, where M = Zn^{2+} and x = 2, and M = Pd^{2+} and x = 1; n = 1 and 16.

4.2.6 Characterisation of the Ligands and Complexes

All compounds were characterised by infrared spectroscopy, mass spectrometry, CHN microanalysis and ^{1}H and ^{13}C NMR spectroscopy.

4.2.6.1 Characterisation of $H_2L^{Dipy\text{-}n}$ and $[M(L^{Dipy\text{-}n})]_x$

The formation of the Schiff-base ligands was evidenced by two imine stretches in the region of 1619 and 1589cm^{-1} in the infrared spectra. Compounds of $[Pd(L^{Dipy\text{-}n})]$ generally showed only one imine stretching vibration at around 1586cm^{-1}, whereas two bands were observed for $[Zn(L^{Dipy\text{-}n})]_2$ at around 1588 and 1557cm^{-1}. All showed strong C-O absorption bands at around 1118cm^{-1}. Alkyl C-H stretches were observed in the region of

2966 – 2827cm^{-1}. Each spectrum was absent of characteristic amine and aldehyde absorptions associated with the starting materials.

MALDI-TOF, FAB and electrospray mass spectrometry displayed peaks corresponding to $[H_2L^{Dipy\text{-}n}]^+$, $[Pd(L^{Dipy\text{-}n})]^+$ and $[Zn(L^{Dipy\text{-}n})]_2^+$, which evidenced the formation of the products and the 1:1 and 2:2 ligand-to-metal stoichiometry of the palladium(II) and zinc(II) complexes, respectively.

Microanalysis revealed the successful formation of the ligands and complexes. The ligands were synthesised in pure form. whereas one or two solvent molecules of H_2O, $CHCl_3$ or CH_2Cl_2 accompanied the complexes.

A singlet peak corresponding to the imine protons at around 8.12ppm in the ^{1}H-NMR spectra of the $H_2L^{Dipy\text{-}n}$ compounds provided evidence of successful Schiff-base condensation reaction. The pyrrolic protons occurred as doublets in the regions of 6.59 and 6.17ppm. Separating these resonances was a singlet peak at 6.37ppm corresponding to the phenyl protons. Completing the spectra were the complicated resonances attributed to the alkyl protons of the peripheral chains from 3.96 – 0.88ppm. Amongst these peaks was the singlet for the pyrrolic methyl protons, which was often obscured, but occasionally visible, at 1.74ppm.

Complexation to palladium(II) was evidenced by shifts in the resonances, relative to the spectra for $H_2L^{Dipy\text{-}n}$. The imine peak was shifted upfield to 7.58ppm, and the occurrence of only one imine peak implied that the complexes were symmetrical species, as predicted. The doublets of the pyrrolic protons experienced significant downfield shifts of 0.3 and 0.13ppm, respectively, whereas the phenyl singlet resonances were shifted upfield by 0.3ppm. Triplets attributed to the protons α to oxygen in the alkoxy chains

were more distinct and separated into central and lateral proton resonances further upfield at 3.83 and 3.63ppm. The remaining aliphatic chain resonances were unaffected, although the methyl protons on the pyrrole core were shifted slightly upfield by 0.6ppm.

Due to the weaker electropositivity of the zinc(II) cation, the metal(II) centre had less of a shielding effect on the protons of the complexes $[Zn(L^{Dipy-n})]_2$ relative to $[Pd(L^{Dipy-n})]$. The ^{1}H-NMR spectra showed the imine proton peak occurring from 8.09 – 8.17ppm. The pyrrole proton resonance doublets occurred at 6.58 and 6.09 or 6.17ppm. The most significant shift relative to the metal-free ligands was for the phenyl protons. In accordance with the complexes $[Pd(L^{Dipy-n})]$ this peak was observed around 0.3ppm further upfield. The protons attributed to the aliphatic chains were in similar positions to the analogous $[Pd(L^{Dipy-n})]$ protons. However, the methyl protons on the pyrrole core occurred at 1.62ppm in the $[Zn(L^{Dipy-1})]$ spectrum, whereas in the longer chain complexes the resonances were obscured by the peaks for the aliphatic chains.

The ^{13}C-NMR spectra for the free ligands and complexes showed nine peaks corresponding to the aromatic and imine carbon resonances, in the regions of 154 - 94ppm for H_2L^{Dipy-n}, 159 – 100ppm for $[Pd(L^{Dipy-n})]$ and 158 – 97ppm for $[Zn(L^{Dipy-n})]_2$. The remaining aliphatic carbon resonances were observed between 74 and 14ppm. However, individual peaks were not always identifiable due to the overlap of some resonances.

4.2.6.2 Characterisation of tc-$H_2L^{Dipy\text{-}n}$ and tc-$[M(L^{Dipy\text{-}n})]_x$

In the infrared spectra the imine stretches for the tetracatenar free ligands were observed at 1620 and 1589cm^{-1}, in common with the hexacatenar analogues. These bands were observed at lower wavenumbers of around 1590 and 1560cm^{-1} for tc-$[Pd(L^{Dipy\text{-}n})]$. For tc-$[Zn(L^{Dipy\text{-}n})]_2$ they were observed at around 1609 and 1580cm^{-1}. A strong C-O absorption band occurred in the region 1134 – 1050cm^{-1} for all compounds. Finally, absence of aldehyde and amine absorption bands evidenced the clean formation of the target compounds.

Electrospray and MALDI-TOF mass spectrometry confirmed the formation of compounds tc-$H_2L^{Dipy\text{-}1}$, tc-$H_2L^{Dipy\text{-}16}$, tc-$[Pd(L^{Dipy\text{-}1})]$, tc-$[Pd(L^{Dipy\text{-}16})]$, tc-$[Zn(L^{Dipy\text{-}1})]_2$ and tc-$[Zn(L^{Dipy\text{-}16})]_2$ with m/z = 501, 1343, 604, 1447, 1128 and 2811, respectively. CHN microanalysis was in agreement with the stoichiometry of the compounds.

Comparative analysis of the ^{1}H-NMR spectra showed that on complexation to palladium(II) the signal corresponding to the imine protons in the free ligands tc-$H_2L^{Dipy\text{-}n}$ was shifted significantly from 8.16ppm to 7.58ppm. The shift on complexation to zinc(II) was a far more subtle upfield shift of 0.06ppm. The singlet imine signal in all spectra revealed the equivalence of the imine protons, which evidenced the formation of symmetrical compounds. The phenyl protons in tc-$H_2L^{Dipy\text{-}n}$ appeared around 6.84 and 6.76ppm as a doublet and a multiplet, respectively. Protons from the pyrrole core were observed as doublets at 6.57 and 6.15ppm. Significant changes were observed on complexation to palladium(II). The three signals from the phenyl protons of tc-$[Pd(L^{Dipy\text{-}n})]$ were separated into a doublet, a

double doublet and a multiplet much further upfield at *ca.* 6.46, 6.36 and 6.31ppm, respectively. The signals arising from the pyrrole protons were shifted to 6.90 and 6.31ppm, the second signal overlapping with one of the peaks for the phenyl protons. The shifts on complexation to zinc(II) were not as considerable as the shifts resulting from palladium(II) complexation. The phenyl proton peaks for tc-$[Zn(L^{Dipy\text{-}n})]_2$ were found *ca.* 6.67 and 6.59ppm as a doublet and a multiplet (for two protons), followed further upfield by the pyrrole proton doublets at 6.23 and 6.13ppm. All signals corresponding to the protons α to the alkoxy oxygen occurred in the region of 3.42 – 3.99ppm, although the signals occurred as well-defined triplets for tc-$[M(L^{Dipy\text{-}16})]_x$ rather than the multiplet found for tc-$H_2L^{Dipy\text{-}16}$. The remaining aliphatic protons for the $n = 16$ compounds were found in the region of 1.83 – 0.88 for tc-$H_2L^{Dipy\text{-}16}$, 1.56 – 0.88 for tc-$[Pd(L^{Dipy\text{-}16})]$ and 1.75 – 0.88 for tc-$[Zn(L^{Dipy\text{-}16})]_2$. These signals obscured the signal for the methyl protons on the pyrrole moiety. However, this signal was visible in the spectra for the methoxy compounds at 1.76ppm, 1.70ppm and 1.60ppm for tc-$H_2L^{Dipy\text{-}1}$, tc-$[Pd(L^{Dipy\text{-}1})]$ and tc-$[Zn(L^{Dipy\text{-}1})]_2$, respectively. The only spectrum to show the presence of the signal corresponding to the pyrrole N-H was that of the tc-$H_2L^{Dipy\text{-}1}$ compound, which displayed a broad singlet at 4.77ppm.

Examination of the ^{13}C-NMR spectra revealed the expected 11 signals in the imine and aromatic regions between 150ppm and 103ppm for tc-$H_2L^{Dipy\text{-}n}$, and 158ppm and 106ppm for tc-$[M(L^{Dipy\text{-}n})]_x$. The *meso* quaternary carbon signal belonging to the free ligands was observed at 36ppm. This was shifted downfield by 3 and 7 ppm on complexation to zinc(II) and palladium(II), respectively. No significant shifts resulting from complexation

were observed for the carbons α to the alkoxy oxygen, nor for carbons in the long aliphatic chains. Once again, as seen in the analogous hexacatenar compounds the close proximity of the aliphatic carbon resonances has led to obscuring of some signals in the region 32 – 14ppm.

4.2.6.3 Characterisation of ex-$H_2L^{Dipy\text{-}n}$ and ex-$[M(L^{Dipy\text{-}n})]_x$

The infrared spectra evidenced the presence of the ester carbonyl with a single absorption band between 1724 and 1741cm^{-1}. Only one imine band was observed for each of the six compounds at *ca.* 1616cm^{-1} for ex-$H_2L^{Dipy\text{-}n}$ and ex-$[Pd(L^{Dipy\text{-}1})]$, and at *ca.* 1605cm^{-1} for ex-$[Pd(L^{Dipy\text{-}16})]$ and ex-$[Zn(L^{Dipy\text{-}n})]_2$. Significant shifts in wavenumber were observed for the C-O stretching vibrations. For ex-$H_2L^{Dipy\text{-}n}$ such bands were observed at *ca.* 1160cm^{-1}, whereas complexation to palladium(II) and zinc(II) resulted in a shift to much lower wavenumber. For ex-$[Pd(L^{Dipy\text{-}1})]$ and ex-$[Pd(L^{Dipy\text{-}16})]$ the bands occurred at 1064 and 1081cm^{-1}, respectively. For ex-$[Zn(L^{Dipy\text{-}1})]_2$ and ex-$[Zn(L^{Dipy\text{-}16})]_2$ the bands occurred at 1021 and 1049cm^{-1}, respectively.

Electrospray mass spectrometry evidenced the formation of the free ligand ex-$H_2L^{Dipy\text{-}1}$ at m/z = 681, but was unable to detect the compound ex-$H_2L^{Dipy\text{-}16}$. However, ex-$H_2L^{Dipy\text{-}16}$ was evidenced by all other techniques. MALDI-TOF mass spectrometry detected the complexes ex-$[Pd(L^{Dipy\text{-}1})]$ and ex-$[Pd(L^{Dipy\text{-}16})]$ at m/z = 784 and 1206, corresponding to the expected 1:1 metal to ligand stoichiometry. The complexes ex-$[Zn(L^{Dipy\text{-}1})]_2$ and ex-$[Zn(L^{Dipy\text{-}16})]_2$ were detected by peaks at m/z = 1488 and 2329, corresponding to the 2:2 stoichiometry. CHN microanalysis satisfactorily characterised the formation of the extended ligands and complexes.

Comparison of the ^{1}H-NMR spectra revealed the effects of complexation to the metal cations palladium(II) and zinc(II). For the metal-free ligand ex-$H_2L^{Dipy\text{-}1}$, the singlet corresponding to the resonance from the imine protons was observed at 8.14ppm, whereas complexation to palladium(II) shifted this resonance upfield to 7.60ppm. On complexation to zinc(II), the singlet was observed at 8.17ppm. The pyrrole protons' resonances were found as doublets at 6.62ppm and 6.17ppm for ex-$H_2L^{Dipy\text{-}1}$, 6.94ppm and 6.34ppm for ex-[Pd($L^{Dipy\text{-}n}$)], and 6.72ppm and 6.21ppm for ex-[Zn($L^{Dipy\text{-}n}$)]$_2$. These signals corresponded to those found for the analogous hexa- and tetracatenar compounds, as described previously.

The additional ester-linked phenyl-ring arms generated accompanying resonances in the aromatic region of the spectra. Doublets corresponding to the protons *ortho-* to the carbon bearing the ester functionality were found at 8.15ppm, 7.89ppm and 8.10ppm for ex-$H_2L^{Dipy\text{-}1}$, ex-[Pd($L^{Dipy\text{-}n}$)] and ex-[Zn($L^{Dipy\text{-}n}$)]$_2$, respectively. The *meta-* protons were observed further upfield at around 6.98, 6.77 and 6.87ppm, respectively. Protons on the phenyl rings grafted to the imine groups often had overlapping doublet resonances occurring at 7.17ppm for ex-$H_2L^{Dipy\text{-}1}$, 6.84ppm for ex-[Pd($L^{Dipy\text{-}n}$)] and 6.98ppm for ex-[Zn($L^{Dipy\text{-}n}$)]$_2$. Alkoxy protons occurred in the region of 4.04 – 3.87ppm and the remaining aliphatic protons resonated in the region 1.92 – 0.88ppm. The singlet corresponding to the pyrrolic methyl protons was observed at 1.67ppm for ex-$H_2L^{Dipy\text{-}1}$, 1.71ppm for ex-[Pd($L^{Dipy\text{-}n}$)] and 1.56ppm for ex-[Zn($L^{Dipy\text{-}n}$)]$_2$.

The ^{13}C-NMR spectra corresponding to ex-$H_2L^{Dipy\text{-}1}$, ex-[Pd($L^{Dipy\text{-}16}$)], ex-[Zn($L^{Dipy\text{-}1}$)]$_2$ and ex-[Zn($L^{Dipy\text{-}16}$)]$_2$ contained the 14 individual resonances

that were assigned to the carbonyl, imine and aromatic carbons in the region of 165 – 107ppm. The complex ex-[Pd(L^{Dipy-1})] was too insoluble for the preparation of a suitably concentrated sample. Due to the similar carbon environments in the aryl region, some of the resonances for ex-$H_2L^{Dipy-16}$ overlapped obscuring four of the expected peaks. From the spectra of the methoxy compounds ex-H_2L^{Dipy-1} and [Zn(L^{Dipy-1})]$_2$ it was apparent that the quaternary carbon resonance occurred at 35ppm for ex-H_2L^{Dipy-1} and 4ppm further downfield for [Zn(L^{Dipy-1})]$_2$. The methyl resonance from the pyrrole core was observed at 28 and 30ppm for ex-H_2L^{Dipy-1} and [Zn(L^{Dipy-1})]$_2$, respectively. Carbon resonances from the aliphatic chains occurred in the region 68 – 14ppm, and once more some of the individual resonances were obscured.

4.2.7 Structure Determination by Single Crystal X-Ray Diffractometry

X-ray crystallographic studies on single crystals of [Zn(L^{Dipy-1})]$_2$, ex-[Pd(L^{Dipy-1})] and ex-[Zn(L^{Dipy-1})]$_2$ revealed the solid state structural geometries of the compounds. Attempts to grow suitable single crystals of [Pd(L^{Dipy-1})], tc-[Zn(L^{Dipy-1})]$_2$ and tc-[Pd(L^{Dipy-1})], as well as the free ligand analogues, were unsuccessful. The two zinc(II) complexes [Zn(L^{Dipy-1})]$_2$ and ex-[Zn(L^{Dipy-1})]$_2$ are dinuclear metallo-helicates with distorted tetrahedral coordination geometry. The palladium(II) complex ex-[Pd(L^{Dipy-1})] was confirmed as being a monomeric species with distorted square planar coordination geometry. Selected bond lengths and angles are shown in Tables 4.1 and 4.2. Herein follows further discussion on the crystallographic data obtained for each complex.

4.2.7.1 Structure Determination of $[Zn(L^{Dipy\text{-}1})]_2$

Crystallographic studies of single crystals of $[Zn(L^{Dipy\text{-}1})]_2$ (Figure 4.12) confirmed that the compounds are binuclear species that crystallise in space group P21/N. The coordination geometry around the zinc(II) cations is distorted tetrahedral, with the four co-ordination sites occupied by one pyrrole nitrogen and one imine nitrogen per ligand. The bridging ligands and tetrahedral co-ordination geometry of the zinc(II) cations result in the formation of a double-stranded helix. The chiral compound crystallises in a centrosymmetric space group, implying that there is a racemic mixture of molecules. Related diiminodipyrromethane double-stranded helicates with manganese(II) and iron(II) cations have been previously prepared at The University of Nottingham by Love and co-workers.[27]

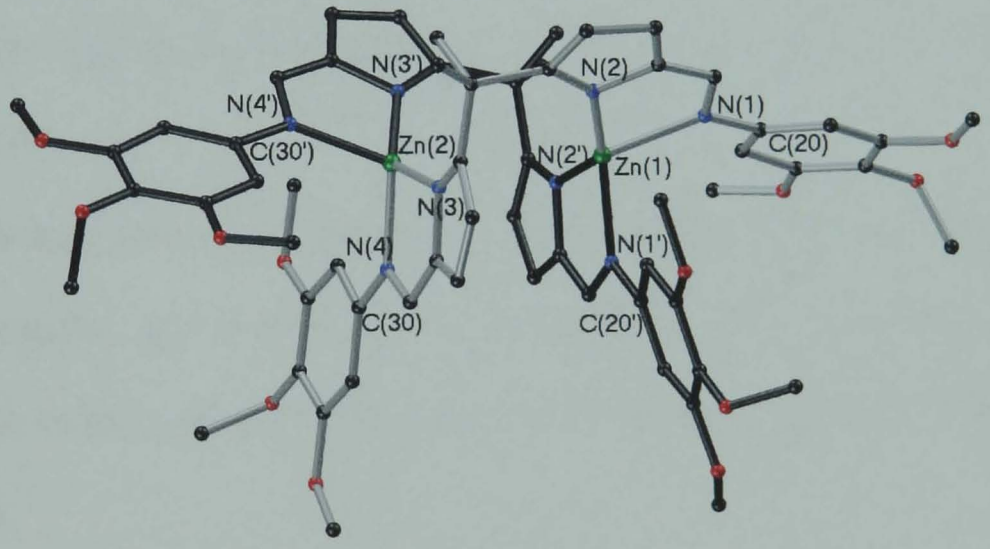

Figure 4.12. Crystal structure of $[Zn(L^{Dipy\text{-}1})]_2$. $0.1CHCl_3.3.35C_4H_{10}O$. Hydrogen atoms and solvents of crystallisation have been omitted for clarity.

For our complex $[Zn(L^{Dipy\text{-}1})]_2$, the bond lengths of the zinc(II) cation to the nitrogen donors are slightly shorter for zinc(II) to the pyrrole nitrogens than for zinc(II) to the imine nitrogens. For example, Zn(1)-N(2) = 1.970(1)Å, Zn(1)-N(2') = 2.022(1)Å, Zn(1)-N(1) = 2.097(1)Å, Zn(1)-N(1') = 2.061(1)Å. The bonds extending from Zn(2) are very similar in length to those from Zn(1) and are detailed in Table 4.1. Bond angles are significantly distorted from

ideal tetrahedral coordination geometry, ranging from 84° to 142°. For example, N(1)-Zn(1)-N(2) = 84.01(4)°, N(1)-Zn(1)-N(2') = 117.72(6)°, N(1)-Zn(1)-N(1') = 106.22(6)°, N(1')-Zn(1)-N(2) = 120.40(7)°, N(1')-Zn(1)-N(2') = 85.20(4)°, N(2)-Zn(1)-N(2') = 141.81(8)°. Selected bond angles for Zn(2) are provided in Table 4.1.

As a result of twisting at the *meso*-carbon, the pyrrole rings from each ligand are twisted relative to each other. The N(3) and N(2) pyrrole rings are twisted by 94.74(5)°, whereas the N(3') and N(2') pyrrole rings are twisted by 84.96°. The phenyl rings do not deviate significantly out of their respective pyrrole planes. The torsion angle between phenyl ring C(30) and pyrrole ring N(3) is 6.869(4)°, between phenyl ring C(20) and pyrrole ring N(2) it is 18.28(1)°, between phenyl ring C(30') and pyrrole ring N(3') the twist is 13.729(8)° and between phenyl ring C(20') and pyrrole ring N(2') it is 16.430(9)°.

Within each dimer there is a distance of 4.076(2)Å between the two zinc(II) cations, and associated with each molecule are 3.35 non-interacting molecules of Et_2O and 0.1 molecules of $CHCl_3$, which occupy voids within the structure.

The packing diagram in Figure 4.13 demonstrates the herringbone layered arrangement of the $[Zn(L^{Dipy\text{-}1})]_2$ molecules. The tilted layers alternate in orientation, so that adjacent layers are arranged 'head-to-tail'. Therefore, between adjacent layers molecules are rotated by 180° and the molecular planes are tilted by approximately 45° between layers (1) and (2), and layers (3) and (4). There is a negligible tilt angle between the molecular planes in layers (2) and (3). Given the separation between neighbouring molecules,

which is greater than 4.40Å from the centroid points of one phenyl ring to an adjacent phenyl ring, there is no indication of significant π-π stacking between molecules.[28]

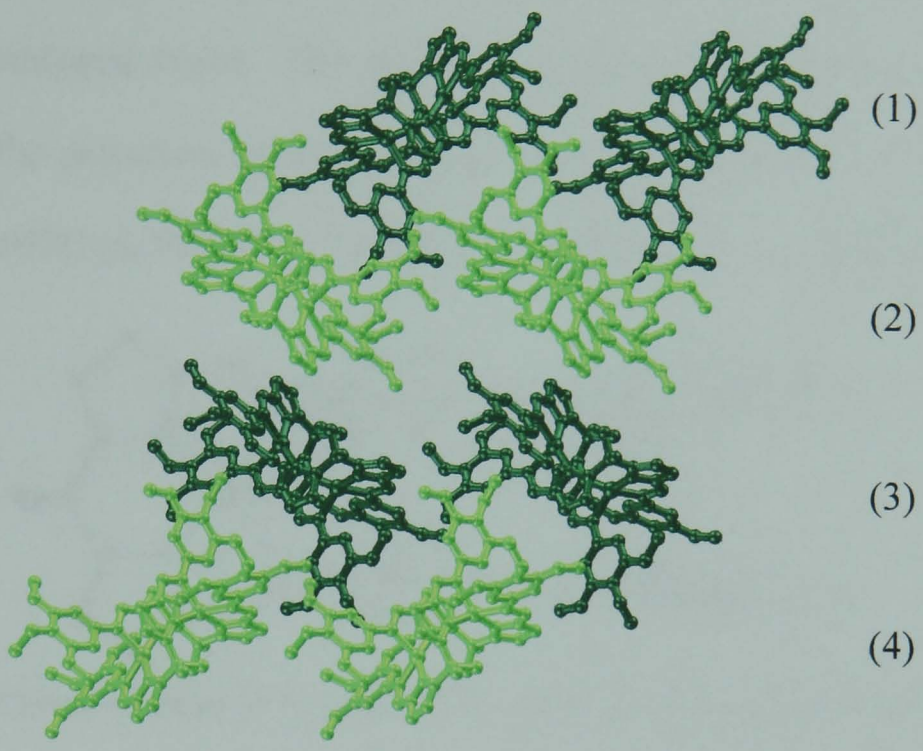

Figure 4.13. Packing diagram of $[Zn(L^{Dipy\text{-}1})]_2.0.1CHCl_3.3.35C_4H_{10}O$ showing the layered herringbone arrangement of the complexes, as viewed along the 'a' axis. The molecules have been colour coded to emphasise the layered structure and the layers have been numbered 1-4 for reference. Hydrogen atoms and solvents of crystallisation have been omitted for clarity.

Table 4.1. Selected bond lengths [Å] and angles [°] for $[Zn(L^{Dipy\text{-}1})]_2.\ 0.1CHCl_3.3.35C_4H_{10}O$

Zn(1)-N(1)	2.097(1)	N(1)-Zn(1)-N(2)	84.01(4)
Zn(1)-N(2)	1.970(1)	N(1)-Zn(1)-N(2')	117.72(6)
Zn(1)-N(1')	2.061(1)	N(1)-Zn(1)-N(1')	106.22(6)
Zn(1)-N(2')	2.002(1)	N(1')-Zn(1)-N(2)	120.40(7)
Zn(2)-N(4)	2.045(1)	N(1')-Zn(1)-N(2')	85.20(4)
Zn(2)-N(3)	1.974(1)	N(2)-Zn(1)-N(2')	141.81(8)
Zn(2)-N(4')	2.090(1)		
Zn(2)-N(3')	1.974(1)	N(4)-Zn(2)-N(3)	85.12(4)
		N(4)-Zn(2)-N(3')	124.70(7)
Twist of N(3) and N(2) pyrrole rings	94.74(5)	N(4)-Zn(2)-N(4')	109.42(6)
Twist of N(3') and N(2') pyrrole rings	84.96(4)	N(4')-Zn(2)-N(3)	112.73(6)

4.2.7.2 Structure Determination of ex-$[Pd(L^{Dipy\text{-}1})]$

The crystal structure of ex-$[Pd(L^{Dipy\text{-}1})]$ revealed the complex crystallises in the triclinic space group P-1, with distorted square planar coordination geometry about the central palladium(II) cation (Figure 4.14).

The bond angles deviate from the ideal angles of 90°, with N(1)-Pd-N(2) = 80.08(9)°, N(2)-Pd-N(3) = 87.69(9)°, N(3)-Pd-N(4) = 79.89(9)°, N(1)-Pd-N(4) = 112.4°. Similar bond lengths extend from the palladium(II) centre to the coordinated nitrogen atoms. The palladium-imine nitrogen bonds are slightly longer than the palladium-pyrrole nitrogen bonds, with Pd-N(1) = 2.089(2)Å, Pd-N(4) = 2.093(2)Å, Pd-N(2) = 1.940(2)Å, and Pd-N(3) = 1.939(2)Å.

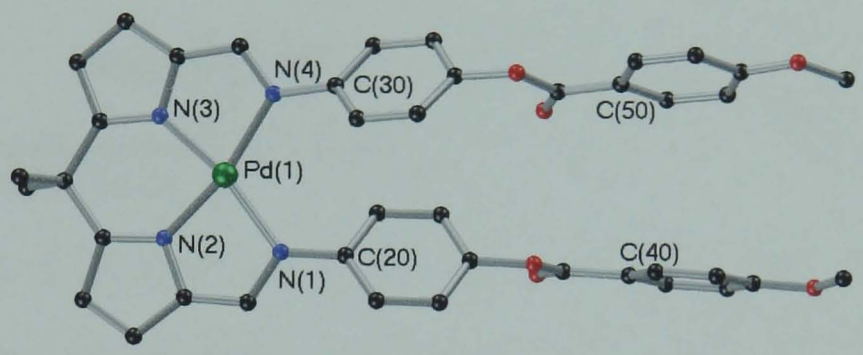

Figure 4.14. Crystal structure of ex-[Pd(L^{Dipy-1})]. Hydrogen atoms have been omitted for clarity.

The square planar geometry of the metal centre constrains the pyrrole rings in an almost planar arrangement, so that the rings experience a twist of just 5.895(6)°, with respect to each other. The palladium(II) cation lies just 0.0458Å out of the square plane defined by the four coordinating nitrogen atoms. Flexibility of the extended arms permits the two sets of phenyl rings to deviate from co-planarity, whereby the C(20) and C(30) rings are twisted 20.97(2)° relative to each other, and the twist of the C(40) and C(50) rings is 16.25(1)°, with respect to each other. The distances between both pairs of rings are 4.035(4)Å for the centroid-centroid distance from the C(20) to the C(30) ring, and 5.107(5)Å for the centroid-centroid distance from the C(40) to the C(50) ring. As is apparent from Figures 4.14 and 4.15 the phenyl rings are also twisted relative to the pyrrole rings. Due to steric restraints the C(20) and C(30) rings are twisted by 34.14(3)° and 40.80(4)° relative to the N(2) and

N(3) pyrrole rings, respectively. The C(40) and C(50) rings are twisted by 92.2° and 103.5° relative to the N(2) and N(3) rings, respectively.

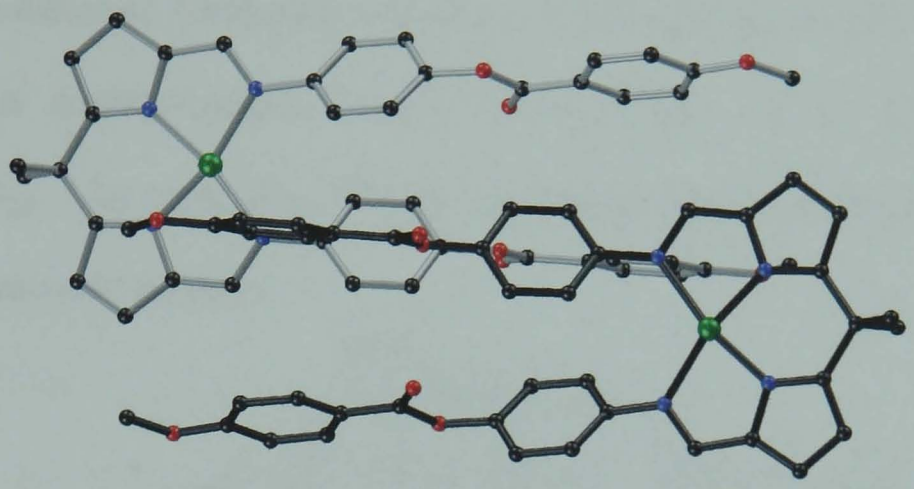

Figure 4.15. Arrangement of 'head-to-tail' monomers of ex-[Pd(L^{Dipy-1})]. Hydrogen atoms have been omitted for clarity.

Figure 4.15 shows the arrangement of nearest-neighbour molecules. The monomers are arranged offset 'head-to-tail', with co-planar dipyrrole cores.

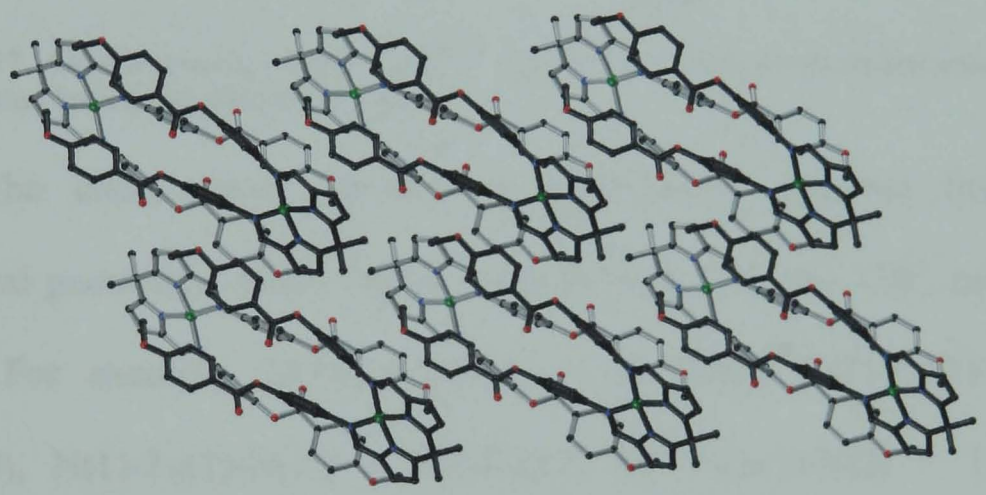

Figure 4.16. Packing diagram of ex-[Pd(L^{Dipy-1})] to show how the molecules are arranged in layers in the solid state, as viewed along the 'a' axis. Hydrogen atoms have been omitted for clarity.

The packing diagram in Figure 4.16 demonstrates how pairs of 'head-to-tail' monomers organise into tilted layers. No molecules of solvent are present in the unit cell.

4.2.7.3 Structure Determination of ex-[Zn(L^{Dipy-1})]$_2$

Single crystal X-ray diffraction confirmed that ex-[Zn(L^{Dipy-1})]$_2$ is a dimeric, binuclear species in space group P-1 (Figure 4.17). The zinc(II)

cations are four-coordinate, and per metal, the coordination sites are provided by one imine nitrogen donor and one pyrrole nitrogen donor from each ligand. Hence, the distorted tetrahedral coordination geometry of the zinc(II) cations result in a double-stranded helical structure, akin to the structure for $[Zn(L^{Dipy\text{-}1})]_2$. As with $[Zn(L^{Dipy\text{-}1})]_2$, the chiral compound ex-$[Zn(L^{Dipy\text{-}1})]_2$ exists as a racemic mixture.

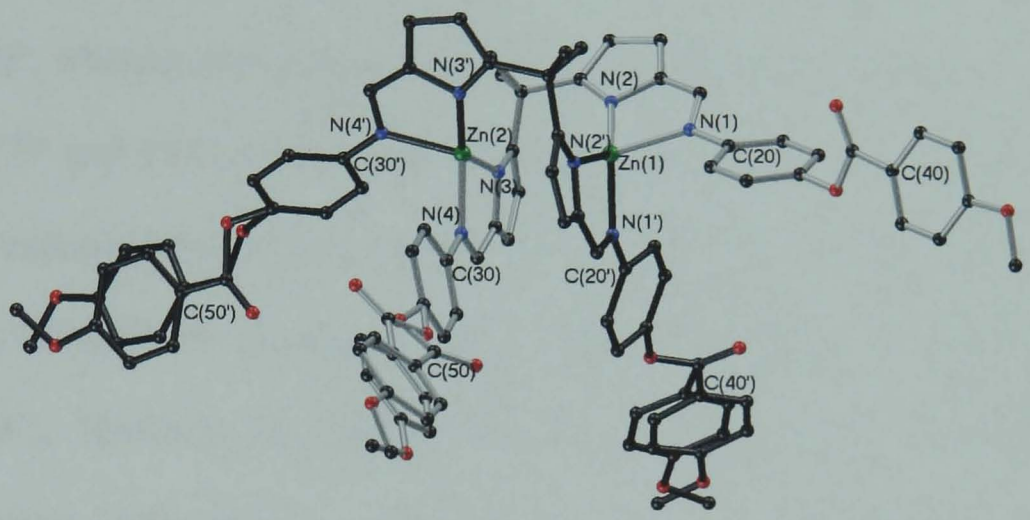

Figure 4.17. Crystal structure of ex-$[Zn(L^{Dipy\text{-}1})]_2.CH_2Cl_2$. Hydrogen atoms and solvents of crystallisation have been omitted for clarity.

The coordination geometry is significantly distorted from ideal tetrahedral geometry. Bond angles range between 84° and 138°, rather than 109°. For example, N(1)-Zn(1)-N(2) = 84.42(6)°, N(1)-Zn(1)-N(2') = 110.81(8), N(1)-Zn(1)-N(1') = 105.81(8)°, N(1')-Zn(1)-N(2) = 130.5(1)°, N(1')-Zn(1)-N(2') = 84.74(6)°, N(2)-Zn(1)-N(2') = 137.4(1)°. Bond lengths are very similar to ex-$[Pd(L^{Dipy\text{-}1})]$ and also to $[Zn(L^{Dipy\text{-}1})]_2$, with Zn(1)-N(1) = 2.096(1)Å, Zn(1)-N(1') = 2.035(1)Å, Zn(1)-N(2) = 1.957(1)Å, Zn(1)-N(2') = 1.988(1)Å. The bond angles and lengths for Zn(2) are very similar to those for Zn(1), see Table 4.2 for details. In each dimer the zinc(II) cations are 3.762(3)Å apart. This distance is shorter than the distance between zinc(II) cations in $[Zn(L^{Dipy\text{-}1})]_2$, possibly as a steric constraint of the longer arms.

The pyrrole rings in each ligand are substantially twisted relative to each other to accommodate the bridging of both metal cations. The N(2)

pyrrole ring is twisted 99.99(7)° relative to the N(3) pyrrole ring, whereas the N(2') pyrrole ring is twisted 79.61(6)° relative to the N(3') pyrrole ring. The phenyl rings are also twisted relative to the pyrrole rings. As is apparent in Figure 4.17, three of the four terminal phenyl rings are disordered. Consequently, their occupancy has been modelled over two sites and each ring experiences a different torsion angle. The phenyl ring C(20') is twisted 29.48(2)°, whereas the disordered phenyl rings C(40'a) and C(40'b) are twisted 102.06(7)° and 103.07(8)° relative to the pyrrole ring N(2'). The phenyl ring C(30') experiences a twist of 29.12(2)°, whereas the disordered phenyl rings C(50'a) and C(50'b) are twisted 33.21(2)° and 50.01(3)° relative to the pyrrole ring N(3'). Similarly, the C(20) phenyl ring has a torsion angle of 25.62° and the terminal C(40) ring a torsion angle of 132.2(1)°, with respect to the N(2) pyrrole ring. Finally, the phenyl ring C(30) has a twist of 18.78(1)° and the disordered terminal rings C(50a) and C(50b) have respective twists of 40.15(3)° and 47.43(3)°, in relation to the N(3) pyrrole ring.

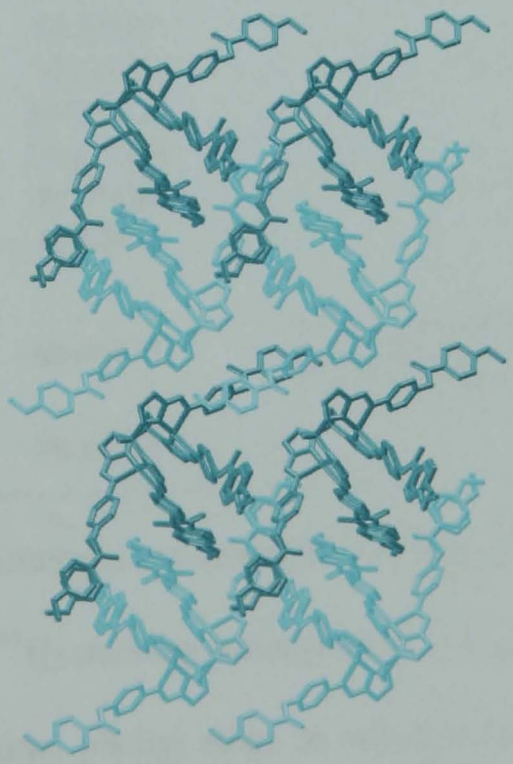

Figure 4.18. Packing diagram of ex-[Zn($L^{Dipy\text{-}1}$)].CH_2Cl_2 showing the layered herringbone arrangement of the complexes, as viewed along the 'a' axis. The molecules have been colour coded to emphasise the layered structure. Hydrogen atoms and solvents of crystallisation have been omitted for clarity.

A packing diagram of ex-$[Zn(L^{Dipy\text{-}1})]_2$ reveals that the molecules are arranged into layers in a herringbone manner (Figure 4.18). Within the voids of the structure resides one non-interacting solvent molecule of CH_2Cl_2 per dimer. This arrangement is similar in structure to that of $[Zn(L^{Dipy\text{-}1})]_2$. However, even though the molecules are rotated by 180° between layers there is no angle of tilt between molecular planes.

Table 4.2. Selected bond lengths [Å] and angles [°] for ex-$[Zn(L^{Dipy\text{-}1})]_2.CH_2Cl_2$ and ex-$[Pd(L^{Dipy\text{-}1})]$.

Zn(1)-N(1)	2.096(1)	Pd(1)-N(1)	2.089(2)
Zn(1)-N(2)	1.957(1)	Pd(1)-N(2)	1.940(2)
Zn(1)-N(1')	2.035(1)	Pd(1)-N(3)	1.939(2)
Zn(1)-N(2')	1.988(1)	Pd(1)-N(4)	2.093(2)
Zn(2)-N(4)	2.032(1)		
Zn(2)-N(3)	1.985(1)		
Zn(2)-N(4')	2.097(1)		
Zn(2)-N(3')	1.958(1)		
N(1)-Zn(1)-N(2)	84.42(6)	N(1)-Pd(1)-N(2)	80.08(9)
N(1)-Zn(1)-N(2')	110.81(8)	N(2)-Pd(1)-N(3)	87.69(9)
N(1)-Zn(1)-N(1')	105.81(8)	N(3)-Pd(1)-N(4)	79.89(9)
N(1')-Zn(1)-N(2)	130.5(1)	N(1)-Pd(1)-N(4)	112.4(1)
N(1')-Zn(1)-N(2')	84.74(6)	N(2)-Pd(1)-N(4)	167.2(1)
N(2)-Zn(1)-N(2')	137.4(1)	N(1)-Pd(1)-N(3)	167.0(1)
N(4)-Zn(2)-N(3)	84.93(6)		
N(4)-Zn(2)-N(3')	131.6(1)		
N(4)-Zn(2)-N(4')	104.80(8)		
N(4')-Zn(2)-N(3)	109.31(8)		
N(4')-Zn(2)-N(3')	84.19(6)		
N(3)-Zn(2)-N(3')	137.5(1)		
Twist of N(3) and N(2) pyrrole rings	99.99(7)	Twist of N(3) and N(2) pyrrole rings	5.895(6)
Twist of N(3') and N(2') pyrrole rings	79.61(6)		

Intermolecular interactions contribute to the stabilisation of the layers within the ex-$[Zn(L^{Dipy\text{-}1})]_2$ packing arrangement. Weak edge-face interactions exist between the terminal phenyl rings in adjacent layers. For example, the C(50) phenyl rings of adjacent dimers are separated by centroid-centroid distances of around 5.910(4)Å, with a torsion angles of approximately

81.21(6)°. Additionally, C(40') and C(50') rings are separated by 4.934(3)Å with the rings at an angle of 69.66(5)° to one another.

Another very weak intermolecular interaction may exist between the C(40) rings of dimers in adjacent layers. The coplanar phenyl rings are off-set by 1.73Å and the plane-plane distance between the two phenyl rings is 3.49Å. The centroid-centroid distance between the two rings is 3.901(3)Å. However, this is just outside of the observed maximum centroid-centroid distance of around 3.8Å for parallel displaced π-π stacking.[28] Hence, it could be a negligible interaction.

4.2.8 Liquid Crystalline Properties of the Dipyrrole-Derived Compounds

The liquid crystalline properties of the compounds were generally studied by polarised optical microscopy and differential scanning calorimetry. Characterisation by small-angle X-ray diffraction was hampered by narrow mesomorphic temperature ranges. Consequently the majority of the following compounds have not been fully characterised. Hence, herein follows a discussion on the mesomorphic character of dipyrrole-derived bent-core compounds derived from preliminary results.

4.2.8.1 Liquid Crystalline Properties of $H_2L^{Dipy\text{-}n}$ and $[M(L^{Dipy\text{-}n})]$

The liquid crystalline behaviour of the ligands $H_2L^{Dipy\text{-}n}$ was studied by polarised optical microscopy and differential scanning calorimetry. The DSC traces only showed the melting temperatures as broad peaks. Given the narrow temperature range of the liquid crystalline phases it is plausible that such broad peaks shielded the remaining clearing temperatures. However, POM was able

to detect both transitions. At the current time the identities of the liquid crystalline phases are unknown.

The transition temperatures of the ligands $H_2L^{Dipy\text{-}n}$ are shown in Chart 4.1 and Table 4.3. The ligands melted into mesophases at temperatures between 42°C and 51°C. As the length of the aliphatic chains increased, the melting temperatures increased, decreased and then increased again as the length went from 10 to 16 carbon atoms. The clearing temperatures behaved in the opposite manner, so that the ligand with n = 14 had the most stable mesophase. But even this existed over a range of only 16°C. All ligands cleared in the range 54°C to 58°C.

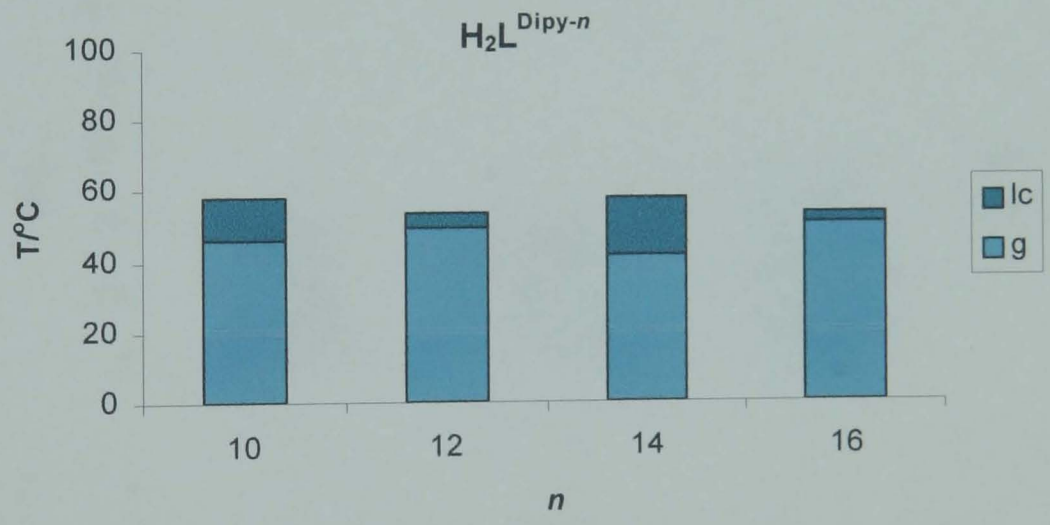

Chart 4.1. Phase diagram representing the transition temperatures of the compounds $H_2L^{Dipy\text{-}n}$ (where lc is an unidentified liquid crystalline phase; g is the glass transition temperature).

Table 4.3. Table showing the combined POM and DSC data to give the mesophase transition temperatures for $H_2L^{Dipy\text{-}n}$, where lc are uncharacterised liquid crystal phases and I is the isotropic liquid.

n	Transitions/°C
10	g 46 lc 58 I
12	g 50 lc 54 I
14	g 42 lc 58 I
16	g 51 lc 54 I

Three of the palladium(II) complexes, $[Pd(L^{Dipy\text{-}12})]$, $[Pd(L^{Dipy\text{-}14})]$ and $[Pd(L^{Dipy\text{-}16})]$, were studied by polarised optical microscopy and differential

scanning calorimetry. In accordance with the metal-free ligands only melting transitions were observed in the DSC traces, whereas both melting and clearing transitions were observed by POM. The results are outlined in Chart 4.2 and Table 4.4.

The complexes melted at just over room temperature. [Pd($L^{Dipy-12}$)], [Pd($L^{Dipy-14}$)] and [Pd($L^{Dipy-16}$)] all melted into currently unidentified liquid crystal phases at 30°C, 30°C and 46°C, respectively. Each cleared into the isotropic liquid at 40°C, 42°C and 52°C. Hence, complexation of the ligand to palladium(II) had a modest stabilising effect on the liquid crystalline phases.

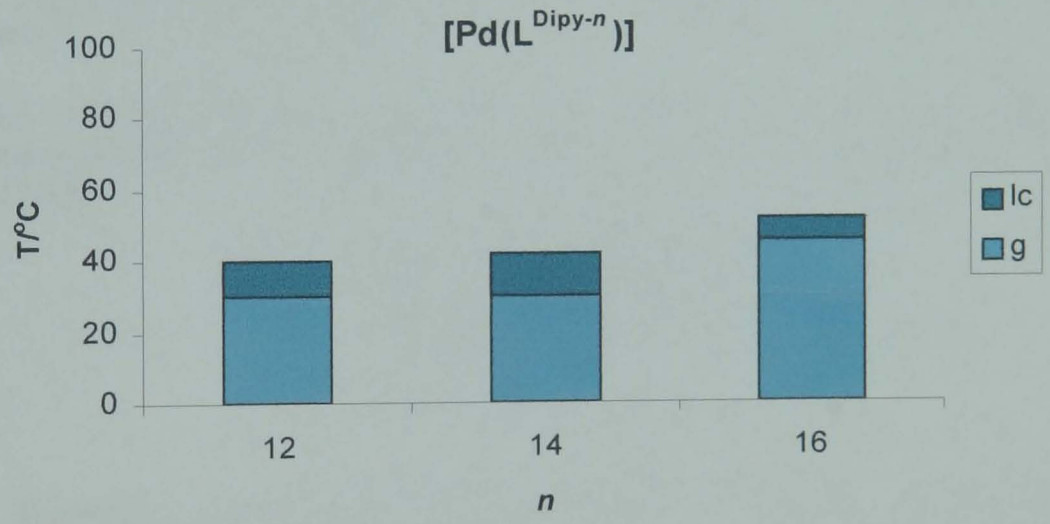

Chart 4.2. Phase diagram representing the transition temperatures of the compounds [Pd(L^{Dipy-n})] (where lc is an unidentified liquid crystalline phase; g is the glass transition temperature).

Table 4.4. Table showing the combined POM and DSC data to give the mesophase transition temperatures for [Pd(L^{Dipy-n})], where lc are uncharacterised liquid crystal phases and I is the isotropic liquid.

n	**Transitions/°C**
12	g 30 lc 40 I
14	g 30 lc 42 I
16	g 46 lc 52 I

The zinc(II) complex $[Zn(L^{Dipy-16})]_2$ was studied by polarised optical microscopy, differential scanning calorimetry and small-angle powder X-ray diffraction. The results, along with a comparative study of the analogous

metal-free ligand $H_2L^{Dipy\text{-}16}$ and the palladium complex $[Pd(L^{Dipy\text{-}16})]$, are shown in Chart 4.3 and Table 4.5.

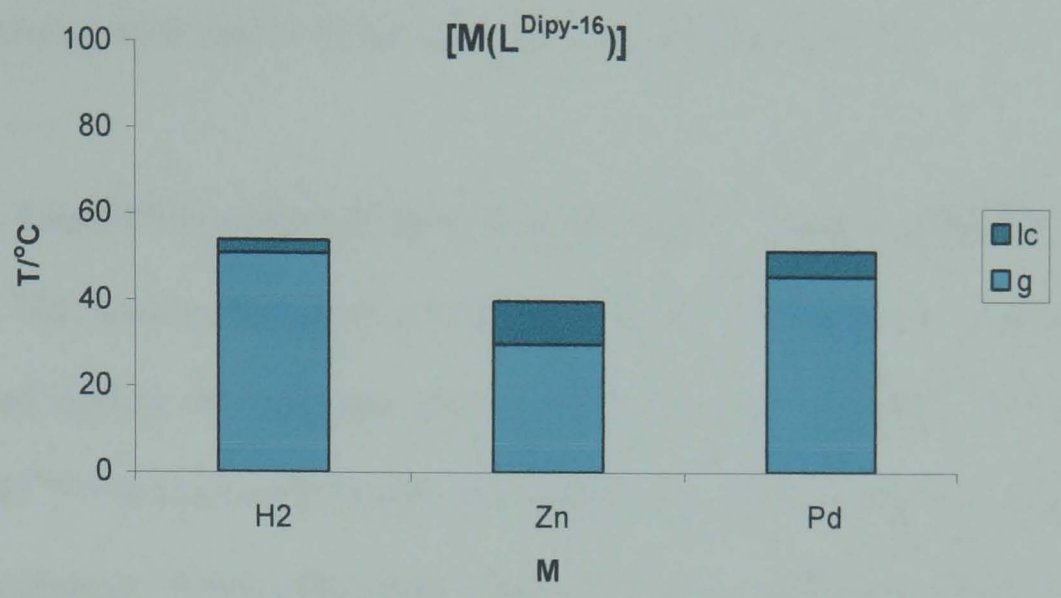

Chart 4.3. Phase diagram representing the transition temperatures of the compounds $[M(L^{Dipy\text{-}16})]_x$ (where lc is an unidentified liquid crystalline phase; g is the glass transition temperature).

Table 4.5. Table showing the combined POM and DSC data to give the mesophase transition temperatures for $[M(L^{Dipy\text{-}16})]_x$, where lc are uncharacterised liquid crystal phases and I is the isotropic liquid.

M	Transitions
H_2	g 51 lc 54 I
Zn	g 30 lc 40 I
Pd	g 46 lc 52 I

Between crossed polarisers $[Zn(L^{Dipy\text{-}16})]_2$ melted into an unidentified liquid crystalline phase at 30°C and cleared at 40°C, which was in agreement with the DSC and XRD findings. Unfortunately, a sufficient diffraction pattern was not obtained to characterise the mesophase. Unsurprisingly, the helical structure of the $[Zn(L^{Dipy\text{-}16})]_2$ dimer served to lower both the melting and clearing temperatures, relative to $H_2L^{Dipy\text{-}16}$ and the planar complex $[Pd(L^{Dipy\text{-}16})]$, as a result of perturbing the close-packing ability of the molecules. The mesophase range had also been further stabilised, but was still somewhat short-lived existing over only a temperature range of 10°C. The ability of tetrahedral zinc(II) complexes to generate mesophases is a rare and

recent phenomenon.[29] However, over the last decade researchers have combined coordination chemistry along with liquid crystal self-organisation processes to successfully achieve supramolecular helical metallomesogen architectures, and these have been reviewed by Serrano and Sierra.[30]

4.2.8.2 Liquid Crystalline Properties of tc-$H_2L^{Dipy\text{-}16}$ and tc-$[M(L^{Dipy\text{-}16})]_x$

The tetracatenar metal-free ligand tc-$H_2L^{Dipy\text{-}16}$ was investigated by polarised optical microscopy, whereas the complexes tc-$[Zn(L^{Dipy\text{-}16})]_2$ and tc-$[Pd(L^{Dipy\text{-}16})]$ were additionally studied by differential scanning calorimetry and small-angle X-ray diffraction. The results are outlined in Chart 4.4 and Table 4.6.

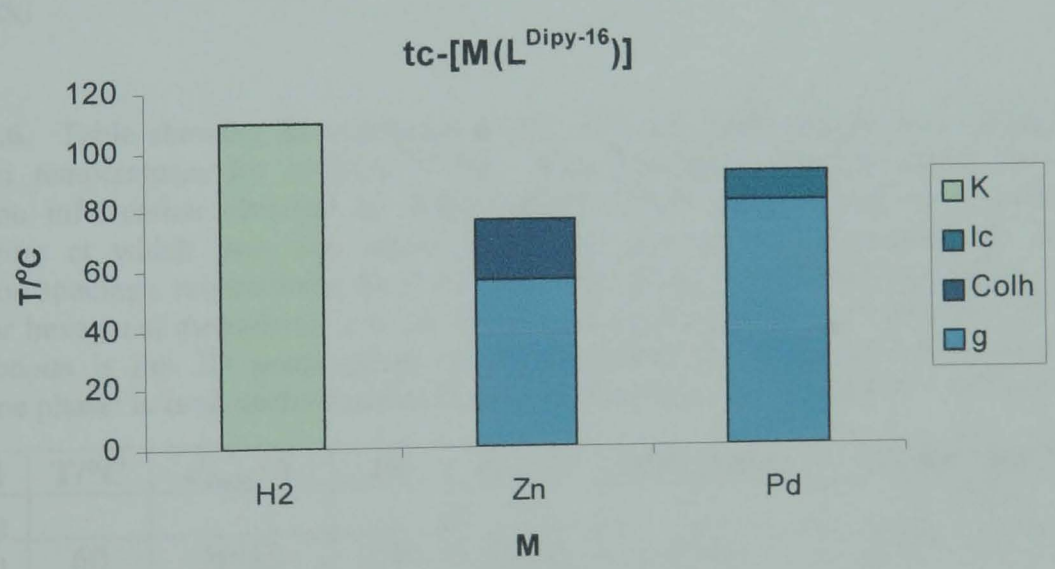

Chart 4.4. Phase diagram representing the transition temperatures of the compounds tc-$[M(L^{Dipy\text{-}16})]_x$ (where lc is an unidentified liquid crystalline phase; Col_h is a columnar hexagonal phase; g is the glass transition temperature; K is the crystalline phase of the non-mesomorphic ligand).

The free ligand was non-mesomorphic, melting at 110°C straight into the isotropic fluid. However, the tc-$[Zn(L^{Dipy\text{-}16})]_2$ and tc-$[Pd(L^{Dipy\text{-}16})]$ complexes were both mesomorphic. The DSC traces showed both melting and clearing temperatures in the first heating cycle in agreement with the POM observations. The tc-$[Zn(L^{Dipy\text{-}16})]_2$ dimer melted into a mesophase at 71°C

and cleared at 77°C, whereas the tc-[Pd($L^{Dipy-16}$)] monomer melted into a mesophase at 83°C and cleared at 93°C. XRD measurements characterised the tc-[Zn($L^{Dipy-16}$)]$_2$ mesophase as Col_h from the one large and three small diffraction peaks in the ratio 1:√3:√4:√7. XRD was unable to characterise the mesophase of tc-[Pd($L^{Dipy-16}$)], although it was able to verify the clearing temperature. Hence, tc-[Zn($L^{Dipy-16}$)] is another rare example of a mesomorphic tetrahedral zinc(II) complex. Using the lattice parameters of tc-[Zn($L^{Dipy-16}$)]$_2$, the number of molecules per column cross-section has been estimated (see Chapter 2, Section 2.2.5.6 for further information). The value of N_h is 1.04. This implies that there is one molecule of tc-[Zn($L^{Dipy-16}$)]$_2$ per column cross-section, which is unsurprising given the dimeric structure of the complex.

Table 4.6. Table showing the combined POM, DSC and XRD data to give the mesophase transition temperatures for tc-[M($L^{Dipy-16}$)]$_x$. Also included, where possible, are detailed indexation information obtained by XRD studies (where **M** = central metal cation; **T** = temperature at which data was taken; d_{meas}, and d_{calc} are the measured and calculated diffraction spacings, respectively; ***hk*** is the indexation of the two-dimensional lattice; Col_h is a columnar hexagonal mesophase; *a* is the lattice parameter and *S* is the lattice area of the Col_h phase; *p6mm* is the 2D space group of the corresponding hexagonal mesophase; K is a crystalline phase; lc is an uncharacterised liquid crystal phase; and I is the isotropic liquid).

M	T/°C	$d_{meas.}$/Å	*hk*	$d_{calc.}$/Å	Mesophase	Transitions/°C
H_2	-	-	-	-	-	K 110 I
Zn	60	30.52	10	30.52	Col_h –	g 57 Col_h 77 I
		17.66	11	17.62	*p6mm*	
		15.23	20	15.26	a = 35.2 Å	
		13.31	21	11.54	S =1076Å^2	
		10.16	22	8.81		
Pd	-	-	-	-	-	g 83 lc 93 I

Comparison of the tetracatenar phase transitions of tc-[M($L^{Dipy-16}$)]$_x$ with those of the hexacatenar complexes [M($L^{Dipy-16}$)]$_x$ showed that reduction in the number of aliphatic chains from six to four had a significant affect on the mesophases. In the first instance, the effect on the metal-free ligands was to eradicate the already limited liquid crystalline behaviour. The effect on the

complexes was to virtually double both the melting and clearing temperatures, which was not surprising considering the reduction in the liquid-like character of the compounds. In addition to the increase in transition temperatures, the mesophase behaviour was also stabilised by reducing the number of chains from six to four per ligand. This could imply that the polar interactions necessary to stabilise the liquid crystalline phase are disturbed by the sterics required to accommodate an additional two chains per ligand.

Although the mesophases of the hexacatenar complexes are currently uncharacterised, the characterisation of the tetracatenar complex tc-[Zn($L^{Dipy\text{-}16}$)]$_2$ has indicated that columnar mesomorphism is not destroyed on removal of two aliphatic chains per ligand. However, given the dimeric nature of tc-[Zn($L^{Dipy\text{-}16}$)]$_2$ it follows that there are eight aliphatic chains per molecule. Therefore, it cannot be assumed that columnar mesomorphism prevails in tc-[Pd($L^{Dipy\text{-}16}$)] with only four aliphatic chains.

4.2.8.3 Liquid Crystalline Properties of ex-$H_2L^{Dipy\text{-}16}$ and ex-[M($L^{Dipy\text{-}16}$)]$_x$

The liquid crystalline properties of ex-$H_2L^{Dipy\text{-}16}$, ex-[Pd($L^{Dipy\text{-}16}$)] and ex-[Zn($L^{Dipy\text{-}16}$)]$_2$ were characterised by polarised optical microscopy and differential scanning calorimetry. The metal-free ligand ex-$H_2L^{Dipy\text{-}16}$ and the dimeric complex ex-[Zn($L^{Dipy\text{-}16}$)]$_2$ are non-mesomorphic, melting directly into the isotropic liquid. However, ex-[Pd($L^{Dipy\text{-}16}$)] was found to have liquid crystalline character. The compound melted into a smectic A phase at 140°C. The mesophase persisted up to high temperature, finally clearing into the isotropic liquid at 230°C. The higher transition temperature of ex-[Pd($L^{Dipy\text{-}16}$)] relative to the (tc)-[M($L^{Dipy\text{-}16}$)]$_x$ complexes reflect the additional attractive

interactions resulting from the extended polar core of supplementary phenyl rings and ester groups.

The complex ex-[Pd($L^{Dipy-16}$)] generated a smectic A mesophase over columnar or banana mesophases. This can be rationalised by several factors. Firstly, the complex is only dicatenar. Consequently, the aliphatic chain density is insufficient to generate the required ratio between the rigid core and aliphatic chains for columnar mesophase formation.[31] Secondly, solid-state single crystal X-ray diffraction of ex-[Pd(L^{Dipy-1})] indicated that the molecule is constrained in a rod-like arrangement, which disfavours both columnar and banana mesophase formation. Thirdly, the dimethyldipyrromethane core may not favour banana mesophase generation due to the lack of conjugation and the narrower bite angle relative to typical banana liquid crystals.[32] Additionally, metallomesogens have yet to generate banana mesophases.

Smectic A mesophase formation is favoured by extended rigid cores due to the sufficiently strong attractive interactions that favour a parallel organisation. Incompatibility between the aliphatic chains and rigid core ensures micro segregation of the core from the flexible chains of adjacent complexes, resulting in a lamellar organisation of molecules.[33] Hence, ex-[Pd($L^{Dipy-16}$)] generates a smectic A mesophase.

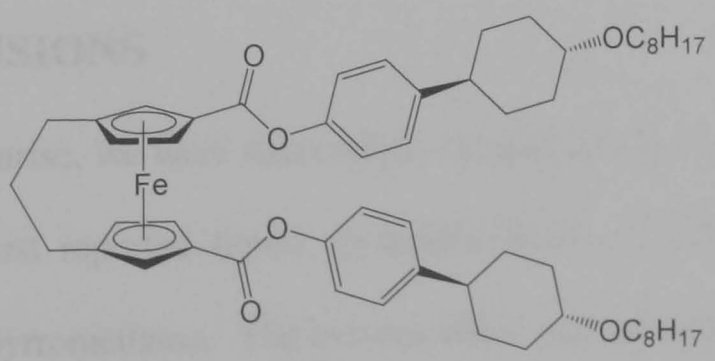

Cr 100 SmC 139.5 N 158 I

Figure 4.19. Liquid crystalline ferrocenophane–derived compound that forms a smectic C and nematic mesophase. Transition temperatures are given in °C.[34]

The formation of calamitic-type mesophases from extended U-shaped structures has been previously demonstrated by a ferrocenophane metallomesogen (Figure 4.19).[34] This complex formed a smectic C mesophase at 100°C, followed by a nematic phase at 139.5°C, before melting into the isotropic liquid at 158°C.

As mentioned above, the metal-free compound ex-$H_2L^{Dipy\text{-}16}$ is non-mesomorphic. The lack of rigidity at the core of the molecule could be responsible for the absence of mesomorphic behaviour. Similarly, the metallo-helicate complex ex-$[Zn(L^{Dipy\text{-}16})]_2$ is also non-mesomorphic. This is probably as a result of a combination of different factors. The tetrahedral geometry at the metal centres reduces the structural anisotropy of the compound and increases steric bulk relative to ex-$[Pd(L^{Dipy\text{-}16})]$. Although this is not a barrier to mesophase formation for $[Zn(L^{Dipy\text{-}16})]_2$ and tc-$[Zn(L^{Dipy\text{-}16})]_2$, the extended core of ex-$[Zn(L^{Dipy\text{-}16})]_2$ has additional polar inter-molecular interactions that could be too strong for mesophase generation. In addition to this, the chain volume of ex-$[Zn(L^{Dipy\text{-}16})]_2$ varies greatly from $[Zn(L^{Dipy\text{-}16})]_2$ and tc-$[Zn(L^{Dipy\text{-}16})]_2$. Hence, the change in balance of rigid and fluid moieties in ex-$[Zn(L^{Dipy\text{-}16})]_2$ may preclude mesophase formation.

4.3 CONCLUSIONS

To summarise, we have successfully synthesised and made preliminary studies on the first reported liquid crystalline bent-core compounds derived from dimethyldipyrromethane. The mesomorphic compounds are $[M(L^{Dipy\text{-}n})]_x$ (M = 2H, x = 1, n = 10, 12, 14,16; M = Pd^{2+}, x = 1, n =12, 14, 16; M = Zn^{2+}, x = 2, n = 16), tc-$[M(L^{Dipy\text{-}16})]_x$ (M = Pd^{2+}, x = 1; M = Zn^{2+}, x = 2) and ex-

$[Pd(L^{Dipy\text{-}n})]_x$, whereas tc-$H_2L^{Dipy\text{-}16}$, ex-$H_2L^{Dipy\text{-}16}$ and ex-$[Zn(L^{Dipy\text{-}16})]_2$ are non-mesomorphic.

The metal-free compounds were prepared by acid-catalysed Schiff-base condensation reactions of the appropriate aniline with 2,2'-diformyl-5,5'-dimethyldipyrromethane. The complexes were generated by deprotonation of the ligand, followed by reaction with the appropriate metal acetate. Characterisation of the compounds confirmed that the target products had been synthesised, and that all zinc(II) complexes, (tc)-$[Zn(L^{Dipy\text{-}n})]_2$ and ex-$[Zn(L^{Dipy\text{-}n})]_2$, are dimeric 2:2 metal-ligand species, whereas all palladium(II) complexes, (tc)-$[Pd(L^{Dipy\text{-}n})]$ and ex-$[Pd(L^{Dipy\text{-}n})]$, are monomeric 1:1 metal-ligand species.

Structural characterisation by single crystal X-ray diffraction of $[Zn(L^{Dipy\text{-}1})]_2$, ex-$[Zn(L^{Dipy\text{-}1})]_2$ and ex-$[Pd(L^{Dipy\text{-}1})]$ revealed that $[Zn(L^{Dipy\text{-}1})]_2$ and ex-$[Zn(L^{Dipy\text{-}1})]_2$ are racemic mixtures of double-stranded helicies with tetrahedrally coordinated zinc(II) centres. The complex ex-$[Pd(L^{Dipy\text{-}1})]$ is monomeric, with distorted square planar coordination geometry. All three complexes pack in layered arrangements, with $[Zn(L^{Dipy\text{-}1})]_2$ and ex-$[Zn(L^{Dipy\text{-}1})]_2$ exhibiting herringbone-type packing.

Characterisation of the mesomorphic behaviour of $[M(L^{Dipy\text{-}n})]_x$ (M = 2H, x = 1, n = 10, 12, 14, 16; M = Pd^{2+}, x = 1, n =12, 14, 16; M = Zn^{2+}, x = 2, n = 16) showed that mesophases exist over narrow temperature ranges, and that complexation of the ligand with n = 16 to zinc(II) and palladium(II) does little to increase the mesomorphic temperature ranges. However, zinc(II) lowers the transition temperatures relative to palladium(II), which itself has transition

temperatures lower than the free-ligand. The mesophase types are currently uncharacterised.

The liquid crystalline behaviour of the complexes tc-$[M(L^{Dipy\text{-}n})]_x$ (M = Pd^{2+}, x = 1; M = Zn^{2+}, x = 2) also exist over narrow temperature ranges, but the mesomorphic range of tc-$[Zn(L^{Dipy\text{-}n})]_2$ is twice that of tc-$[Pd(L^{Dipy\text{-}n})]$. In accordance with the hexacatenar compounds, the transition temperatures of tc-$[Zn(L^{Dipy\text{-}n})]_2$ are lower than tc-$[Pd(L^{Dipy\text{-}n})]$. The 2D symmetry of the tc-$[Zn(L^{Dipy\text{-}n})]_2$ mesophase has been characterised as columnar hexagonal.

Comparison of the behaviour of the mesomorphic complexes $[M(L^{Dipy\text{-}n})]_x$ (M = Pd^{2+}, x = 1, *n* =12, 14, 16; M = Zn^{2+}, x = 2, *n* = 16) with tc-$[M(L^{Dipy\text{-}16})]_x$ (M = Pd^{2+}, x = 1; M = Zn^{2+}, x = 2) reveals that reducing the aliphatic chain density gives rise to higher transition temperatures. Although the only compound to have full mesophase characterisation is tc-$[Zn(L^{Dipy\text{-}16})]_2$, the columnar hexagonal character of the mesophase suggests that reducing the number of aliphatic chains from six to four per ligand does not preclude columnar mesophase formation.

Out of the three extended compounds under investigation, namely ex-$H_2L^{Dipy\text{-}16}$, ex-$[Zn(L^{Dipy\text{-}16})]_2$ and ex-$[Pd(L^{Dipy\text{-}16})]$, only ex-$[Pd(L^{Dipy\text{-}16})]$ had mesomorphic character. The complex did not generate banana mesophases, but formed a smectic A phase over a pronounced temperature range.

4.4 EXPERIMENTAL

NMR spectra were recorded on either a Bruker DPX300 FT-NMR spectrometer operating at 300.13 MHz for ^{1}H and 75.48 MHz for broadband proton decoupled ^{13}C, or a Jeol EX270 FT-NMR spectrometer operating at

270.17 MHz for ^{1}H and 67.93MHz for broadband proton decoupled ^{13}C. Chemical shifts are referenced with respect to residual proton and carbon solvent (with δ_H = 7.26 ppm and δ_C = 77.0 ppm for $CDCl_3$). IR spectra were obtained on a Nicolet AVATAR 360 FT-IR spectrometer as KBr pellets. FAB mass spectra were obtained on a Finnigan MAT TSQ-700 spectrometer at the University of Wales, Swansea, with 3-nitrobenzyl alcohol (NOBA) as matrix. MALDI-TOF mass spectra were obtained on a Voyager-DE-STR spectrometer at the University of Wales, Swansea, with *trans*-2-[3-(4-tert-butylphenyl)-2-methylprop-2-enylidene]malononitrile (DCTB) as matrix. EI and ES mass spectra were recorded by the Mass Spectrometry Service at the University of Nottingham. Elemental analyses (C, H, N) were carried out by the Analytical Department of the University of Nottingham.

Analysis by polarised optical microscopy was carried out using a Zeiss Labpol, or Olympus BH40 microscope equipped with a Link-Am HFS91 hot stage, TMS92 controller and LNP2 cooling unit. Analysis by DSC was carried out on either a Perkin-Elmer DSC7 instrument or a TA DSC 2920 instrument, using heating and cooling rates of either 5 or 10°C min^{-1}. For analysis by XRD the powdered sample was filled in Lindemann capillaries of 1mm diameter. A linear monochromatic Cu-K_α beam (λ = 1.5405Å) obtained with a sealed-tube generator (900W) and a bent quartz monochromator were used. The diffraction patterns were registered with a curved counter Inel CPS 120, for which the sample temperature was controlled within ± 0.05°C. Periodicidies up to 60Å could be measured. An X-ray pattern was recorded every 20°C for each compound from the crystalline state up to the isotropic liquid.

4.4.1 Synthesis of 5,5'-Dimethyldipyrromethane

Under an atmosphere of argon, trifluoroacetic acid (0.680g, 5.96mmol) was added to a solution of excess pyrrole (100g, 1.49mol) and acetone (3.46g, 0.0596mol). The solution was stirred for 5 mins and the reaction was quenched with 0.1M NaOH to give a basic solution. EtOAc (200cm^3) was added and the organic phase was washed with H_2O (3 x 100cm^3) and dried over $MgSO_4$. The solvent was removed *in vacuo* to give a brown oil. Distillation on the Kugelrohr gave a white, crystalline solid (4.35g, 41.9%). Microanalysis: Calculated for $C_{11}H_{14}N_2.0.1H_2O$ C 75.05, H 8.13, N 15.91; found C 74.61, H 8.10, N 16.08. ^{1}H-NMR (300.13MHz, $CDCl_3$, 298K): δ_H 7.60 (2H, br s, N<u>H</u>), 6.58 (2H, m, Ar<u>H</u>), 6.13 (4H, m, Ar<u>H</u>), 1.64 (6H, s, C<u>H</u>$_3$) ppm. ^{13}C-NMR (67.93MHz, $CDCl_3$, 298K): δ_C 139.4, 117.52, 108.0, 104.1, 35.4, 29.6 ppm. EI MS: m/z = 174 $(L)^+$.

4.4.2 Synthesis of 5,5'-Diformyl-2,2'-dimethyldipyrromethane

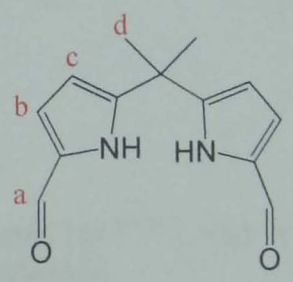

Figure 4.20. 5,5'-Diformyl-2,2'-dimethyldipyrromethane, with selected hydrogen atoms labelled a – d in reference to ^{1}H-NMR assignments.

A stirred solution of 5,5'-dimethyldipyrromethane (4.14g, 0.0238mol) in DMF (80cm^3) was degassed with Ar for 5 mins. The solution was cooled to 0°C then $POCl_3$ (4.45cm^3, 0.0476mol) was added dropwise. The orange/red solution was stirred at room temperature for 1 hour, over which time the solution became deep red. H_2O (60cm^3) was added and the reaction was quenched with 2M KOH until strongly basic. The resulting orange precipitate

was filtered off and washed with EtOH (3.94g, 71.9%). Microanalysis: Calculated for $C_{13}H_{14}N_2O_2$ C 67.81, H 6.13, N 12.17; found C 67.51, H 6.18, N 11.92. IR (KBr): ν = 2971m (N-H), 2820m (N-H), 1660vs (C=O), 1492s (C=C) cm^{-1}. ^{1}H-NMR (300.13MHz, $CDCl_3$, 298K): δ_H 10.54 (2H, br s, N<u>H</u>), 9.30 (2H, s, C<u>H</u>$_a$O), 6.87 (2H, dd, $^3J_{AM}$ = 3.90Hz, $^4J_{AX}$ = 1.5Hz, <u>H</u>$_b$), 6.23 (2H, dd, $^3J_{AM}$ = 3.90Hz, $^4J_{AX}$ = 1.34Hz, <u>H</u>$_c$), 1.75 (6H, s, <u>H</u>$_d$) ppm. ^{13}C-NMR (67.93MHz, $CDCl_3$, 298K): δ_C 179.4, 148.0, 132.5, 122.7, 108.3, 36.3, 28.1 ppm. ES MS: m/z = 231 $(L)^+$.

4.4.3 Synthesis of the Metal-Free Ligands, $H_2L^{Dipy\text{-}n}$

Similar preparations were used for all compounds, so one example of the free ligand preparation is given.

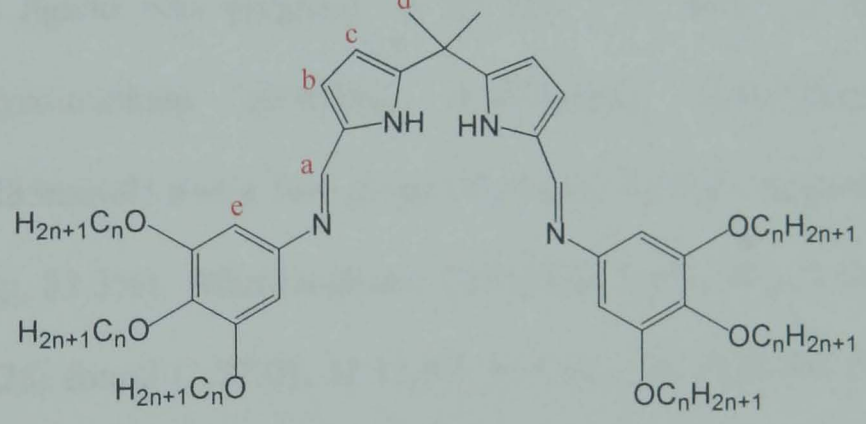

Figure 4.21. Structure of the ligands $H_2L^{Dipy\text{-}n}$, with selected hydrogen atoms labelled a-e in reference to the NMR spectral assignments.

4.4.3.1 Synthesis of $H_2L^{Dipy\text{-}1}$

3,4,5-Trimethoxyaniline (0.801g, 4.37mmol) in a solution of $CHCl_3$ (10cm^3) was added to 2,2'-diformyl-5,5'-dimethyldipyrromethane (0.504g, 2.19mmol) in warm MeOH (100cm^3). After the yellow/orange solution was stirred, a few drops of glacial AcOH were added and the solution was stirred at room temperature for 1h. The solvent volume was reduced *in vacuo*, resulting in the precipitation of a yellow solid, which was washed with Et_2O and dried.

The solid was recrystallised from $CHCl_3$ and EtOH (0.808g, 87.9%). Microanalysis: Calculated for $C_{31}H_{36}N_4O_6$ C 66.41, H 6.47, N 9.99; found C 66.30, H 6.42, N 10.17. IR (KBr pellet): ν = 2936m (C-H), 2827m (C-H), 1619s (C=N), 1589s (C=N), 1501s (C=C), 1484s (C=C), 1121s (C-O) cm^{-1}. ^{1}H-NMR (300.13MHz, $CDCl_3$, 298K): δ_H 8.16 (2H, s, $\underline{H}_aC$=N), 6.61 (2H, d, $^3J_{AX}$ = 3.86Hz, $\underline{H}_b$), 6.39 (4H, s, $\underline{H}_e$), 6.19 (2H, d, $^3J_{AX}$ = 3.70Hz, $\underline{H}_c$), 3.86 (12H, s, lateral OC$\underline{H}_3$), 3.84 (6H, s, central OC$\underline{H}_3$), 1.74 (6H, s, $\underline{H}_d$) ppm. ^{13}C-NMR (67.93MHz, $CDCl_3$, 298K): δ_C 153.5, 149.0, 147.6, 144.3, 136.0, 130.4, 117.4, 107.2, 98.0, 60.9, 56.0, 36.0, 28.6 ppm. ES MS: m/z = 561 $(H_2L^{Dipy\text{-}1})^+$.

4.4.3.2 Synthesis of $H_2L^{Dipy\text{-}10}$

This ligand was prepared as for $H_2L^{Dipy\text{-}1}$, from 2,2'-diformyl-5,5'-dimethyldipyrromethane (0.0326g, 0.142mmol), 3,4,5-tridecyloxyaniline (0.160g, 0.285mmol) and a few drops of glacial AcOH. Appearance: yellow solid (0.154g, 82.3%). Microanalysis: Calculated for $C_{85}H_{144}N_4O_6$ C 77.45, H 11.01, N 4.25; found C 77.01, H 11.59, N 4.22. IR (KBr pellet): ν = 2966s (C-H), 2929s (C-H), 1591s (C=N), 1505s (C=C), 1464s (C=C), 1116s (C-O) cm^{-1}. ^{1}H-NMR (300.13MHz, $CDCl_3$, 298K): δ_H 8.12 (2H, s, $\underline{H}_aC$=N), 6.59 (2H, br d, $\underline{H}_b$), 6.37 (4H, s, $\underline{H}_e$), 6.16 (2H, d, $^3J_{AX}$ = 3.53Hz, $\underline{H}_c$), 3.94 (12H, m, OC$\underline{H}_2$) , 1.81-1.26 (96H + 6H, m, C$\underline{H}_2$ + $\underline{H}_d$), 0.88 (18H, 2 overlapping triplets, C$\underline{H}_3$) ppm. MALDI-TOF MS: m/z = 1317 $(H_2L^{Dipy\text{-}10})^+$.

4.4.3.3 Synthesis of $H_2L^{Dipy-12}$

This compound was prepared as for H_2L^{Dipy-1}, from 2,2`-diformyl-5,5`-dimethyldipyrromethane (0.0818g, 0.355mmol), 3,4,5-tridodecyloxyaniline (0.459g, 0.710mmol) and a few drops of glacial AcOH. Appearance: beige/yellow solid (0.384g, 72.7%). Microanalysis: Calculated for $C_{97}H_{168}N_4O_6$ C 78.38, H 11.39, N 3.77; found C 78.19, H 11.65, N 3.58. IR (KBr pellet): ν = 2916vs (C-H), 2848vs (C-H), 1616m (C=N), 1528s (C=N), 1505m (C=C), 1486s (C=C), 1468s (C=C), 1117vs (C-O) cm^{-1}. ^{1}H-NMR (300.13MHz, $CDCl_3$, 298K): δ_H 8.12 (2H, s, $\underline{H}_aC$=N), 6.59(2H, br d, $\underline{H}_b$), 6.37 (4H, s, $\underline{H}_e$), 6.17 (2H, d, $^3J_{AX}$ = 3.35Hz, $\underline{H}_c$), 3.94 (12H, 2 overlapping triplets, O$C\underline{H}_2$), 1.83-1.25 (120H + 6H, m, $C\underline{H}_2$ + $\underline{H}_d$), 0.87 (18H, 2 overlapping triplets, CH_3) ppm. ^{13}C-NMR (75.48MHz, $CDCl_3$, 298K): δ_C 153.7, 148.6, 142.4, 136.3, 130.1, 117.5, 107.2, 99.4, 94.5, 73.5, 69.1, 36.5, 32.0, 30.0, 29.9, 29.8, 29.8, 29.5, 29.5, 29.5, 28.9, 26.4, 22.8, 14.2 ppm. MALDI-TOF MS: m/z = 1486 $(H_2L^{Dipy-12})^+$.

4.4.3.4 Synthesis of $H_2L^{Dipy-14}$

This compound was prepared as for H_2L^{Dipy-1}, from 2,2`-diformyl-5,5`-dimethyldipyrromethane (0.159g, 0.690mmol), 3,4,5-tritetradecyloxyaniline (1.00g, 1.37mmol) and a few drops of glacial AcOH. Appearance: Yellow solid (0.868g, 76.0%). Microanalysis: Calculated for $C_{109}H_{192}N_4O_6$ C 79.12, H 11.70, N 3.39; found C 78.77, H 11.86, N 3.63. IR (KBr pellet): ν = 2919vs (C-H), 2851vs (C-H), 1619m (C=N), 1584s (C=N), 1505w (C=C), 1486m (C=C), 1471s (C=C), 1118s (C-O) cm^{-1}. ^{1}H-NMR (300.13MHz, $CDCl_3$, 298K): δ_H 8.13 (2H, s, $\underline{H}_aC$=N), 6.57 (2H, d, $^3J_{AX}$ = 3.62Hz, $\underline{H}_b$), 6.36 (4H, s,

$\underline{H}_e$), 6.16 (2H, d, $^3J_{AX}$ = 3.65Hz, $\underline{H}_c$), 3.96 (12H, m, $OC\underline{H}_2$), 1.83-1.25 (144H, m, $C\underline{H}_2$), 174(6H, s, $\underline{H}_d$), 0.88 (18H, 2 overlapping triplets, $C\underline{H}_3$) ppm. ^{13}C-NMR (75.48MHz, $CDCl_3$, 298K): δ_C 153.5, 136.2, 115.4, 99.3, 73.5, 69.0, 31.9, 30.3, 29.7, 29.7, 29.4, 28.5, 26.1, 22.7, 14.1 ppm (four alkyl carbons obscured). MALDI-TOF MS: m/z = 1654 $(H_2L^{Dipy\text{-}14})^+$.

4.4.3.5 Synthesis of $H_2L^{Dipy\text{-}16}$

This compound was prepared as for $H_2L^{Dipy\text{-}1}$, from 2,2'-diformyl-5,5'-dimethyldipyrromethane (0.0760g, 0.330mmol), 3,4,5-trihexadecyloxyaniline (0.534g, 0.656mmol) and a few drops of glacial AcOH. Appearance: mustard yellow solid (0.400g, 66.5%). Microanalysis: Calculated for $C_{121}H_{216}N_4O_6$ C 79.72, H 11.94, N 3.07; found C 79.48, H 12.22, N 2.96. IR (KBr pellet): ν = 2919s (C-H), 2849s (C-H), 1615m (C=N), 1582s (C=N), 1505w (C=C), 1468m (C=C), 1417s (C=C), 1119s (C-O) cm^{-1}. ^{1}H-NMR (300.13MHz, $CDCl_3$, 298K): δ_H 8.13 (2H, s, $\underline{H}_aC$=N), 6.57 (2H, d, $^3J_{AX}$ = 3.52Hz, $\underline{H}_b$), 6.36 (4H, s, $\underline{H}_e$), 6.16 (2H, d, $^3J_{AX}$ = 3.63Hz, $\underline{H}_c$), 3.92 (12H, 2 overlapping triplets, $OC\underline{H}_2$), 1.80-1.25 (168H + 6H, m, $C\underline{H}_2$ + $\underline{H}_d$), 0.88 (18H, 2 overlapping triplets, $C\underline{H}_3$) ppm. ^{13}C-NMR (75.48MHz, $CDCl_3$, 298K): δ_C 153.7, 153.4, 148.2, 142.3, 136.3, 132.4, 108.0, 99.3, 94.4, 73.5, 68.9, 31.9, 30.3, 29.7, 29.4, 26.1, 22.7, 14.1 ppm (nine alkyl carbons obscured). MALDI-TOF MS: m/z = 1823 $(H_2L^{Dipy\text{-}16})^+$.

4.4.4 Synthesis of the Complexes, $[M(L^{Dipy\text{-}n})]$

Similar preparations were used for all compounds, so one example for each series of complexes is given.

4.4.4.1 Synthesis of $[Zn(L^{Dipy-1})]_2$

A methanolic ($5cm^3$) solution of $Zn(OAc)_2.2H_2O$ (0.0345g, 0.161mmol) was added to a solution of H_2L^{Dipy-1} (0.0847g, 0.151mmol) in CH_2Cl_2 ($20cm^3$). The orange solution was stirred for 30 mins. A few drops of NEt_3 were added and the solution was stirred for 24 hours. The solution was reduced in volume under vacuum and MeOH was added to precipitate yellow crystals, which were recrystallised from $CHCl_3$ and Et_2O (0.0799g, 84.8%). Microanalysis: Calculated for $C_{31}H_{34}N_4O_6Zn_1.CH_2Cl_2.H_2O$ C 53.02, H 5.23, N 7.73; found C 53.27, H 5.22, 7.80. IR (KBr pellet): ν = 2964w (C-H), 2934w (C-H), 1588s (C=N), 1557s (C=N), 1512s (C=C), 1495s (C=C), 1464m (C=C), 1127s (C-O) cm^{-1}. ^{1}H-NMR (300.13MHz, $CDCl_3$, 298K): δ_H 8.17 (2H, s, $\underline{H}_aC=N$), 6.66 (2H, d, $^3J_{AX}$ = 3.62Hz, $\underline{H}_b$), 6.17 (2H, d, $^3J_{AX}$ = 3.63Hz, $\underline{H}_c$), 6.09 (4H, s, $\underline{H}_e$), 3.74 (6H, s, central $OC\underline{H}_3$), 3.56 (12H, s, lateral $OC\underline{H}_3$) 1.62 (6H, s, $\underline{H}_d$) ppm. ^{13}C-NMR (75.48MHz, $CDCl_3$, 298K): δ_C 158.3, 153.4, 149.0, 141.9, 135.8, 135.3, 122.0, 111.8, 97.0, 60.9, 55.7, 39.3, 29.7 ppm. FAB (LSI)MS: m/z = 1248 $[Zn(L^{Dipy-1})]_2^+$.

4.4.4.2 Synthesis of $[Zn(L^{Dipy-10})]_2$

This compound was prepared as for $[Zn(L^{Dipy-1})]_2$, from $H_2L^{Dipy-10}$ (0.0896g, 0.0680mmol), $Zn(OAc)_2.2H_2O$ (0.0224g, 0.102mmol) and a few drops of NEt_3. Appearance: brown oil (0.0477g, 49.9%). Microanalysis: Calculated for $C_{85}H_{166}N_4O_6Zn_1.CHCl_3.H_2O$ C 67.03, H 11.05, N 3.64: found C 66.81, H 9.22, 3.09. IR (KBr liquid film): ν = 2922vs (C-H), 2853vs (C-H), 1586s (C=N), 1558s (C=N), 1511m (C=C), 1495m (C=C), 1471m (C=C), 1116m (C-O) cm^{-1}. ^{1}H-NMR (300.13MHz, $CDCl_3$, 298K): δ_H 8.10 (2H, s,

$\underline{H}_aC=N$), 6.58 (2H, d, $^3J_{AX}$ = 3.44Hz, $\underline{H}_b$), 6.09 (2H, d, $^3J_{AX}$ = 3.00Hz, $\underline{H}_c$), 6.04 (4H, s, $\underline{H}_e$), 3.89 (4H, t, $^3J_{AX}$ = 6.66Hz, central $OC\underline{H}_2$) , 3.59 (8H, t, $^3J_{AX}$ = 6.43Hz, lateral $OC\underline{H}_2$) 1.87-1.26 (96H + 6H, m, $C\underline{H}_2$ + $\underline{H}_d$), 0.88 (18H, 2 overlapping triplets, $C\underline{H}_3$) ppm. ^{13}C-NMR (75.48MHz, $CDCl_3$, 298K): δ_C 156.7, 153.2, 149.0, 141.5, 135.8, 135.4, 112.0, 107.4, 98.4, 73.4, 69.6, 31.9, 30.3, 29.7, 29.5, 29.3, 29.2, 28.1, 26.1, 25.8, 22.7, 14.1 ppm. MALDI-TOF MS: m/z = 2762 $[Zn(L^{Dipy\text{-}10})]_2^+$.

4.4.4.3 Synthesis of $[Zn(L^{Dipy\text{-}12})]_2$

This compound was prepared as for $[Zn(L^{Dipy\text{-}1})]_2$, from $H_2L^{Dipy\text{-}12}$ (0.0929g, 0.0635mmol), $Zn(OAc)_2.2H_2O$ (0.0154g, 0.0702mmol) and a few drops of NEt_3. Appearance: yellow solid (0.0922g, 95.2%). Microanalysis: Calculated for $C_{97}H_{166}N_4O_6Zn_1.0.5CHCl_3$ C 72.76, H 10.43, N 3.48; found C 72.23, H 10.51, N 3.58. IR (KBr pellet): ν = 2922vs (C-H), 2853vs (C-H), 1582m (C=N), 1556s (C=N), 1509m (C=C), 1492m (C=C), 1471m (C=C), 1116m (C-O) cm^{-1}. ^{1}H-NMR (300.13MHz, $CDCl_3$, 298K): δ_H 8.09 (2H, s, $\underline{H}_aC=N$), 6.58 (2H, d, $^3J_{AX}$ = 3.05Hz, $\underline{H}_b$), 6.09 (2H, d, $^3J_{AX}$ = 2.82Hz, $\underline{H}_c$), 6.04 (4H, s, $\underline{H}_e$), 3.82 (4H, t, $^3J_{AX}$ = 6.49Hz, central $OC\underline{H}_2$) , 3.59 (8H, t, $^3J_{AX}$ = 6.37Hz, lateral $OC\underline{H}_2$) 1.69-1.27 (120H + 6H, m, $C\underline{H}_2$ + $\underline{H}_d$), 0.88 (18H, 2 overlapping triplets, $C\underline{H}_3$) ppm. ^{13}C-NMR (67.93MHz, $CDCl_3$, 298K): δ_C 158.0, 153.3, 148.8, 141.6, 135.7, 135.4, 121.6, 111.6, 98.5, 73.5, 68.7, 39.2, 32.0, 30.3, 29.7, 29.5, 29.4, 29.3, 26.1, 22.7, 14.1 ppm (three alkyl carbons obscured). MALDI-TOF MS: m/z = 3099 $[Zn(L^{Dipy\text{-}12})]_2^+$.

4.4.4.4 Synthesis of $[Zn(L^{Dipy\text{-}14})]_2$

This compound was prepared as for $[Zn(L^{Dipy\text{-}1})]_2$, from $H_2L^{Dipy\text{-}14}$ (0.167g, 0.101mmol), $Zn(OAc)_2.2H_2O$ (0.0265g, 0.121mmol) and a few drops of NEt_3. Appearance: brown solid (0.138g, 79.5%). Microanalysis: Calculated for $C_{109}H_{190}N_4O_6Zn_1.CHCl_3.2H_2O$ C 70.52, H 10.49, N 2.99; found C 70.56, H 10.93, N 2.72. IR (KBr pellet): ν = 2925vs (C-H), 2852vs (C-H), 1580s (C=N), 1559s (C=N), 1511m (C=C), 1493m (C=C), 1468m (C=C), 1118vs (C-O) cm^{-1}. ^{1}H-NMR (300.13MHz, $CDCl_3$, 298K): δ_H 8.13 (2H, s, $\underline{H}_aC$=N), 6.58 (2H, d, $^3J_{AX}$ = 2.94Hz, $\underline{H}_b$), 6.16 (2H, d, $^3J_{AX}$ = 3.70Hz, $\underline{H}_c$), 6.03 (4H, s, $\underline{H}_e$), 3.90 (4H, m, central $OC\underline{H}_2$), 3.61 (8H, m, lateral $OC\underline{H}_2$), 1.75-1.26 (144H + 6H, m, $C\underline{H}_2$ + $\underline{H}_d$), 0.88 (18H, 2 overlapping triplets, $C\underline{H}_3$) ppm. ^{13}C-NMR (67.93MHz, $CDCl_3$, 298K): δ_C 158.0, 153.2, 148.8, 141.5, 135.8, 135.4 121.6, 111.5, 98.4, 73.4, 68.7, 39.2, 31.9, 30.3, 29.7, 29.5, 29.4, 26.1, 22.7, 14.1 ppm (six alkyl carbons obscured). MALDI-TOF MS: m/z = 3436 $[Zn(L^{Dipy\text{-}14})]_2^+$.

4.4.4.5 Synthesis of $[Zn(L^{Dipy\text{-}16})]_2$

This compound was prepared as for $[Zn(L^{Dipy\text{-}1})]_2$, from $H_2L^{Dipy\text{-}16}$ (0.108g, 0.0592mmol), $Zn(OAc)_2.2H_2O$ (0.0141g, 0.0643mmol) and a few drops of NEt_3. Appearance: yellow/brown solid (0.0930g, 83.3%). Microanalysis: Calculated for $C_{121}H_{214}N_4O_6Zn_1.H_2O$ C 76.31, H 11.43, N 2.94; found C 76.43, H 11.71, N 2.89. IR (KBr pellet): ν = 2911vs (C-H), 2850vs (C-H), 1593s (C=N), 1566m (C=N), 1507m (C=C), 1467s (C=C), 1119vs (C-O) cm^{-1}. ^{1}H-NMR (300.13MHz, $CDCl_3$, 298K): δ_H 8.09 (2H, s, $\underline{H}_aC$=N), 6.58 (2H, br d, $\underline{H}_b$), 6.09 (2H, br d, $\underline{H}_c$), 6.03 (4H, s, $\underline{H}_e$), 3.81 (4H, t, $^3J_{AX}$ = 6.48Hz, central $OC\underline{H}_2$), 3.59 (8H, t, $^3J_{AX}$ = 6.41Hz, lateral $OC\underline{H}_2$), 1.81-

1.24 (168H + 6H, m, C$\underline{H}_2$ + $\underline{H}_d$), 0.88 (18H, 2 overlapping triplets, C$\underline{H}_3$) ppm. ^{13}C-NMR (67.93MHz, $CDCl_3$, 298K): δ_C 153.2, 148.8, 141.5, 135.8, 135.4, 121.6, 111.4, 109.3, 98.4, 73.4, 68.6, 39.2, 31.9, 30.3, 30.1, 29.8, 29.7, 29.6, 29.5, 29.4, 26.1, 22.7, 14.1 ppm (five alkyl carbons obscured). MALDI-TOF MS: m/z = 3771 $[Zn(L^{Dipy\text{-}16})]_2^+$.

4.4.4.6 Synthesis of [Pd($L^{Dipy\text{-}1}$)]

To a solution of $H_2L^{Dipy\text{-}1}$ (0.104g, 0.185mmol) in CH_2Cl_2 (15cm^3) was added $Pd(OAc)_2$ (0.0416g, 0.185mmol) in CH_2Cl_2 (3cm^3). The yellow/orange solution was stirred for 30 mins. A few drops of NEt_3 were added and the solution became orange in colour. This was stirred for 24 hours. The solution was reduced in volume under vacuum and MeOH was added to precipitate the yellow product. The solid was recrystallised from $CHCl_3$ and EtOH (0.0824g, 67.2%). Microanalysis: Calculated for $C_{31}H_{34}N_4O_6Pd_1.H_2O$ C 54.51, H 5.31, N 8.20; found C 54.49, H 5.28, 8.48. IR (KBr pellet): ν = 2936w (C-H), 2833w (C-H), 1585s (C=N), 1505s (C=C), 1464m (C=C), 1418m (C=C), 1128s (C-O) cm^{-1}. ^{1}H-NMR (300.13MHz, $CDCl_3$, 298K): δ_H 7.61 (2H, s, $\underline{H}_aC$=N), 6.93 (2H, d, $^3J_{AX}$ = 3.97Hz, $\underline{H}_b$), 6.33 (2H, d, $^3J_{AX}$ = 3.98Hz, $\underline{H}_c$), 6.15 (4H, s, $\underline{H}_e$), 3.80 (6H, s, central OC$\underline{H}_3$) , 3.64 (12H, s, lateral OC$\underline{H}_3$) 1.69 (6H, s, $\underline{H}_d$) ppm. ^{13}C-NMR (75.48MHz, $CDCl_3$, 298K): δ_C 158.5, 153.0, 152.4, 145.7, 136.3, 135.9, 119.5, 108.2, 99.7, 60.8, 55.6, 43.1, 32.1 ppm. FAB (LSI)MS: m/z = 664 $[Pd(L^{Dipy\text{-}1})]^+$.

4.4.4.7 Synthesis of [Pd($L^{Dipy-10}$)]

This compound was prepared as for [Pd(L^{Dipy-1})], from $H_2L^{Dipy-10}$ (0.311g, 0.236mmol), $Pd(OAc)_2$ (0.0534g, 0.238mmol) and a few drops of NEt_3. Appearance: yellow solid (0.311g, 92.6%). Microanalysis: Calculated for $C_{85}H_{142}N_4O_6Pd_1.H_2O$ C 70.87, H 10.08, N 3.89; found C 70.36, H 9.60, N 3.72. IR (KBr pellet): ν = 2920s (C-H), 1589s (C=N), 1505s (C=C), 1471s (C=C), 1435s (C=C), 1118s (C-O) cm^{-1}. ^{1}H-NMR (300.13MHz, $CDCl_3$, 298K): δ_H 7.58 (2H, s, $\underline{H}_aC$=N), 6.89 (2H, d, $^3J_{AX}$ = 3.91Hz, $\underline{H}_b$), 6.30 (2H, d, $^3J_{AX}$ = 3.93Hz, $\underline{H}_c$), 6.08 (4H, s, $\underline{H}_e$), 3.83 (4H, t, $^3J_{AX}$ = 6.45Hz, central O$C\underline{H}_2$), 3.63 (8H, t, $^3J_{AX}$ = 6.51Hz, lateral O$C\underline{H}_2$) 1.74-1.28 (96H + 6H, m, $C\underline{H}_2$ + $\underline{H}_d$), 0.88 (18H, overlapping triplets, $C\underline{H}_3$) ppm. ^{13}C-NMR (75.48MHz, $CDCl_3$, 298K): δ_C 158.4, 152.9, 152.0, 145.0, 136.3, 136.1, 119.0, 107.8, 100.4, 73.4, 68.5, 43.0, 32.0, 30.6, 29.9, 29.7, 29.5, 29.4, 26.3, 26.2, 22.7, 14.1 ppm. MALDI-TOF MS: m/z = 1421 [Pd($L^{Dipy-10}$)]$^+$.

4.4.4.8 Synthesis of [Pd($L^{Dipy-12}$)]

This compound was prepared as for [Pd(L^{Dipy-1})], from $H_2L^{Dipy-12}$ (0.103g, 0.0693mmol), $Pd(OAc)_2$ (0.0169g, 0.0753mmol) and a few drops of NEt_3. Appearance: sticky brown solid (0.109g, 98.9%). Microanalysis: Calculated for $C_{97}H_{166}N_4O_6Pd_1.CHCl_3.H_2O$ C 68.11, H 9.86, N 3.24: found C 68.07, H 10.43, N 3.63. IR (KBr pellet): ν = 2922s (C-H), 1586m (C=N), 1505m (C=C), 1468m (C=C), 1432m (C=C), 1116s (C-O) cm^{-1}. ^{1}H-NMR (300.13MHz, $CDCl_3$, 298K): δ_H 7.58 (2H, s, $\underline{H}_aC$=N), 6.89 (2H, d, $^3J_{AX}$ = 3.66Hz, $\underline{H}_b$), 6.30 (2H, d, $^3J_{AX}$ = 3.90Hz, $\underline{H}_c$), 6.08 (4H, s, $\underline{H}_e$), 3.85 (4H, t, $^3J_{AX}$ = 6.41Hz, central O$C\underline{H}_2$), 3.63 (8H, t, $^3J_{AX}$ = 6.61Hz, lateral O$C\underline{H}_2$) 1.71-1.27

(120H + 6H, m, $C\underline{H}_2$ + $\underline{H}_d$), 0.88 (18H, overlapping triplets. $C\underline{H}_3$) ppm. ^{13}C-NMR (75.48MHz, $CDCl_3$, 298K): δ_C 158.4, 152.8, 152.0, 144.9, 136.2, 136.0, 119.0, 107.8, 100.3, 73.3, 68.4, 42.8, 32.1, 32.0, 31.8, 30.5, 29.6, 29.3, 26.2, 26.1, 22.6, 22.5, 14.0 ppm. MALDI-TOF MS: m/z = 1589 $[Pd(L^{Dipy\text{-}12})]^+$.

4.4.4.9 Synthesis of $[Pd(L^{Dipy\text{-}14})]$

This compound was prepared as for $[Pd(L^{Dipy\text{-}1})]$, from $H_2L^{Dipy\text{-}14}$ (0.103g, 0.0622mmol), $Pd(OAc)_2$ (0.0148g, 0.0659mmol) and a few drops of NEt_3. Appearance: brown solid (0.107g, 97.8%). Microanalysis: Calculated for $C_{109}H_{190}N_4O_6Pd_1.H_2O$ C 73.67, H 10.89, N 3.15; found C 73.45, H 10.78, N 3.13. IR (KBr pellet): ν = 2911vs (C-H), 2849vs (C-H), 1586s (C=N), 1502m (C=C), 1468m (C=C), 1468m (C=C), 1120s (C-O) cm^{-1}. ^{1}H-NMR (300.13MHz, $CDCl_3$, 298K): δ_H 7.58 (2H, s, $\underline{H}_aC$=N), 6.89 (2H, d, $^3J_{AX}$ = 3.95Hz, $\underline{H}_b$), 6.30 (2H, d, $^3J_{AX}$ = 3.95Hz, $\underline{H}_c$), 6.08 (4H, s, $\underline{H}_e$), 3.83 (4H, t, $^3J_{AX}$ = 6.36Hz, central $OC\underline{H}_2$), 3.63 (8H, t, $^3J_{AX}$ = 6.49Hz, lateral $OC\underline{H}_2$) 1.68-1.26 (144H + 6H, m, $C\underline{H}_2$ + $\underline{H}_d$), 0.88 (18H, overlapping triplets, $C\underline{H}_3$) ppm. ^{13}C-NMR (67.93MHz, $CDCl_3$, 298K): δ_C 158.5, 153.0, 152.2, 145.1, 136.4, 136.2, 119.1, 107.9, 100.5, 73.5, 68.7, 43.0, 32.2, 31.9, 30.9, 30.6, 29.9, 29.8, 29.7, 29.6, 29.5, 29.4, 29.2, 26.3, 22.8, 14.2 ppm. MALDI-TOF MS: m/z = 1758 $[Pd(L^{Dipy\text{-}14})]^+$.

4.4.4.10 Synthesis of $[Pd(L^{Dipy\text{-}16})]$

This compound was prepared as for $[Pd(L^{Dipy\text{-}1})]$, from $H_2L^{Dipy\text{-}16}$ (0.196g, 0.107mmol), $Pd(OAc)_2$ (0.0251g, 0.112mmol) and a few drops of NEt_3. Appearance: yellow solid (0.191g, 92.7%). Microanalysis: Calculated

for $C_{121}H_{214}N_4O_6Pd_1.H_2O$ C 74.70, H 11.19, N 2.88; found C 74.73, H 11.40, N 2.77. IR (KBr pellet): ν = 2919vs (C-H), 2850vs (C-H), 1585m (C=N), 1561s (C=N), 1502s (C=C), 1468s (C=C), 1432m (C=C), 1120s (C-O) cm^{-1}. ^{1}H-NMR (300.13MHz, $CDCl_3$, 298K): δ_H 7.58 (2H, s, $\underline{H}_aC$=N), 6.89 (2H, d, $^3J_{AX}$ = 3.91Hz, $\underline{H}_b$), 6.30 (2H, d, $^3J_{AX}$ = 3.93Hz, $\underline{H}_c$), 6.07 (4H, s, $\underline{H}_e$), 3.83 (4H, t, $^3J_{AX}$ = 6.49Hz, central $OC\underline{H}_2$), 3.62 (8H, t, $^3J_{AX}$ = 6.34Hz, lateral $OC\underline{H}_2$) 1.71-1.26 (168H, m, $C\underline{H}_2$), 1.57 (6H, s, $\underline{H}_d$), 0.88 (18H, overlapping triplets, $C\underline{H}_3$) ppm. ^{13}C-NMR (75.48MHz, $CDCl_3$, 298K): δ_C 158.9, 152.9, 152.1, 145.0, 136.3, 136.1, 119.0, 107.8, 100.5, 73.4, 68.6, 43.0, 32.2, 31.9, 30.9, 30.6, 29.8, 29.3, 26.3, 26.2, 22.7, 14.1 ppm (six alkyl carbons obscured). MALDI-TOF MS: m/z = 1926 $[Pd(L^{Dipy\text{-}16})]^+$.

4.4.5 Synthesis of the Tetracatenar Free Ligands, tc-$H_2L^{Dipy\text{-}n}$

Similar preparations were used for both ligands, so one synthetic procedure is given.

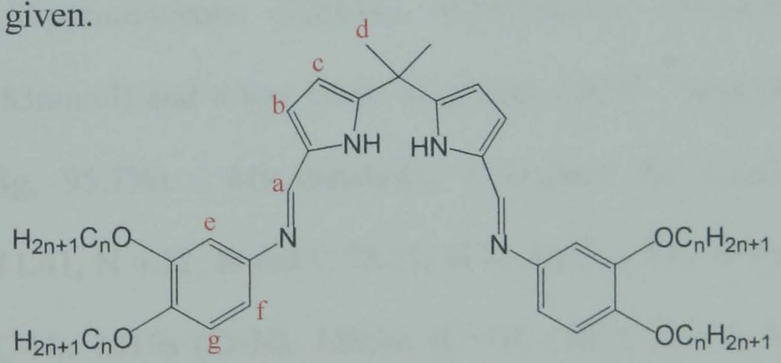

Figure 4.22. Structure of the ligands tc-$H_2L^{Dipy\text{-}n}$, with selected hydrogen atoms labelled a-g in reference to the NMR spectral assignments.

4.4.5.1 Synthesis of tc-$H_2L^{Dipy\text{-}1}$

To a warm, methanolic ($75cm^3$) solution of 2,2'-diformyl-5,5'-dimethyldipyrromethane (0.309g, 1.34mmol) was added 3,4-dimethoxyaniline (0.416g, 2.72mmol) in $CHCl_3$ ($20cm^3$). A few drops of glacial AcOH were added and the orange/brown solution was stirred for 1 hour and left to stand for

a further 18 hours. The resulting yellow precipitate was collected and recrystallised from EtOH and $CHCl_3$ (0.496g, 73.9%). Microanalysis: Calculated for $C_{29}H_{32}N_4O_4.CHCl_3.H_2O$ C 56.48, H 5.53, N 8.78: found C 56.66, H 5.27, N 8.78. IR (KBr pellet): ν = 2964w (C-H), 2836w (C-H), 1620s (C=N), 1589s (C=N), 1507s (C=C), 1480s (C=C), 1441s (C=C), 1127s (C-O) cm^{-1}. ^{1}H-NMR (300.13MHz, $CDCl_3$, 298K): δ_H 8.16 (2H, s, $\underline{H}_aC$=N), 6.84 (2H, d, $^3J_{AB}$ = 8.35Hz, $\underline{H}_g$), 6.76(4H, m, $\underline{H}_e$ + $\underline{H}_f$), 6.57 (2H, d, $^3J_{AX}$ = 3.67Hz, $\underline{H}_b$), 6.15 (2H, d, $^3J_{AX}$ = 3.69Hz, $\underline{H}_c$), 4.77 (2H, br s, N$\underline{H}$), 3.87 (12H, s, OC$\underline{H}_3$), 1.76 (6H, s, $\underline{H}_d$) ppm. ^{13}C-NMR (75.48MHz, $CDCl_3$, 298K): δ_C 149.3, 148.3, 147.2, 144.9, 144.1, 130.2, 117.0, 112.0, 111.5, 106.8, 105.0, 56.0, 55.8, 35.9, 28.4 ppm. ES MS: m/z = 501 $(tc\text{-}H_2L^{Dipy\text{-}1})^+$.

4.4.5.2 Synthesis of tc-$H_2L^{Dipy\text{-}16}$

This compound was prepared as for tc-$H_2L^{Dipy\text{-}1}$, from 2,2'-diformyl-5,5'-dimethyldipyrromethane (0.0444g, 0.193mmol), 3,4-didecyloxyaniline (0.220g, 0.383mmol) and a few drops of glacial AcOH. Appearance: yellow solid (0.248g, 95.7%). Microanalysis: Calculated for $C_{89}H_{152}N_4O_4.H_2O$ C 78.59, H 11.41, N 4.12; found C 78.41, H 11.40, N 4.38. IR (KBr pellet): ν = 2844vs (C-H), 1619s (C=N), 1589m (C=N), 1512s (C=C), 1486s (C=C), 1467s (C=C), 1131s (C-O) cm^{-1}. ^{1}H-NMR (300.13MHz, $CDCl_3$, 298K): δ_H 8.15 (2H, s, $\underline{H}_aC$=N), 6.84 (2H, d, $^3J_{AB}$ = 8.50Hz, $\underline{H}_g$), 6.72 (4H, m, $\underline{H}_e$ + $\underline{H}_f$), 6.55 (2H, d, $^3J_{AX}$ = 3.62Hz, $\underline{H}_b$), 6.15 (2H, d, $^3J_{AX}$ = 3.64Hz, $\underline{H}_c$), 3.99 (8H, m, OC$\underline{H}_2$), 1.83 – 1.25 (112H + 6H, m, C$\underline{H}_2$ + $\underline{H}_d$), 0.88 (12H, overlapping triplets, C$\underline{H}_3$) ppm. ^{13}C-NMR (75.48MHz, $CDCl_3$, 298K): δ_C 149.7 148.0, 147.3, 144.9, 144.2, 130.3, 117.0, 114.5, 112.5, 107.2, 102.7, 69.7, 69.1, 36.0,

31.9, 29.7, 29.6, 29.4, 29.3, 28.5, 26.0, 22.7, 14.1 ppm (seven alkyl carbons obscured). ES MS: m/z = 1343 $(tc\text{-}H_2L^{Dipy\text{-}16} + H)^+$.

4.4.6 Synthesis of the Tetracatenar Complexes, tc- $[M(L^{Dipy\text{-}n})]_x$

Similar preparations were used for all complexes, so one synthetic procedure is given.

4.4.6.1 Synthesis of tc-$[Zn(L^{Dipy\text{-}1})]_2$

A solution of $Zn(OAc)_2.2H_2O$ (0.0520g, 0.237mmol) in MeOH ($10cm^3$) was added to a solution of $tc\text{-}H_2L^{Dipy\text{-}1}$ (0.119g, 0.238mmol) in CH_2Cl_2 ($20cm^3$). A few drops of NEt_3 were added and the yellow solution was stirred for 18 hours at room temperature. Slow evaporation of the mother liquor resulted in the precipitation of a yellow solid. This was recrystallised from $CHCl_3$ and EtOH (0.0806g, 60.3%). Microanalysis: Calculated for $[C_{29}H_{30}N_4O_4Zn_1]_2.CH_2Cl_2.H_2O$ C 57.57, H 5.24, N 9.10: found C 57.58, H 5.18, N 9.06. IR (KBr pellet): ν = 2964w (C-H), 2931w (C-H), 1609s (C=N), 1580s (C=N), 1521br,s (C=C), 1466s (C=C), 1050s (C-O) cm^{-1}. ^{1}H-NMR (300.13MHz, $CDCl_3$, 298K): δ_H 8.16 (2H, s, $\underline{H}_aC$=N), 6.67 (2H, d, $^3J_{AB}$ = 8.70Hz, $\underline{H}_g$), 6.59 (4H, m, $\underline{H}_e$ + $\underline{H}_f$), 6.23 (2H, d, $^3J_{AB}$ = 2.40Hz, $\underline{H}_b$), 6.13 (2H, d, $^3J_{AB}$ = 2.40Hz, $\underline{H}_c$), 3.89 (6H, s, $OC\underline{H}_3$), 3.43 (6H, s, $OC\underline{H}_3$), 1.60 (6H, s, $\underline{H}_d$) ppm. ^{13}C-NMR (75.48MHz, $CDCl_3$, 298K): δ_C 157.9, 149.1, 146.2, 140.1, 135.9, 121.3, 111.3, 108.7, 106.1, 56.0, 55.3, 39.2, 29.8 ppm. MALDI-TOF MS: m/z = 1128 $(tc\text{-}[ZnL^{Dipy\text{-}1}]_2)^+$.

4.4.6.2 Synthesis of tc-[Zn($L^{Dipy-16}$)]$_2$

This compound was prepared as for tc-[Zn(L^{Dipy-1})]$_2$, from tc-$H_2L^{Dipy-16}$ (0.105g, 0.0782mmol), $Zn(OAc)_2$ (0.0215g, 0.0979mmol) and a few drops of NEt_3. Appearance: yellow solid (0.0992g, 90.2%). Microanalysis: Calculated for $C_{89}H_{150}N_4O_4Zn_1.H_2O$ C 75.09, H 10.76, N 3.94; found C 75.34, H 10.91, N 4.05. IR (KBr pellet): ν = 2916vs (C-H), 2850vs (C-H), 1606m (C=N), 1576s (C=C), 1517s (C=C), 1468s (C=C), 1051s (C-O) cm^{-1}. ^{1}H-NMR (300.13MHz, $CDCl_3$, 298K): δ_H 8.10 (2H, s, $\underline{H}_aC$=N), 6.66 (2H, d, $^3J_{AB}$ = 8.72Hz, $\underline{H}_g$), 6.53 (4H, m, $\underline{H}_e$ + $\underline{H}_f$), 6.20 (2H, d, $^3J_{AB}$ = 2.37Hz, $\underline{H}_b$), 6.10 (2H, d, $^3J_{AB}$ = 3.35, $\underline{H}_c$), 3.87 (4H, t, $^3J_{AX}$ = 6.69Hz, O$\underline{CH}_2$), 3.42 (4H, t, $^3J_{AX}$ = 6.56Hz, O$\underline{CH}_2$), 1.75 – 1.26 (112H + 6H, m, $C\underline{H}_2$ + $\underline{H}_d$), 0.88 (12H, 2 overlapping triplets, $C\underline{H}_3$) ppm. ^{13}C-NMR (75.48MHz, $CDCl_3$, 298K): δ_C 158.1, 152.2, 149.1, 146.0, 140.1, 135.9, 121.1, 114.3, 111.1, 108.6, 107.9, 69.8, 67.8, 39.3, 32.0, 29.9, 29.8, 29.7, 29.6, 29.5, 29.2, 26.1, 22.8, 14.2 ppm (six alkyl carbons obscured). MALDI-TOF MS: m/z =2811 (tc-[Zn$L^{Dipy-16}$]$_2$)$^+$.

4.4.6.3 Synthesis of tc-[Pd(L^{Dipy-1})]

$Pd(OAc)_2$ (0.0458g, 0.204mmol) in CH_2Cl_2 (10cm^3) was added to a solution of tc-H_2L^{Dipy-1} (0.101g, 0.202mmol) in CH_2Cl_2 (20cm^3). A few drops of NEt_3 were added and the orange solution was stirred for 18 hours. Slow evaporation of the mother liquor resulted in the precipitation of orange microcrystals, which were recrystallised from $CHCl_3$ and EtOH (0.0650g, 53.2%). Microanalysis: Calculated for $C_{29}H_{30}N_4O_4Pd_1.CHCl_3$ C 49.74, H 4.31, N 7.73; found C 50.12, H 4.78, N 8.01. IR (KBr pellet): ν = 2961w (C-H), 2931w (C-H), 1592m (C=N), 1557s (C=N), 1506s (C=C), 1463m

(C=C), 1437m (C=C), 1083s (C-O) cm^{-1}. ^{1}H-NMR (300.13MHz, $CDCl_3$, 298K): δ_H 7.58 (2H, s, $\underline{H}_aC=N$), 6.90 (2H, d, $^3J_{AX}$ = 3.90Hz, $\underline{H}_b$), 6.48 (2H, d, $^3J_{AB}$ = 8.40Hz, $\underline{H}_g$), 6.41 (2H, dd, $^3J_{AB}$ = 8.40Hz, $^4J_{AM}$ = 2.40Hz, $\underline{H}_f$), 6.32 (4H, overlapping doublets, $\underline{H}_e$ + $\underline{H}_c$), 3.81 (6H, s, $OC\underline{H}_3$), 3.60 (6H, s, $OC\underline{H}_3$), 1.70 (6H, s, $\underline{H}_d$) ppm. ^{13}C-NMR (75.48MHz, $CDCl_3$, 298K): δ_C 158.1, 152.1, 148.8, 147.0, 143.1, 136.2, 118.9, 113.5, 110.9, 107.7, 106.4, 56.1, 55.4, 43.1, 32.2ppm. MALDI-TOF MS: m/z = 604 (tc-[$PdL^{Dipy\text{-}1}$])$^+$.

4.4.6.4 Synthesis of tc-[Pd($L^{Dipy\text{-}16}$)]

This compound was prepared as for tc-[Pd($L^{Dipy\text{-}1}$)], from tc-$H_2L^{Dipy\text{-}16}$ (0.306g, 0.228mmol), $Pd(OAc)_2$ (0.0531g, 0.237mmol) and a few drops of NEt_3. Appearance: yellow solid (0.296g, 89.9%). Microanalysis: Calculated for $C_{89}H_{150}N_4O_4Pd_1$ C 73.89, H 10.45, N 3.87; found C 73.52, H 10.52, N 3.86. IR (KBr pellet): ν = 2925s (C-H), 2850s (C-H), 1589w (C=N), 1564s (C=N), 1515s (C=C), 1471m (C=C), 1422w (C=C), 1134s (C-O) cm^{-1}. ^{1}H-NMR (300.13MHz, $CDCl_3$, 298K): δ_H 7.56 (2H, s, $\underline{H}_aC=N$), 6.88 (2H, d, $^3J_{AX}$ = 3.90Hz, $\underline{H}_b$), 6.46 (2H, d, $^3J_{AB}$ = 8.32Hz, $\underline{H}_g$), 6.36 (2H, dd, $^3J_{AB}$ = 8.39Hz, $^4J_{AM}$ = 2.13Hz, $\underline{H}_f$), 6.31 (4H, overlapping doublets, $\underline{H}_e$ + $\underline{H}_c$), 3.87 (4H, t, $^3J_{AX}$ = 6.59Hz, $OC\underline{H}_2$), 3.58 (4H, t, $^3J_{AX}$ = 6.67Hz, $OC\underline{H}_2$), 1.76 (6H, s, $\underline{H}_d$), 1.56 – 1.26 (112H, m, $C\underline{H}_2$), 0.88 (12H, 2 overlapping triplets, $C\underline{H}_3$) ppm. ^{13}C-NMR (75.48MHz, $CDCl_3$, 298K): δ_C 158.3, 152.0, 149.4, 147.1, 143.5, 136.4, 118.8, 113.1, 113.7, 108.2, 107.7, 70.0, 68.5, 43.1, 32.2, 31.9, 29.8, 29.7, 29.5, 29.4, 29.3, 26.2, 26.1, 22.6, 14.1 ppm (five alkyl carbons obscured). MALDI-TOF MS: m/z = 1447 (tc-[$PdL^{Dipy\text{-}16}$])$^+$.

4.4.7 Synthesis of the Extended Dipyrrole Ligands, ex-$H_2L^{Dipy\text{-}n}$

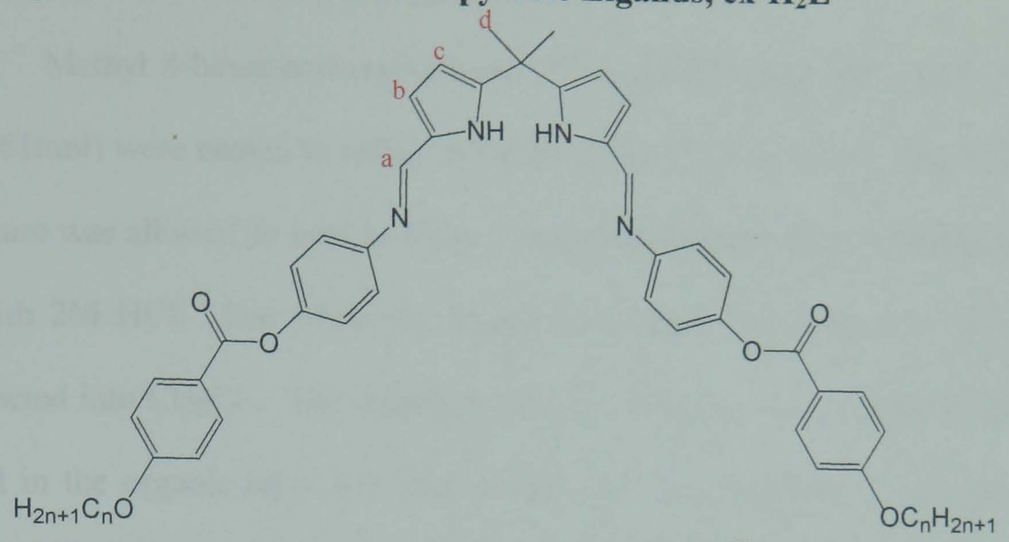

Figure 4.23. Structure of the extended dipyrrole ligands, ex-$H_2L^{Dipy\text{-}n}$, with selected hydrogen atoms labelled a-d in reference to the NMR spectral assignments.

4.4.7.1 Synthesis of Methyl 4-Hexadecyloxybenzoate

Under an atmosphere of N_2, 1-bromohexadecane (10.1g, 0.0331mol), excess Cs_2CO_3 (11.7g, 0.0359mol) and a few drops of Aliquat 336 were added to methyl 4-hydroxybenzoate (5.04g, 0.0331mol) in CH_3CN ($100cm^3$) and heated to reflux for 24 hours. CH_2Cl_2 ($100cm^3$) was added and the salt was removed by filtration. The organic solution was reduced in volume *in vacuo* to give a white solid (11.2g, 89.8%). Microanalysis: Calculated for $C_{24}H_{40}O_3$ C 76.55, H 10.71, N 0.00; found C 76.13, H 10.48, N 0.00. IR (KBr pellet): υ = 2910vs (C-H), 1719s (C=O), 1610s (C=C), 1511s (C=C), 1107s (C-O) cm^{-1}. ^{1}H-NMR (300.13MHz, $CDCl_3$, 298K): δ_H 7.98 (2H, d, $J_{AA'XX'}$ = 8.93Hz, *o*-$\underline{H}ArCO_2Me$), 6.90 (2H, d, $J_{AA'XX'}$ = 8.94Hz, *m*-$\underline{H}ArCO_2Me$), 4.00 (2H, t, $^3J_{AX}$ = 6.56Hz, $OC\underline{H}_2$), 3.88 (3H, s, $OC\underline{H}_3$), 1.80 (2H, m, $OCH_2C\underline{H}_2$-), 1.56-1.25 (28H, m, $C\underline{H}_2$), 0.88 (3H, t, $^3J_{AX_2}$ = 6.68Hz, $C\underline{H}_3$) ppm. ^{13}C-NMR (75.48MHz, $CDCl_3$, 298K): δ_C 166.8, 162.9, 131.5, 122.2, 113.9, 68.1, 51.7, 31.9, 29.6, 29.5, 29.3, 29.1, 25.9, 22.6, 14.1 ppm (seven alkyl carbons obscured). CI MS: m/z = 376 $(L)^+$.

4.4.7.2 Synthesis of 4-Hexadecyloxybenzoic Acid

Methyl 4-hexadecyloxybenzoate (10.4g, 0.0276mol) and KOH (31.5g, 0.0561mol) were heated to reflux in EtOH (250cm^3) for 2 hours. The reaction mixture was allowed to cool to room temperature and was then acidified to pH 1 with 2M HCl. The white precipitate was filtered off, added to H_2O and extracted into CH_2Cl_2. The organic and aqueous layers were separated and the solid in the organic layer was filtered off and washed with Et_2O to give the white solid 4-hexadecyloxybenzoic acid (9.83g, 98.2%). Microanalysis: Calculated for $C_{23}H_{38}O_3.CH_2Cl_2.H_2O$ C 61.93, H 9.09, N 0.00; found C 62.06, H 8.54, N 0.00. IR (KBr pellet): υ = 2999br,s (O-H), 2817br,vs (C-H), 1693vs (C=O), 1613s (C=C), 1599s (C=C), 1577s (C=C), 1108s (C-O) cm^{-1}. ^{1}H-NMR (300.13MHz, $CDCl_3$, 298K): δ_H 8.04 (2H, d, $J_{AA'XX'}$ = 8.84Hz, *o*-HArCO$_2$Me), 6.93 (2H, d, $J_{AA'XX'}$ = 8.92Hz, *m*-HArCO$_2$Me), 4.02 (2H, t, $^3J_{AX}$ = 6.55Hz, OCH$_2$), 1.80 (2H, m, OCH$_2$CH$_2$-), 1.46-1.25 (28H, m, CH$_2$), 0.88 (3H, t, $^3J_{AX}$ = 6.66Hz, CH$_3$) ppm. EI MS m/z = 362 (L)$^+$.

4.4.7.3 Synthesis of (4-(Methoxy)benzoyl)oxy)-4-Nitrobenzene

Under an atmosphere of N_2, *p*-anisic acid (2.76g, 0.0181mol) was added to a solution of 4-nitrophenol (2.52g, 0.0181mol), DCC (3.73g, 0.0181mol) and DMAP (0.220g, 1.81mmol) in CH_2Cl_2 (150cm^3) and stirred for 19 hours. The solid was removed by filtration and the yellow filtrate was reduced *in vacuo* to a yellow solid. This was recrystallised from hot EtOH to give an off-white solid (4.02g, 81.3%). Microanalysis: Calculated for $C_{14}H_{11}N_1O_5$ C 61.54, H 4.06, N 5.13; found C 61.55, H 4.07, N 4.89. IR (KBr pellet): υ = 2849w (C-H), 1730s (C=O), 1616s (C=C), 1591s (C=C), 1510m

($C\text{-}NO_2$), 1351s ($C\text{-}NO_2$), 1111s (C-O) cm^{-1}. ^{1}H-NMR (300.13MHz, $CDCl_3$, 298K): δ_H 8.32 (2H, d, $J_{AA'XX'}$ = 9.13Hz, *o*-$\underline{H}ArNO_2$), 8.15 (2H, d, $J_{AA'XX'}$ = 8.95Hz, *o*-$\underline{H}ArCO_2$-), 7.41 (2H, d, $J_{AA'XX'}$ = 9.14Hz, *m*-$\underline{H}ArNO_2$), 7.01 (2H, d, $J_{AA'XX'}$ = 8.96Hz, *m*-$\underline{H}ArCO_2$-), 3.91 (3H, s, $OC\underline{H}_3$) ppm. ^{13}C-NMR (75.48MHz, $CDCl_3$, 298K): δ_C 164.4, 163.9, 155.9, 145.2, 132.5, 125.2, 122.6, 120.6, 114.0, 55.6 ppm. CI MS: m/z = 274 $(L)^+$.

4.4.7.4 Synthesis of (4-(Hexadecyloxy)benzoyl)oxy)-4-Nitrobenzene

4-Hexadecyloxybenzoic acid (3.03g, 8.36mmol) was added to a solution of 4-nitrophenol (1.16g, 8.36mmol), DCC (1.72g, 8.34mmol) and DMAP (0.02g, 0.164mmol) in CH_2Cl_2 (200cm^3) under an atmosphere of N_2. This was stirred for 19 hours then filtered. The filtrate was reduced *in vacuo*, giving a light yellow solid, which was washed with MeOH and dried (3.05g, 75.4%). Microanalysis: Calculated for $C_{29}H_{41}N_1O_5.0.5H_2O$ C 70.70, H 8.59, N 2.84; found C 71.13, H 8.42, N 3.00. IR (KBr pellet): υ = 2935vs (C-H), 2846vs (C-H), 1720s (C=O), 1626s (C=C), 1597s (C=C), 1577s (C=C), 1515m ($C\text{-}NO_2$), 1347s ($C\text{-}NO_2$), 1175s (C-O) cm^{-1}. ^{1}H-NMR (300.13MHz, $CDCl_3$, 298K): δ_H 8.31 (2H, d, $J_{AA'XX'}$ = 9.02Hz, *o*-$\underline{H}ArNO_2$), 8.13 (2H, d, $J_{AA'XX'}$ = 8.85Hz, *o*-$\underline{H}ArCO_2$-), 7.40 (2H, d, $J_{AA'XX'}$ = 9.05Hz, *m*-$\underline{H}ArNO_2$), 6.98 (2H, d, $J_{AA'XX'}$ = 8.89Hz, *m*-$\underline{H}ArCO_2$-), 4.05 (2H, t, $^3J_{AX}$ = 6.55Hz, $OC\underline{H}_2$), 1.85-1.25 (28H, m, $C\underline{H}_2$), 0.87 (3H, t, $^3J_{AX}$ = 6.66Hz, $C\underline{H}_3$) ppm. ^{13}C-NMR (75.48MHz, $CDCl_3$, 298K): δ_C 163.8, 155.9, 145.1, 132.4, 126.0, 125.1, 122.6, 120.2, 114.4, 68.3, 33.8, 31.9, 29.6, 29.5, 29.3, 29.0, 25.9, 24.8, 22.6, 14.0 ppm (five alkyl carbons obscured). CI MS: expected ions not observed.

4.4.7.5 Synthesis of ((4-(Methoxy)benzoyl)oxy-4-Aniline

Under an atmosphere of Ar, $SnCl_2.2H_2O$ (14.04g, 0.0621mol) was added to a suspension of (4-(methoxy)benzoyl)oxy)-4-nitrobenzene (3.40g, 0.0124mol) in absolute EtOH ($50cm^3$). After heating to reflux for 17 hours, the yellow solution was allowed to cool to room temperature and poured onto ice. The pH was adjusted to pH 8 by addition of 2M NaOH and the organic layer was extracted with EtOAc (3 x $100cm^3$). The extracts were dried over Na_2SO_4 and the filtrate reduced down to give a white solid, which was washed with EtOH and dried (1.75g, 57.9%). Microanalysis: Calculated for $C_{14}H_{13}N_1O_3$ C 69.12, H 5.39, N 5.76; found C 69.02, H 5.44, N 5.41. IR (KBr pellet): υ = 3468m (NH_2), 3385m (NH_2), 2837w (C-H), 1710s (C=O), 1628s (C=C), 1607s (C=C), 1579s (C=C), 1083s (C-O) cm^{-1}. ^{1}H-NMR (300.13MHz, $CDCl_3$, 298K): δ_H 8.14 (2H, d, $J_{AA'XX'}$ = 8.92Hz, *o*-$\underline{H}ArCO_2$-), 6.98 (4H, overlapping doublets, *m*-$\underline{H}ArCO_2$- + *m*-$\underline{H}ArNH_2$), 6.70 (2H, d, $J_{AA'XX'}$ = 6.51Hz, *o*-$\underline{H}ArNH_2$), 3.89 (3H, s, $OC\underline{H}_3$), 3.65 (2H, br s, $N\underline{H}_2$) ppm. ^{13}C-NMR (75.48MHz, $CDCl_3$, 298K): δ_C 165.4, 163.6, 144.1, 142.9, 132.1, 122.2, 122.0, 115.5, 113.6, 55.4 ppm. CI MS: m/z = 243 $(L)^+$.

4.4.7.6 Synthesis of ((4-(Hexadecyloxy)benzoyl)oxy-4-Aniline

Under an inert atmosphere, (4-(hexadecyloxy)benzoyl)oxy)-4-nitrobenzene (2.00g, 4.13mmol) followed by addition of $SnCl_2.2H_2O$ (4.67g, 0.0207mol) were heated to reflux in absolute EtOH ($50cm^3$) for 18 hours. The solution was allowed to cool to room temperature and poured onto ice. After 2m NaOH was added to adjust the pH to 8, the product was extracted into EtOAc (4 x $100cm^3$). The organic layers were combined and dried over

Na_2SO_4. The solution was reduced in volume *in vacuo*, resulting in a white solid, which was washed with EtOH and dried (0.872g, 46.5%). Microanalysis: Calculated for $C_{29}H_{43}N_1O_3$ C 76.78, H 9.55, N 3.09: found C 76.64, H 9.33, N 2.80. IR (KBr pellet): υ = 3425m (NH_2), 3340m (NH_2), 2854s (C-H), 1719vs (C=O), 1628m (C=C), 1608s (C=C), 1583w (C=C), 1087s (C-O) cm^{-1}. ^{1}H-NMR (270.17MHz, $CDCl_3$, 298K): δ_H 8.11 (2H, d, $J_{AA'XX'}$ = 8.64Hz, *o*-HArCO$_2$-), 6.95 (4H, overlapping doublets, *m*-HArCO$_2$- + *m*-HArNH$_2$), 6.69 (2H, d, $J_{AA'XX'}$ = 6.51Hz, *o*-HArNH$_2$), 4.02 (2H, t, $^3J_{AX}$ = 6.62Hz, OCH$_2$), 3.70 (2H, br s, NH$_2$) 1.80 –1.25 (28H, m, CH$_2$), 0.87 (3H, t, $^3J_{AX}$ = 6.62Hz, CH$_3$) ppm. ^{13}C-NMR (75.48MHz, $CDCl_3$, 298K): δ_C 165.5, 163.3, 144.0, 143.2, 132.1, 122.4, 121.8, 115.7, 114.2, 68.3, 31.9, 29.7, 29.4, 29.1, 26.0, 22.7, 14.1 ppm (eight alkyl carbons obscured). CI MS: m/z = 453 $(L)^+$.

4.4.7.7 Synthesis of ex-H_2L^{Dipy-1}

((4-(Methoxy)benzoyl)oxy-4-aniline (0.510g, 2.10mmol) in THF (20cm^3) was added to a warm solution of 2,2'-diformyl-5,5'-dimthyldipyrromethane (0.241g, 1.05mmol) in EtOH (80cm^3). A few drops of glacial AcOH were added and the orange solution was stirred at room temperature for 4 hours. The solution was reduced in volume under vacuum and washed with EtOH to give a beige solid. This was recrystallised from $CHCl_3$ and MeOH to give a yellow solid (0.523g, 73.2%). Microanalysis: Calculated for $C_{41}H_{36}N_4O_6.H_2O$ C 70.47, H 5.48, N 8.02: found C 70.84, H 5.20, N 7.97. IR (KBr pellet): υ = 2972w (C-H), 1724vs (C=O), 1616s (C=N), 1608s (C=C), 1593s (C=C), 1158s (C-O) cm^{-1}. ^{1}H-NMR (270.17MHz, $CDCl_3$,

298K): δ_H 8.15 (4H, d, $J_{AA'XX'}$ = 6.68Hz, *o*-HArCO$_2$-), 8.14 (2H, s, H_aC=N), 7.17 (8H, overlapping doublets, *o*-HArN=C- + *m*-HArN=C-), 6.98 (4H, d, $J_{AA'XX'}$ = 8.96Hz, *m*-HArCO$_2$), 6.62 (2H, d, $^3J_{AX}$ = 3.67Hz, H_b), 6.17 (2H, d, $^3J_{AX}$ = 3.70 Hz, H_c), 3.89 (6H, s, OCH_3), 1.67 (6H, s, H_d) ppm. ^{13}C-NMR (75.48MHz, d-DMSO, 298K): δ_C 164.4, 163.7, 151.0, 150.2, 147.8, 145.2, 132.0, 130.4, 122.6, 121.5, 121.0, 117.2, 114.3, 106.6, 55.7, 35.4, 27.6 ppm. ES MS: m/z = 681 (ex-$H_2L^{Dipy\text{-}1}$)$^+$.

4.4.7.8 Synthesis of ex-$H_2L^{Dipy\text{-}16}$

To a warm ethanolic (80cm^3) solution of 2,2'diformyl-5,5'-dimethyldipyrromethane (0.105g, 0.456mmol) was added ((4-(hexadecyloxy)benzoyl)oxy-4-aniline (0.412g, 0.908mmol) in THF (20cm^3). A few drops of glacial AcOH were added and the yellow/orange solution was stirred for 4 hours. The solution was reduced in volume under vacuum to give a beige solid. This was recrystallised from $CHCl_3$ and MeOH to give a yellow solid (0.396g, 78.8%). Microanalysis: Calculated for $C_{71}H_{96}N_4O_6.H_2O$ C 76.17, H 8.82, N 5.00; found C 75.92, H 8.62, N 5.51. IR (KBr pellet): υ = 2908s (C-H), 2847vs (C-H), 1734s (C=O), 1614s (C=N), 1600s (C=C), 1160s (C-O) cm^{-1}. ^{1}H-NMR (300.13MHz, $CDCl_3$, 298K): δ_H 8.15 (2H, s, H_aC=N), 8.13 (4H, d, $J_{AA'XX'}$ = 8.87Hz, *o*-HArCO$_2$-), 7.16 (8H, overlapping doublets, *o*-HArN=C- + *m*-HArN=C-), 6.97 (4H, d, $J_{AA'XX'}$ = 8.89Hz, *m*-HArCO$_2$), 6.72 (2H, br d, H_b), 6.23 (2H, d, $^3J_{AX}$ = 3.45 Hz, H_c), 4.04 (4H, t, $^3J_{AX}$ = 6.56Hz, OCH_2), 1.86 – 1.26 (22H, m, CH_2), 0.88 (6H, t, $^3J_{AX}$ = 6.60Hz, H_d) ppm. ^{13}C-NMR (75.48MHz, $CDCl_3$, 298K): δ_C 165.0, 163.5, 148.7, 132.2, 122.3, 121.8, 121.7, 121.5, 115.7, 114.3, 68.3, 31.9, 29.7, 29.3,

29.1, 28.6, 26.0, 22.7, 14.1 ppm (eight alkyl plus four aromatic carbons obscured). ES MS: expected ions not found.

4.4.8 Synthesis of the Extended Dipyrrole Complexes, ex-[M(L^{Dipy-n})]$_x$

4.4.8.1 Synthesis of ex-[Zn(L^{Dipy-1})]$_2$

$Zn(OAc)_2.2H_2O$ (0.0332g, 0.151mol) in MeOH (3cm^3) was added to a solution of ex-H_2L^{Dipy-1} (0.101g, 0.148mmol) in CH_2Cl_2 (20cm^3) and stirred at room temperature for 30 mins. A few drops of NEt_3 were added and the solution was stirred for a further 24 hours. The solution was reduced in volume *in vacuo* to give a yellow solid, recrystallised from $CHCl_3$ and MeOH (0.0869g, 77.3%). Microanalysis: Calculated for $C_{41}H_{34}N_4O_6Zn_1$ C 66.18, H 4.61, N 7.53; found C 65.59, H 4.66, N 7.22. IR (KBr pellet): υ = 2968w (C-H), 2933w (C-H), 1741vs (C=O), 1605s (C=N), 1568s (C=C), 1553s (C=C), 1021s (C-O) cm^{-1}. ^{1}H-NMR (300.13MHz, $CDCl_3$, 298K): δ_H 8.17 (2H, s, $\underline{H}_aC$=N), 8.10 (4H, d, $J_{AA'XX'}$ = 6.96Hz, *o*-$\underline{H}ArCO_2$-), 6.98 (8H, overlapping doublets, *o*-$\underline{H}$ArN=C- + *m*-$\underline{H}$ArN=C-), 6.87 (4H, d, $J_{AA'XX'}$ = 8.77Hz, *m*-$\underline{H}ArCO_2$), 6.72 (2H, d, $^3J_{AX}$ = 3.56Hz, $\underline{H}_b$), 6.21 (2H, d, $^3J_{AX}$ = 3.60Hz, $\underline{H}_c$), 3.88 (6H, s, OC$\underline{H}_3$), 1.56 (6H, s br, $\underline{H}_d$) ppm. ^{13}C-NMR (75.48MHz, $CDCl_3$, 298K): δ_C 164.9, 163.8, 158.8, 150.9, 147.8, 144.2, 135.9, 132.2, 122.6, 122.4, 121.8, 120.6, 113.8, 111.9, 55.5, 39.4, 29.8 ppm. MALDI-TOF MS: m/z = 1488 ex-[Zn(L^{Dipy-1})]$_2^+$.

4.4.8.2 Synthesis of ex-[Zn($L^{Dipy-16}$)]$_2$

$Zn(OAc)_2.2H_2O$ (0.0266g, 0.121mmol) in MeOH (3cm^3) was added to a solution of ex-$H_2L^{Dipy-16}$ (0.127g, 0.115mmol) in CH_2Cl_2 (40cm^3). The

solution was stirred for 30 mins then a few drops of NEt_3 were added and the solution was stirred for a further 24 hours. The solution was reduced in volume *in vacuo* to give a yellow solid, which was recrystallised from $CHCl_3$ and EtOH (0.0871g, 65.1%). Microanalysis: Calculated for $C_{71}H_{94}N_4O_6.H_2O$ C 72.09, H 8.18, N 4.74; found C 72.12, H 8.20, N 4.72. IR (KBr pellet): υ = 2924s (C-H), 2852s (C-H), 1734s (C=O), 1605s (C=N), 1570s (C=C), 1513s (C=C), 1049s (C-O) cm^{-1}. ^{1}H-NMR (300.13MHz, $CDCl_3$, 298K): δ_H 8.17 (2H, s, $\underline{H}_aC$=N), 8.11 (4H, d, $J_{AA'XX'}$ = 9.41Hz, *o*-$\underline{H}ArCO_2$-), 7.00 (4H, d, $J_{AA'XX'}$ = 8.90Hz, *o*-$\underline{H}ArN$=C-), 6.94 (4H, d, $J_{AA'XX'}$ = 8.99Hz, *m*-$\underline{H}ArN$=C-), 6.86 (4H, d, $J_{AA'XX'}$ = 8.93Hz, *m*-$\underline{H}ArCO_2$), 6.72 (2H, d, $^3J_{AX}$ = 3.64Hz, $\underline{H}_b$), 6.21 (2H, d, $^3J_{AX}$ = 3.70Hz, $\underline{H}_c$), 4.04 (4H, t, $^3J_{AX}$ = 6.57Hz, $OC\underline{H}_2$), 1.83-1.26 (23H, m, $C\underline{H}_2$), 1.55 (6H, s, $\underline{H}_d$), 0.88 (6H, t, $^3J_{AX}$ = 6.66Hz, $C\underline{H}_3$) ppm. ^{13}C-NMR (75.48MHz, $CDCl_3$, 298K): δ_C 164.9, 163.4, 158.8, 150.9, 147.8, 144.2, 135.9, 132.2, 122.4, 121.5, 120.6, 114.2, 68.3, 39.4, 31.9, 29.7, 29.3, 29.1, 26.0, 22.7, 14.1 ppm (nine alkyl carbons plus two aromatic carbons obscured). MALDI-TOF MS: m/z = 2329 ex-$[Zn(L^{Dipy\text{-}16})]_2^+$.

4.4.8.3 Synthesis of ex-[Pd($L^{Dipy\text{-}1}$)]

$Pd(OAc)_2$ (0.0340g, 0.151mmol) in CH_2Cl_2 (5cm^3) was added to a solution of ex-$H_2L^{Dipy\text{-}1}$ (0.101g, 0.148mmol) in CH_2Cl_2 (20cm^3) and stirred at room temperature for 30 mins. A few drops of NEt_3 were added and the solution was stirred for a further 24 hours. The resulting bright yellow solid was recrystallised from $CHCl_3$ and MeOH (0.0607g, 52.2%). Microanalysis: Calculated for $C_{41}H_{34}N_4O_6Pd_1$ C 62.72, H 4.36, N 7.14; found C 62.18, H 4.26, N 7.17. IR (KBr pellet): υ = 2977w (C-H), 2930w (C-H), 1723vs (C=O),

1616s (C=N), 1597s (C=C), 1580s (C=C), 1064s (C-O) cm^{-1}. ^{1}H-NMR (300.13MHz, $CDCl_3$, 298K): δ_H 7.89 (4H, d, $J_{AA'XX'}$ = 6.96Hz, *o*-$\underline{H}ArCO_2$-), 7.60 (2H, s, $\underline{H}_aC$=N), 6.94 (2H, d, $^3J_{AX}$ = 3.94Hz, $\underline{H}_b$), 6.84 (8H, overlapping doublets, *o*-$\underline{H}$ArN=C- + *m*-$\underline{H}$ArN=C), 6.77 (4H, d, $J_{AA'XX'}$ = 8.85Hz, *m*-$\underline{H}ArCO_2$), 6.34 (2H, d, $^3J_{AX}$ = 3.95Hz, $\underline{H}_c$), 3.87 (6H, s, $OC\underline{H}_3$), 1.71 (6H, s, $\underline{H}_d$) ppm. MALDI-TOF MS: m/z = 784 ex-$[Pd(L^{Dipy\text{-}1})]^+$.

4.4.8.4 Synthesis of ex-[Pd($L^{Dipy\text{-}16}$)]

$Pd(OAc)_2$ (0.0250g, 0.111mmol) in CH_2Cl_2 ($3cm^3$) was added to a solution of ex-$H_2L^{Dipy\text{-}16}$ (0.114g, 0.103mmol) in CH_2Cl_2 ($40cm^3$) and stirred for 30 mins. A few drops of NEt_3 were added and the yellow/orange solution was stirred at room temperature for 24 hours. The solution was reduced in volume in *vacuo* to give a yellow solid, which was recrystallised from $CHCl_3$ and EtOH (0.0843g, 67.9%). Microanalysis: Calculated for $C_{71}H_{94}N_4O_6Pd_1.2H_2O$ C 68.66, H 7.95, N 4.51; found C 69.00, H 7.72, N 4.46. IR (KBr pellet): υ = 2919m (C-H), 2550m (C-H), 1728s (C=O), 1606s (C=N), 1560s (C=C), 1511s (C=C), 1081s (C-O) cm^{-1}. ^{1}H-NMR (300.13MHz, $CDCl_3$, 298K): δ_H 7.88 (4H, d, $J_{AA'XX'}$ = 8.74Hz, *o*-$\underline{H}ArCO_2$-), 7.60 (2H, s, $\underline{H}_aC$=N), 6.94 (2H, d, $^3J_{AX}$ = 3.90Hz, $\underline{H}_b$), 6.84 (8H, overlapping doublets, *m*-$\underline{H}$ArN=C- + *m*-$\underline{H}$ArN=C-), 6.75 (4H, d, $J_{AA'XX'}$ = 8.74Hz, *m*-$\underline{H}ArCO_2$), 6.34 (2H, d, $^3J_{AX}$ = 3.93Hz, $\underline{H}_c$), 3.99 (4H, t, $^3J_{AX}$ = 6.51Hz, $OC\underline{H}_2$), 1.92-1.27 (56H, m, $C\underline{H}_2$), 1.71 (6H, s, $\underline{H}_d$), 0.88 (6H, t, $^3J_{AX}$ = 6.57Hz, $C\underline{H}_3$) ppm. ^{13}C-NMR (75.48MHz, $CDCl_3$, 298K): δ_C 164.5, 163.2, 158.5, 152.2, 148.6, 146.5, 136.4, 132.1, 123.1, 122.1, 121.5, 119.4, 114.0, 108.1, 68.2, 43.2, 32.1, 31.9, 29.7, 29.5,

29.4, 29.2, 26.0, 22.7, 14.1 ppm (five alkyl carbons obscured). MALDI-TOF MS: m/z = 1206 ex-$[Pd(L^{Dipy\text{-}16})]^+$.

4.5 REFERENCES

[1] B. Donnio, D. Guillon, R. Deschenaux and D. W. Bruce, *Comprehensive Coord. Chem. II*, ed. J. A. McCleverty and T. J. Meyer, Oxford: Elsevier, 2004, **7**, 357.

[2] C. Piechocki, J. Simon, A. Skoulios, D. Guillon and P. Weber, *J. Am. Chem. Soc.*, 1982, **104**, 5245.

[3] (a) D. Guillon, A. Skoulios, C. Piechocki, J. Simon and P. Weber, *Mol. Cryst. Liq. Cryst.*, 1983, **100**, 275; (b) C. Piechocki and J. Simon, *Nouv. J. Chim.*, 1985, **9**, 159; (c) P. Weber, D. Guillon and A. Skoulios, *Liq. Cryst.*, 1991, **9**, 369; (d) D. Markovitsti, T. H. Tran-Thi, V. Briois, J. Simon and K. Ohta, *J. Am. Chem. Soc.*, 1988, **110**, 2001.

[4] (a) D. Guillon, P. Weber, A. Skoulios, C. Piechocki and J. Simon, *Mol. Cryst. Liq. Cryst.*, 1985, **130**, 223; (b) M. Hanack, A. Beck and H. Lehmann, *Synthesis*, 1987, 703; (c) D. M. Knawby and T. M. Swager, *Chem. Mater.*, 1997, **9**, 535.

[5] K. Hatsusaka, K. Ohta, I. Yamamoto and H. Shirai, *J. Mater. Chem.*, 2001, **11**, 423.

[6] M. Kimura, H. Narikawa, K. Ohta, K. Hanabusa, H. Shirai and N. Kobayashi, *Chem. Mater.*, 2002, **14**, 2711.

[7] J. W. Goodby, P. S. Robinson, B. K. Teo and P. E. Cladis, *Mol. Cryst. Liq. Cryst., Lett. Sect.*, 1980, **56**, 303.

[8] B. A. Gregg, M. A. Fox and A. J. Bard, *J. Chem. Soc., Chem. Commun.*, 1987, **15**, 1134.

[9] V. Paganuzzi, P. Guatteri, P. Riccardi, T. Sacchelli, J. Barberá, M. Costa and E. Dalcanale, *Eur. J. Org. Chem.*, 1999, **7**, 1527.

[10] (a) Y. Shimizu, M. Miya, A. Nagata, K. Ohta, A. Matsumura, I. Yamamoto and S. Kusabayashi, *Chem. Lett.*, 1991, **1**, 25; (b) Y. Shimizu, M. Miya, A. Nagata, K. Ohta, I. Yamamoto and S. Kusabayashi, *Liq. Cryst.*, 1993, **14**, 795.

[11] M. A. Fox, J. V. Grant, D. Melamed, T. Torimoto, C. Y. Liu and A. J. Bard, *Chem. Mater.*, 1998, **10**, 1771.

[12] B. R. Patel and K. S. Suslick, *J. Am. Chem. Soc.*, 1998, **120**, 11802.

[13] (a) Q. M. Wang and D. W. Bruce, *Chem. Commun.*, 1996, 2505: (b) Q. M. Wang and D. W. Bruce, *Angew. Chem. Int. Ed. Engl.*, 1997, **36**, 150.

[14] H. Goto and K. Akagi, *J. Polym. Sci. A1*, 2005, **43**, 616.

[15] M. Kijima, H. Hasegawa and H. Shirakawa, *J. Polym. Sci. A1*, 1998, **36**, 2691.

[16] Y. Chen, C. T. Imrie and K. S. Ryder, *J. Mater. Chem.*, 2001, **11**, 990.

[17] Z. Bao, W. K. Chan and L. Yu, *J. Am. Chem. Soc.*, 1995, **117**, 12426.

[18] K. Praefcke, M. Jachmann, D. Blunk and M. Horn, *Liq. Cryst.*, 1998, **24**, 153.

[19] S. J. Nugent, Q. M. Wang and D. W. Bruce, *New J. Chem.*, 1996, **20**, 669.

[20] A. Krówczyński, W. Pyżuk and E. Górecka, *Polish J. Chem.*, 1994, **68**, 281.

[21] B. Donnio and D. W. Bruce, *J. Chem. Soc., Dalton Trans.*, 1997, 2745.

[22] G. Pelzl, S. Diele and W. Weissflog, *Adv. Mater.*, 1999, **11**, 707.

[23] (a) B. J. Littler, M. A. Miller, C.-H. Hung, R. W. Wagner, D. F. O'Shea, P. D. Boyle and J. S. Lindsey, *J. Org. Chem.*, 1999, **64**, 1391. (b) J. B. Love, A. J. Blake, C. Wilson, S. D. Reid, A. Novak and P. B. Hitchcock, *Chem. Commun.*, 2003, 1682.

[24] M. Veber, H. Strzelecka and C. Jallabert, *Mol. Cryst. Liq. Cryst. Inc. Nomlin. Opt.*, 1988, **156**, 347.

[25] V. Percec, C.-H. Ahn, T. K. Bera, G. Ungar and D. J. P. Yeardley, *Chem. Eur. J.*, 1999, **5**, 3, 1070.

[26] S. Morrone, D. Guillon and D. W. Bruce, *Inorg. Chem.*, 1996, **35**, 7041.

[27] S. D. Reid, A. J. Blake, W. Köckenberger, C. Wilson and J. B. Love, *Dalton Trans.*, 2003, 4387.

[28] C. Janiak, *J. Chem. Soc., Dalton Trans.*, 2000, 3885.

[29] (a) G. Barberio, A. Bellusci, A. Crispini, M. Ghedini, A. Golemme, P. Prus and D. Pucci, *Eur. J. Inorg. Chem.*, 2005, 181; (b) R. Giménez, A. B. Manrique, S. Uriel, J. Barberá and J. L. Serrano, *Chem. Commun.*, 2004, 2064; (c) C. K. Lee, M. J. Ling and I. J. B. Lin, *Dalton Trans.*, 2003, **24**, 4731.

[30] J. L. Serrano and T. Sierra, *Coord. Chem. Rev.*, 2003, **242**, 73.

[31] B. Donnio and D. W. Bruce, *J. Chem. Soc. Dalton Trans.*, 1997, 2745.

[32] G. Pelzl, S. Diele and W. Weissflog, *Adv. Mater.*, 1999, **11**, 707.

[33] C. Tschierske, *J. Mater. Chem.*, 1998, **8**, 1485.

[34] A. Werner and W. Friedrichsen, *J. Chem. Soc., Chem. Commun.*, 1994, 365.

Appendix I

Crystallographic Refinement Details and Data For $[MnCl_2(L^{Phen\text{-}1})]_2.2CH_2Cl_2$

Single-crystal diffraction data were collected on a Bruker SMART1000 CCD area detector diffractometer, equipped with an Oxford Cryosystem open-flow nitrogen cryostat, using graphite-monochromated Mo-K_α radiation (λ=0.71073 Å). Integrated intensities, corrected for Lorentz and polarisation effects, were obtained using the Bruker SAINT package, as were the cell parameters. All data were corrected for absorption using a multi-scan correction. The structure was solved by direct methods and refined by full-matrix least squares using SHELXL-97. All further non-hydrogen atoms were located in subsequent difference Fourier syntheses. The disorder in carbon atom C2R in a methoxy group was modelled over two sites with 80% and 20% occupancies and had suitable geometry restraints. Close contact between one H of the minor component (20%) and H8a improved through use of HFIX 137, although the atoms were still close. All hydrogen atoms were placed in geometrically calculated positions and refined using a riding model. All non-hydrogen atoms (except C2R) were refined with anisotropic displacement parameters. Crystal structure diagrams were generated using OLEX, version 2.54.[1]

Identification code	mnme3c
Crystal data	
Chemical formula	$C_{64}H_{60}Cl_4Mn_2N_8O_{12}.2(CH_2Cl_2)$
M_r	1554.73
Cell setting, space group	Triclinic, *P*-1
a, b, c (Å)	10.0772 (10), 13.8008 (14), 13.9813 (15)
α, β, γ (°)	92.992 (2), 109.004 (2), 108.673 (2)

V (Å^3)	1714.9 (3)
Z	1
D_x (Mg m^{-3})	1.505
Radiation type	Mo $K\alpha$
No. of reflections for cell parameters	3065
θ range (°)	2.3–25.5
μ (mm^{-1})	0.75
Temperature (K)	150 (2)
Crystal form, colour	Column, orange/brown
Crystal size (mm)	0.22 × 0.14 × 0.06
Data collection	
Diffractometer	Bruker SMART1000 CCD area detector
Data collection method	ω
Absorption correction	Multi-scan (based on symmetry-related measurements)
T_{min}	0.884
T_{max}	1.000
No. of measured, independent and observed parameters	15147, 7679, 4706
Criterion for observed reflections	$I > 2\sigma(I)$
R_{int}	0.031
θ_{max} (°)	27.5
Range of h, k, l	$-13 \rightarrow h \rightarrow 12$ $-17 \rightarrow k \rightarrow 17$ $-18 \rightarrow l \rightarrow 18$
Refinement	
Refinement on	F^2
$R[F^2 > 2\sigma(F^2)]$, $wR(F^2)$, S	0.053, 0.165, 1.01
No. of relections	7674 reflections
No. of parameters	439
H-atom treatment	Riding model, Me as rigid rotor
Weighting scheme	Calculated $w = 1/[\sigma^2(F_o^2) + (0.0781P)^2 + 1.765P]$ where $P = (F_o^2 + 2F_c^2)/3$
$(\Delta/\sigma)_{max}$	0.001
$\Delta\rho_{max}$, $\Delta\rho_{min}$ (e Å^{-3})	1.08, –0.62

Computer programs: *Bruker SMART version 5.624* (Bruker, 2001); *Bruker SAINT version 6.36a* (Bruker, 2002); *Bruker SAINT; Bruker SHELXTL* (Bruker, 2001); *SHELXS-97* (Sheldrick, 1990); *SHELXL-97* (Sheldrick, 1997); *enCIFer*(Allen et al.,2004);*PLATON*(Spek,2003).

Appendix II

Crystallographic Refinement Details and Data For $[CoCl_2(L^{Phen\text{-}1})].2CHCl_3$

Single-crystal diffraction data were collected on a Bruker SMART1000 CCD area detector diffractometer, equipped with an Oxford Cryosystem open-flow nitrogen cryostat, using graphite-monochromated Mo-K_α radiation (λ=0.71073 Å). Integrated intensities, corrected for Lorentz and polarisation effects, were obtained using the Bruker SAINT package, as were the cell parameters. All data were corrected for absorption using a multi-scan correction. The structure was solved by direct methods and refined by full-matrix least squares using SHELXL-97. All further non-hydrogen atoms were located in subsequent difference Fourier syntheses. All hydrogen atoms were placed in geometrically calculated positions and refined using a riding model. All non-hydrogen atoms were refined with anisotropic displacement parameters. The largest residual electron density peak may be solvent, but no recognisable model could be found. Crystal structure diagrams were generated using OLEX, version 2.54.[1]

Identification code	phmeco
Crystal data	
Chemical formula	$C_{32}H_{30}Cl_2CoN_4O_6.2(CHCl_3)$
M_r	935.17
Cell setting, space group	Triclinic, *P*-1
a, *b*, *c* (Å)	10.891 (2), 13.178 (2), 16.020 (2)
α, β, γ (°)	96.280 (2), 99.859 (2), 110.725 (2)
V (Å^3)	2082.3 (6)
Z	2
D_x (Mg m^{-3})	1.491

Radiation type	Mo $K\alpha$
No. of reflections for cell parameters	3419
θ range (°)	2.2–23.1
μ (mm^{-1})	0.97
Temperature (K)	150 (2)
Crystal form, colour	Needle, orange
Crystal size (mm)	0.71 × 0.08 × 0.06
Data collection	
Diffractometer	Bruker SMART APEX CCD area detector
Data collection method	ω
Absorption correction	Multi-scan (based on symmetry-related measurements)
T_{min}	0.888
T_{max}	1.000
No. of measured, independent and observed parameters	17711, 9131, 6782
Criterion for observed reflections	$I > 2\sigma(I)$
R_{int}	0.027
θ_{max} (°)	28.2
Range of h, k, l	$-14 \rightarrow h \rightarrow 13$ $-16 \rightarrow k \rightarrow 16$ $-21 \rightarrow l \rightarrow 20$
Refinement	
Refinement on	F^2
$R[F^2 > 2\sigma(F^2)]$, $wR(F^2)$, S	0.069, 0.203, 1.02
No. of relections	9131 reflections
No. of parameters	484
H-atom treatment	Constrained to parent site
Weighting scheme	Calculated $w = 1/[\sigma^2(F_o^2) + (0.1085P)^2 + 3.9717P]$ where $P = (F_o^2 + 2F_c^2)/3$
$(\Delta/\sigma)_{max}$	<0.0001
$\Delta\rho_{max}$, $\Delta\rho_{min}$ (e $Å^{-3}$)	1.28, –1.38

Computer programs: *Bruker SMART version 5.625* (Bruker, 2001); *Bruker SAINT version 6.02a* (Bruker, 2000); *Bruker SAINT; Bruker SHELXTL* (Bruker, 1997); *SHELXS-97* (Sheldrick, 1990); *SHELXL-97* (Sheldrick, 1997); *SHELXL-97; PLATON* (Spek, 2002).

Appendix III

Crystallographic Refinement Details and Data For $[NiCl_2(L^{Phen\text{-}1})]_2.2CHCl_3 2.5EtOH$

Single-crystal diffraction data were collected on a Nonius kappa CCD area detector diffractometer, equipped with an Oxford Cryosystem open-flow nitrogen cryostat, using confocal mirrored-monochromated Mo-K_α radiation (λ=0.71073 Å). Integrated intensities, corrected for Lorentz and polarisation effects, were obtained using the DENZO and COLLECT packages, as were the cell parameters. All data were corrected for absorption using a multi-scan correction. The structure was solved by direct methods and refined by full-matrix least squares using SHELXL-97. All further non-hydrogen atoms were located in subsequent difference Fourier syntheses. The solvent molecule EtOH exhibited a severe crystallographic disorder, which could not be sensibly modelled in terms of atomic sites. The PLATON SQUEEZE procedure was used to treat regions of diffuse electron density and to estimate the number of residual electrons. The number of electrons located was 10 electrons per unit cell, which equates to half a molecule of EtOH per dimer. The largest residual electron peak was in the region of $CHCl_3$. All hydrogen atoms were placed in geometrically calculated positions and refined using a riding model. All non-hydrogen atoms were refined with anisotropic displacement parameters. Crystal structure diagrams were generated using OLEX, version 2.54.[1]

Identification code	nioman
Crystal data	
Chemical formula	$C_{64}H_{60}Cl_4N_8Ni_2O_{12}.2(CHCl_3).2.5(C_2H_5OH)$
M_r	1746.33

Cell setting, space group	Triclinic, *P*-1
a, *b*, *c* (Å)	10.0340 (3), 13.8630 (5), 15.7797 (6)
α, β, γ (°)	104.115 (2), 98.845 (2), 109.786 (2)
V (Å^3)	1934.71 (12)
Z	1
D_x (Mg m^{-3})	1.499
Radiation type	Mo *K*α
No. of reflections for cell parameters	33232
θ range (°)	2.9–27.5
μ (mm^{-1})	0.90
Temperature (K)	150 (2)
Crystal form, colour	Needle, yellow
Crystal size (mm)	0.20 × 0.03 × 0.02
Data collection	
Diffractometer	Bruker-Nonius 95mm CCD camera on κ-goniostat
Data collection method	φ & ω scans
Absorption correction	?
T_{min}	0.802
T_{max}	1.000
No. of measured, independent and observed parameters	40914, 8992, 6270
Criterion for observed reflections	$I > 2\sigma(I)$
R_{int}	0.104
θ_{max} (°)	27.8
Range of *h*, *k*, *l*	$-13 \rightarrow h \rightarrow 13$ $-18 \rightarrow k \rightarrow 18$ $-20 \rightarrow l \rightarrow 20$
Refinement	
Refinement on	F^2
$R[F^2 > 2\sigma(F^2)]$, $wR(F^2)$, S	0.079, 0.207, 1.02
No. of relections	8992 reflections
No. of parameters	454
H-atom treatment	Mixture of independent and constrained refinement
Weighting scheme	Calculated $w = 1/[\sigma^2(F_o^2) + (0.087P)^2 + 7.5005P]$ where $P = (F_o^2 + 2F_c^2)/3$

$(\Delta/\sigma)_{max}$	<0.0001
$\Delta\rho_{max}$, $\Delta\rho_{min}$ (e Å^{-3})	2.04, –1.16

Computer programs: *COLLECT* (Hooft, 1998); *DENZO* (Otwinowski & Minor, 1997) & *COLLECT* (Hooft, 1998); *DENZO & COLLECT*; *SHELXS-97* (Sheldrick, 1990); *SHELXL-97* (Sheldrick, 1997); *enCIFer(Allen et al.,2004; PLATON(Spek,2003).*

Appendix IV

Crystallographic Refinement Details and Data For $[CuCl_2(L^{Phen\text{-}0})].2CHCl_3$

Single-crystal diffraction data were collected on a Bruker SMART1000 CCD area detector diffractometer, equipped with an Oxford Cryosystem open-flow nitrogen cryostat, using graphite-monochromated Mo-K_α radiation (λ=0.71073 Å). Integrated intensities, corrected for Lorentz and polarisation effects, were obtained using the Bruker SAINT package, as were the cell parameters. All data were corrected for absorption using a multi-scan correction. The structure was solved by direct methods and refined by full-matrix least squares using SHELXL-97. All further non-hydrogen atoms were located in subsequent difference Fourier syntheses. The disorder in one solvent molecule of $CHCl_3$ was modelled over two sites with 65% and 35% occupancies and suitable geometry restraints. All hydrogen atoms were placed in geometrically calculated positions and refined using a riding model. All non-hydrogen atoms were refined with anisotropic displacement parameters, with the exception of C2S and C2S' from $CHCl_3$. Crystal structure diagrams were generated using OLEX, version 2.54.[1]

Identification code	cuanpc
Crystal data	
Chemical formula	$C_{26}H_{18}Cl_2CuN_4.0.5(C_2H_2Cl_6).CHCl_3$
M_r	759.62
Cell setting, space group	Triclinic, *P*-1
a, *b*, *c* (Å)	9.586 (2), 11.468 (2), 14.003 (3)
α, β, γ (°)	81.306 (3), 85.236 (3), 84.859 (3)
V (Å^3)	1511.8 (5)
Z	2
D_x (Mg m^{-3})	1.669
Radiation type	Mo $K\alpha$
No. of reflections for cell parameters	5307
θ range (°)	2.5–27.5
μ (mm^{-1})	1.46
Temperature (K)	150 (2)
Crystal form, colour	Tablet, red
Crystal size (mm)	0.44 × 0.33 × 0.14
Data collection	
Diffractometer	Bruker SMART APEX CCD area detector
Data collection method	ω
Absorption correction	MULTI-SCAN
T_{min}	0.810
T_{max}	1.000
No. of measured, independent and observed parameters	12916, 6815, 5962
Criterion for observed reflections	$I > 2\sigma(I)$
R_{int}	0.015
θ_{max} (°)	27.5
Range of *h*, *k*, *l*	$-12 \rightarrow h \rightarrow 12$
	$-14 \rightarrow k \rightarrow 14$
	$-18 \rightarrow l \rightarrow 18$
Refinement	
Refinement on	F^2
$R[F^2 > 2\sigma(F^2)]$, $wR(F^2)$, S	0.040, 0.108, 1.06
No. of relections	6815 reflections
No. of parameters	396
H-atom treatment	Riding model

Weighting scheme	Calculated $w = 1/[\sigma^2(F_o^2) + (0.0578P)^2 + 1.3572P]$ where $P = (F_o^2 + 2F_c^2)/3$
$(\Delta/\sigma)_{max}$	0.001
$\Delta\rho_{max}$, $\Delta\rho_{min}$ (e Å^{-3})	0.96, –0.77

Computer programs: *Bruker SMART version 5.625* (Bruker, 2001); *Bruker SAINT version 6.36a* (Bruker, 2000); *Bruker SAINT; Bruker SHELXTL* (Bruker, 2001); *SHELXS-97* (Sheldrick, 1990); *SHELXL-97* (Sheldrick, 1997); *enCIFer* (CCDC, 2003); *PLATON* (Spek, 2003).

Appendix V

Crystallographic Refinement Details and Data For $[ZnCl_2(L^{Phen\text{-}1})].2CHCl_3$

Single-crystal diffraction data were collected on a Bruker SMART1000 CCD area detector diffractometer, equipped with an Oxford Cryosystem open-flow nitrogen cryostat, using graphite-monochromated Mo-K_α radiation (λ=0.71073 Å). Integrated intensities, corrected for Lorentz and polarisation effects, were obtained using the Bruker SAINT package, as were the cell parameters. All data were corrected for absorption using a multi-scan correction. The structure was solved by direct methods and refined by full-matrix least squares using SHELXL-97. All further non-hydrogen atoms were located in subsequent difference Fourier syntheses. Both $CHCl_3$ solvent molecules were disordered, and consequently most chlorine atoms in $CHCl_3$, Cl6, Cl7, Cl8, Cl9, were anisotropically modelled over two sites with applied restraints. The hydrogen atom on C2S was omitted. All hydrogen atoms were placed in geometrically calculated positions and refined using a riding model. All non-hydrogen atoms were refined with anisotropic displacement

parameters. Crystal structure diagrams were generated using OLEX, version 2.54.[1]

Identification code	znphen
Crystal data	
Chemical formula	$C_{32}H_{30}Cl_2N_4O_6Zn.2(CHCl_3)$
M_r	941.61
Cell setting, space group	Triclinic, *P*-1
a, *b*, *c* (Å)	10.9144 (6), 13.2193 (7), 16.0353 (9)
α, β, γ (°)	96.2070 (10), 100.3980 (10), 110.9150 (10)
V (Å^3)	2087.8 (2)
Z	2
D_x (Mg m^{-3})	1.498
Radiation type	Mo $K\alpha$
No. of reflections for cell parameters	9573
θ range (°)	2.1–28.6
μ (mm^{-1})	1.15
Temperature (K)	150 (2)
Crystal form, colour	Column, orange-yellow
Crystal size (mm)	0.50 × 0.20 × 0.13
Data collection	
Diffractometer	Bruker SMART1000 CCD area detector
Data collection method	ω
Absorption correction	Multi-scan (based on symmetry-related measurements)
T_{min}	0.865
T_{max}	1.000
No. of measured, independent and observed parameters	18562, 9466, 7711
Criterion for observed reflections	$I > 2\sigma(I)$
R_{int}	0.019
θ_{max} (°)	28.6
Range of *h*, *k*, *l*	$-14 \rightarrow h \rightarrow 14$
	$-17 \rightarrow k \rightarrow 16$
	$-20 \rightarrow l \rightarrow 21$

Refinement	
Refinement on	F^2
$R[F^2 > 2\sigma(F^2)]$, $wR(F^2)$, S	0.060, 0.184, 1.02
No. of relections	9455 reflections
No. of parameters	490
H-atom treatment	Riding model
Weighting scheme	Calculated $w = 1/[\sigma^2(F_o^2) + (0.1033P)^2 + 4.750P]$ where $P = (F_o^2 + 2F_c^2)/3$
$(\Delta/\sigma)_{max}$	0.002
$\Delta\rho_{max}$, $\Delta\rho_{min}$ (e Å^{-3})	1.49, –1.88

Computer programs: *Bruker SMART version 5.054* (Bruker, 1998); *Bruker SAINT version 6.02a* (Bruker, 2000); *Bruker SAINT; Bruker SHELXTL* (Bruker, 1997); *SHELXS-97* (Sheldrick, 1990); *SHELXL-97* (Sheldrick, 1997); *SHELXL-97; PLATON* (Spek, 2000).

Appendix VI

Crystallographic Refinement Details and Data For $[MnCl_2(L^{Bipy\text{-}1})].0.5EtOH$

Single-crystal diffraction data were collected on a Bruker SMART1000 CCD area detector diffractometer, equipped with an Oxford Cryosystem open-flow nitrogen cryostat, using graphite-monochromated Mo-K_α radiation (λ=0.71073 Å). Integrated intensities, corrected for Lorentz and polarisation effects, were obtained using the Bruker SAINT package, as were the cell parameters. All data were corrected for absorption using a multi-scan correction. The structure was solved by direct methods and refined by full-matrix least squares using SHELXL-97. All further non-hydrogen atoms were located in subsequent difference Fourier syntheses. The solvent molecule EtOH lies across a symmetry site, so C1S is fully occupied and O1S is half occupied. Hydrogens (except O-H's) have been omitted from the solvent molecule. All hydrogen atoms were placed in geometrically calculated

positions and refined using a riding model. All non-hydrogen atoms were refined with anisotropic displacement parameters. Crystal structure diagrams were generated using OLEX, version 2.54. [1]

Identification code	mnclom
Crystal data	
Chemical formula	$C_{30}H_{30}Cl_2MnN_4O_6.0.5(C_2H_5OH)$
M_r	691.45
Cell setting, space group	Monoclinic, *I*2/*a*
a, *b*, *c* (Å)	18.331 (2), 13.9424 (12), 24.431 (2)
β (°)	100.392 (2)
V (Å^3)	6141.4 (16)
Z	8
D_x (Mg m^{-3})	1.496
Radiation type	Mo $K\alpha$
No. of reflections for cell parameters	6069
θ range (°)	2.4–27.6
μ (mm^{-1})	0.66
Temperature (K)	150 (2)
Crystal form, colour	Block, orange
Crystal size (mm)	0.30 × 0.28 × 0.20
Data collection	
Diffractometer	Bruker SMART1000 CCD area detector
Data collection method	ω
Absorption correction	Multi-scan (based on symmetry-related measurements)
T_{min}	0.784
T_{max}	1.000
No. of measured, independent and observed parameters	19058, 7235, 5259
Criterion for observed reflections	$I > 2\sigma(I)$
R_{int}	0.030
θ_{max} (°)	27.5
Range of *h*, *k*, *l*	$-23 \rightarrow h \rightarrow 23$
	$-16 \rightarrow k \rightarrow 18$
	$-31 \rightarrow l \rightarrow 24$

Refinement	
Refinement on	F^2
$R[F^2 > 2\sigma(F^2)]$, $wR(F^2)$, S	0.037, 0.100, 1.02
No. of relections	6960 reflections
No. of parameters	407
H-atom treatment	Riding model
Weighting scheme	Calculated $w = 1/[\sigma^2(F_o^2) + (0.044P)^2 + 8.74P]$ where $P = (F_o^2 + 2F_c^2)/3$
$(\Delta/\sigma)_{max}$	0.001
$\Delta\rho_{max}$, $\Delta\rho_{min}$ (e Å^{-3})	0.64, –0.29

Computer programs: *Bruker SMART version 5.624* (Bruker, 2001): *Bruker SAINT version 6.36a* (Bruker, 2000); *Bruker SAINT; Bruker SHELXTL* (Bruker, 2001); *SHELXS-97* (Sheldrick, 1990); *SHELXL-97* (Sheldrick, 1997); *enCIFer* (CCDC, 2003); *PLATON* (Spek, 2003).

Appendix VII

Crystallographic Refinement Details and Data For $[CoCl_2(L^{Bipy\text{-}1})].5CHCl_3$

Single-crystal diffraction data were collected on a Bruker SMART1000 CCD area detector diffractometer, equipped with an Oxford Cryosystem open-flow nitrogen cryostat, using graphite-monochromated Mo-K_α radiation (λ=0.71073 Å). Integrated intensities, corrected for Lorentz and polarisation effects, were obtained using the Bruker SAINT package, as were the cell parameters. All data were corrected for absorption using a multi-scan correction. The structure was solved by direct methods and refined by full-matrix least squares using SHELXL-97. All further non-hydrogen atoms were located in subsequent difference Fourier syntheses. Attempts to model disorder in two of the molecules of $CHCl_3$ included in the asymmetric unit gave unsatisfactory results, with peaks of ~3 e-/Å^3 remaining in positions which do not form part of a sensible disorder model. The PLATON SQUEEZE

model was used to account for this electron density, calculating 212 electrons per unit cell, which equates to approximately four molecules of $CHCl_3$ per unit cell. This has been included in the cell contents and used for all values derived from this. All hydrogen atoms were placed in geometrically calculated positions and refined using a riding model. All non-hydrogen atoms were refined with anisotropic displacement parameters. Crystal structure diagrams were generated using OLEX, version 2.54. [1]

Identification code	coclom
Crystal data	
Chemical formula	$C_{30}H_{30}Cl_2CoN_4O_6.5(CHCl_3)$
M_r	1269.25
Cell setting, space group	Triclinic, *P*-1
a, *b*, *c* (Å)	11.0076 (12), 14.914 (2), 16.549 (2)
α, β, γ (°)	89.747 (2), 70.871 (2), 89.298 (2)
V (Å^3)	2566.7 (8)
Z	2
D_x (Mg m^{-3})	1.642
Radiation type	Mo *K*α
No. of reflections for cell parameters	5914
θ range (°)	2.4–26.9
μ (mm^{-1})	1.26
Temperature (K)	150 (2)
Crystal form, colour	Column, orange
Crystal size (mm)	0.23 × 0.18 × 0.11
Data collection	
Diffractometer	Bruker SMART1000 CCD area detector
Data collection method	ω
Absorption correction	Multi-scan (based on symmetry-related measurements)
T_{min}	0.896
T_{max}	1.000
No. of measured, independent and observed parameters	23499, 11483, 7897

Criterion for observed reflections	$I > 2\sigma(I)$
R_{int}	0.030
θ_{max} (°)	27.5
Range of h, k, l	$-14 \rightarrow h \rightarrow 14$ $-19 \rightarrow k \rightarrow 19$ $-21 \rightarrow l \rightarrow 20$
Refinement	
Refinement on	F^2
$R[F^2 > 2\sigma(F^2)]$, $wR(F^2)$, S	0.050, 0.136, 1.06
No. of relections	11472 reflections
No. of parameters	496
H-atom treatment	Riding model
Weighting scheme	Calculated $w = 1/[\sigma^2(F_o^2) + (0.0703P)^2 + 0.1618P]$ where $P = (F_o^2 + 2F_c^2)/3$
$(\Delta/\sigma)_{max}$	0.001
$\Delta\rho_{max}$, $\Delta\rho_{min}$ (e Å^{-3})	0.98, –0.78

Computer programs: *Bruker SMART version 5.624* (Bruker, 2001); *Bruker SAINT version 6.36a* (Bruker, 2002); *Bruker SAINT; Bruker SHELXTL* (Bruker, 2001); *SHELXS-97* (Sheldrick, 1990); *SHELXL-97* (Sheldrick, 1997); *enCIFer*(Allen et al.,2004);*PLATON*(Spek,2003).

Appendix VIII

Crystallographic Refinement Details and Data For $[NiCl_2(L^{Bipy\text{-}1})].5CHCl_3$

Single-crystal diffraction data were collected on a Bruker SMART1000 CCD area detector diffractometer, equipped with an Oxford Cryosystem open-flow nitrogen cryostat, using graphite-monochromated Mo-K_α radiation (λ=0.71073 Å). Integrated intensities, corrected for Lorentz and polarisation effects, were obtained using the Bruker SAINT package, as were the cell parameters. All data were corrected for absorption using a multi-scan correction. The structure was solved by direct methods and refined by full-

matrix least squares using SHELXL-97. All further non-hydrogen atoms were located in subsequent difference Fourier syntheses. Disorder in one $CHCl_3$ group, hence chlorine atoms were modelled over 2 sites, with occupancies of 85% and 15%, respectively. Residual electron density was found in the region of the other $CHCl_3$ solvent molecule but does not form part of a sensible disorder model. All hydrogen atoms were placed in geometrically calculated positions and refined using a riding model. All non-hydrogen atoms were refined with anisotropic displacement parameters, except the minor components of the disorder model. Crystal structure diagrams were generated using OLEX, version 2.54.[1]

Identification code	niclom
Crystal data	
Chemical formula	$C_{30}H_{30}Cl_2N_4NiO_6.5(CHCl_3)$
M_r	1269.03
Cell setting, space group	Triclinic, *P*-1
a, *b*, *c* (Å)	11.037 (6), 14.889 (8), 16.636 (9)
α, β, γ (°)	89.426 (9), 70.934 (8), 89.356 (8)
V (Å^3)	2584 (4)
Z	2
D_x (Mg m^{-3})	1.631
Radiation type	Mo *K*α
No. of reflections for cell parameters	8784
θ range (°)	2.4–27.5
μ (mm^{-1})	1.30
Temperature (K)	150 (2)
Crystal form, colour	Plate, orange
Crystal size (mm)	0.41 × 0.38 × 0.03
Data collection	
Diffractometer	Bruker SMART1000 CCD area detector
Data collection method	ω
Absorption correction	Multi-scan (based on symmetry-related measurements)

	related measurements)
T_{min}	0.636
T_{max}	1.000
No. of measured, independent and observed parameters	19561, 10952, 8729
Criterion for observed reflections	$I > 2\sigma(I)$
R_{int}	0.026
θ_{max} (°)	27.5
Range of h, k, l	$-13 \rightarrow h \rightarrow 14$ $-19 \rightarrow k \rightarrow 19$ $-21 \rightarrow l \rightarrow 19$
Refinement	
Refinement on	F^2
$R[F^2 > 2\sigma(F^2)]$, $wR(F^2)$, S	0.061, 0.195, 1.03
No. of relections	10944 reflections
No. of parameters	580
H-atom treatment	Riding model
Weighting scheme	Calculated $w = 1/[\sigma^2(F_o^2) + (0.105P)^2 + 8.765P]$ where $P = (F_o^2 + 2F_c^2)/3$
$(\Delta/\sigma)_{max}$	0.005
$\Delta\rho_{max}$, $\Delta\rho_{min}$ (e Å^{-3})	1.83, –1.25

Computer programs: *Bruker SMART version 5.624* (Bruker, 2001); *Bruker SAINT version 6.36a* (Bruker, 2000); *Bruker SAINT; Bruker SHELXTL* (Bruker, 2001); *SHELXS-97* (Sheldrick, 1990); *SHELXL-97* (Sheldrick, 1997); *enCIFer* (CCDC, 2003); *PLATON* (Spek, 2003).

Appendix IX

Crystallographic Refinement Details and Data For $[ZnCl_2(L^{Bipy\text{-}1})].CHCl_3$

Single-crystal diffraction data were collected on a Bruker SMART1000 CCD area detector diffractometer, equipped with an Oxford Cryosystem open-flow nitrogen cryostat, using graphite-monochromated Mo-K_α radiation (λ=0.71073 Å). The crystal used for the data collection was split and the data

were processed using two orientation matrices, related by a rotation of -1.67° about the (-1, 0.16, 0.03) direct lattice direction. Subsequent refinement showed the fraction of each component approximately 0.5. Integrated intensities, corrected for Lorentz and polarisation effects, were obtained using the Bruker SAINT package, as were the cell parameters. All data were corrected for absorption using a multi-scan correction. The structure was solved by direct methods and refined by full-matrix least squares using SHELXL-97. All further non-hydrogen atoms were located in subsequent difference Fourier syntheses. The largest residual electron density peak was adjacent to the zinc(II) cation. All hydrogen atoms were placed in geometrically calculated positions and refined using a riding model. All non-hydrogen atoms were refined with anisotropic displacement parameters. Crystal structure diagrams were generated using OLEX, version 2.54.[1]

Identification code	znomim
Crystal data	
Chemical formula	$C_{30}H_{30}Cl_2N_4O_6Zn.CHCl_3$
M_r	798.22
Cell setting, space group	Triclinic, *P*-1
a, *b*, *c* (Å)	7.986 (5), 13.563 (9), 16.562 (11)
α, β, γ (°)	87.363 (11), 78.345 (13), 88.200 (12)
V (Å^3)	1755 (2)
Z	2
D_x (Mg m^{-3})	1.511
Radiation type	Mo $K\alpha$
No. of reflections for cell parameters	804
θ range (°)	2.6–24.7
μ (mm^{-1})	1.13
Temperature (K)	150 (2)
Crystal form, colour	Block, yellow
Crystal size (mm)	0.23 × 0.18 × 0.12

Data collection	
Diffractometer	Bruker SMART1000 CCD area detector
Data collection method	ω
Absorption correction	Multi-scan (based on symmetry-related measurements)
T_{min}	0.467
T_{max}	1.000
No. of measured, independent and observed parameters	16114, 9050, 5912
Criterion for observed reflections	$I > 2\sigma(I)$
R_{int}	0.057
θ_{max} (°)	27.6
Range of h, k, l	$-10 \rightarrow h \rightarrow 10$ $-17 \rightarrow k \rightarrow 17$ $-21 \rightarrow l \rightarrow 21$
Refinement	
Refinement on	F^2
$R[F^2 > 2\sigma(F^2)]$, $wR(F^2)$, S	0.086, 0.264, 1.01
No. of relections	9050 reflections
No. of parameters	425
H-atom treatment	Riding model
Weighting scheme	Calculated $w = 1/[\sigma^2(F_o^2) + (0.1788P)^2]$ where $P = (F_o^2 + 2F_c^2)/3$
$(\Delta/\sigma)_{max}$	0.005
$\Delta\rho_{max}$, $\Delta\rho_{min}$ (e Å^{-3})	1.63, −1.40

Computer programs: *Bruker SMART version 5.624* (Bruker, 2001); *Bruker SAINT version 6.36a* (Bruker, 2000); *Bruker SAINT; Bruker SHELXTL* (Bruker, 2001); *SHELXS-97* (Sheldrick, 1990); *SHELXL-97* (Sheldrick, 1997); *enCIFer* (CCDC, 2003); *PLATON* (Spek, 2003).

Appendix X

Crystallographic Refinement Details and Data For $[Zn(L^{Dipy-1})]_2.0.1CHCl_3.3.35C_2H_{10}O$

Single-crystal diffraction data were collected on a Bruker SMART1000 CCD area detector diffractometer, equipped with an Oxford Cryosystem open-flow nitrogen cryostat, using graphite-monochromated Mo-K_α radiation (λ=0.71073 Å). Integrated intensities, corrected for Lorentz and polarisation effects, were obtained using the Bruker SAINT package, as were the cell parameters. All data were corrected for absorption using a multi-scan correction. The structure was solved by direct methods and refined by full-matrix least squares using SHELXL-97. All further non-hydrogen atoms were located in subsequent difference Fourier syntheses. Several molecules of solvent were included in the lattice. One ordered, fully occupied molecule of Et_2O (O1s). One Et_2O with $CHCl_3$ overlaid modelled as 0.85 occupancy and $CHCl_3$ as 0.15 with one Cl disordered over 2 equally occupied (0.075) sites. Further Et_2O lies with O (O3s) on an inversion site and adjacent C atom disordered over two half occupied sites (half a molecule in the asymmetric unit). O4s has two orientations of Et_2O overlapping, with occupancies 0.60 and 0.40. O3s and O4s Et_2O molecules were modelled with isotropic adsorptions. All have suitable geometric restraints applied. All hydrogen atoms were placed in geometrically calculated positions and refined using a riding model. All non-hydrogen, non-disordered atoms were refined with anisotropic displacement parameters. Crystal structure diagrams were generated using OLEX, version 2.54.[1]

Identification code	znpyro
Crystal data	
Chemical formula	$C_{62}H_{68}N_8O_{12}Zn_2.0.1(CHCl_3).3.35(C_2H_{10}O)$
M_r	1498.74
Cell setting, space group	Monoclinic, $P2_1/n$
a, b, c (Å)	13.1924 (9), 15.0537 (10), 38.352 (3)
β (°)	94.166 (2)
V (Å^3)	7596.4 (9)
Z	4
D_x (Mg m^{-3})	1.310
Radiation type	Mo $K\alpha$
No. of reflections for cell parameters	11345
θ range (°)	3.6–27.3
μ (mm^{-1})	0.71
Temperature (K)	150 (2)
Crystal form, colour	Lath, yellow
Crystal size (mm)	0.54 × 0.20 × 0.07
Data collection	
Diffractometer	Bruker SMART APEX CCD area detector
Data collection method	ω
Absorption correction	Multi-scan (based on symmetry-related measurements)
T_{min}	0.830
T_{max}	1.000
No. of measured, independent and observed parameters	57078, 13308, 10794
Criterion for observed reflections	$I > 2\sigma(I)$
R_{int}	0.049
θ_{max} (°)	25.0
Range of h, k, l	$-15 \rightarrow h \rightarrow 15$
	$-17 \rightarrow k \rightarrow 17$
	$-45 \rightarrow l \rightarrow 45$
Refinement	
Refinement on	F^2
$R[F^2 > 2\sigma(F^2)]$, $wR(F^2)$, S	0.068, 0.157, 1.14
No. of relections	13308 reflections

No. of parameters	904
H-atom treatment	Constrained to parent site
Weighting scheme	Calculated $w = 1/[\sigma^2(F_o^2) + (0.0463P)^2 + 24.3343P]$ where $P = (F_o^2 + 2F_c^2)/3$
$(\Delta/\sigma)_{max}$	0.001
$\Delta\rho_{max}$, $\Delta\rho_{min}$ (e Å^{-3})	0.82, –0.75

Computer programs: *Bruker SMART version 5.625* (Bruker, 2001); *Bruker SAINT version 6.36a* (Bruker, 2000); *Bruker SAINT; Bruker SHELXTL* (Bruker, 2001); *SHELXS-97* (Sheldrick, 1990); *SHELXL-97* (Sheldrick, 1997); *enCIFer* (CCDC, 2003); *PLATON* (Spek, 2003).

Appendix XI

Crystallographic Refinement Details and Data For ex-[Zn(L^{Dipy-1})]$_2$.CH_2Cl_2

Single-crystal diffraction data were collected on a Bruker SMART1000 CCD area detector diffractometer, equipped with an Oxford Cryosystem open-flow nitrogen cryostat, using graphite-monochromated Mo-K_α radiation (λ=0.71073 Å). Integrated intensities, corrected for Lorentz and polarisation effects, were obtained using the Bruker SAINT package, as were the cell parameters. All data were corrected for absorption using a multi-scan correction. The structure was solved by direct methods and refined by full-matrix least squares using SHELXL-97. All further non-hydrogen atoms were located in subsequent difference Fourier syntheses. Disorder in several terminal groups was modelled over two half occupied sites with isotropic adsorptions and some geometry restraints. All hydrogen atoms were placed in geometrically calculated positions and refined using a riding model. All non-hydrogen atoms, except disordered terminal groups, were refined with

anisotropic displacement parameters. Crystal structure diagrams were generated using OLEX, version 2.54. [1]

Identification code	znmees
Crystal data	
Chemical formula	$C_{82}H_{68}N_8O_{12}Zn_2.CH_2Cl_2$
M_r	1573.11
Cell setting, space group	Triclinic, *P*-1
a, *b*, *c* (Å)	10.8280 (14), 13.868 (2), 24.757 (3)
α, β, γ (°)	86.729 (2), 83.778 (2), 79.859 (2)
V (Å^3)	3635.2 (8)
Z	2
D_x (Mg m^{-3})	1.437
Radiation type	Mo *K*α
No. of reflections for cell parameters	5493
θ range (°)	2.2–23.6
μ (mm^{-1})	0.80
Temperature (K)	150 (2)
Crystal form, colour	Block, orange
Crystal size (mm)	0.20 × 0.16 × 0.11
Data collection	
Diffractometer	Bruker SMART1000 CCD area detector
Data collection method	ω
Absorption correction	Multi-scan (based on symmetry-related measurements)
T_{min}	0.880
T_{max}	1.000
No. of measured, independent and observed parameters	32028, 16161, 10094
Criterion for observed reflections	$I > 2\sigma(I)$
R_{int}	0.046
θ_{max} (°)	27.5
Range of *h*, *k*, *l*	$-13 \rightarrow h \rightarrow 14$
	$-17 \rightarrow k \rightarrow 17$
	$-31 \rightarrow l \rightarrow 32$

Refinement	
Refinement on	F^2
$R[F^2 > 2\sigma(F^2)]$, $wR(F^2)$, S	0.058, 0.152, 1.01
No. of relections	16161 reflections
No. of parameters	926
H-atom treatment	Constrained to parent site
Weighting scheme	Calculated $w = 1/[\sigma^2(F_o^2) + (0.0595P)^2 + 4.4192P]$ where $P = (F_o^2 + 2F_c^2)/3$
$(\Delta/\sigma)_{max}$	0.001
$\Delta\rho_{max}$, $\Delta\rho_{min}$ (e Å^{-3})	0.67, –0.92

Computer programs: *Bruker SMART version 5.624* (Bruker, 2001); *Bruker SAINT version 6.36a* (Bruker, 2002); *Bruker SAINT; Bruker SHELXTL* (Bruker, 2001); *SIR-92* (Altomare et al, 1992); *SHELXL-97* (Sheldrick, 1997); *enCIFer*(Allen et al.,2004);*PLATON*(Spek,2003).

Appendix XII

Crystallographic Refinement Details and Data For ex-[Pd(L^{Dipy-1})]

Single-crystal diffraction data were collected on a Bruker SMART1000 CCD area detector diffractometer, equipped with an Oxford Cryosystem open-flow nitrogen cryostat, using graphite-monochromated Mo-K_α radiation (λ=0.71073 Å). Integrated intensities, corrected for Lorentz and polarisation effects, were obtained using the Bruker SAINT package, as were the cell parameters. All data were corrected for absorption using a multi-scan correction. The structure was solved by direct methods and refined by full-matrix least squares using SHELXL-97. All further non-hydrogen atoms were located in subsequent difference Fourier syntheses. Twinning was present, with 180° rotation about 011 rl direction. Twin law (-1 0 0, -0.24 0.2 0.8, -0.24 1.2 -0.2) was used. Rotax was used to identify the twin law and WINGX was used to write hklf5 format data file. The twin component fraction refines

to approximately 16%. All hydrogen atoms were placed in geometrically calculated positions and refined using a riding model. All non-hydrogen atoms were refined with anisotropic displacement parameters. Crystal structure diagrams were generated using OLEX, version 2.54. [1]

Identification code	pdmesb
Crystal data	
Chemical formula	$C_{41}H_{34}N_4O_6Pd$
M_r	785.12
Cell setting, space group	Triclinic, *P*-1
a, *b*, *c* (Å)	10.723 (2), 12.353 (2), 13.847 (3)
α, β, γ (°)	68.143 (3), 89.402 (3), 80.348 (3)
V (Å^3)	1675.5 (9)
Z	2
D_x (Mg m^{-3})	1.556
Radiation type	Mo *K*α
No. of reflections for cell parameters	5554
θ range (°)	2.4–26.9
μ (mm^{-1})	0.61
Temperature (K)	150 (2)
Crystal form, colour	Lath, yellow
Crystal size (mm)	0.25 × 0.12 × 0.06
Data collection	
Diffractometer	Bruker SMART1000 CCD area detector
Data collection method	ω
Absorption correction	Multi scan
T_{min}	0.773
T_{max}	1.00
No. of measured, independent and observed parameters	14506, 7424, 6205
Criterion for observed reflections	$I > 2\sigma(I)$
R_{int}	0.040
θ_{max} (°)	27.6
Range of *h*, *k*, *l*	$-13 \rightarrow h \rightarrow 13$
	$-15 \rightarrow k \rightarrow 16$

	$-17 \rightarrow l \rightarrow 17$
Refinement	
Refinement on	F^2
$R[F^2 > 2\sigma(F^2)]$, $wR(F^2)$, S	0.046, 0.123, 1.07
No. of relections	7424 reflections
No. of parameters	470
H-atom treatment	Riding model
Weighting scheme	Calculated $w = 1/[\sigma^2(F_o^2) + (0.0557P)^2 + 2.642P]$ where $P = (F_o^2 + 2F_c^2)/3$
$(\Delta/\sigma)_{max}$	0.005
$\Delta\rho_{max}$, $\Delta\rho_{min}$ (e Å^{-3})	1.19, –1.46

Computer programs: *Bruker SMART version 5.624* (Bruker, 2001); *sadabs version 2.05*; *SHELXS-97* (Sheldrick, 1990); *ROTAX/WINGX*; *SHELXL-97* (Sheldrick, 1997).

[1] O. V. Dolomanov, A. J. Blake, N. R. Champness, C. Wilson and M. Schröder, *J. Appl. Cryst.*, 2003, **36**, 1283.